frontiers | Research Topics

Gene regulation mediated by competing RNA: From benchside to bedside

Edited by
Yumei Luo, Detu Zhu and Jian-Hong Fang

Published in
Frontiers in Genetics

ISSN 1664-8714
ISBN 978-2-83250-982-1
DOI 110.3389/978-2-83250-982-1

About Frontiers

Frontiers is more than just an open access publisher of scholarly articles: it is a pioneering approach to the world of academia, radically improving the way scholarly research is managed. The grand vision of Frontiers is a world where all people have an equal opportunity to seek, share and generate knowledge. Frontiers provides immediate and permanent online open access to all its publications, but this alone is not enough to realize our grand goals.

Frontiers journal series

The Frontiers journal series is a multi-tier and interdisciplinary set of open-access, online journals, promising a paradigm shift from the current review, selection and dissemination processes in academic publishing. All Frontiers journals are driven by researchers for researchers; therefore, they constitute a service to the scholarly community. At the same time, the *Frontiers journal series* operates on a revolutionary invention, the tiered publishing system, initially addressing specific communities of scholars, and gradually climbing up to broader public understanding, thus serving the interests of the lay society, too.

Dedication to quality

Each Frontiers article is a landmark of the highest quality, thanks to genuinely collaborative interactions between authors and review editors, who include some of the world's best academicians. Research must be certified by peers before entering a stream of knowledge that may eventually reach the public - and shape society; therefore, Frontiers only applies the most rigorous and unbiased reviews. Frontiers revolutionizes research publishing by freely delivering the most outstanding research, evaluated with no bias from both the academic and social point of view. By applying the most advanced information technologies, Frontiers is catapulting scholarly publishing into a new generation.

What are Frontiers Research Topics?

Frontiers Research Topics are very popular trademarks of the *Frontiers journals series*: they are collections of at least ten articles, all centered on a particular subject. With their unique mix of varied contributions from Original Research to Review Articles, Frontiers Research Topics unify the most influential researchers, the latest key findings and historical advances in a hot research area.

Find out more on how to host your own Frontiers Research Topic or contribute to one as an author by contacting the Frontiers editorial office: frontiersin.org/about/contact

Gene regulation mediated by competing RNA: From benchside to bedside

Topic editors

Yumei Luo — The Third Affiliated Hospital of Guangzhou Medical University, China

Detu Zhu — Cornell University, United States

Jian-Hong Fang — Sun Yat-sen University, China

Citation

Luo, Y., Zhu, D., Fang, J.-H., eds. (2022). *Gene regulation mediated by competing RNA: From benchside to bedside*. Lausanne: Frontiers Media SA.

doi: 10.3389/978-2-83250-982-1

Table of contents

frontiers | Frontiers in Genetics

TYPE Editorial
PUBLISHED 23 November 2022
DOI 10.3389/fgene.2022.1085155

OPEN ACCESS

EDITED BY
William C. Cho,
QEH, Hong Kong SAR, China

REVIEWED BY
Chen Xu,
Shanghai Changzheng Hospital, China
Yu-Hang Xing,
Massachusetts General Hospital Cancer Center, United States

*CORRESPONDENCE
Yumei Luo,
mei.2002@163.com
Detu Zhu,
clover_jato@163.com

SPECIALTY SECTION
This article was submitted to RNA, a section of the journal Frontiers in Genetics

RECEIVED 31 October 2022
ACCEPTED 14 November 2022
PUBLISHED 23 November 2022

CITATION
Luo Y, Zhu D and Fang J-H (2022), Editorial: Gene regulation mediated by competing RNA: From benchside to bedside.
Front. Genet. 13:1085155.
doi: 10.3389/fgene.2022.1085155

Editorial: Gene regulation mediated by competing RNA: From benchside to bedside

Yumei Luo[1,2,3]*, Detu Zhu[1,4]* and Jian-Hong Fang[5]

[1]Department of Obstetrics and Gynecology, Key Laboratory for Major Obstetric Diseases of Guangdong Province, The Third Affiliated Hospital of Guangzhou Medical University, Guangzhou, China, [2]Guangzhou Laboratory, Guangzhou, China, [3]Institute of Biological Products, National Institutes for Food and Drug Control, Beijing, China, [4]Department of Genetic Medicine, Weill Cornell Medical College, New York, NY, United States, [5]MOE Key Laboratory of Gene Function and Regulation, School of Life Sciences, Sun Yat-sen University, Guangzhou, China

KEYWORDS

microRNA, long non-coding RNA, circular RNA, competing endogenous RNA network, gene regulation, CRISPR, SARS-CoV-2

Editorial on the Research Topic
Gene regulation mediated by competing RNA: From benchside to bedside

In addition to DNA methylation and chromatin structure, another important level of epigenetic regulation for gene expression is non-coding RNA (ncRNA) (Luo et al., 2019). NcRNAs facilitate post-transcriptional gene regulation *via* competitively interacting with the regulatory elements of target genes (Zhang et al., 2022). The course of various biological processes, the development of diseases, and the susceptibility to therapy are all significantly influenced by competitive ncRNA gene regulation (Panni et al., 2020). Numerous studies have demonstrated that important functional genes could be regulated by these ncRNAs *via* competing endogenous RNA (ceRNA) network (Salmena et al., 2011; Tay et al., 2011; Tay et al., 2014). Moreover, a large number of therapeutic means have been developed based on these mechanisms (Luo and Zhu, 2014). Thus, competitive RNA is expected to be used not only for basic research but also as a promising tool for applications in therapy. In this Research Topic, the essential functions and mechanisms of ncRNAs are further identified and investigated.

Circular RNAs (circRNAs) are ncRNAs that play a regulatory role in many biological processes, such as cell proliferation, senescence, and apoptosis (Visci et al., 2020). Many studies have found that circRNAs can play their regulatory role as microRNA (miRNA) sponges in human physiological and pathological processes (Peng et al., 2021). Whether as a diagnostic biomarker or as a therapeutic target, circRNAs have important values for studying the pathogenesis of diseases owing to their unique properties.

Aberrant alterations in nucleus pulposus cells (NPCs) are the most significant aspect of the pathological process of intervertebral disk degeneration (IDD) (Fontana et al., 2015; Oichi et al., 2020). In this context, Li et al. investigated circRNAs and miRNAs associated

with NPC metabolism under the IDD condition. They identified that circ_0040039 might aggravate IDD by stabilizing miR-874-3p and thus upregulate the miR-874-3p-ESR1 pathway, which lead to NPC degeneration and worsen IDD. In another study, Duan et al. demonstrated that circMTO1 could accelerate the progression of polycystic ovary syndrome (PCOS) by increasing MCL1 expression through interaction with miR-320b, offering novel insights into the development of diagnosis and treatment for PCOS. Furthermore, Cai et al. revealed that hsa_circRNA_0001400 is substantially expressed in cervical cancer tissues and promotes tumor progression *via* the circRNA_0001400-miR-326-Akt pathway. Knockdown of circRNA_0001400 by siRNA might potentially developed as a new method for cervical cancer therapy.

Long non-coding RNAs (lncRNAs), like circRNAs, can serve as miRNA sponges to provide indirect regulation of gene expression (Zhang et al., 2018). Besides, artificial lncRNAs have recently drawn a lot of interest as novel disease therapy tools to be utilized in gene regulatory activities (Tang et al., 2016).

Atrial fibrillation (AF), the most prevalent kind of arrhythmia, poses a great challenge in patient diagnosis and therapy (Hindricks et al., 2021), and further research into the pathophysiology of AF is of urgent need. Liu et al. constructed a ceRNA network associated to AF susceptibility and persistence, and then prioritized the selected lncRNAs using an innovative application of the improved RWR-M algorithm. Myocardial infarction-associated transcripts (MIAT) and LINC00964 were identified as featured lncRNAs in the network. These discoveries are in line with a prior study (Deshmukh et al., 2015), and they also suggested that ceRNA network analysis might shed light on the basic mechanisms underlying AF and offer promising therapeutic and diagnostic tools. In another study, kidney stones are hypothesized to be caused by Randall's plaque (RP) (Daudon et al., 2015). Xia et al. investigated the rate of immune cell infiltration as well as the ceRNA network in RPs from renal stone patients and validated the results both *in vivo* and *in vitro*. They then found that the lncRNA-associated differentially expressed mRNAs were significantly associated with renal interstitial fibrosis in extracellular matrix tissues, regulatory cell responses to growth factor stimulation, and collagen-containing extracellular matrices. In addition, Wu et al. summarized the recent research progress of LINC00467, detailing its biological mechanisms as an oncogene and clinical values as a prognostic predictor in various types of cancers.

MiRNAs as a class of small ncRNAs play a crucial role in downregulating gene expression by competitively interacting with the mRNA 3′UTR region and mediating RNA degradation through the RISC complex (Zhou et al., 2022). MiRNAs have two main applications. On the one hand, artificial miRNAs are often developed as genetic tools based on their downregulation mechanism to affect gene expression (Zhu et al., 2018). On the other hand, miRNAs are often utilized in targeted gene therapy due to the characteristic that miRNA targets can be used to attain tissue or cell-type specific transgene expression (Luo et al., 2015a).

MiRNAs have important roles in the emergence of epilepsy due to their capacity to regulate a variety of mRNAs. Previous studies have shown that miRNAs could alter neuronal excitability, which has an impact on the incidence of epilepsy (Henshall et al., 2016). Su et al. constructed a miRNA-mRNA regulation network that regulates ion channel genes in the mesial temporal lobe epilepsy (mTLE). They identified that miR-27a-3p might control a number of ion channel genes associated with mTLE, pointing to the possibility of using it as a diagnostic biomarker for mTLE.

In addition, the human induced pluripotent stem cells (hiPSCs) and embryonic stem cells (hESCs) are powerful tools for genetic studies in the recent years (Luo et al., 2021a). Some previous studies have illustrated the roles of several lncRNA-miRNA-mRNA circuits in regulating the pluripotent genes in hESCs (Wang et al., 2013; Xu et al., 2016). In this Research Topic, Chen et al. systematically reviewed the current progress in applying iPSC-derived models to study the regulatory role of miRNAs in developmental processes.

As sequencing technologies advance quickly, the expression profiles of different classes of ncRNAs are feasible to be characterized simultaneously in disease models, such as dilated cardiomyopathy (DCM) (Lin et al., 2021). Based on sex differences in DCM, Liu et al. constructed an immune-related ceRNA network including 5 lncRNAs, 6 miRNAs, and 29 mRNAs that might regulate several immune-related signaling pathways. Among these genes, CBL, CXCL12, and IL6ST were found to be connected to immune cell infiltration.

Here we assembled a compendium of 11 manuscripts including nine original researches and two reviews that cover the scope of this Research Topic, summarizing the critical aspects of the gene regulation mediated by competing RNAs in various diseases.

Additionally, we would also like to highlight other novel forms of competing RNA-mediated gene regulation that are yet to be included in the above compendium. Guide RNA (gRNA) is an important class of artificial small ncRNA that competitively bind with elements on the genome with the CRISPR/Cas complex (Luo et al., 2015b). Besides genome editing, the RNA-guided gene targeting technology has also been exploited quickly and extensively for diverse purposes, including gene regulation (Luo et al., 2016).

Recently, RNA viruses, such as SARS-CoV-2, have been found to act as exogenous competing RNAs and thus regulate endogenous gene expression, which may contribute to the disease progression (Bertolazzi et al., 2020). And in the current COVID-19 pandemic, it is of great interest to focus

on the role of SARS-CoV-2 in competing RNA-mediated gene regulation (Luo et al., 2021b).

Author contributions

YL, DZ, and J-HF wrote and edited the manuscript. All authors have approved the manuscript for publication.

Funding

This study was supported by the National Natural Science Foundation of China (82002774), Guangdong Basic and Applied Basic Research Foundation (2020A1515010065), Guangzhou City Science and Technology Project (202201020208), Guangzhou City Science, Technology and Innovation Commission (202002030077), Guangdong Province Outstanding Youth Medical Talent Program (110217110) and Lin He's Academician Workstation of New Medicine and Clinical Translation at The Third Affiliated Hospital of Guangzhou Medical University (2021HLKY05).

Acknowledgments

We thank all authors, reviewers and the Frontiers journal editorial team for their contributions to this Research Topic.

Conflict of interest

The authors declare that the research was conducted in the absence of any commercial or financial relationships that could be construed as a potential conflict of interest.

Publisher's note

References

Bertolazzi, G., Cipollina, C., Benos, P. V., Tumminello, M., and Coronnello, C. (2020). miR-1207-5p can contribute to dysregulation of inflammatory response in COVID-19 via targeting SARS-CoV-2 RNA. *Front. Cell. Infect. Microbiol.* 10, 586592. doi:10.3389/fcimb.2020.586592

Daudon, M., Bazin, D., and Letavernier, E. (2015). Randall's plaque as the origin of calcium oxalate kidney stones. *Urolithiasis* 43 (S1), 5–11. doi:10.1007/s00240-014-0703-y

Deshmukh, A., Barnard, J., Sun, H., Newton, D., Castel, L., Pettersson, G., et al. (2015). Left atrial transcriptional changes associated with atrial fibrillation susceptibility and persistence. *Circ. Arrhythm. Electrophysiol.* 8 (1), 32–41. doi:10.1161/CIRCEP.114.001632

Fontana, G., See, E., and Pandit, A. (2015). Current trends in biologics delivery to restore intervertebral disc anabolism. *Adv. Drug Deliv. Rev.* 84, 146–158. doi:10.1016/j.addr.2014.08.008

Henshall, D. C., Hamer, H. M., Pasterkamp, R. J., Goldstein, D. B., Kjems, J., Prehn, J. H. M., et al. (2016). MicroRNAs in epilepsy: pathophysiology and clinical utility. *Lancet. Neurol.* 15 (13), 1368–1376. doi:10.1016/S1474-4422(16)30246-0

Hindricks, G., Potpara, T., Dagres, N., Arbelo, E., Bax, J. J., Blomström-Lundqvist, C., et al. (2021). 2020 ESC Guidelines for the diagnosis and management of atrial fibrillation developed in collaboration with the European Association for Cardio-Thoracic Surgery (EACTS): The Task Force for the diagnosis and management of atrial fibrillation of the European Society of Cardiology (ESC) Developed with the special contribution of the European Heart Rhythm Association (EHRA) of the ESC. *Eur. Heart J.* 42 (5), 373–498. doi:10.1093/eurheartj/ehaa612

Lin, Z., Zhao, Y., Dai, F., Su, E., Li, F., and Yan, Y. (2021). Analysis of changes in circular RNA expression and construction of ceRNA networks in human dilated cardiomyopathy. *J. Cell. Mol. Med.* 25 (5), 2572–2583. doi:10.1111/jcmm.16251

Luo, Y., and Zhu, D. (2014). Combinatorial control of transgene expression by hypoxia-responsive promoter and MicroRNA regulation for neural stem cell-based cancer therapy. *Biomed. Res. Int.* 2014, 751397. doi:10.1155/2014/751397

Luo, Y., Zhu, D., Lam, D. H., Huang, J., Tang, Y., Luo, X., et al. (2015a). A double-switch cell fusion-inducible transgene expression system for neural stem cell-based antiglioma gene therapy. *Stem Cells Int.* 2015, 649080. doi:10.1155/2015/649080

Luo, Y., Zhu, D., Zhang, Z., Chen, Y., and Sun, X. (2015b). Integrative analysis of CRISPR/Cas9 target sites in the human *HBB* gene. *Biomed. Res. Int.* 2015, 514709. doi:10.1155/2015/514709

Luo, Y., Xu, X., An, X., Sun, X., Wang, S., and Zhu, D. (2016). Targeted inhibition of the miR-199a/214 cluster by CRISPR interference augments the tumor tropism of human induced pluripotent stem cell-derived neural stem cells under hypoxic condition. *Stem Cells Int.* 2016, 3598542. doi:10.1155/2016/3598542

Luo, Y., Huang, J., Tang, Y., Luo, X., Ge, L., Sheng, X., et al. (2019). Regional methylome profiling reveals dynamic epigenetic heterogeneity and convergent hypomethylation of stem cell quiescence-associated genes in breast cancer following neoadjuvant chemotherapy. *Cell Biosci.* 9 (1), 16. doi:10.1186/s13578-019-0278-y

Luo, Y., Chen, Y., Zhang, M., Ma, X., Zhu, D., and Chen, Y. (2021a). Generation of an induced pluripotent stem cell line GZHMCi008-A derived from a patient with SRY-positive 46, XX testicular disorder of sex development. *Stem Cell Res.* 57, 102583. doi:10.1016/j.scr.2021.102583

Luo, Y., Zhang, M., Chen, Y., Chen, Y., and Zhu, D. (2021b). Application of human induced pluripotent stem cell-derived cellular and organoid models for COVID-19 research. *Front. Cell Dev. Biol.* 9, 720099. doi:10.3389/fcell.2021.720099

Oichi, T., Taniguchi, Y., Oshima, Y., Tanaka, S., and Saito, T. (2020). Pathomechanism of intervertebral disc degeneration. *JOR Spine* 3 (1), 1076. doi:10.1002/jsp2.1076

Panni, S., Lovering, R. C., Porras, P., and Orchard, S. (2020). Non-coding RNA regulatory networks. *Biochim. Biophys. Acta. Gene Regul. Mech.* 1863 (6), 194417. doi:10.1016/j.bbagrm.2019.194417

Peng, F., Gong, W., Li, S., Yin, B., Zhao, C., Liu, W., et al. (2021). circRNA_010383 acts as a sponge for miR-135a, and its downregulated expression contributes to renal fibrosis in diabetic nephropathy. *Diabetes* 70 (2), 603–615. doi:10.2337/db20-0203

Salmena, L., Poliseno, L., Tay, Y., Kats, L., and Pandolfi, P. P. (2011). A ceRNA hypothesis: the rosetta stone of a hidden RNA language? *Cell* 146 (3), 353–358. doi:10.1016/j.cell.2011.07.014

Tang, S., Tan, G., Jiang, X., Han, P., Zhai, B., Dong, X., et al. (2016). An artificial lncRNA targeting multiple miRNAs overcomes sorafenib resistance in hepatocellular carcinoma cells. *Oncotarget* 7 (45), 73257–73269. doi:10.18632/oncotarget.12304

Tay, Y., Kats, L., Salmena, L., Weiss, D., Tan, S. M., Ala, U., et al. (2011). Coding-independent regulation of the tumor suppressor PTEN by competing endogenous mRNAs. *Cell* 147 (2), 344–357. doi:10.1016/j.cell.2011.09.029

Tay, Y., Rinn, J., and Pandolfi, P. P. (2014). The multilayered complexity of ceRNA crosstalk and competition. *Nature* 505 (7483), 344–352. doi:10.1038/nature12986

Visci, G., Tolomeo, D., Agostini, A., Traversa, D., Macchia, G., and Storlazzi, C. T. (2020). CircRNAs and Fusion-circRNAs in cancer: New players in an old game. *Cell. Signal.* 75, 109747. doi:10.1016/j.cellsig.2020.109747

Wang, Y., Xu, Z., Jiang, J., Xu, C., Kang, J., Xiao, L., et al. (2013). Endogenous miRNA sponge lincRNA-RoR regulates Oct4, Nanog, and Sox2 in human embryonic stem cell self-renewal. *Dev. Cell* 25 (1), 69–80. doi:10.1016/j.devcel.2013.03.002

Xu, C., Zhang, Y., Wang, Q., Xu, Z., Jiang, J., Gao, Y., et al. (2016). Long non-coding RNA GAS5 controls human embryonic stem cell self-renewal by maintaining NODAL signalling. *Nat. Commun.* 7, 13287. doi:10.1038/ncomms13287

Zhang, Z. K., Li, J., Guan, D., Liang, C., Zhuo, Z., Liu, J., et al. (2018). A newly identified lncRNA MAR1 acts as a miR-487b sponge to promote skeletal muscle differentiation and regeneration: MAR1 sponges miR-487b to promote muscle differentiation. *J. Cachexia Sarcopenia Muscle* 9 (3), 613–626. doi:10.1002/jcsm.12281

Zhang, Y., Yang, M., Yang, S., and Hong, F. (2022). Role of noncoding RNAs and untranslated regions in cancer: A review. *Medicine* 101 (33), e30045. doi:10.1097/MD.0000000000030045

Zhou, G., Zhang, M., Zhang, J., Feng, Y., Xie, Z., Liu, S., et al. (2022). The gene regulatory role of non-coding RNAs in non-obstructive azoospermia. *Front. Endocrinol.* 13, 959487. doi:10.3389/fendo.2022.959487

Zhu, D., Zhao, Z., Cui, G., Chang, S., Hu, L., See, Y. X., et al. (2018). Single-cell transcriptome analysis reveals estrogen signaling coordinately augments one-carbon, polyamine, and purine synthesis in breast cancer. *Cell Rep.* 25 (8), 2285–2298. doi:10.1016/j.celrep.2018.10.093

frontiers in Genetics

ORIGINAL RESEARCH
published: 11 June 2021
doi: 10.3389/fgene.2021.656759

Circ_0040039 May Aggravate Intervertebral Disk Degeneration by Regulating the MiR-874-3p-ESR1 Pathway

*Yongjin Li[1,2,3†], Xuke Wang[2,4†], Haiwei Xu[2†], Guowang Li[1,2,3†], Zhenxin Huo[1,2,3], Lilong Du[1,2,3], Kaihui Zhang[1,2,3], Li Shen[1,2,3], Hao Li[1,2,3] and Baoshan Xu[1,2,3]**

[1] Department of Minimally Invasive Spine Surgery, Tianjin Hospital, Tianjin, China, [2] Graduate School, Tianjin Medical University, Tianjin, China, [3] Tianjin Hospital, Orthopedic Research Institute, Tianjin, China, [4] Department of Minimally Invasive Spine Surgery, Luoyang Orthopedic- Traumatological Hospital, Luoyang, China

OPEN ACCESS

Edited by:
Yumei Luo,
Third Affiliated Hospital of Guangzhou Medical University, China

Reviewed by:
Jun Zou,
Soochow University, China
Hui Liu,
The First Affiliated Hospital of Sun Yat-sen University, China
Wenbin Hua,
Huazhong University of Science and Technology, China
Sidong Yang,
Third Hospital of Hebei Medical University, China

***Correspondence:**
Baoshan Xu
baoshanxu99@tmu.edu.cn

[†] These authors have contributed equally to this work

Specialty section:
This article was submitted to RNA, a section of the journal Frontiers in Genetics

Received: *21 January 2021*
Accepted: *15 April 2021*
Published: *11 June 2021*

Citation:
Li Y, Wang X, Xu H, Li G, Huo Z, Du L, Zhang K, Shen L, Li H and Xu B (2021) Circ_0040039 May Aggravate Intervertebral Disk Degeneration by Regulating the MiR-874-3p-ESR1 Pathway. Front. Genet. 12:656759. doi: 10.3389/fgene.2021.656759

The functional alteration of nucleus pulposus cells (NPCs) exerts a crucial role in the occurrence and progression of intervertebral disk degeneration (IDD). Circular RNAs and microRNAs (miRs) are critical regulators of NPC metabolic processes such as growth and apoptosis. In this study, bioinformatics tools, encompassing Gene Ontology pathway and Venn diagrams analysis, and protein–protein interaction (PPI) network construction were used to identify functional molecules related to IDD. PPI network unveiled that ESR1 was one of the most critical genes in IDD. Then, a key IDD-related circ_0040039-miR-874-3p-ESR1 interaction network was predicted and constructed. Circ_0040039 promoted miR-874-3p and repressed ESR1 expression, and miR-874-3p repressed ESR1 expression in NPCs, suggesting ESR1 might be a direct target of miR-874-3p. Functionally, circ_0040039 could enhance NPC apoptosis and inhibit NPC growth, revealing that circ_0040039 might aggravate IDD by stabilizing miR-874-3p and further upregulating the miR-874-3p-ESR1 pathway. This signaling pathway might provide a novel therapeutic strategy and targets for the diagnosis and therapy of IDD-related diseases.

Keywords: circular RNA, ESR1, apoptosis, intervertebral disk degeneration, miR-874-3p

INTRODUCTION

The intervertebral disk (IVD), especially the nucleus pulposus (NP) tissue in its center, plays a crucial role in harboring complex mechanical stress and maintaining spine stability (Humzah and Soames, 1988). NP cell (NPC) degeneration is often regarded as the initiating factor of intervertebral disk degeneration (IDD). The abnormal increase in the degradation of NPC extracellular matrix (ECM) components, such as aggrecan and collagen II (Roughley, 2004; Fontana et al., 2015; Oichi et al., 2020); NPC apoptosis (Ding et al., 2013; Fontana et al., 2015; Oichi et al., 2020); and levels of proinflammatory cytokines, such as tumor necrosis factor α (TNF-α) and interleukin 1β (IL-1β) secreted by NPCs (Risbud and Shapiro, 2014; Fontana et al., 2015; Oichi et al., 2020; Wang et al., 2020), are the most important pathological characteristics during IDD. The functional changes in NPCs can trigger the loss of IVD function and further facilitate the progression of IDD (Roughley, 2004; Ding et al., 2013;

Risbud and Shapiro, 2014; Fontana et al., 2015; Oichi et al., 2020; Wang et al., 2020). Thus, exploring the specific pathomechanism of IDD at the level of NPCs is of far-reaching significance.

Non-coding RNAs (ncRNAs), such as circular RNAs (circRNAs) and microRNAs (miRNAs, miRs), are vitally important regulatory elements encoded by the genome. Accumulating studies have constantly uncovered that the dysfunction of NPCs induced by proinflammatory cytokines or compression or other inducers can be recovered by differentially expressed circRNAs and miRNAs in IDD (Cheng et al., 2018; Wang et al., 2018; Xie et al., 2019; Cazzanelli and Wuertz-Kozak, 2020; Xiang et al., 2020). Mechanistically, circRNA-mediated alteration in the expression levels of miRNAs can be divided into two modes. One is the canonical sponge mechanism, in which circRNAs repress or do not affect miRNA expression (Piwecka et al., 2017; Cheng et al., 2018; Wang et al., 2018; Xie et al., 2019; Xiang et al., 2020); another is the stabilization mechanism, in which circRNAs elevate miRNA expression (Piwecka et al., 2017; Chen et al., 2019). MiRNAs are small, single-stranded, ncRNAs, which inhibit mRNA expression by inhibiting mRNA translation or inducing mRNA degradation through forming an RNA-induced silencing complex with argonaute 2 protein and directly interacting with the 3′-untranslated region (UTR) of the target mRNA (Pasquinelli, 2012; Piwecka et al., 2017; Cheng et al., 2018; Ji et al., 2018; Wang et al., 2018; Chen et al., 2019; Xie et al., 2019; Xiang et al., 2020). Circ-VMA21 (Cheng et al., 2018), circ-CIDN (Xiang et al., 2020), circ-4099 (Wang et al., 2018), circ-ERCC2 (Xie et al., 2019), and miR-141 inhibitor (Ji et al., 2018) were reported to be involved in regulating NPC apoptosis and ECM metabolism and also alleviate IDD *in vitro* and *in vivo*. However, the current treatment of IDD remains a challenge. Therefore, novel key molecules to maintain the normal physiological function of NPCs and block the pathological process of IDD are urgently needed.

In this study, IDD-related circRNA (GSE67566), miRNA (GSE63492/GSE116726), and mRNA (GSE56081) microarray datasets downloaded from the Gene Expression Omnibus (GEO) database[1], which reposits publicly available gene expression and other functional genomic datasets, were reanalyzed (Clough and Barrett, 2016). Then, a circ_0040039-miR-874-3p-ESR1 interaction network was constructed by bioinformatics analysis, and it was confirmed that circ_0040039 could upregulate the miR-874-3p-ESR1 pathway. Finally, the overexpression of circ_0040039 was found to promote NPC degeneration.

MATERIALS AND METHODS

Selection and Analysis of GEO Datasets

After Lan et al. (2016); Ji et al. (2018), and Wan et al. (2014) sequenced normal and degenerative NP tissues, respectively, they uploaded circRNA (GSE67566), miRNA (GSE63492/GSE116726), and mRNA (GSE56081) microarray datasets to GEO database. Detailed information for each dataset is shown in **Table 1**. In terms of GSE67566/GSE63492/GSE116726, the raw data were read and analyzed using the limma package in R (Ritchie et al., 2015), as well as normalized and log2-transformed. By default, the false-positive results of adjusted *P*-value were corrected using Benjamini and Hochberg false discovery rate (FDR). We identified differentially expressed miRNAs (DEMs) with the criterion of the absolute value of log2 fold change (FC) > 2 and $-\log_{10}$ (FDR) > 2 based on the analysis of GSE116726. The GSE56081 dataset was obtained from Lan et al. (2016) analytical result (FC > 2 or < -2, $P < 0.05$).

Venn Analysis

The upstream miRNAs of ESR1 were predicted by Targetscanhuman 7.2[2] (Agarwal et al., 2015), mirDIP[3] (Tokar et al., 2018), starBase[4] (Li et al., 2014), miRTarBase[5] (Chou et al., 2018), miRDB[6] (Chen and Wang, 2020), and miRWalk 3.0[7] (Dweep and Gretz, 2015) databases, and GSE63492/GSE116726 datasets. Targetscanhuman 7.2 (Agarwal et al., 2015), starBase (Li et al., 2014), miRTarBase (Chou et al., 2018), miRDB (Chen and Wang, 2020), miRWalk 3.0 (Dweep and Gretz, 2015), and miRanda[8] (John et al., 2004), and GSE56081 dataset were used to predict miR-874-3p targets genes. Additionally, the upstream circRNAs of miR-874-3p were predicted via circbank[9] (Liu et al., 2019), starBase (Li et al., 2014) databases, and GSE67566 dataset to select IDD-related circRNAs.

Gene Ontology Enrichment Analyses and Protein–Protein Interaction Network Construction

Based on the miR-874-3p targets genes predicted by miRTarBase database (Chou et al., 2018), the Cytoscape software was utilized to display these genes (Otasek et al., 2019). Furthermore, Gene Ontology (GO) enrichment analyses was conducted using the Search Tool for the Retrieval of Interacting Genes (STRING)[10] (Szklarczyk et al., 2019), and the predominant enrichment pathways were further visualized by SangerBox tool[11]. The $P < 0.05$ was regarded as statistically significant. In addition, protein–protein interaction (PPI) network was constructed, and the degree centrality of the nodes in the PPI network was speculated through the cytoHubba plug-in in Cytoscape software (Chin et al., 2014; Szklarczyk et al., 2019), of which the higher nodes degrees were considered as the hub genes (Zotenko et al., 2008).

[1]http://www.ncbi.nlm.nih.gov/geo

[2]http://www.targetscan.org/vert_72/

[3]http://ophid.utoronto.ca/mirDIP/

[4]http://starbase.sysu.edu.cn/index.php

[5]http://mirtarbase.mbc.nctu.edu.tw

[6]http://www.mirdb.org/miRDB/

[7]https://zmf.umm.uni-heidelberg.de/

[8]http://www.microrna.org/microrna/home.do

[9]www.circbank.cn

[10]http://www.string-db.org/

[11]http://sangerbox.com/tool

TABLE 1 | Basic information of the microarray datasets.

Data source(GEO)	Platform	Samples size(D/N)	RNA types	First author	References
GSE67566	GPL19978	5/5	circRNA	Lan PH	Lan et al., 2016
GSE63492	GPL19449	5/5	miRNA	Lan PH	Lan et al., 2016
GSE116726	GPL20712	3/3	miRNA	Ji ML	Ji et al., 2018
GSE56081	GPL15314	5/5	mRNA	Wan ZY	Wan et al., 2014

GEO, Gene Expression Omnibus; D, degeneration, N, normal; circRNA, circular RNA; miRNA, microRNA; mRNA, messenger RNA.

Acquirement, Culture, and Treatment of Human NPCs

The specific method was described in our previous study (Li et al., 2021). Human NPCs were purchased from ScienCell Research Laboratories (ScienCell, Cat. #4800, United States), which were isolated from the NP of human intervertebral disc. NPCs were cultured in Nucleus Pulposus Cell Medium (Cat. #4801, ScienCell, United States) containing 10 mL fetal bovine serum, 5 mL NPC growth supplement, and 5 mL penicillin/streptomycin solution and then were incubated at 37°C in a humidified environment with 5% CO_2. The medium was changed every 2 days. The NPCs were passaged once a week, and well-grown NPCs were taken for subsequent experiments. To simulate the microenvironment of IDD, TNF-α, and IL-1β (10 ng/mL, Proteintech) were employed to stimulate NPCs for 24 h.

Plasmids Construction and NPC Transfection

The miR-874-3p mimic, miR-874-3p inhibitor, and their corresponding negative controls (NCs) were obtained from JIAMAY BIOLAB (Beijing, China). The empty vector: pcDNA3.1 + Circ Mini (5,607 bp) and overexpression vector: pcDNA3.1 + Circ Mini-circ_0040039 (6,333 bp) and pcDNA3.1 + Circ Mini- circ_0004354 (5,765 bp) were designed and synthesized by HyCell Biotechnology (Wuhan, China). As for NPC transfection, culture plates were incubated at 37°C in a humidified environment with 5% CO_2. CircRNAs plasmids or miR-874-3p mimic or inhibitor or corresponding NCs were transfected into NPCs with Lipofectamine 8000 (Beyotime, China) based on the manufacturer's protocols. After 48-h transfection, NPCs were collected to conduct the next experiments.

Quantitative Real-Time Reverse Transcriptase–Polymerase Chain Reaction

Total RNAs was extracted from NPCs using TRIzol Reagent (Life Technologies, Thermo Fisher Scientific, United States) according to the manufacturer's protocols. First, 1 μg total RNA and 1 μL Geneseed® Enzyme Mix (Geneseed, Guangzhou, China) were used to reverse into 20 μL complementary DNA (cDNA) through Geneseed® II First Strand cDNA Synthesis Kit (Geneseed, Guangzhou, China). Next, 10 μL Geneseed® quantitative polymerase chain reaction (qPCR) SYBR® Green Master Mix (Geneseed, Guangzhou, China), 0.5 μL forward (F) primer (10 μM), and 0.5 μL reverse (R) primer (10 μM) were made up and used to conduct quantitative reverse transcriptase (RT)–PCR on ABI7500 system (Applied Biosystems, CA, United States). All specific primers were shown as follows: (1) GAPDH: F1: AGAAGGCTGGGGCTCATTTG, R1: GCAGGAGGCATTGCTGATGAT; (2) ESR1: F2: 5′-ACCCTCC ATGATCAGGTCCA-3′, R2: 5′-AGATCTCCACCATGCCCT CT-3′; (3) miR-874-3p: F3: ATGGTTCGTGGGCTGCCCTGGC, Com R3: GTGCAGGGT CCGAGGT, RT3: GTCGTATCCAG TGCAGGGTCCGAGGTATTCGCACTGGATA.

CGACCtcggtccc; (4) U6: F4: CTCGCTTCGGCAGCACA, R4: AACGCTTCACGA ATTTGCGT, RT4: GTCGTATC CAGTGCAGGGTCCGAGGTATTCGCACTGGATA CGACCAAATATGGAAC. Among them, GAPDH was used as circ_0040039, circ_0004354, and ESR1 control, whereas U6 was used as miR-874-3p control. Their relative expression levels were measured based on the $2^{-\Delta\Delta}$ Ct method described by Livak and Schmittgen (2001).

Cell Counting Kit-8

The well-grown NPCs were inoculated into six-hole cell culture plates at a density of 5×10^5 cells per well. Then, 200 μL diluted RNAs–Lipofectamine 8000 (Beyotime, China) complex was added to the cell wells that had been replaced with 800 μL serum-free medium. The NPCs were then cultured for 0, 1, 2, and 3 days at 37°C incubator. For Cell Counting Kit-8 (CCK8) assay, 10 μL CCK8 solution was added to each well and for incubation for another 1.5 h. The NPC growth was evaluated by CCK8 detection kit according to manufacturer's protocols (Yeasen, Shanghai, China). The absorbance was determined at OD 450 nm. NPC growth rates were calculated based on the formula: Day*n* OD value/Day0 average OD value (same processing sample).

Flow Cytometry

The well-grown NPCs were inoculated into 6 hole cell culture plates at a density of 5×10^5 cells per well. After circ_0040039 or circ_0004354 overexpression vector were transfected into NPCs using Lipofectamine 8000 (Beyotime, China), the NPC apoptosis rates were evaluated by annexin V–APC apoptosis detection kit according to manufacturer's protocols (keyGEN, KGA1024, China). Annexin V–APC is matched with 7-AAD to distinguish NPCs in different stages of apoptosis. The NPCs were stained with 5 μL annexin V–APC and 5 μL 7-AAD, and then the data were analyzed with FlowJo VX10 software. On the scatterplot of the bivariate flow cytometry (FCM), annexin V + /7-AAD + (Q2) represented the late apoptotic

and necrotic NPCs; annexin V + /7-AAD- (Q3) represented the early apoptotic NPCs, whereas annexin V–/7-AAD− (Q4) represented living NPCs.

Dual-Luciferase Reporter Assays

MiRanda database (John et al., 2004) was used to predict the potential binding sites of miR-874-3p with ESR1 mRNA 3′-UTR. Luciferase reporter vectors: psiCHECK2–Firefly luciferase–Renilla luciferase containing ESR1–700-bp wild-type (WT) sequences or corresponding mutant (MUT) sequences, were constructed by Geneseed Biotech Co. (Guangzhou, China). Human embryonic kidney (HEK) 293T cells were plated on 24-well plates at a density of 1×10^5 cells per well. Subsequently, 1 μg vector and 100 μL miR-874-3p mimic or mimic NC were cotransfected into HEK-293T cells using 2 μL Lipofectamine 8000 (Beyotime, China). After 48-h transfection, the relative luciferase activity was measured using the Dual Luciferase Assay Kit (Promega E1910, Madison, WI, United States) according to the manufacturer's directions. The activation degrees of the target reporter genes were calculated between different samples according to the obtained ratio of the relative light unit (RLU) value measured by Renilla luciferase divided by the RLU value measured by Firefly luciferase.

Western Blotting Assay

The specific method was described in our previous study (Li et al., 2021). RIPA lysis buffer containing phenylmethanesulfonyl fluoride (Beyotime, Shanghai, China) was used to extract the total protein from NPCs. The protein concentrations were quantified using the Micro Bicinchoninic Acid Protein Assay kit (Beyotime, Shanghai, China). After making sodium dodecyl sulfate–polyacrylamide gel electrophoresis (SDS-PAGE) gels, the proteins were isolated through SDS-PAGE and then transferred to polyvinylidene difluoride (PVDF) membranes (Bio-Rad, CA, United States) at 350 mA for 70 min. Subsequently, the PVDF membranes were blocked by 5% non-fat milk and incubated overnight at 4°C with primary antibody, including anti-ESR1 antibody (diluted 1:1,000; Abcam, ab32063) and anti–β-actin antibody (diluted 1:5,000; Proteintech, 66009-1-Ig), followed by incubation with a secondary antibody. Phosphate-buffered saline with Tween-20 was utilized to wash the PVDF membranes. Finally, the signals were tested by BeyoECL Star Luminescence kit (Beyotime, Shanghai, China) and a chemiluminescence system (Bio-Rad, CA, United States).

Statistical Analysis

All the experiments were performed at least three times. GraphPad Prism software 6 version was used to analyze the data. The statistical significances between the two groups were compared using unpaired Student's *t*-test, where the differences among more than two groups were assessed using one-way analysis of variance followed by Tukey multiple-comparisons test. The $P < 0.05$ was considered as statistically significant.

RESULTS

Prediction of ESR1 Was One of the Most Critical Differentially Expressed Genes in IDD

A large number of studies have indicated the involvement of a multitude of DEMs in regulating IDD via repressing their target genes. However, which target genes were the most important remains unanswered. To address this question, the key differentially expressed genes (KDEGs) of these DEMs were summarized and are listed in **Supplementary Table 1**. A total of 97 different target genes were reported as IDD-related KDEGs. Given that the STRING website can provide experimental and predicted PPI information, and PPI is the most appropriate tool for studying the potential interrelationship among multiple genes, this study mapped the 97 KDEGs into the STRING website, followed by the analysis of their interaction using cytoHubba plug-in in Cytoscape software. The results unveiled that estrogen receptor α (ESR1) ranked the highest and was a hub gene, suggesting that ESR1 could regulate a series of IDD-related genes, encompassing protective factors, such as SIRT1, Sox9, HIF-1α, and IGF1R, as well as catabolic factors, such as IL-6, MMP2/9, and CASP3 (**Figures 1A,B**). The Kyoto Encyclopedia of Genes and Genomes analysis of the estrogen signaling pathway revealed that ESR1 might regulate the expression of related genes (**Figure 1C**) to mediate various signaling pathways, including canonical mitogen-activated protein kinase, PI3K-Akt, and estrogen pathways, thereby affecting cell cycle progression, growth, apoptosis, and other pathological processes (**Figure 1D**). Furthermore, Cai et al. (2020) demonstrated that the mRNA and protein expression levels of ESR1 were significantly decreased in patients with IDD diseases. Collectively, these results predicted that ESR1 might be one of the most KDEGs in IDD.

Prediction of the Upstream MiRNAs of ESR1

MiRNAs can degrade mRNAs and inhibit their translation via directly binding to the 3′-UTR of their target mRNAs (Pasquinelli, 2012; Ji et al., 2018). The upstream miRNAs of ESR1 were predicted and analyzed by bioinformatics analysis. The datasets used in this study were obtained from human NP specimens. Two overlapped IDD-related miRNAs were predicted by merging miRDB, TargetScan, miRTarBase, mirDIP, and miRwalk databases and GSE116726/63492 datasets (**Figure 2A**). Volcano plots revealed two DEMs in GSE116726; the expression of miR-874-3p was lower than that of miR-130b-3p in IDD (**Figure 2B**). Conversely, ESR1 was predicted to the target gene of miR-874-3p by intersecting different algorithms, including the GSE56081 dataset (**Figure 2C**). The potential binding sites of miR-874-3p with ESR1 mRNA 3′-UTR were predicted using the miRanda database (John et al., 2004). An ESR1 fragment with WT or MUT complementary binding sites for miR-874-3p was established and inserted into psiCHECK2 luciferase reporter vectors to confirm further the interaction between miR-874-3p and ESR1 (**Figure 2D**). MiR-874-3p mimic significantly repressed the luciferase activity of the ESR1-WT vector, whereas

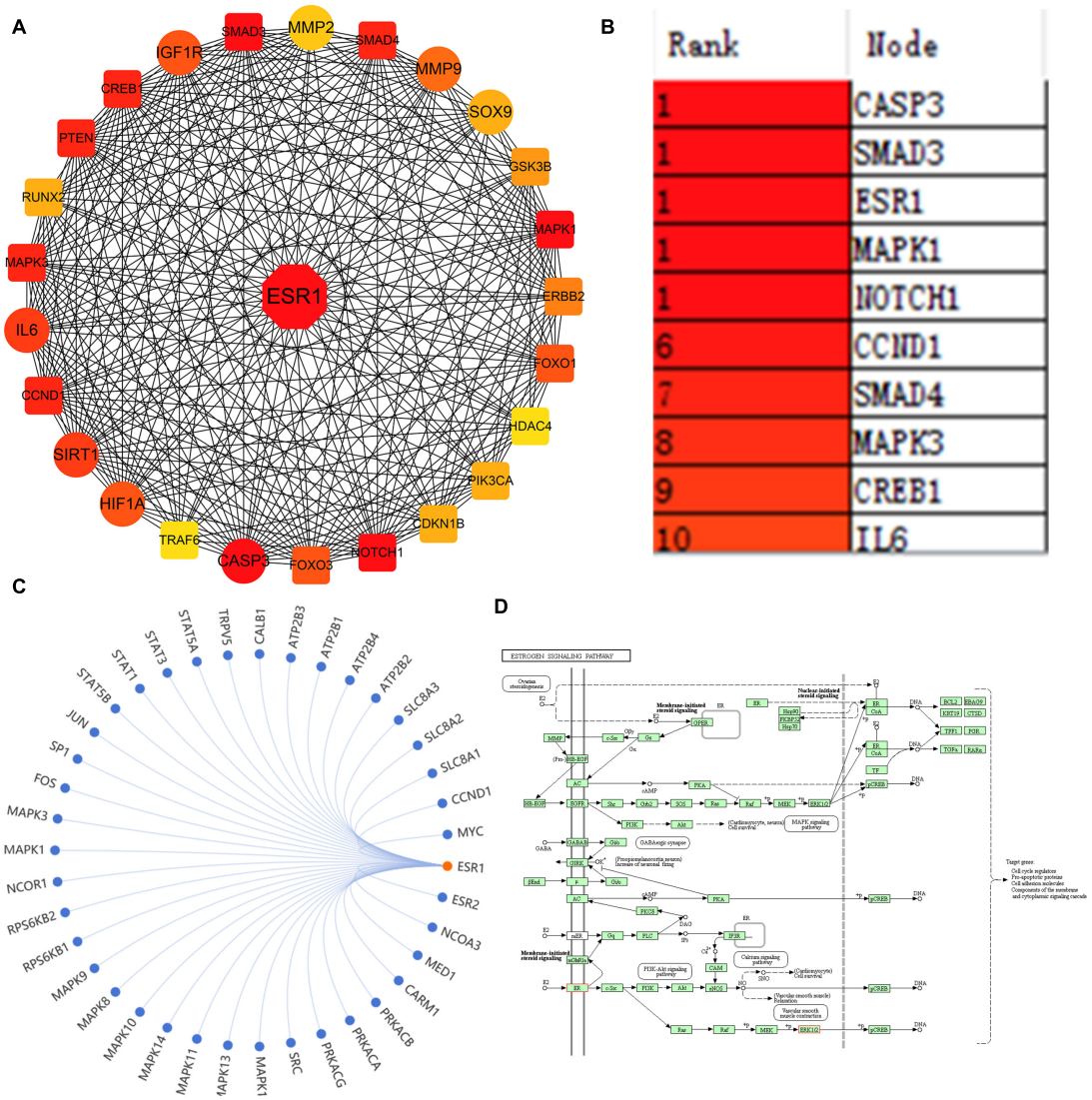

FIGURE 1 | ESR1 was identified as one of the most critical genes in IDD. **(A)** PPI network showing IDD-related miRNA target genes. The line between the circle nodes indicates the interaction between the two genes. Red indicates the most key hub genes; the depth of the color is related to the association of other genes in the PPI network. **(B)** Top 10 genes in the PPI network ranked by the maximal clique centrality method, of which ESR1 ranked the highest. **(C)** Other genes regulated by ESR1 were predicted and visualized using the SangerBox tool. **(D)** Kyoto Encyclopedia of Genes and Genomes analysis of estrogen signaling pathway displayed that ESR1 might be involved in regulating various pathways.

such overexpression could not change the activity of the ESR1-MUT vector, revealing that miR-874-3p could directly bind to the 3′-UTR of ESR1 (**Figure 2E**). Moreover, miR-874-3p mimic repressed and miR-874-3p inhibitor increased the mRNA level of ESR1 (**Figure 2F**). Thus, miR-874-3p was determined as a key miRNA in this study.

Bioinformatics Analysis of miR-874-3p Target Genes Predicted Using the miRTarBase Database

miRTarBase: The experimentally (luciferase reporter assay, Western blot, microarray, and next-generation sequencing experiments) validated miRNA–target interaction database (Chou et al., 2018) was used to predict the target genes of miR-874-3p. The 77 miR-874-3p target genes predicted using the miRTarBase database were then visualized using Cytoscape software (**Figure 3A**). As shown in **Figure 3B**, the analysis result of PPI revealed that ESR1 was the most key hub gene of the miR-874-3p target genes. Subsequently, GO functional enrichment analysis for these target genes was conducted using the STRING website, which predominantly included three aspects: biological process (BP), molecular function (MF), and cellular component (CC). The bubble diagram (**Figure 3C**) and GO chord diagram (**Figure 3D**) of the GO analysis of BP indicated that miR-874-3p might be

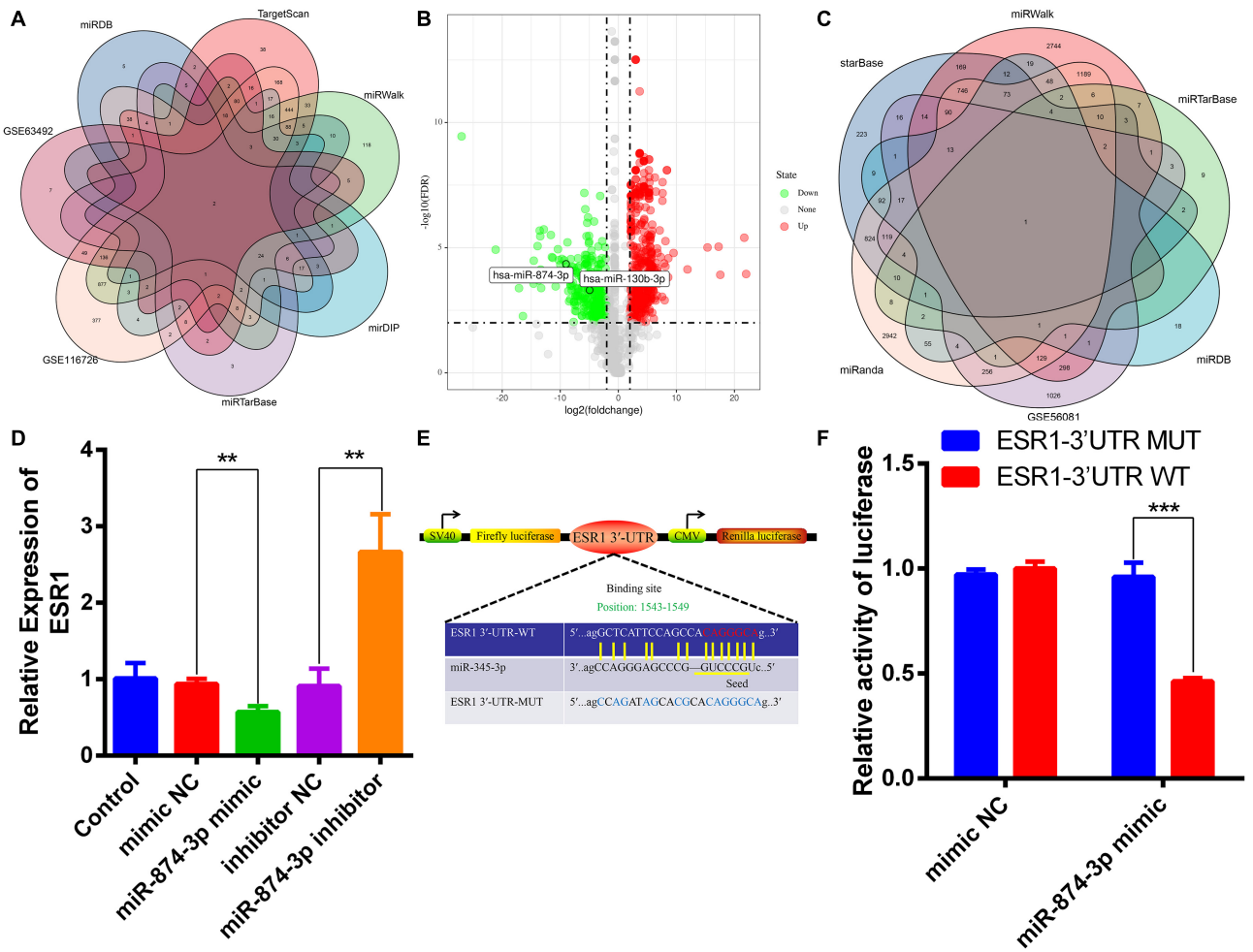

FIGURE 2 | MiR-874-3p was predicted to be the upstream miRNA of ESR1. **(A)** Upstream miRNAs of ESR1 were predicted using different algorithms. **(B)** Volcano plot shows the predicted upstream miRNAs of ESR1 based on the analysis of GSE116726. Green points represent downregulated miRNAs (left side), and red points represent upregulated miRNAs (right side); miR-874-3p and miR-130b-3p are presented. **(C)** Venn analysis of miR-874-3p downstream target genes using different algorithms. **(D)** ESR1 expression level was measured in NPCs after transfected with miR-874-3p mimic or miR-874-3p inhibitor or corresponding NCs using the qRT-PCR assay. **(E)** Binding site of miR-874-3p and ESR1. **(F)** Luciferase reporter vectors carrying ESR1 WT or MUT sequences were cotransfected into HEK-293T cells with miR-874-3p mimic or mimic negative control (NC). Relative luciferase activity was detected in HEK-293T cells. Data are represented as the mean ± SD. $^{**}P < 0.01$, $^{***}P < 0.001$.

mainly involved in regulating different signaling pathways through targeting ESR1/signal transducer and activator of transcription 3 (STAT3)/poly(ADP-ribose) polymerase 1 (PARP1)/cyclin-dependent kinase 9 (CDK9)/histone deacetylases 1 (HDAC1), encompassing negative regulation of macromolecule metabolic process, negative regulation of gene expression, negative regulation of cellular metabolic process, and cell population growth. MF included organic cyclic compound binding, heterocyclic compound binding, RNA binding, nucleic acid binding, and single-stranded RNA binding (**Figure 3E**). The most enriched in CC were nucleoplasm, intracellular organelle, membrane-bound organelle, cytoplasmic ribonucleoprotein granule, and protein-containing complex (**Figure 3F**). These results indicated that miR-874-3p might modulate NPC growth and apoptosis to mediate IDD through binding to ESR1 or other mRNAs in the cytoplasm.

Prediction and Verification of the Upstream CircRNAs of MiR-874-3p

Accumulating evidence has uncovered that miRNAs can be adsorbed or even repressed by circRNAs via a ceRNA-dependent mechanism (Piwecka et al., 2017; Cheng et al., 2018; Wang et al., 2018; Xie et al., 2019; Xiang et al., 2020). The upstream circRNAs of miR-874-3p were predicted and analyzed to explore further the novel unidentified circRNAs affecting miR-874-3p function. Circbank is a comprehensive database of human circRNAs containing beyond 140,000 annotated circRNAs from different sources, which can be used to predict the upstream

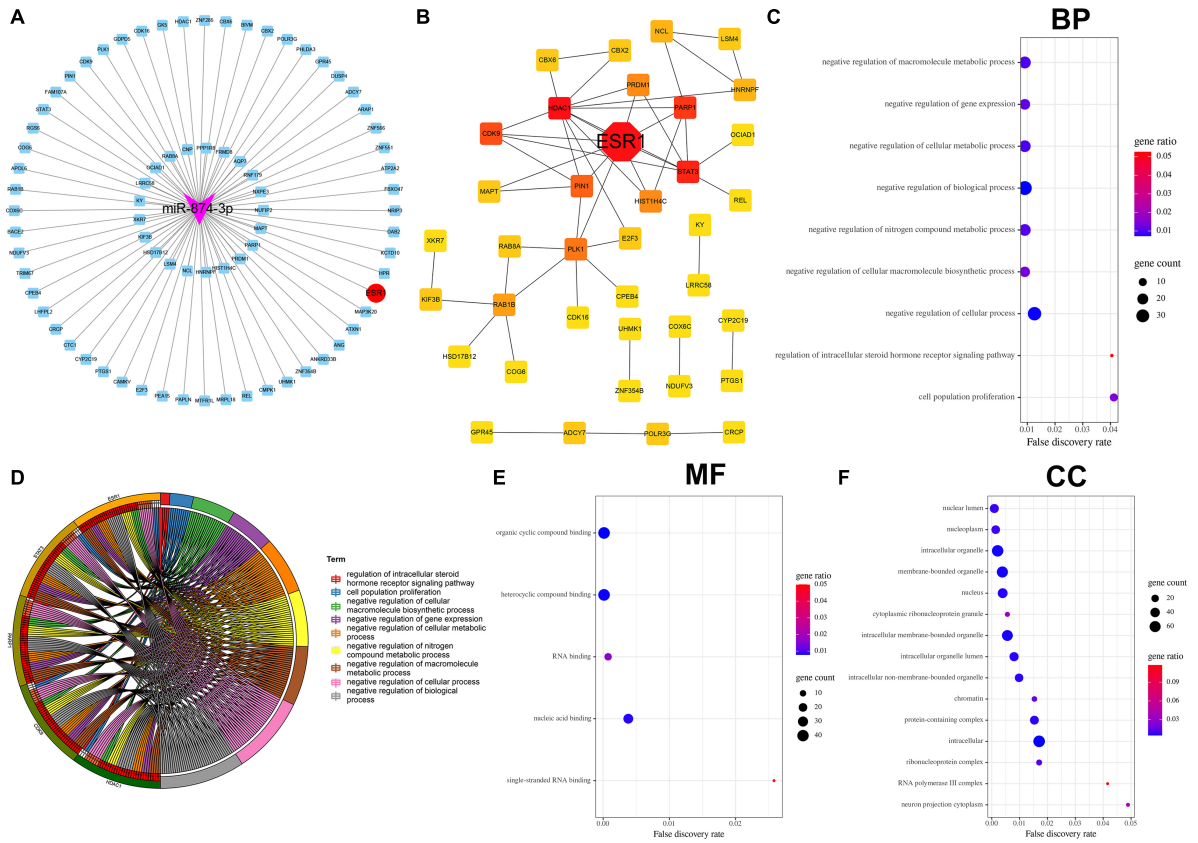

FIGURE 3 | Bioinformatics analysis of miR-874-3p target genes predicted using the miRTarbase database. **(A)** Cytoscape software was used to visualize the miR-874-3p target genes, of which miR-874-3p and ESR1 were indicated with red ellipse and purple triangles, respectively. **(B)** ESR1 was identified as a key hub gene in the PPI network using the Cytoscape plug-in cytoHubba, of which ESR1 is indicted with a red diamond. **(C–F)** GO analysis of miR-874-3p target genes through the STRING website. FDR < 0.05 was regarded as statistically significant. **(C)** Bubble diagram shows the main biological process. The *x*-axis represents the FDR, the left *y*-axis represents the GO terms, and the right *y*-axis represents the gene ratio (up) and gene count (down). **(D)** GO chord diagram shows the five hub genes involved in the main biological process. The left outside of the circle represents the genes, whereas the left inside of the circle represents the FDR. **(E)** Bubble diagram shows the enrichment of molecular function. **(F)** Enrichment of the cellular component is shown by bubble diagram.

circRNAs of miRNAs (Liu et al., 2019). Eight overlapped circRNAs were predicted by intersecting starBase and circbank databases and the GSE67566 dataset (**Figure 4A**). Furthermore, a circRNA-miR-874-3p-ESR1 interaction network was constructed and visualized using Cytoscape software (**Figure 4B**). The two most upregulated IDD-related circRNAs circ_0040039 and circ_0004354, both derived from the syntrophin β2 gene, were predicted to bind to miR-874-3p together (data not shown). Thus, circ_0040039 and circ_0004354 were selected for further investigation. Subsequently, the empty vector (**Figure 4C**) and overexpression vector of circ_0040039 (**Figure 4D**) and circ_0004354 (**Figure 4F**) were constructed. The expression levels of circ_0040039 (**Figure 4E**) and circ_0004354 (**Figure 4G**) significantly increased after transfecting their overexpression vector into NPCs. Unexpectedly, both circ_0040039 and circ_0004354 elevated (but not repressed) the miR-874-3p expression level; the role of circ_0040039 was more significant (**Figure 4H**). In addition, circ_0004354 slightly elevated ESR1 expression without any statistically significant difference, whereas circ_0040039 remarkably repressed the ESR1 expression level (**Figure 4I**). **Figure 4J** displayed that circ_0040039 was the most upregulated circRNA in IDD group through the analysis of GSE67566. Furthermore, Western blotting assay demonstrated that circ_0040039 inhibited the protein expression level of ESR1 (**Figure 4K**). Taken together, these data suggested that circ_0040039 might regulate the miR-874-3p-ESR1 pathway via a stabilization mechanism rather than a canonical ceRNA mechanism, as previously reported (Piwecka et al., 2017; Chen et al., 2019).

Demonstration of the Expression Levels of Circ_0040039, Circ_0004354, MiR-874-3p, and ESR1 in Proinflammatory Cytokine-Treated NPCs

Considering that the elevated expression of TNF-α and IL-1β is a hallmark trait during NPC degeneration (Risbud and Shapiro, 2014; Fontana et al., 2015; Oichi et al., 2020; Wang et al., 2020), many researchers used them to simulate the microenvironment of IDD *in vitro* (Cheng et al., 2018;

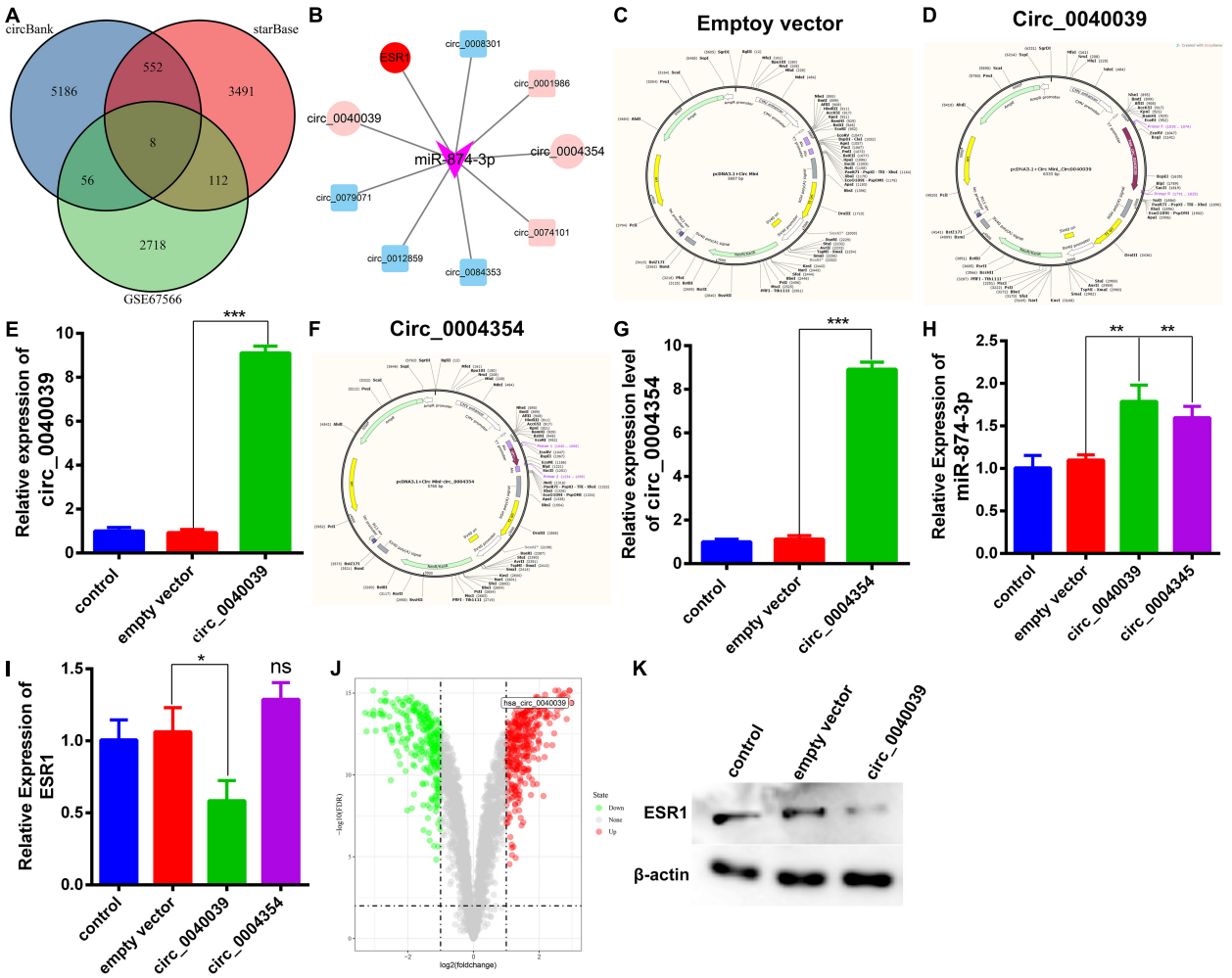

FIGURE 4 | Prediction and verification of the upstream circRNAs of miR-874-3p. **(A)** Venn diagram was used to select the overlapping upstream circRNAs of miR-874-3p through the intersection of circbank and starBase databases, and the GSE67566 dataset. **(B)** CircRNAs-miR-874-3p-ESR1 interaction network was established using Cytoscape software. Light red represents upregulated circRNAs, and light green represents downregulated circRNAs. Circ_0040039, circ_0004354, and ESR1 were exhibited with a red ellipse, whereas miR-874-3p was represented by purple triangles. **(C)** CircRNA empty vector atlas. **(D)** Circ_0040039 overexpression vector atlas. **(E)** Overexpression effect of circ_0040039 was validated in NPCs using the qRT-PCR assay. **(F)** Circ_0004354 overexpression vector atlas. **(G)** qRT-PCR assay corroborated that the expression of circ_0004354 significantly increased in circ_0004354-transfected NPCs. **(H)** qRT-PCR assay confirmed that the expression level of miR-874-3p was elevated in NPCs after transfection with circ_0040039 or circ_0004354. **(I)** ESR1 expression level was measured in NPCs after transfection with circ_0040039 or circ_0004354 or corresponding NC using the qRT-PCR assay. **(J)** Volcano plot shows the predicted circ_0040039 based on the analysis of GSE67566. Green points represent downregulated circRNAs (left side), and red points represent upregulated circRNAs (right side); circ_0040039 is presented. **(K)** Western blotting assay demonstrated that circ_0040039 inhibits the protein expression level of ESR1. Data are represented as the mean ± SD. $^{*}P < 0.05$, $^{**}P < 0.01$, $^{***}P < 0.001$.

Wang et al., 2018, 2020). Consistent with the predicted result, the expression level of circ_0040039 significantly increased in proinflammatory cytokine–treated NPCs (**Figure 5A**). On the contrary, circ_0004354 expression significantly decreased in IL-1β–treated NPCs (**Figure 5B**). The expression level of miR-874-3p significantly increased but not decreased under the treatment of IL-1β, whereas its expression was not altered in response to TNF-α alone or both TNF-α and IL-1β treatments (**Figure 5C**). Surprisingly, only IL-1β remarkably enhanced ESR1 mRNA expression, whereas using TNF-α and IL-1β at the same time slightly inhibited its expression without reaching statistically significant differences (**Figure 5D**). However, this result was inconsistent with previous study. Recently, Song et al. (2021) validated that TNF-α can inhibit ESR1 expression in NPCs. Another literature has indicated that ESR1 silencing can elevate IL-1β and TNF-α expression (Sheng et al., 2018). The difference in experimental results may be related to the state of the NPCs and the different experimental conditions. We cannot rule out that IL-1β might act as a buffer to transiently enhance miR-874-3p and ESR1 expression, thereby delaying the development of IDD. The specific mechanisms of TNF-α and IL-1β do not affect or even increase ESR1 mRNA levels in NPCs, and its

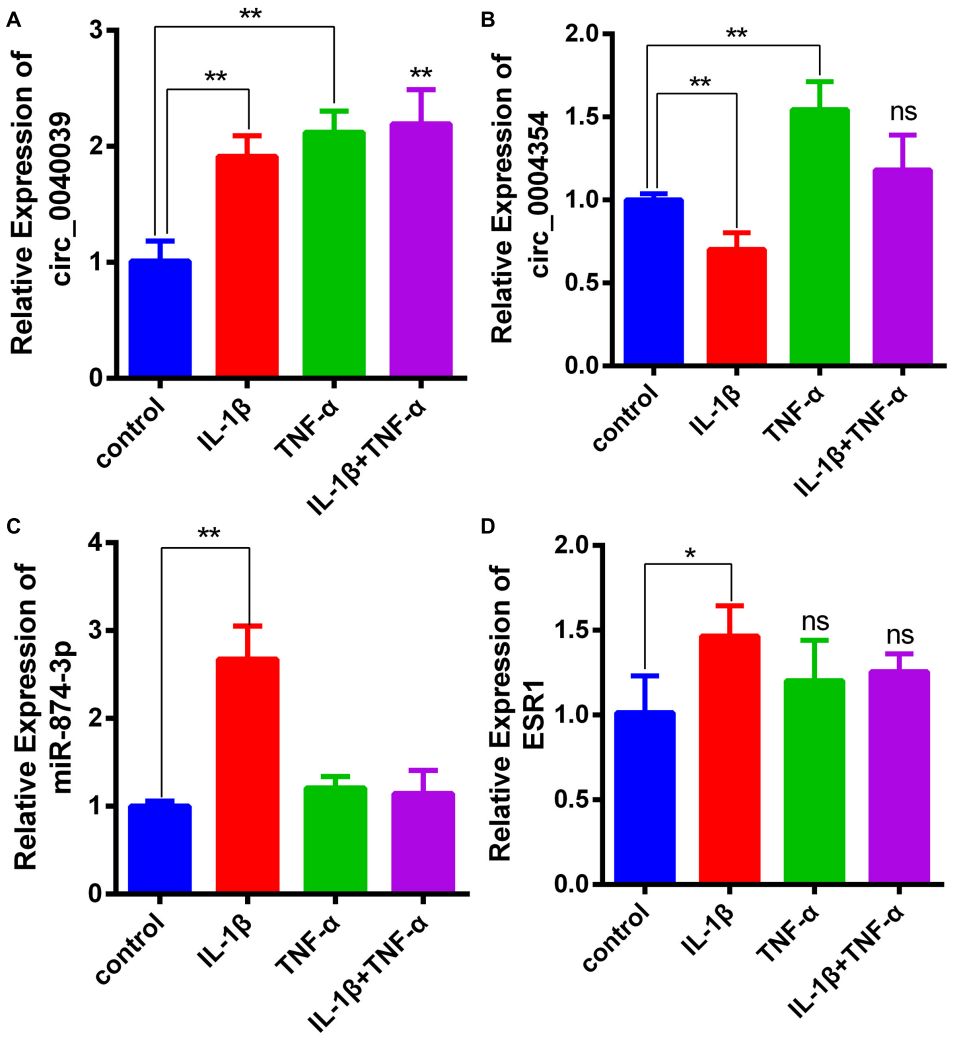

FIGURE 5 | Demonstration of the expression levels of circ_0040039, circ_0004354, miR-874-3p, and ESR1 in proinflammatory cytokine–treated NPCs. **(A–D)** Expression levels of circ_0040039, circ_0004354, miR-874-3p, and ESR1 in NPCs were detected using the qRT-PCR assay in response to different proinflammatory cytokine treatments. Among these, circ_0040039, miR-874-3p, and ESR1 expression levels increased in IL-1β–treated NPCs. Data are represented as the mean ± SD. $^{*}P < 0.05$, $^{**}P < 0.01$.

biological significance needs future investigation to elucidate. Based on these results, IL-1β was used to simulate the IDD microenvironment for further investigation.

Biofunction of Circ_0040039 in NPCs

CCK8 and FCM detection assays were performed in circ_0040039-overexpressing NPCs to validate the biofunction of circ_0040039 in NPCs. Compared with empty vector and control, circ_0040039 significantly promoted NPC apoptosis (**Figures 6A,B**) and repressed NPC growth (**Figure 6C**) in response to 20 ng/mL IL-1β treatments. Given that circ_0040039 promoted miR-874-3p (**Figure 4H**) but repressed ESR1 expression (**Figures 4I,J**), and miR-874-3p repressed ESR1 expression in NPCs (**Figure 2D**), it was speculated that circ_0040039 promoted NPC degeneration possibly via activating the miR-874-3p-ESR1 signaling pathway.

DISCUSSION

Yang et al. (2020) summarized that estrogen can inhibit NPC apoptosis and ECM degradation by repressing proinflammatory cytokines expression and oxidative damage, as well as promoting the PI3K/Akt pathway, autophagy, and integrin expression. *Esr1* gene, which encodes the estrogen receptor α, can be activated by estrogen. Sheng and colleagues validated that ESR1 silencing or the decreased expression of ESR1 induced by miR-221 overexpression can weaken the protective effects of estrogen on IDD via inhibiting ECM synthesis, as well as elevating NPC apoptosis and IL-1β and TNF-α expression (Sheng et al., 2018).

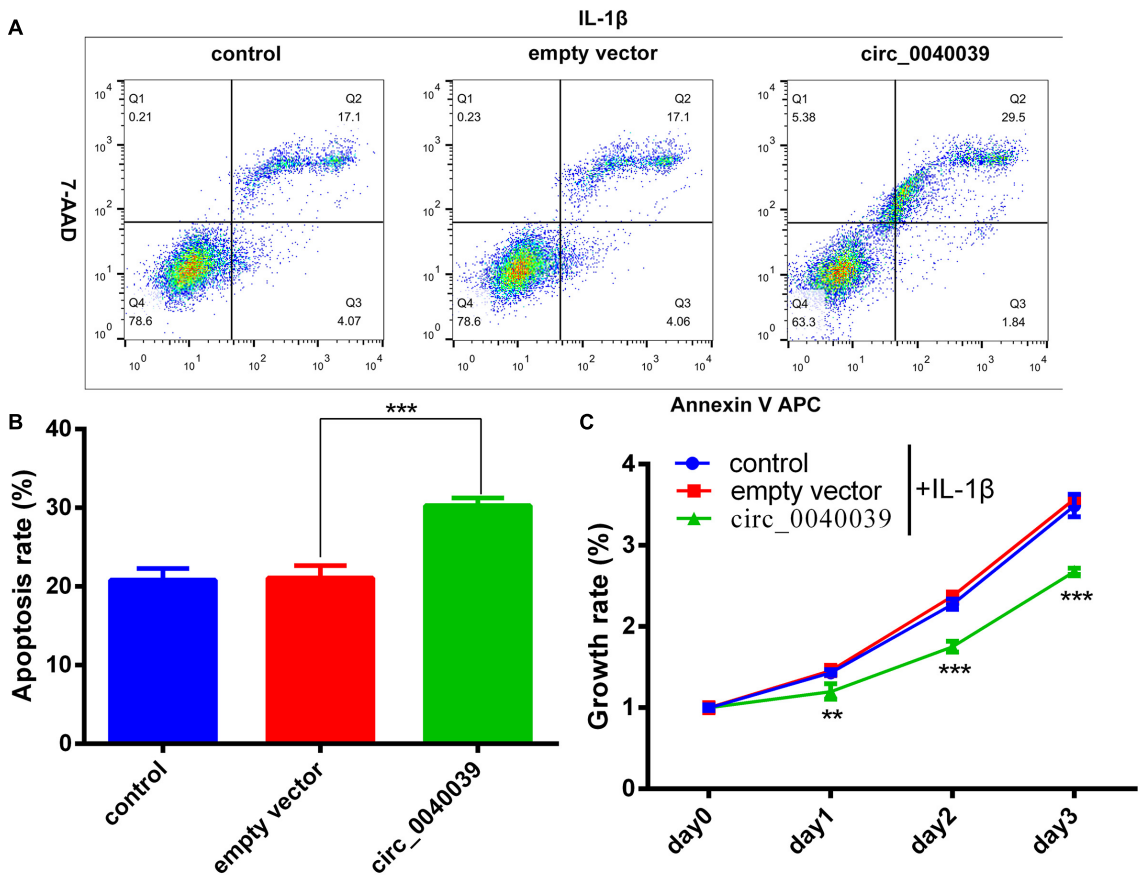

FIGURE 6 | Circ_0040039 promoted NPC degeneration. **(A,B)** Circ_0040039 overexpression vector or empty vector was transfected into NPCs, and then 20 ng/mL IL-1β was added to each group to treat NPCs. **(A)** NPC apoptosis was evaluated using the flow cytometry detection assay. **(B)** Quantitative analysis of the NPC apoptosis rate. **(C)** CCK8 assay was used to detect the growth rate of NPCs. $^{**}P < 0.01$, $^{***}P < 0.001$.

Upregulation of ESR1 was demonstrated to protect TNF-α–induced NPC degeneration through the activation of CCN5 by binding to its promoter (Song et al., 2021). Moreover, ESR1 has a negative correlation with the severity of IDD, and its mRNA and protein levels are downregulated in the NP tissues of patients with high-grade IDD compared with patients with low-grade IDD (Song et al., 2014; Cai et al., 2020). A series of studies demonstrated that the activity and biofunction of ESR1 could be regulated by circRNAs and miRNAs (Sheng et al., 2018; Cai et al., 2020; Taheri et al., 2020). The available evidence showed the interactions between ESR1 and miRNAs were implicated in the pathomechanism of IDD. For example, miR-221 (Sheng et al., 2018) and miR-203-3p (Cai et al., 2020) were reported to promote IDD via directly repressing ESR1 expression. Additionally, ESR1-associated circRNAs also have been identified in patients with cancer (Yuan et al., 2019; Xiao et al., 2020). Yuan et al. (2019) demonstrated that circ_0087378 was downregulated in patients with ER^+ breast cancer. ESR1 was proven to inhibit circRNA-SMG1.72 expression by directly binding to the 5′ promoter region of its host gene SMG1, thereby suppressing hepatocellular carcinoma progression (Xiao et al., 2020). However, the ESR1-associated circRNAs in IDD have not been investigated. The present study found that circ_0040039 repressed whereas circ_0004354 promoted ESR1 expression. Under the stimulation of IL-1β, the expression of circ_0040039 and ESR1 was elevated in NPCs. The gain-of-function experiments revealed that circ_0040039 hindered NPC survival. Given that Lan et al. (2016) predicted and demonstrated that the expression level of circ_0040039 was remarkably upregulated in IDD, it was hypothesized that the upregulation of circ_0040039 might disrupt the normal function of IVD by inhibiting ESR1 expression and functions during IDD. The participation of circ_0040039-ESR1 pathway in regulating the ECM metabolism and the production of proinflammatory factors by NPCs, as well as the biological significance of the circ_0004354-ESR1 pathway in IDD, need further investigation.

MiR-874-3p has been implicated in regulating the apoptosis and growth of various cells. Dai et al. (2020) recently found that miR-874-3p aggravated renal podocyte apoptosis by directly inhibiting MsrB3. Leong et al. (2017) demonstrated that the activation of the miR-874-3p-PIN1 pathway promoted the apoptosis of hepatocellular carcinoma cells and repressed growth. Xia et al. (2018) also uncovered that the upregulation of miR-874-3p enhanced the apoptosis of epithelial ovarian cancer cells and

inhibited growth. Huang et al. (2018) found that silencing circ_0000977 promoted the apoptosis of pancreatic ductal adenocarcinoma cells by stimulating miR-874-3p and inhibiting PLK1 expression. However, miR-874-3p has been confirmed to inhibit the apoptosis of brain tissue (Jiang et al., 2019; Xie et al., 2020) and cavernosal smooth muscle cells (Huo et al., 2020). The different roles of miR-874-3p may be related to cell state and type. This study verified that circ_0040039 and circ_0004354 promoted miR-874-3p expression, and ESR1 might be a direct target of miR-874-3p. It seemed whether miR-874-3p promoted or inhibited NPC apoptosis was not important; it might play a role as a bridge.

The cross-talk between circRNAs and miRNAs is not single. A growing body of evidence has revealed that circRNAs are widely involved in the regulation of the occurrence and progression of various chronic diseases by acting as miRNA sponges, encompassing IDD (Cheng et al., 2018; Wang et al., 2018; Xie et al., 2019; Xiang et al., 2020), osteoarthritis (Zhou et al., 2019; Chen et al., 2020), and cancers (Huang et al., 2018; Chen et al., 2019; Zhao et al., 2020), as well as cardiovascular (Garikipati et al., 2019) and neurodegenerative (Zhang et al., 2020) diseases. For instance, circ-VMA21 was demonstrated to mitigate proinflammatory cytokine–induced NPC apoptosis and ECM degradation by suppressing the miR-200c-XIAP signaling pathway (Cheng et al., 2018). Our group previously also reported that circ-FAM169A might modulate the pathological process of IDD through downregulating miR-583 (Li et al., 2021). In addition, circRNA involved in compression-induced damage of NPCs (circRNA-CIDN) (Xiang et al., 2020), circ-4099 (Wang et al., 2018), and circ-ERCC2 (Xie et al., 2019) were all corroborated to mediate the progression of IDD via negatively regulated miRNA expression. Besides adsorbing miRNA, circRNAs can also stabilize and upregulate miRNA expression. CircCSNK1G3 can positively regulate miR-181b/d expression levels to promote prostate cancer cell growth, as reported by Chen et al. (2019). Piwecka et al. (2017) found that the miR-7 expression level was downregulated and miR-7 targets were upregulated in *CDR1as*, a gene encoding circRNA Cdr1as, in knockout mouse brains. The present study also showed that circ_0040039 could enhance miR-874-3p and repress ESR1 expression levels, further supporting the existence of miRNA stabilization mechanism. However, the underlying stabilization mechanisms remain to be clarified in the future.

However, the present study also had several limitations. First, the data were obtained only from the GEO database, and hence the verification of clinical samples was lacking. Second, the study was devoid of rescue experiments and *in vivo* investigation. Third, whether circ_0040039 regulated miR-874-3p expression through a stabilization mechanism still remained unclear.

CONCLUSION

Taken together, the results uncovered that circ_0040039 might inhibit ESR1 expression via upregulating miR-874-3p, thereby facilitating NPC apoptosis and inhibiting NPC growth. The findings might enhance the understanding of the pathogenesis of IDD and provide a new treatment strategy against IDD diseases in the future. The precise role and mutual regulatory mechanism of the circ_0040039-miR-874-3p-ESR1 pathway in IDD need further investigation.

DATA AVAILABILITY STATEMENT

Publicly available datasets were analyzed in this study. This data can be found here: circRNA (GSE67566), miRNA (GSE63492/GSE116726), and mRNA (GSE56081) microarray datasets.

AUTHOR CONTRIBUTIONS

BX and YL conceived and designed the experiments. YL, XW, HX, and GL conducted the experiments and analyzed the data. YL wrote the manuscript. ZH and KZ provided significant suggestions for the study. LS and HL searched the literature and collected important reference information. BX reviewed and revised the manuscript. All authors have read and approved the final version of the manuscript.

FUNDING

This study was supported by the grants from the National Natural Science Foundation of China (Nos. 82072491, 31670983, and 31900967) and the Natural Science Foundation of Tianjin city (Nos. 20JCYBJC00820 and 19JCQNJC09300).

ACKNOWLEDGMENTS

We would like to thank all the reviewers who participated in the review and MJEditor (www.mjeditor.com) for its linguistic assistance during the preparation of this manuscript.

SUPPLEMENTARY MATERIAL

The Supplementary Material for this article can be found online at: https://www.frontiersin.org/articles/10.3389/fgene.2021.656759/full#supplementary-material

REFERENCES

Agarwal, V., Bell, G. W., Nam, J. W., and Bartel, D. P. (2015). Predicting effective microRNA target sites in mammalian mRNAs. *Elife* 4:e05005.

Cai, Z., Li, K., Yang, K., Luo, D., and Xu, H. (2020). Suppression of miR-203-3p inhibits lipopolysaccharide induced human intervertebral disc inflammation and degeneration through upregulating estrogen receptor alpha. *Gene Ther.* 27, 417–426. doi: 10.1038/s41434-019-0118-z

Cazzanelli, P., and Wuertz-Kozak, K. (2020). MicroRNAs in intervertebral disc degeneration, apoptosis, inflammation, and mechanobiology. *Int. J. Mol. Sci.* 21:3601. doi: 10.3390/ijms21103601

Chen, C., Yin, P., Hu, S., Sun, X., and Li, B. (2020). Circular RNA-9119 protects IL-1beta-treated chondrocytes from apoptosis in an osteoarthritis cell model by intercepting the microRNA-26a/PTEN axis. *Life Sci.* 256:117924. doi: 10.1016/j.lfs.2020.117924

Chen, S., Huang, V., Xu, X., Livingstone, J., Soares, F., Jeon, J., et al. (2019). Widespread and functional RNA circularization in localized prostate cancer. *Cell* 176, 831–843.e22.

Chen, Y., and Wang, X. (2020). miRDB: an online database for prediction of functional microRNA targets. *Nucleic Acids Res.* 48, D127–D131.

Cheng, X., Zhang, L., Zhang, K., Zhang, G., Hu, Y., Sun, X., et al. (2018). Circular RNA VMA21 protects against intervertebral disc degeneration through targeting miR-200c and X linked inhibitor-of-apoptosis protein. *Ann. Rheum. Dis.* 77, 770–779. doi: 10.1136/annrheumdis-2017-212056

Chin, C. H., Chen, S. H., Wu, H. H., Ho, C. W., Ko, M. T., and Lin, C. Y. (2014). cytoHubba: identifying hub objects and sub-networks from complex interactome. *BMC Syst. Biol.* 8(Suppl. 4):S11.

Chou, C. H., Shrestha, S., Yang, C. D., Chang, N. W., Lin, Y. L., Liao, K. W., et al. (2018). miRTarBase update 2018: a resource for experimentally validated microRNA-target interactions. *Nucleic Acids Res.* 46, D296–D302.

Clough, E., and Barrett, T. (2016). The gene expression omnibus database. *Methods Mol. Biol.* 1418, 93–110. doi: 10.1007/978-1-4939-3578-9_5

Dai, Y., Gao, M., Li, L., Mao, Z., Xu, L., Yin, L., et al. (2020). MicroRNA-874-3p aggravates doxorubicin-induced renal podocyte injury via targeting methionine sulfoxide reductase B3. *Oxid. Med. Cell. Longev.* 2020:9481841.

Ding, F., Shao, Z. W., and Xiong, L. M. (2013). Cell death in intervertebral disc degeneration. *Apoptosis* 18, 777–785. doi: 10.1007/s10495-013-0839-1

Dweep, H., and Gretz, N. (2015). miRWalk2.0: a comprehensive atlas of microRNA-target interactions. *Nat. Methods* 12:697. doi: 10.1038/nmeth.3485

Fontana, G., See, E., and Pandit, A. (2015). Current trends in biologics delivery to restore intervertebral disc anabolism. *Adv. Drug Deliv. Rev.* 84, 146–158. doi: 10.1016/j.addr.2014.08.008

Garikipati, V., Verma, S. K., Cheng, Z., Liang, D., Truongcao, M. M., Cimini, M., et al. (2019). Circular RNA CircFndc3b modulates cardiac repair after myocardial infarction via FUS/VEGF-A axis. *Nat. Commun.* 10:4317.

Huang, W. J., Wang, Y., Liu, S., Yang, J., Guo, S. X., Wang, L., et al. (2018). Silencing circular RNA hsa_circ_0000977 suppresses pancreatic ductal adenocarcinoma progression by stimulating miR-874-3p and inhibiting PLK1 expression. *Cancer Lett.* 422, 70–80. doi: 10.1016/j.canlet.2018.02.014

Humzah, M. D., and Soames, R. W. (1988). Human intervertebral disc: structure and function. *Anat. Rec.* 220, 337–356. doi: 10.1002/ar.1092200402

Huo, W., Li, H., Zhang, Y., and Li, H. (2020). Epigenetic silencing of microRNA-874-3p implicates in erectile dysfunction in diabetic rats by activating the Nupr1/Chop-mediated pathway. *FASEB J.* 34, 1695–1709. doi: 10.1096/fj.201902086r

Ji, M. L., Jiang, H., Zhang, X. J., Shi, P. L., Li, C., Wu, H., et al. (2018). Preclinical development of a microRNA-based therapy for intervertebral disc degeneration. *Nat. Commun.* 9:5051.

Jiang, D., Sun, X., Wang, S., and Man, H. (2019). Upregulation of miR-874-3p decreases cerebral ischemia/reperfusion injury by directly targeting BMF and BCL2L13. *Biomed. Pharmacother.* 117:108941. doi: 10.1016/j.biopha.2019.108941

John, B., Enright, A. J., Aravin, A., Tuschl, T., Sander, C., and Marks, D. S. (2004). Human MicroRNA targets. *PLoS Biol.* 2:e363. doi: 10.1371/journal.pbio.0020363

Lan, P. H., Liu, Z. H., Pei, Y. J., Wu, Z. G., Yu, Y., Yang, Y. F., et al. (2016). Landscape of RNAs in human lumbar disc degeneration. *Oncotarget* 7, 63166–63176. doi: 10.18632/oncotarget.11334

Leong, K. W., Cheng, C. W., Wong, C. M., Ng, I. O., Kwong, Y. L., and Tse, E. (2017). miR-874-3p is down-regulated in hepatocellular carcinoma and negatively regulates PIN1 expression. *Oncotarget* 8, 11343–11355. doi: 10.18632/oncotarget.14526

Li, J. H., Liu, S., Zhou, H., Qu, L. H., and Yang, J. H. (2014). starBase v2.0: decoding miRNA-ceRNA, miRNA-ncRNA and protein-RNA interaction networks from large-scale CLIP-Seq data. *Nucleic Acids Res.* 42, D92–D97.

Li, Y., Pan, D., Liu, S., Xing, X., Zhou, H., Zhang, B., et al. (2021). Identification of circ-FAM169A sponges miR-583 involved in the regulation of intervertebral disc degeneration. *J. Orthop. Transl.* 26, 121–131. doi: 10.1016/j.jot.2020.07.007

Liu, M., Wang, Q., Shen, J., Yang, B. B., and Ding, X. (2019). Circbank: a comprehensive database for circRNA with standard nomenclature. *RNA Biol.* 16, 899–905. doi: 10.1080/15476286.2019.1600395

Livak, K. J., and Schmittgen, T. D. (2001). Analysis of relative gene expression data using real-time quantitative PCR and the 2(-Delta Delta C(T)) method. *Methods* 25, 402–408. doi: 10.1006/meth.2001.1262

Oichi, T., Taniguchi, Y., Oshima, Y., Tanaka, S., and Saito, T. (2020). Pathomechanism of intervertebral disc degeneration. *JOR Spine* 3:e1076.

Otasek, D., Morris, J. H., Boucas, J., Pico, A. R., and Demchak, B. (2019). Cytoscape automation: empowering workflow-based network analysis. *Genome Biol.* 20:185.

Pasquinelli, A. E. (2012). MicroRNAs and their targets: recognition, regulation and an emerging reciprocal relationship. *Nat. Rev. Genet.* 13, 271–282. doi: 10.1038/nrg3162

Piwecka, M., Glazar, P., Hernandez-Miranda, L. R., Memczak, S., Wolf, S. A., Rybak-Wolf, A., et al. (2017). Loss of a mammalian circular RNA locus causes miRNA deregulation and affects brain function. *Science* 357:eaam8526. doi: 10.1126/science.aam8526

Risbud, M. V., and Shapiro, I. M. (2014). Role of cytokines in intervertebral disc degeneration: pain and disc content. *Nat. Rev. Rheumatol.* 10, 44–56. doi: 10.1038/nrrheum.2013.160

Ritchie, M. E., Phipson, B., Wu, D., Hu, Y., Law, C. W., Shi, W., et al. (2015). limma powers differential expression analyses for RNA-sequencing and microarray studies. *Nucleic Acids Res.* 43:e47. doi: 10.1093/nar/gkv007

Roughley, P. J. (2004). Biology of intervertebral disc aging and degeneration: involvement of the extracellular matrix. *Spine* 29, 2691–2699. doi: 10.1097/01.brs.0000146101.53784.b1

Sheng, B., Yuan, Y., Liu, X., Zhang, Y., Liu, H., Shen, X., et al. (2018). Protective effect of estrogen against intervertebral disc degeneration is attenuated by miR-221 through targeting estrogen receptor alpha. *Acta Biochim. Biophys. Sin.* 50, 345–354. doi: 10.1093/abbs/gmy017

Song, M. X., Ma, X. X., Wang, C., Wang, Y., Sun, C., Xu, D. R., et al. (2021). Protective effect of estrogen receptors (ERα/β) against the intervertebral disc degeneration involves activating CCN5 via the promoter. *Eur. Rev. Med. Pharmacol. Sci.* 25, 1811–1820.

Song, X. X., Yu, Y. J., Li, X. F., Liu, Z. D., Yu, B. W., and Guo, Z. (2014). Estrogen receptor expression in lumbar intervertebral disc of the elderly: gender- and degeneration degree-related variations. *Joint Bone Spine* 81, 250–253. doi: 10.1016/j.jbspin.2013.09.002

Szklarczyk, D., Gable, A. L., Lyon, D., Junge, A., Wyder, S., Huerta-Cepas, J., et al. (2019). STRING v11: protein-protein association networks with increased coverage, supporting functional discovery in genome-wide experimental datasets. *Nucleic Acids Res.* 47, D607–D613.

Taheri, M., Shoorei, H., Dinger, M. E., and Ghafouri-Fard, S. (2020). Perspectives on the role of non-coding RNAs in the regulation of expression and function of the estrogen receptor. *Cancers* 12:2162.

Tokar, T., Pastrello, C., Rossos, A., Abovsky, M., Hauschild, A. C., Tsay, M., et al. (2018). mirDIP 4.1-integrative database of human microRNA target predictions. *Nucleic Acids Res.* 46, D360–D370.

Wan, Z. Y., Song, F., Sun, Z., Chen, Y. F., Zhang, W. L., Samartzis, D., et al. (2014). Aberrantly expressed long noncoding RNAs in human intervertebral disc degeneration: a microarray related study. *Arthritis Res. Ther.* 16:465.

Wang, H., He, P., Pan, H., Long, J., Wang, J., Li, Z., et al. (2018). Circular RNA circ-4099 is induced by TNF-alpha and regulates ECM synthesis by blocking miR-616-5p inhibition of Sox9 in intervertebral disc degeneration. *Exp. Mol. Med.* 50, 1–14.

Wang, Y., Che, M., Xin, J., Zheng, Z., Li, J., and Zhang, S. (2020). The role of IL-1beta and TNF-alpha in intervertebral disc degeneration. *Biomed. Pharmacother.* 131:110660.

Xia, B., Lin, M., Dong, W., Chen, H., Li, B., Zhang, X., et al. (2018). Upregulation of miR-874-3p and miR-874-5p inhibits epithelial ovarian cancer malignancy via SIK2. *J. Biochem. Mol. Toxicol.* 32:e22168.

Xiang, Q., Kang, L., Wang, J., Liao, Z., Song, Y., Zhao, K., et al. (2020). CircRNA-CIDN mitigated compression loading-induced damage in human nucleus pulposus cells via miR-34a-5p/SIRT1 axis. *EBioMedicine* 53:102679.

Xiao, Y., Liu, G., Sun, Y., Gao, Y., Ouyang, X., Chang, C., et al. (2020). Targeting the estrogen receptor alpha (ERalpha)-mediated circ-SMG1.72/miR-141-3p/Gelsolin signaling to better suppress the HCC cell invasion. *Oncogene* 39, 2493–2508.

Xie, K., Cai, Y., Yang, P., Du, F., and Wu, K. (2020). Upregulating microRNA-874-3p inhibits CXCL12 expression to promote angiogenesis and suppress inflammatory response in ischemic stroke. *Am. J. Physiol. Cell Physiol.* 319, C579–C588.

Xie, L., Huang, W., Fang, Z., Ding, F., Zou, F., Ma, X., et al. (2019). CircERCC2 ameliorated intervertebral disc degeneration by regulating mitophagy and apoptosis through miR-182-5p/SIRT1 axis. *Cell Death Dis.* 10:751.

Yang, S., Zhang, F., Ma, J., and Ding, W. (2020). Intervertebral disc ageing and degeneration: the antiapoptotic effect of oestrogen. *Ageing Res. Rev.* 57:100978.

Yuan, C., Zhou, L., Zhang, L., Yin, K., Peng, J., Sha, R., et al. (2019). Identification and integrated analysis of key differentially expressed circular RNAs in ER-positive subtype breast cancer. *Epigenomics* 11, 297–321.

Zhang, N., Gao, Y., Yu, S., Sun, X., and Shen, K. (2020). Berberine attenuates Abeta42-induced neuronal damage through regulating circHDAC9/miR-142-5p axis in human neuronal cells. *Life Sci.* 252:117637.

Zhao, B., Song, X., and Guan, H. (2020). CircACAP2 promotes breast cancer proliferation and metastasis by targeting miR-29a/b-3p-COL5A1 axis. *Life Sci.* 244:117179.

Zhou, Z. B., Huang, G. X., Fu, Q., Han, B., Lu, J. J., Chen, A. M., et al. (2019). circRNA.33186 contributes to the pathogenesis of osteoarthritis by sponging miR-127-5p. *Mol. Ther.* 27, 531–541.

Zotenko, E., Mestre, J., O'Leary, D. P., and Przytycka, T. M. (2008). Why do hubs in the yeast protein interaction network tend to be essential: reexamining the connection between the network topology and essentiality. *PLoS Comput. Biol.* 4:e1000140. doi: 10.1371/journal.pcbi.1000140

Conflict of Interest: The authors declare that the research was conducted in the absence of any commercial or financial relationships that could be construed as a potential conflict of interest.

frontiers in Genetics

ORIGINAL RESEARCH
published: 23 June 2021
doi: 10.3389/fgene.2021.653474

Identifying ceRNA Networks Associated With the Susceptibility and Persistence of Atrial Fibrillation Through Weighted Gene Co-Expression Network Analysis

*Yaozhong Liu, Na Liu, Fan Bai and Qiming Liu**

Department of Cardiovascular Medicine, Second Xiangya Hospital, Central South University, Changsha, China

Background: Atrial fibrillation (AF) is the most common arrhythmia. We aimed to construct competing endogenous RNA (ceRNA) networks associated with the susceptibility and persistence of AF by applying the weighted gene co-expression network analysis (WGCNA) and prioritize key genes using the random walk with restart on multiplex networks (RWR-M) algorithm.

Methods: RNA sequencing results from 235 left atrial appendage samples were downloaded from the GEO database. The top 5,000 lncRNAs/mRNAs with the highest variance were used to construct a gene co-expression network using the WGCNA method. AF susceptibility- or persistence-associated modules were identified by correlating the module eigengene with the atrial rhythm phenotype. Using a module-specific manner, ceRNA pairs of lncRNA–mRNA were predicted. The RWR-M algorithm was applied to calculate the proximity between lncRNAs and known AF protein-coding genes. Random forest classifiers, based on the expression value of key lncRNA-associated ceRNA pairs, were constructed and validated against an independent data set.

Results: From the 21 identified modules, magenta and tan modules were associated with AF susceptibility, whereas turquoise and yellow modules were associated with AF persistence. ceRNA networks in magenta and tan modules were primarily involved in the inflammatory process, whereas ceRNA networks in turquoise and yellow modules were primarily associated with electrical remodeling. A total of 106 previously identified AF-associated protein-coding genes were found in the ceRNA networks, including 16 that were previously implicated in the genome-wide association study. Myocardial infarction–associated transcript (MIAT) and LINC00964 were prioritized as key lncRNAs through RWR-M. The classifiers based on their associated ceRNA pairs were able to distinguish AF from sinus rhythm with respective AUC values of 0.810 and 0.940 in the training set and 0.870 and 0.922 in the independent test set. The AF-related single-nucleotide polymorphism rs35006907 was found in the intronic region of LINC00964 and negatively regulated the LINC00964 expression.

OPEN ACCESS

Edited by:
Detu Zhu,
Cornell University, United States

Reviewed by:
Liangjiang Wang,
Clemson University, United States
Pengcheng Yang,
Independent Researcher,
Beijing, China
Yong Xu,
First Hospital of Shanxi Medical University, China

***Correspondence:**
Qiming Liu
qimingliu@csu.edu.cn

Specialty section:
This article was submitted to RNA, a section of the journal Frontiers in Genetics

Received: *14 January 2021*
Accepted: *15 April 2021*
Published: *23 June 2021*

Citation:
Liu Y, Liu N, Bai F and Liu Q (2021) Identifying ceRNA Networks Associated With the Susceptibility and Persistence of Atrial Fibrillation Through Weighted Gene Co-Expression Network Analysis. Front. Genet. 12:653474. doi: 10.3389/fgene.2021.653474

Conclusion: Our study constructed AF susceptibility- and persistence-associated ceRNA networks, linked genetics with epigenetics, identified MIAT and LINC00964 as key lncRNAs, and constructed random forest classifiers based on their associated ceRNA pairs. These results will help us to better understand the mechanisms underlying AF from the ceRNA perspective and provide candidate therapeutic and diagnostic tools.

Keywords: atrial fibrillation, susceptibility, persistence, ceRNA, WGCNA, RWR-M

INTRODUCTION

Atrial fibrillation (AF) is the most common type of cardiac arrhythmia and poses a significant burden to patients and physicians (Hindricks et al., 2020). The currently estimated global prevalence of AF is between 2 and 4% (Hindricks et al., 2020; Virani et al., 2020), and by the middle of the 21st century, AF will be diagnosed in an estimated 72 million individuals in Asia, 16 million in America, and 14 million in Europe (Kornej et al., 2020). Well-known risk factors contribute to AF susceptibility, including aging, male sex, alcohol consumption, obesity, and smoking as well as comorbidities such as heart failure, diabetes, obstructive sleep apnea, and inflammatory disease (Chung et al., 2020). AF is also heritable (Weng et al., 2017), and two large-scale genome-wide association studies (GWAS) identified more than 100 loci associated with AF (Nielsen et al., 2018; Roselli et al., 2018). AF increases the risk of stroke, dementia, and depression and contributes to a 1.5–3.5-fold increase in mortality (Hindricks et al., 2020). Despite its epidemiological importance, the fundamental mechanisms that underlie AF remain poorly understood.

The basic mechanisms that underlie AF include ectopic firing and reentry circuits, both of which are associated with atrial electrical and structural remodeling (Iwasaki et al., 2011). Electrical remodeling refers to changes in the expression or function of the ion channels that affect the electrical activity of cardiomyocytes, whereas structural remodeling refers to alterations that occur in the tissue architecture, such as atrial fibrosis and dilation (Nattel and Harada, 2014). Both electrical and structural remodeling provide the substrates for ectopic firing and reentry circuits. Some newly proposed physiological processes, including oxidative stress, inflammation, and mitochondrial damage, have the potential to trigger atrial remodeling and represent promising therapeutic targets in AF (Nattel et al., 2020).

Depending on the presentation, duration, and spontaneous termination of AF, five patterns have been classified, including first-diagnosed, paroxysmal, persistent, long-standing persistent, and permanent AF (Hindricks et al., 2020). The self-perpetuating nature of AF represents a major challenge that has limited the success of pharmacological or ablation therapies and might serve as the leading mechanism that contributes to the development of paroxysmal to persistent to permanent AF (Nattel et al., 2014). Rapid, irregular pacing causes abnormalities to develop in the underlying electrical or structural properties of the atria, and these remodeling events can further promote AF development (Nattel et al., 2014), leading to a vicious cycle of "AF begetting AF." Therefore, identifying the regulators that mediate the pathogenic biological processes that underlie atrial remodeling has become a primary goal in AF-related clinical and experimental studies. The recent discovery of a new group of mediators, known as competing endogenous RNAs (ceRNAs), offers a unique opportunity for deciphering this complex heart rhythm disorder.

Numerous microRNA (miRNA) binding sites have been identified on messenger RNAs (mRNAs), long non-coding RNAs (lncRNAs), circular RNAs, and pseudogenes (Tay et al., 2014), leading to the hypothesis that RNA transcripts containing miRNA-binding sites can "communicate" or regulate each other by competing for shared miRNAs, acting as ceRNAs (Salmena et al., 2011). This hypothesis has been widely adopted in investigations of the roles played by non-coding RNAs in disease pathogenesis, especially lncRNAs. A great example is cardiac apoptosis–related lncRNA (CARL), which competitively binds to miR-539, preventing the miR-539-dependent downregulation of prohibitin 2 (PHB2), allowing PHB2 to inhibit mitochondrial fission and apoptosis in cardiomyocytes (Wang et al., 2014). However, the functions of ceRNA pairs in AF have not yet been well-illustrated. As the "language" of ceRNAs, many miRNAs have been demonstrated to promote AF development by causing atrial electrical and structural remodeling (Luo et al., 2015), suggesting the existence of ceRNA crosstalk in AF pathogenesis. Previous research has attempted to identify ceRNA pairs associated with AF by identifying differentially expressed lncRNAs/mRNAs between patients with AF and those with sinus rhythm (SR) (Qian et al., 2019). However, differentially expressed gene (DEG) analysis ignores the interconnections between ceRNAs and may filter out genes with high centralities that engage in high levels of ceRNA crosstalk. In addition, DEGs were identified by comparing the expression patterns between a persistent AF and an SR group; however, these genes could be associated with either increased susceptibility or persistence, and the distinction between susceptibility- and persistence-associated ceRNA pairs is not possible in comparisons of AF and SR genes.

The characteristics and underlying molecular mechanisms associated with AF susceptibility might differ from those associated with AF persistence. A previous microarray study (Deshmukh et al., 2015) compared the transcriptomic profiles of left atrial appendages from three types of patients (no AF history, AF history in SR at surgery, AF history in AF at surgery) and found that AF susceptibility was associated with changes in the activities of several transcription factor targets related to inflammation, oxidation, and cellular stress responses, whereas AF persistence was associated with the remodeling of ion channel

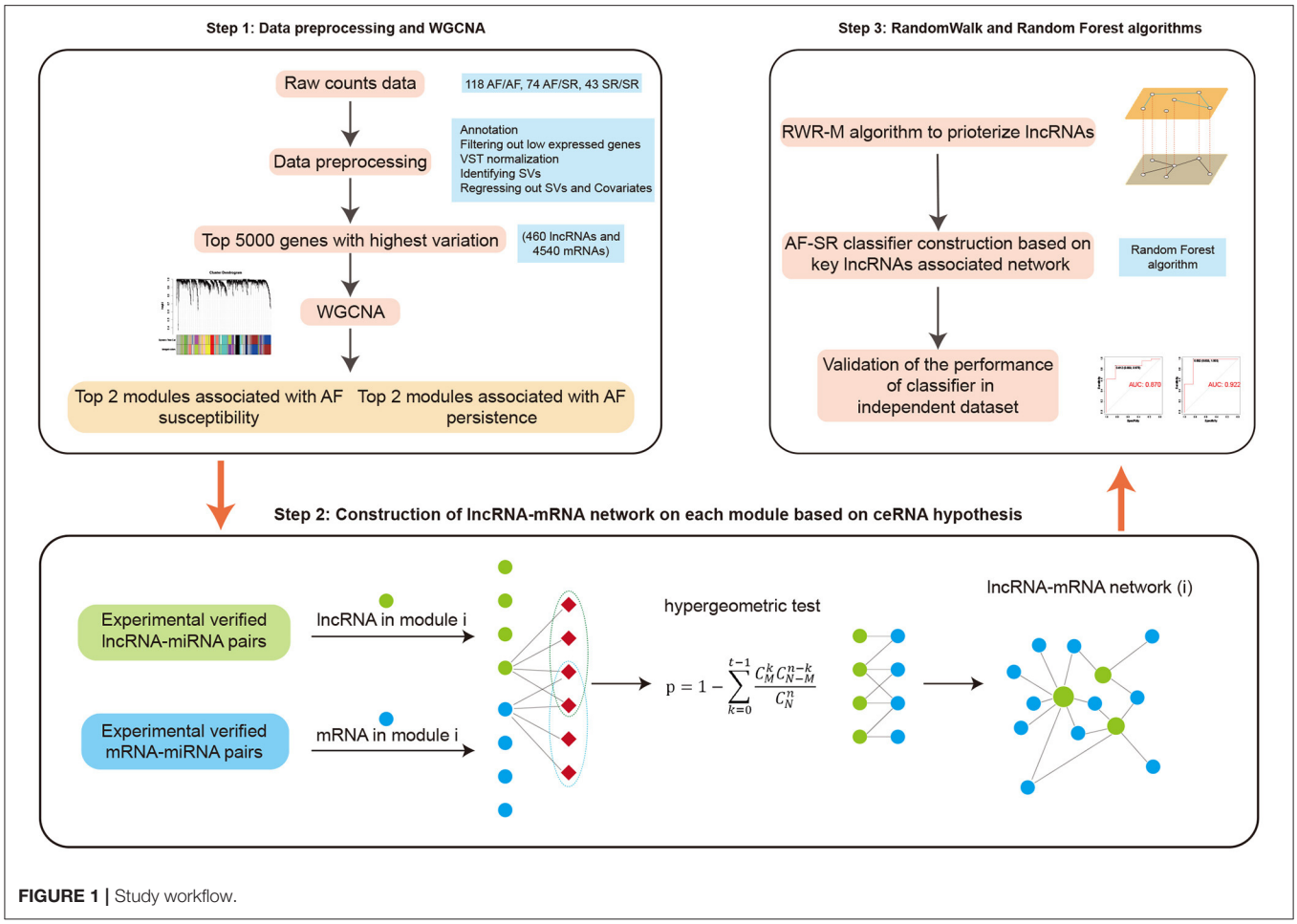

FIGURE 1 | Study workflow.

expression. Many of these changes corroborate the findings of previous clinical and electrophysiology studies of AF. On the one hand, inflammatory disease, cardiovascular comorbidities, and increased serum inflammatory biomarkers have been associated with an increased risk of AF (Chung et al., 2020; Li and Brundel, 2020), which supports the idea that inflammation and oxidative stress contribute to AF susceptibility. On the other hand, GWAS studies and gain and loss of function studies have identified various genes related to ion channel expression that are associated with AF persistence (Roselli et al., 2020). Drugs that target ion channel currents represent the current pharmacological strategies used to treat AF patients. However, the application of anti-inflammatory agents for AF prevention has generally failed to establish AF-specific indications, and the efficiency of anti-arrhythmia drugs in AF treatment remains relatively unsatisfactory (Chung et al., 2020). Therefore, the identification of new regulators to prevent the initiation and progression of this complex arrhythmia could provide new therapeutic and diagnostic targets.

In this study, we introduce a method known as the weighted gene co-expression network analysis (WGCNA), which can cluster highly correlated genes into association modules and then relate each module to external clinical traits (Langfelder and Horvath, 2008). The construction of a ceRNA network within a disease-related module ensures that the identified nodes are highly co-expressed and enhances the reliability and significance of the network. Our present study used a large cohort ($n = 235$) of left atrial tissue samples derived from patients from three types of atrial rhythm. By analyzing the relationships between the modules and the various phenotypes, we were able to identify AF susceptibility- and persistence-associated ceRNA networks, which will inform future research. We also applied a newly proposed algorithm, known as the random walk with restart on multiple networks (RWR-M), to prioritize lncRNAs by analyzing the "proximity score" of each lncRNA to known disease-related genes. Moreover, by applying the random forest classification algorithm, we demonstrate that key lncRNA-associated ceRNA pairs could distinguish AF from SR patients in both training and independent test sets. In general, our study generates a state-of-the-art pipeline for the construction of disease-associated ceRNA networks and the prioritization of newly identified disease-associated genes (**Figure 1**). These results provide information to promote a better understanding of the mechanisms that underlie AF from the ceRNA perspective and identify new candidate therapeutic and diagnostic targets.

MATERIALS AND METHODS

Data Acquisition and Preprocessing

The GSE69890 data set was used to obtain the RNA sequencing results generated from left atrial appendage (LAA) tissue samples derived from 235 subjects of European descent (Hsu et al., 2018). These 235 subjects were divided into three groups according to their atrial rhythm phenotypes: no history of AF and in SR at the time of surgery (SR/SR, $n = 43$), a history of AF but in SR at the time of surgery (AF/SR, $n = 74$), and a history of AF and flutter at the time of surgery (AF/AF, $n = 118$). The raw count file was downloaded from the NCBI Gene Expression Omnibus (GEO) database (https://www.ncbi.nlm.nih.gov/). We annotated the Ensemble ID identifier with the Ensembl Release 99 (https://www.ensembl.org/index.html), retaining rows that (1) had an official symbol name and (2) belonged to the lncRNA or mRNA category and removing rows that had duplicated gene names. Genes with counts of <10 in more than 80% of samples were filtered out, and the remaining data were variance-stabilized and transformed using the R package DESeq2 (Love et al., 2014). Surrogate variables (SVs) were calculated using the sva package (Leek et al., 2012), and the expression of each gene was adjusted by the sex covariate and the identified SVs. Finally, the top 5,000 genes with the highest variance were selected for the construction of a gene co-expression network.

For validation, the GSE41177 data set (Yeh et al., 2013), which includes microarray data from a total of 38 left atrial tissues from 6 persistent AF and 32 SR patients, was downloaded from the GEO database. The raw CEL files were obtained and preprocessed using a robust multiarray average (RMA) algorithm with the affy package (Gautier et al., 2004) for background correction and quantile normalization. The median expression values among all multiple probe IDs were selected to represent the corresponding gene.

Construction of a Weighted Gene Co-Expression Network

WGCNA is one of the most widely used methods for the construction of a gene co-expression network (Langfelder and Horvath, 2008). In this study, we focused only on positive gene correlations; therefore, a signed network was constructed. First, a signed adjacency matrix was generated between genes based on their correlation. The adjacency value, *signed* a_{ij}, for genes i and j, is defined as

$$\text{signed a}_{\text{ij}} = |\left(1 + \text{cor}\left(x_i, x_j\right)\right)/2|^{\beta},$$

where $cor\left(x_i, x_j\right)$ is the Pearson's correlation coefficient between gene i and gene j, and β is an integer to let the network display a scale-free topology property. A value of $\beta = 12$ was selected in this study because this satisfied a degree of independence of 0.9 with the minimum value. Then, a topological overlap measure (TOM) was created to reduce the network sensitivity to spurious connections or random noise (Ravasz et al., 2002). Hierarchical clustering was performed on the matrix 1 – TOM and the dynamic tree cut method was applied to generate modules of highly co-expressed genes with parameters set to a deepSplit of 2, minModuleSize of 30, and height cutoff of 0.25 as recommended (Zhang and Horvath, 2005). The module eigengene (ME) is defined as the first principal component of a given module and can, therefore, present the gene expression profiles in a module (Langfelder and Horvath, 2008).

Association Between Modules and Clinical Information

Pearson's correlation analysis was applied to correlate the atrial rhythms with the MEs from each module. Associations between modules and AF susceptibility were determined by evaluating the correlations between the MEs and the atrial rhythm phenotypes in the 117 AF/SR and SR/SR samples (AF/SR was assigned one and SR/SR was assigned zero). Similarly, associations between modules and AF persistence were determined by evaluating the correlation between MEs and atrial rhythm phenotypes in the 192 AF/AF and AF/SR samples (AF/AF was assigned one and AF/SR was assigned zero). To reduce the probability of statistical error, we only chose the four most significant modules associated with AF (two for susceptibility and two for persistence) for further analysis.

Preparation of miRNA Targets Database

DIANA-LncBase v2.0 (http://www.microrna.gr/LncBase) is a reference repository that contains experimentally supported non-coding RNA–miRNA pairs (Paraskevopoulou et al., 2016). DIANA-TarBase v8 (http://www.microrna.gr/tarbase) is a reference database with experimentally supported mRNA-miRNA pairs (Karagkouni et al., 2018). We annotated the Ensemble ID identifiers in the two data sets, as described above, and retained only the identified lncRNA–miRNA and mRNA–miRNA pairs, resulting in 26,178 lncRNA–miRNA pairs and 418,758 mRNA–miRNA pairs, which were used for further ceRNA pair prediction.

ceRNA Network Construction

For each of the selected modules, the mRNAs and lncRNAs were co-expressed and closely related to AF. Thus, we predicted their communications by identifying shared miRNAs between lncRNAs and mRNAs. We used a strict prediction and selection method as follows: (a) prediction of lncRNA–miRNA interactions; (b) prediction of mRNA–miRNA interactions; (c) hypergeometric test: for each lncRNA–mRNA pair with shared miRNAs, we calculated the pair's significance by performing a hypergeometric test using the phyper function in the stata packages in R software. The p-values were calculated as follows:

$$\text{p} = 1 - \sum_{k=0}^{t-1} \frac{C_M^k C_{N-M}^{n-k}}{C_N^n},$$

where N represents the total number of miRNAs in the prepared lncRNA–miRNA and mRNA–miRNA pairs ($N = 923$), t represents the number of shared miRNAs between the given lncRNA and mRNA, n represents the number of miRNAs that target the lncRNA, and M represents the number of miRNAs that target the mRNA. Those pairs with $p < 0.05$ were selected to construct the ceRNA network. We also calculated an adjusted

p-value using the Benjamini–Hochberg (BH) method. Those pairs with adjusted $p < 0.05$ were used in the following sensitivity analysis.

Enrichment Analysis

For a given gene list, a gene ontology biological process (GO BP) enrichment analysis was conducted using the ClusterProfiler (Yu et al., 2012) package in R software.

Random Walk With Restart on Multiplex Networks

RWR-M is a state-of-the-art algorithm in network computational biology (Valdeolivas et al., 2019). It can be applied to prioritize candidate disease genes by calculating the proximity score of other nodes to known disease genes (seed nodes) in multiple interaction networks. Consider a multiplex graph G of L undirected graphs that share the same sets of n nodes. Each layer $\alpha = 1,\ldots L$, is defined by its n × n adjacency matrix $A^{[\alpha]} = (A^{[\alpha]}(i,j))_{i,j=1,\ldots n}$, where $A^{[\alpha]}(i,j) = 0$ if nodes i and j are not directly connected on layer α and one otherwise. Specifically, $A^{[\alpha]}(i,i) = 0, i = 1,\ldots n$. The multiplex graph is then defined as G = (V, E), where $V = \{v_i^\alpha \; i = 1,\ldots n, \alpha = 1,\ldots L\}$; $E = \{(v_i^\alpha \; v_j^\alpha), i,j = 1,\ldots n, \alpha = 1,\ldots L, A^{[\alpha]}(i,j) \neq 0\} \bigcup \{(v_i^\alpha, v_i^\beta), i = 1,\ldots n, \alpha \neq \beta\}$.

For each iteration, an imaginary particle can walk from its current node v_i^α to its neighbors within a layer or jump to v_i^β ($\alpha \neq \beta$) in another layer. An $nL \times nL$ matrix M can be defined as

$$M = \begin{pmatrix} (1-\delta)A^{[1]} & \frac{\delta}{L-1}I & \ldots & \frac{\delta}{L-1}I \\ \frac{\delta}{L-1}I & (1-\delta)A^{[2]} & \ldots & \frac{\delta}{L-1}I \\ \vdots & \vdots & \ddots & \vdots \\ \frac{\delta}{L-1}I & \frac{\delta}{L-1}I & \ldots & (1-\delta)A^{[L]} \end{pmatrix},$$

where I is the n × n identity matrix. The parameter $\delta \in [0,1]$ is the probability of staying in a layer or jumping to another layer and was set as 0.5 in this study. The RWR-M equation can be defined as

$$\overline{p}_{t+1}^T = (1-r)M\overline{p}_t^T + r\overline{p}_{RS}^T,$$

where M is the column normalization transition matrix of M; $\overline{p}_t^T = [p_t^1,\ldots p_t^L]$ and $\overline{p}_{t+1}^T = [p_{t+1}^1,\ldots p_{t+1}^L]$ are n × L vectors with each element representing the probability of the walking particle in G; r ∈ [0, 1] is the restart probability that the particle can restart by jumping to seed nodes at each iteration in the graph and was set as 0.7. The $\overline{p}_{RS}$ is defined as $\overline{p}_{RS} = \tau \cdot \overline{p}_0$, where $\overline{p}_0$ represents the initial probability distribution. The seed nodes are assigned $1/k$ (k is the number of seeds), and other nodes are assigned zero. $\tau = [\tau 1,\ldots, \tau L]$ is the measurement of each layer's weight. After enough iterations, the difference between $\overline{p}_{t+1}$ and $\overline{p}_t$ becomes negligible, and the stationary probability distribution is reached. The elements in the distribution matrix then represent a proximity measure from every node to the seed(s). Nodes with a high "global proximity score" were, therefore, prioritized as new disease genes.

First, the lncRNA–mRNA pairs in the four ceRNA networks were aggregated into a single large network, which was set as the first layer. We then used the top 50% of evidence-supported gene–gene interactions with the highest confidence scores from the cardiac muscle data identified by the GIANT project (Greene et al., 2015). The GIANT project collected genome-wide, functional interaction networks in tissue- and cell-specific manners for more than 100 human tissues and cell types. We only extracted those edges for which the two nodes both existed in the aggregated ceRNA network. Then, we conducted the RWR-M algorithm with two layers (L = 2, aggregated ceRNA network, and GIANT-guided network) using the RandomWalkRestartMH package (Valdeolivas et al., 2019). For the RWR-M analysis, seed nodes must first be defined. We searched the DISEASE (Pletscher-Frankild et al., 2015), DisgeNET (Piñero et al., 2017), and MALACARD (Rappaport et al., 2017) databases to identify known AF protein-coding genes, and those presented in the network were set as seed nodes. For RWR-M, the layer weight was set to $\tau = [\frac{2}{(1+R)}, \frac{2\times R}{(1+R)}]$, where R is the ratio of the number of ceRNA-guided interactions in the first layer to the number of GIANT project-guided interactions in the second layer. After performing the RWR-M algorithm, the top two scoring lncRNAs were selected as the key lncRNAs associated with AF.

Gene Set Variation Analysis

To further investigate the function of the prioritized lncRNAs and eliminate the effects of atrial rhythm, we conducted a GSVA. GSVA (Hänzelmann et al., 2013) is an unsupervised method that computes the enrichment score of a given gene set in each sample. We downloaded the latest GO BP gene sets from the Molecular Signatures Database v7.2 (https://www.gsea-msigdb.org/) (Mootha et al., 2003) and excluded those with gene sizes smaller than 10 or larger than 500. For each gene set, we identified the correlation with the prioritized lncRNAs by fitting a linear model as the GSVA score–atrial rhythm + expression value of lncRNA. The regression coefficient and p-value for each lncRNA were calculated using the stata package.

Construction of Random Forest Classifiers and Validation

For each prioritized lncRNA, the expression values of the lncRNA and its mRNA pairs were used to construct a random forest classifier using the randomForest package (Liaw and Wiener, 2002) in R. The performance of the classifier was first validated in the training set using a six-fold cross-validation method and was further evaluated using an independent test data set. First, because RNA sequencing and microarray results can be characterized by substantial heterogeneity, the expression values of selected features in 118 AF/AF samples, 43 SR/SR samples, and 38 microarray samples were merged, and batch effects were removed using the combat function of the sva package in R, without specifying the covariate of interest (AF or SR). The RNA sequencing samples were used as the training set, and the remaining 38 microarray samples were used as the test set. The performance of the established classifier was evaluated using the receiver operating characteristic curve and the value of the area under the curve (AUC).

RESULTS

Data Preparation

After data preprocessing, we obtained a large gene expression matrix consisting of 16,905 unique genes (1,994 lncRNAs and 14,911 mRNAs) rows by 235 sample columns (AF/AF, $n = 118$; AF/SR, $n = 74$; and SR/SR, $n = 43$). An SV analysis was performed to identify potential large effectors of gene expression that might potentially introduce spurious correlations between genes, including technical variables, such as batch effects and read depths; genetic variables; and environmental variables, such as any history of structural heart disease and age (Leek and Storey, 2007; Leek et al., 2010; Parsana et al., 2019). Two SVs were identified when specifying the interest of atrial rhythm and covariate of sex. We then fit the gene expression matrix with a linear model that included atrial rhythm, sex, and the identified SVs (expression–atrial rhythm + sex + SVs) and regressed out the sex variable and the SVs. The cleaned expression matrix was used for further analyses, and the GSE41177 data set was used for validation.

Construction of Co-Expression Modules and the Identification of Key Modules

The top 5,000 genes with the highest variation (including 460 lncRNAs and 4,540 mRNAs) were selected for the construction of a gene co-expression network. The β value was set to 12. A total of 21 modules were generated using dynamic tree cutting (**Figure 2A**). We then analyzed the correlation between each module and the clinical traits by calculating the correlation coefficient between each ME and the atrial rhythm phenotype. As shown in **Figure 2B**, the magenta ($r = 0.42$, $p = 3e{-}6$) and tan ($r = 0.35$, $p = 9e{-}5$) modules represent the top two AF susceptibility-associated modules, whereas the turquoise ($r = -0.54$, $p = 1e{-}15$) and yellow ($r = 0.6$, $p = 6e{-}20$) modules represent the top two AF persistence-associated modules. In addition, the magenta and tan modules did not significantly correlate with AF persistence, and the turquoise and yellow modules did not significantly correlate with AF susceptibility, indicating that the selected modules each have specificity for either AF susceptibility or persistence. **Supplementary Table 1** summarizes the basic and functional information for all 21 modules. **Figures 2C–F** show the top 10 GO BP enrichment results for the four selected modules. The magenta module is primarily associated with the type I interferon signaling pathway, and the tan module is primarily associated with T cell activation. Both the turquoise and yellow modules are associated with muscle contraction and the regulation of membrane potential. These results indicate that immune system activation is closely associated with AF susceptibility, and electrical remodeling is more closely associated with AF persistence.

Construction of ceRNA Networks in a Module-Specific Manner

The key design of our study was the construction of the ceRNA network among highly co-expressed genes. We reasoned that, if two genes exist in different modules, their ceRNA interactions would likely be less strong. Thus, we did not consider any intermodule ceRNA pairs. For each of the four AF modules, we identified the intramodule lncRNA–mRNA ceRNA pairs through the prediction and selection methods described in section Association between modules and clinical information. We obtained four independent ceRNA networks, two associated with AF susceptibility and two associated with AF persistence (**Figure 3**). The GO BP enrichment analysis (**Figure 4**) shows that the magenta ceRNA network was primarily associated with the defense response to virus and type I interferon signaling pathway, the tan ceRNA network was associated with T cell differentiation and T cell activation, the turquoise ceRNA network was primarily associated with synapse organization and regulation of membrane potential, and the yellow ceRNA network was primarily associated with cardiac muscle tissue development and muscle contraction.

We successfully constructed two inflammation-associated ceRNA networks related to AF susceptibility and two cardiac conduction or electrical remodeling-associated ceRNA networks related to AF persistence. Based on **Figure 3**, the majority of the nodes in each network appear to be able to communicate with each other through ceRNA language-guided interactions, either directly (lncRNA–mRNA) or indirectly (an mRNA–lncRNA–mRNA–lncRNA axis). These lncRNAs and mRNAs represent valuable therapeutic targets to prevent AF progression as they were not only co-expressed but also functionally correlated. Moreover, a total of 106 previously identified AF protein-coding genes were included in the established ceRNA networks (**Figure 3**, red nodes), including 49 in the turquoise ceRNA network, 32 in the yellow ceRNA network, 15 in the magenta ceRNA network, and 10 in the tan ceRNA network. The hypergeometric test showed a p-value of 8e−10 for the AF enrichment. These findings further demonstrate the significance of the constructed networks. More interestingly, 16 of the identified protein-coding genes have been implicated in the GWAS of AF conducted by Roselli et al. (2018, 2020) and Nielsen et al. (2018), including *AGBL4*, *COG5*, *DGKB*, *HSF2*, *KCND3*, *KCNN2*, *SLC27A6*, *SYNE2*, and *SYNPO2L* in the turquoise ceRNA network and *MYH7*, *MYOCD*, *MYO18B*, *NAV2*, *PHLDB2*, *RPL3L*, and *SMAD7* in the yellow ceRNA network. These results indicate that the roles of these GWAS-related genes in AF are likely associated with atrial electrical remodeling. Detailed information for each ceRNA network, including shared miRNAs between any lncRNA–mRNA pair, can be found in **Supplementary Table 2**.

Prioritizing Key lncRNAs Associated With AF Using the RWR-M Algorithm

We then aimed to prioritize key lncRNAs associated with AF (**Figure 5**). We defined the hub lncRNAs with high graphical proximity to known AF genes. We applied the latest RWR-M algorithm with two different layers (the aggregated ceRNA network and the GIANT project-guided network; **Figure 5A**). The calculated RWR-M score can be considered a measure of the proximity between the seed(s) and all other nodes in the graph. Those genes with high RWR-M scores are then identified as hub genes. After performing the RWR-M algorithms, MIAT and LINC00964 were identified as the genes with the top two highest RWR-M scores and were identified as hub genes associated with AF (**Figure 5A**; scores for all lncRNAs in the

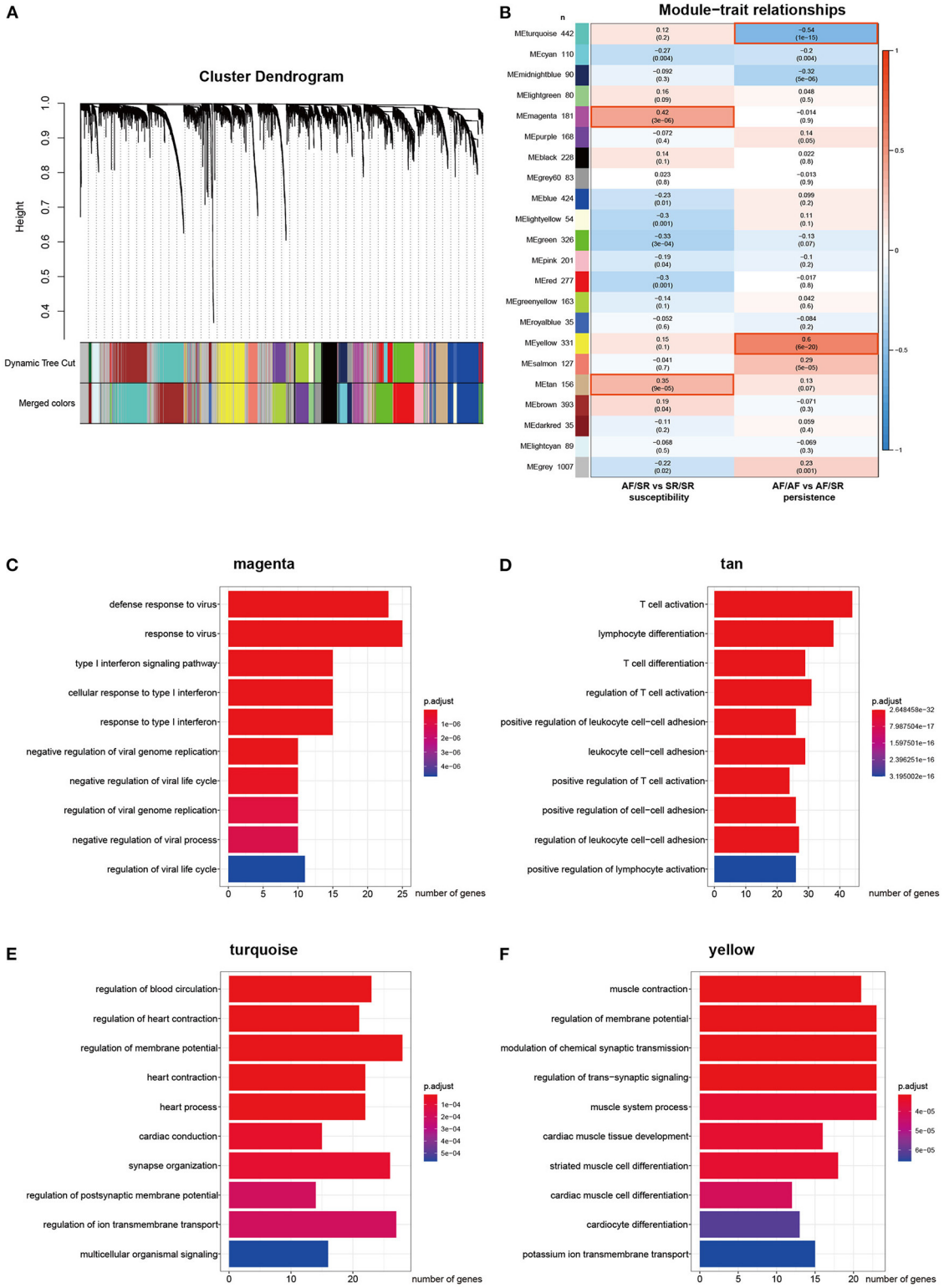

FIGURE 2 | Construction of the weighted co-expression network and module analysis. **(A)** Cluster dendrogram. The two colored rows below represent the original and merged modules. **(B)** Heat map of the correlation between AF susceptibility/persistence and module eigengenes. Each row corresponds to a different module eigengene, and each column corresponds to a different AF trait. Each cell contains the corresponding correlation (first line) and *p*-value (second line). **(C–F)** Top 10 enriched biological processes associated with the AF-related modules.

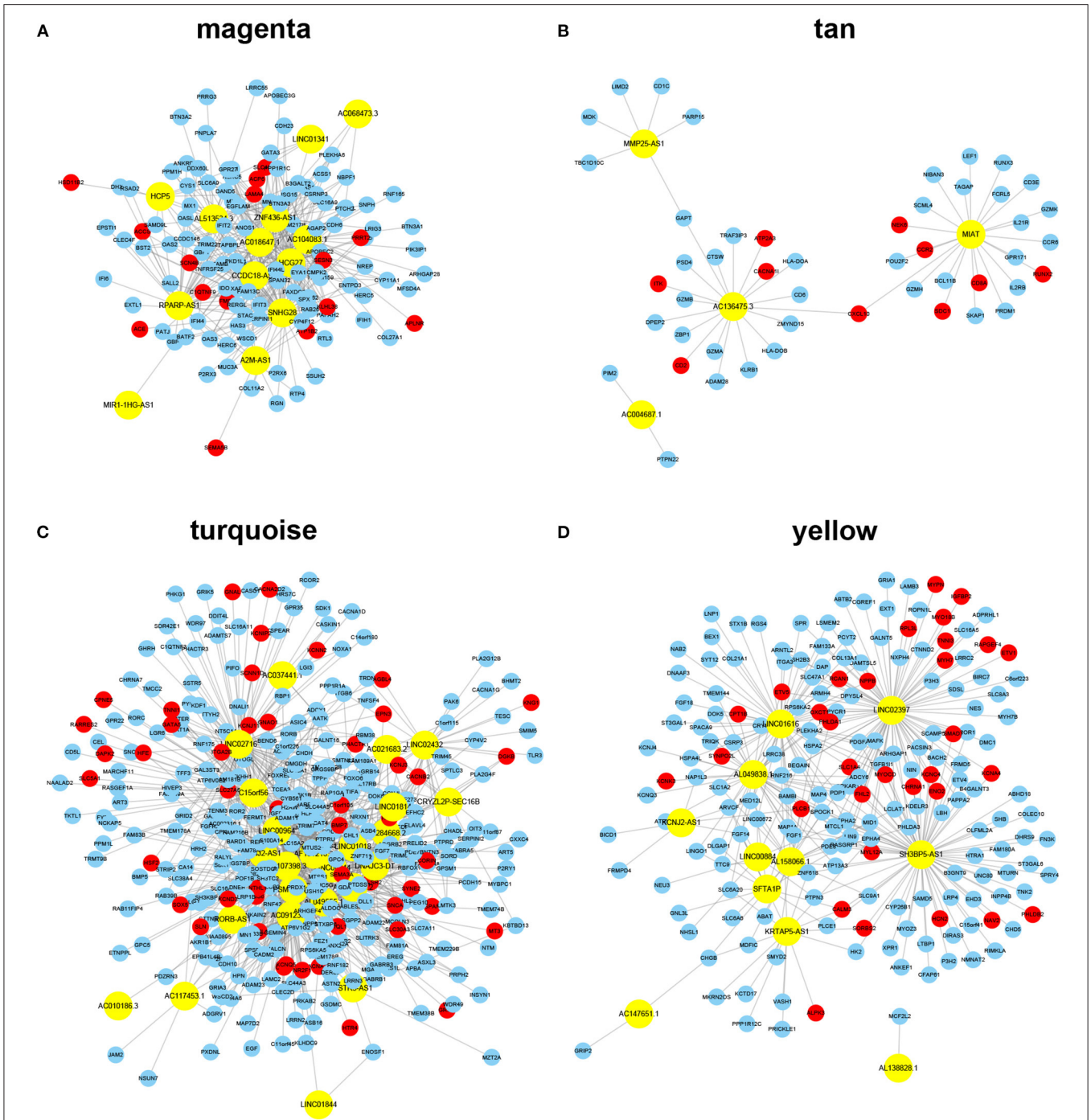

FIGURE 3 | ceRNA networks for each module. Note: the yellow color represents lncRNAs, whereas the red color represents known AF protein-coding genes identified from DISEASE, DisgeNET, and MALACARD databases. **(A–D)** lncRNA-mRNA ceRNA networks identified using a module-specific manner in AF susceptibility-associated magenta **(A)** and tan **(B)** modules, and AF persistence-associated turquoise **(C)** and yellow **(D)** modules.

network and their diagnostic efficiency for distinguishing AF from SR are described in **Supplementary Table 3**). We also tested whether using BH-adjusted *p*-values in step 2.5 would substantially change the results. After filtering lncRNA–mRNA pairs with an adjusted $p < 0.05$ and conducting the subsequent protocols, MIAT and LINC00964 remained among the top five high RWR-M scoring lncRNAs. The lncRNA MIAT belongs to the AF susceptibility-associated tan module, whereas the lncRNA LNIC00964 belongs to the AF persistence-associated turquoise module. The miRNA partners of MIAT-mediated ceRNA pairs include 19 miRNAs (**Supplementary Table 2**), some of which have previously been implicated in AF, such as miR-27b-3 (Lv

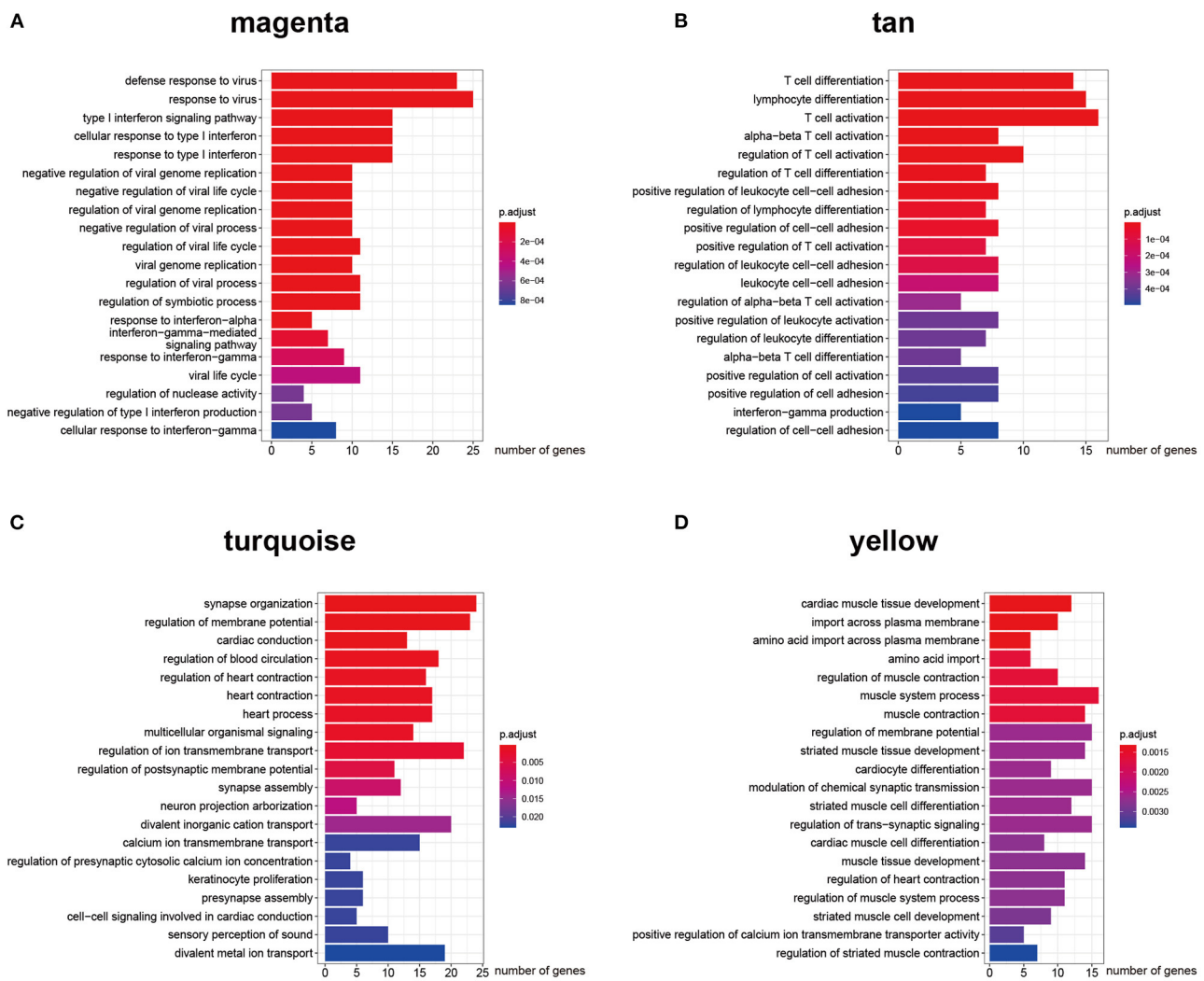

FIGURE 4 | Gene ontology biological process enrichment analysis for each ceRNA network. **(A–D)** Top 20 enriched gene ontology biological process terms of protein-coding genes in AF susceptibility-associated magenta **(A)** and tan **(B)** ceRNA networks, and AF persistence-associated turquoise **(C)** and yellow **(D)** ceRNA networks.

et al., 2019) and miR-23b-3p (Yang et al., 2019). The miRNA partners of LINC00964-mediated ceRNA pairs only included miR-34a-5p. Interestingly, a previous study has demonstrated that miR-34a promoted atrial electrical remodeling by enhancing intracellular Ca^{2+} signaling (Zhu et al., 2018). These results revealed that these miRNA-mediated ceRNA pairs likely served critical roles during AF development.

Identifying Biological Processes Correlated With MIAT and LINC00964

The lncRNA MIAT has 23 direct mRNA targets in the tan module, including six known AF genes. GO BP enrichment analysis identified the 23 genes associated with MIAT as being primarily involved in lymphocyte differentiation and T cell activation (data not shown). The lncRNA LINC00964 has 89 direct mRNA targets in the turquoise module, including 13 known AF genes. No significant term was enriched among these 89 mRNAs based on Fisher's exact test with BH adjustment, indicating that the 89 direct targets of LINC00964 have multiple biological functions. These genes are significantly associated with atrial electrical remodeling because they (1) were co-expressed with atrial electrical remodeling-related genes in the turquoise ceRNA network and (2) co-interacted with atrial electrical remodeling-related genes in the turquoise ceRNA network through ceRNA-guided interactions. To further investigate the biological functions of MIAT and LINC00964, we conducted a GSVA and correlated the GSVA score of each pathway (a total of 5,348 gene sets) with the expression value of each lncRNA while adjusting for the AF phenotype (**Supplementary Table 4** for MIAT and **Supplementary Table 5** for LINC00964). For MIAT, all of the top 10 positively correlated pathways were identified as T cell activation–related pathways, with T_Helper_17_Cell_Lineage_Commitment having the highest regression coefficient of 0.384. For LINC00964,

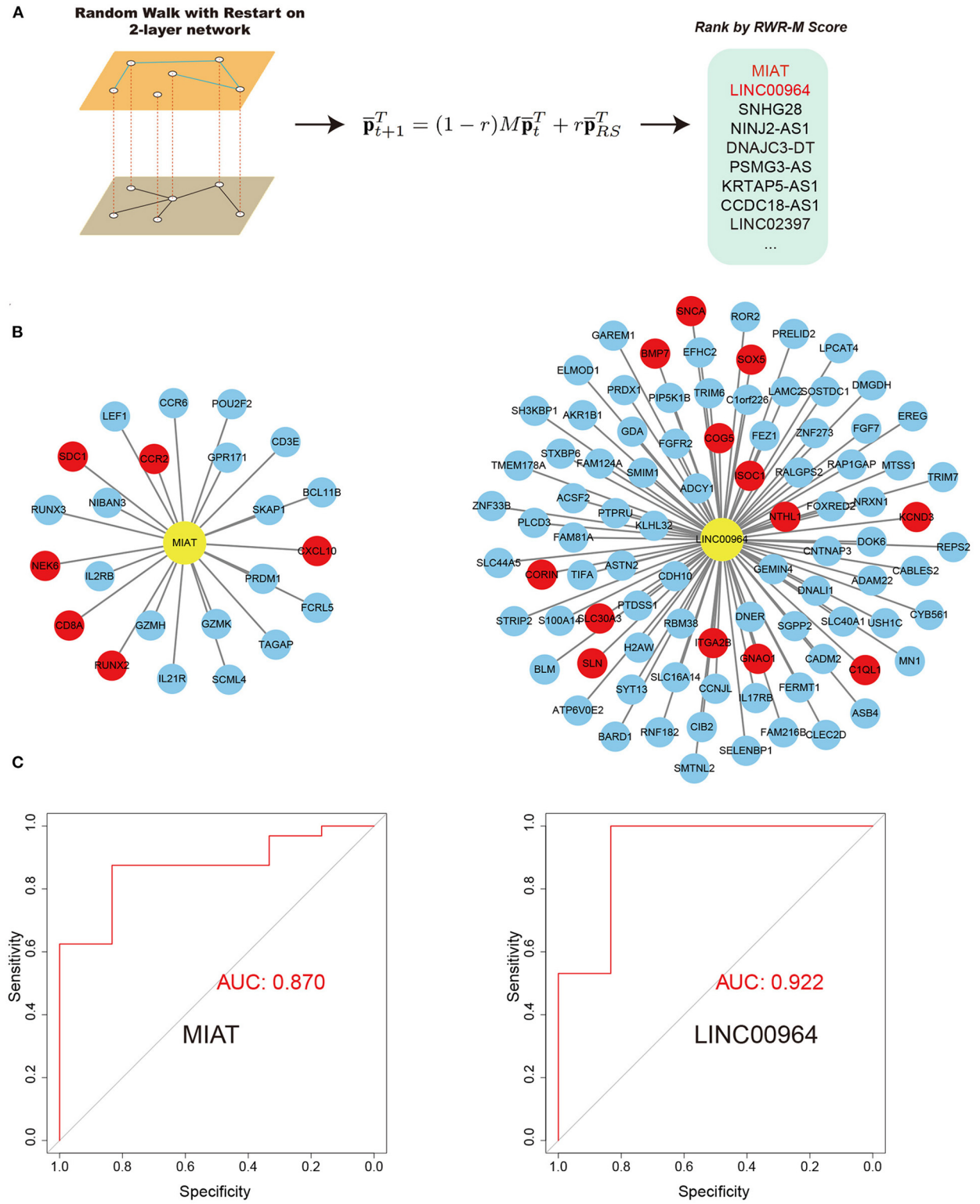

FIGURE 5 | RWR-M algorithm and the performance of random forest classifiers in the test set. **(A)** Process of RWR-M. **(B)** MIAT-related ceRNA pairs (left) and LINC00964-related ceRNA pairs (right). Yellow color represents lncRNAs and red color represents known AF protein-coding genes. **(C)** Performance of the MIAT-related ceRNA pairs-based classifier (left) and the LINC00964-related ceRNA pairs-based classifier (right), as reflected by their respective receiver operating characteristic curves.

the top 10 positively correlated gene sets were primarily involved in rhythm control-related processes. In addition, nearly all of the cardiac conduction–associated pathways were significantly positively correlated with LINC00964. For example, the Atrial_Cardiac_Muscle_Cell_Membrane_Repolarization pathway was correlated with LINC00964 with a regression coefficient of 0.178 and a *p*-value of 0.015. Taken together, these findings suggest that MIAT was closely associated with T cell activation, whereas LINC00964 was closely associated with atrial electrical remodeling.

Establishing a Classifier Based on Key lncRNA–mRNA Pairs

We reasoned that if MIAT and LINC00964 were important in AF, the expression values of their related ceRNA pairs would have the ability to discriminate persistent AF from SR. For each of the two lncRNAs, we extracted related ceRNA pairs in the network (**Figure 5B**) and constructed a classifier based on their expression values, using random forest algorithms. Before the random forest algorithm, we removed the batch effects associated with the microarray samples and the RNA sequencing samples that did not fit the interest (AF or SR) into the model to increase the power of the classifier as the microarray data and RNA sequencing data have high heterogeneity. The classifiers were first validated in the training set using a six-fold cross-validation method. Both MIAT-based and LINC00964-based classifiers showed a strong ability to discriminate AF from SR in the training set with AUC values of 0.810 and 0.940, respectively. We then evaluated their performances in the independent microarray data set. Promisingly, high AUC values were obtained for both classifiers, including 0.870 for the MIAT-based classifier and 0.922 for the LINC00964-based classifier (**Figure 5C**). These results further indicate the importance of these ceRNA pairs in AF pathogenesis and might provide new diagnostic tools for AF. In the sensitivity analysis, we determined the effects of retaining the batch effects, which resulted in the AUC values of the MIAT- and LINC00964-based classifiers for the independent test set being reduced to 0.75 and 0.70, respectively. This result highlights the importance of removing batch effects before constructing classifiers.

DISCUSSION

To our knowledge, this is the first study to identify AF susceptibility- and persistence-specific gene modules and ceRNA networks. The large sample size ensures that these results are more reliable than most previously conducted AF bioinformatic studies. By comparing the MEs from patients in SR who differed according to a history of previous AF (AF/SR vs. SR/SR), we identified two co-expression modules associated with AF susceptibility, both of which were primarily associated with inflammatory processes. By comparing the MEs from patients in AF rhythm with those from patients with a history of AF but in SR (AF/AF vs. AF/SR), we identified two co-expression modules associated with AF persistence, both of which primarily associated with the processes of electrical remodeling. These results were consistent with those of a previous study that compared the genome-wide mRNA microarray profiling of LAA tissues between AF/AF, AF/SR, and SR/SR patients (Deshmukh et al., 2015), in which altered transcriptional activity associated with inflammation and the remodeling of ion channel expression were also associated with AF susceptibility and persistence, respectively.

Our next goal was to construct ceRNA networks based on gene co-expression modules, which differed from a previous study (Qian et al., 2019) that used identified DEGs to predict AF-associated ceRNA pairs, which does not account for any interactions between genes. For each ceRNA network, the nodes were not only co-expressed, but also interacted functionally, and most of the nodes could communicate either directly or indirectly. The function of each network was closely associated with a specific feature of atrial remodeling, which could provide a better understanding of gene functions. For example, the identification of a gene in the turquoise ceRNA network could indicate a role in AF through the regulation of genes involved in electrical remodeling. This information might also help to relate genetics with epigenetics and disease phenotypes as 16 AF-GWAS-related genes were identified in the currently constructed electrical remodeling-related networks.

Another innovation of the present study was the application of the state-of-the-art RWR-M algorithm, which is an improvement on the RWR algorithm, to prioritize lncRNAs. Most previous studies (Song et al., 2016; Qian et al., 2019; Wang et al., 2020) use the RWR algorithm to identify new disease genes based on a single network. However, this approach ignores functional interactions, such as co-expression networks and co-annotation networks, and each type of network has different relationships, advantages, and biases (Lee et al., 2019). One should note that the RWR-M algorithm differs from the simple aggregation of various types of interactions into an aggregated network, which would dismiss the individual features and topologies of each network and has been shown to be less effective for prioritizing new disease genes than the RWR-M algorithm (Valdeolivas et al., 2019). By applying the RWR-M algorithm based on ceRNA language-guided and evidence-supported interactions identified by a previously published data set (Greene et al., 2015), MIAT and LINC00964 were identified as the top two genes with the highest proximities to known AF genes. After adjusting for the covariate of atrial rhythm, MIAT was significantly correlated with T cell activation, especially T helper 17 cells, whereas LINC00964 was correlated with rhythm control. Moreover, LINC00964 was also significantly correlated with the atrial electrical remodeling–related process. Using the random forest algorithm, we further demonstrated that their associated ceRNA pairs could distinguish persistent AF from SR patients in both the training set and an independent test set, further indicating the importance of MIAT and LINC00964 in AF susceptibility and persistence, respectively.

MIAT has been shown to promote cardiac fibrosis through the MIAT/miR-24/Furin/transforming growth factor (TGF)-beta 1 axis (Qu et al., 2017), promote cardiac hypertrophy through the miR-150/P300 axis (Zhu et al., 2016) and miR-93/TLR4 axis (Li et al., 2018), promote extracellular matrix deposition through the miR-29/COL1A1 and COL3A1 axes (Chuang et al., 2020), and regulate vascular endothelial cell function through the miR-150-5p/VEGF axis (Yan et al., 2015). Our study indicates that MIAT is a T cell activation–associated lncRNA, especially

Th17 cells, and is closely associated with AF susceptibility. This corroborates a recent study that found that cinnamaldehyde can ameliorate ulcerative colitis through the suppression of Th17 cells and the regulation of MIAT (Qu et al., 2020). The knockdown of MIAT has been shown to alleviate the inflammatory response and reduce intracellular oxidative stress in LPS-stimulated atrial HL-1 cells (Xing et al., 2020) and attenuate AF and AF-induced atrial fibrosis by targeting miR-133a-3p (Yao et al., 2020). Th17 cells are also suggested to contribute to AF susceptibility. Elevated plasma levels of Th17-related cytokines have been associated with a high risk of AF (Wu et al., 2016), and serum IL-17A levels are associated with AF recurrence (Xu et al., 2019). Experiments have also shown that Th17-produced IL-17A contributes to the development of AF by promoting inflammation and cardiac fibrosis (Fu et al., 2015). Other types of T cells, such as Th1, Th2, and Tregs, have also been implicated in AF (Liu et al., 2018). These studies are consistent with our finding and suggest the involvement of MIAT in AF through the mediation of T cell activation and inflammation. Targeting MIAT might prevent AF occurrence and recurrence.

We also identified LINC00964 as a central AF persistence-related lncRNA that is closely associated with atrial electrical remodeling. The function of LINC00964 has not previously been investigated. However, by searching the results of GWAS, we found that an AF-related single-nucleotide polymorphism (SNP), rs35006907, exists in the intronic region of LINC00964. The presence of SNPs in the promoter, intronic, or exonic regions of lncRNAs can affect transcription, structure, or function (Castellanos-Rubio and Ghosh, 2019). For example, the SNP rs11672691, located in the promoter region of lncRNA PCAT19, modulates the function and expression of PCAT19, promoting prostate cancer progression through the upregulation of cell cycle gene expression (Hua et al., 2018). By searching the expression quantitative trait loci (eQTLs) results from the Genotype-Tissue Expression (GTEx) consortium database (http://www.gtexportal.org/home/) version 8 (GTEx Consortium, 2015), rs35006907 was identified as being negatively correlated with LINC00964 expression levels, in both heart-atrial appendage tissue (normalized effect size $= -0.28$, $p = 2.7e{-}8$) and heart-left ventricle tissue (normalized effect size $= -0.35$, $p = 4.3e{-}13$). This direct evidence between SNP and gene expression indicates that the r35006907 SNP could promote AF persistence by negatively regulating the expression of LINC00964. The downregulation of LINC00964 expression would promote AF electrical remodeling by affecting the expression of ion channel–related genes in the turquoise ceRNA network.

Several limitations should be acknowledged in this study. First, the RNA sequencing technique that was used for GSE68868 was not specialized for the identification of lncRNAs; thus, only a small number of lncRNAs were available after filtering out low-expression genes. Second, lncRNAs can affect protein-coding gene function through diverse pathways, and we only considered the effects of the ceRNA mechanism. Third, lncRNAs or mRNAs can also communicate with each other through the ceRNA language, which was not analyzed. Finally, no attempt was made to validate the functions of the identified ceRNA pairs using an experimental model, and the causal relationships remain unclear.

In conclusion, our study constructed AF susceptibility- and persistence-associated ceRNA networks, identified relationships between genetic and epigenetic pathways, prioritized MIAT and LINC00964 as key lncRNAs, and constructed random forest classifiers based on their associated ceRNA pairs. These results will help us to better understand the mechanisms underlying AF from the ceRNA perspective and provide candidate therapeutic and diagnostic tools.

DATA AVAILABILITY STATEMENT

The original contributions presented in the study are included in the article/**Supplementary Material**, further inquiries can be directed to the corresponding author/s. A copy of the code used in this analysis is available at: https://github.com/Yaozhong-Liu/ceRNA_in_af.

AUTHOR CONTRIBUTIONS

YL performed the bioinformatic analysis and was a major contributor in writing the manuscript. NL and FB made important modifications to the manuscript. YL and QL designed the research project and created the final revision of the manuscript. All authors read and approved the final version of the manuscript.

FUNDING

This work was supported by grants from the National Key Research and Development Program of China (No. 2016YFC1301005) and the National Natural Science Foundation of China (No. 81770337).

ACKNOWLEDGMENTS

YL would like to thank Miss Wan Ziwei for her love.

SUPPLEMENTARY MATERIAL

The Supplementary Material for this article can be found online at: https://www.frontiersin.org/articles/10.3389/fgene.2021.653474/full#supplementary-material

REFERENCES

Castellanos-Rubio, A., and Ghosh, S. (2019). Disease-associated SNPs in inflammation-related lncRNAs. *Front. Immunol.* 10:420. doi: 10.3389/fimmu.2019.00420

Chuang, T. D., Ansari, A., Yu, C., Sakurai, R., Harb, A., Liu, J., et al. (2020). Mechanism underlying increased cardiac extracellular matrix deposition in perinatal nicotine-exposed offspring. *Am. J. Physiol. Heart Circ. Physiol.* 319, H651–60. doi: 10.1152/ajpheart.00021.2020

Chung, M. K., Refaat, M., Shen, W.-K., Kutyifa, V., Cha, Y.-M., Di Biase, L., et al. (2020). Atrial fibrillation: JACC council perspectives. *J. Am. Coll. Cardiol.* 75, 1689–1713. doi: 10.1016/j.jacc.2020.02.025

Deshmukh, A., Barnard, J., Sun, H., Newton, D., Castel, L., Pettersson, G., et al. (2015). Left atrial transcriptional changes associated with atrial fibrillation susceptibility and persistence. *Circ. Arrhyth. Electrophysiol.* 8, 32–41. doi: 10.1161/CIRCEP.114.001632

Fu, X. X., Zhao, N., Dong, Q., Du, L. L., Chen, X. J., Wu, Q. F., et al. (2015). Interleukin-17A contributes to the development of post-operative atrial fibrillation by regulating inflammation and fibrosis in rats with sterile pericarditis. *Int. J. Mol. Med*. 36, 83–92. doi: 10.3892/ijmm.2015.2204

Gautier, L., Cope, L., Bolstad, B. M., and Irizarry, R. A. (2004). affy-analysis of Affymetrix GeneChip data at the probe level. *Bioinformatics* 20, 307–315. doi: 10.1093/bioinformatics/btg405

Greene, C., Krishnan, A., Wong, A., Ricciotti, E., Zelaya, R., Himmelstein, D., et al. (2015). Understanding multicellular function and disease with human tissue-specific networks. *Nat. Genet.* 47, 569–576. doi: 10.1038/ng.3259

GTEx Consortium (2015). The genotype-tissue expression (GTEx) pilot analysis: multitissue gene regulation in humans. *Science* 348, 648–660. doi: 10.1126/science.1262110

Hänzelmann, S., Castelo, R., and Guinney, J. (2013). GSVA: gene set variation analysis for microarray and RNA-seq data. *BMC Bioinform.* 14:7. doi: 10.1186/1471-2105-14-7

Hindricks, G., Potpara, T., Dagres, N., Arbelo, E., Bax, J. J., Blomström-Lundqvist, C., et al. (2020). 2020 ESC guidelines for the diagnosis and management of atrial fibrillation developed in collaboration with the European Association of Cardio-Thoracic Surgery (EACTS). *Eur. Heart J.* 42, 373–498. doi: 10.1093/eurheartj/ehaa612

Hsu, J., Gore-Panter, S., Tchou, G., Castel, L., Lovano, B., Moravec, C., et al. (2018). Genetic control of left atrial gene expression yields insights into the genetic susceptibility for atrial fibrillation. *Circ. Genom. Precis. Med.* 11:e002107. doi: 10.1161/CIRCGEN.118.002107

Hua, J. T., Ahmed, M., Guo, H., Zhang, Y., Chen, S., Soares, F., et al. (2018). Risk SNP-mediated promoter-enhancer switching drives prostate cancer through lncRNA PCAT19. *Cell* 174, 564–75.e518. doi: 10.1016/j.cell.2018.06.014

Iwasaki, Y. K., Nishida, K., Kato, T., and Nattel, S. (2011). Atrial fibrillation pathophysiology: implications for management. *Circulation* 124, 2264–2274. doi: 10.1161/CIRCULATIONAHA.111.019893

Karagkouni, D., Paraskevopoulou, M., Chatzopoulos, S., Vlachos, I., Tastsoglou, S., Kanellos, I., et al. (2018). DIANA-TarBase v8: a decade-long collection of experimentally supported miRNA-gene interactions. *Nucleic Acids Res.* 46, D239–D245. doi: 10.1093/nar/gkx1141

Kornej, J., Börschel, C. S., Benjamin, E. J., and Schnabel, R. B. (2020). Epidemiology of atrial fibrillation in the 21st century: novel methods and new insights. *Circ. Res.* 127, 4–20. doi: 10.1161/CIRCRESAHA.120.316340

Langfelder, P., and Horvath, S. (2008). WGCNA: an R package for weighted correlation network analysis. *BMC Bioinform.* 9:559. doi: 10.1186/1471-2105-9-559

Lee, B., Zhang, S., Poleksic, A., and Xie, L. (2019). Heterogeneous multi-layered network model for omics data integration and analysis. *Front. Genet.* 10:1381. doi: 10.3389/fgene.2019.01381

Leek, J., Johnson, W., Parker, H., Jaffe, A., and Storey, J. (2012). The sva package for removing batch effects and other unwanted variation in high-throughput experiments. *Bioinformatics* 28, 882–883. doi: 10.1093/bioinformatics/bts034

Leek, J., Scharpf, R., Bravo, H., Simcha, D., Langmead, B., Johnson, W., et al. (2010). Tackling the widespread and critical impact of batch effects in high-throughput data. *Nat. Rev. Genet.* 11, 733–739. doi: 10.1038/nrg2825

Leek, J., and Storey, J. (2007). Capturing heterogeneity in gene expression studies by surrogate variable analysis. *PLoS Genet.* 3, 1724–1735. doi: 10.1371/journal.pgen.0030161

Li, N., and Brundel, B. (2020). Inflammasomes and proteostasis novel molecular mechanisms associated with atrial fibrillation. *Circ. Res.* 127, 73–90. doi: 10.1161/CIRCRESAHA.119.316364

Li, Y., Wang, J., Sun, L., and Zhu, S. (2018). LncRNA myocardial infarction-associated transcript (MIAT) contributed to cardiac hypertrophy by regulating TLR4 via miR-93. *Eur. J. Pharmacol.* 818, 508–517. doi: 10.1016/j.ejphar.2017.11.031

Liaw, A., and Wiener, M. (2002). Classification and regression by randomForest. *R News* 23, 18–22. doi: 10.1057/9780230509993

Liu, Y., Shi, Q., Ma, Y., and Liu, Q. (2018). The role of immune cells in atrial fibrillation. *J. Mol. Cell Cardiol.* 123, 198–208. doi: 10.1016/j.yjmcc.2018.09.007

Love, M., Huber, W., and Anders, S. (2014). Moderated estimation of fold change and dispersion for RNA-seq data with DESeq2. *Genome Biol.* 15:550. doi: 10.1186/s13059-014-0550-8

Luo, X., Yang, B., and Nattel, S. (2015). MicroRNAs and atrial fibrillation: mechanisms and translational potential. *Nat. Rev. Cardiol.* 12, 80–90. doi: 10.1038/nrcardio.2014.178

Lv, X., Li, J., Hu, Y., Wang, S., Yang, C., Li, C., et al. (2019). Overexpression of miR-27b-3p targeting Wnt3a regulates the signaling pathway of Wnt/β-catenin and attenuates atrial fibrosis in rats with atrial fibrillation. *Oxid. Med. Cell. Longev.* 2019:5703764. doi: 10.1155/2019/5703764

Mootha, V. K., Lindgren, C. M., Eriksson, K.-F., Subramanian, A., Sihag, S., Lehar, J., et al. (2003). PGC-1α-responsive genes involved in oxidative phosphorylation are coordinately downregulated in human diabetes. *Nat. Genet.* 34, 267–273. doi: 10.1038/ng1180

Nattel, S., Guasch, E., Savelieva, I., Cosio, F., Valverde, I., Halperin, J., et al. (2014). Early management of atrial fibrillation to prevent cardiovascular complications. *Eur. Heart J.* 35, 1448–1456. doi: 10.1093/eurheartj/ehu028

Nattel, S., and Harada, M. (2014). Atrial remodeling and atrial fibrillation: recent advances and translational perspectives. *J. Am. Coll. Cardiol.* 63, 2335–2345. doi: 10.1016/j.jacc.2014.02.555

Nattel, S., Heijman, J., Zhou, L., and Dobrev, D. (2020). Molecular basis of atrial fibrillation pathophysiology and therapy: a translational perspective. *Circ. Res.* 127, 51–72. doi: 10.1161/CIRCRESAHA.120.316363

Nielsen, J. B., Thorolfsdottir, R. B., Fritsche, L. G., Zhou, W., Skov, M. W., Graham, S. E., et al. (2018). Biobank-driven genomic discovery yields new insight into atrial fibrillation biology. *Nat. Genet.* 50, 1234–1239. doi: 10.1038/s41588-018-0171-3

Paraskevopoulou, M., Vlachos, I., Karagkouni, D., Georgakilas, G., Kanellos, I., Vergoulis, T., et al. (2016). DIANA-LncBase v2: indexing microRNA targets on non-coding transcripts. *Nucleic Acids Res.* 44, D231–238. doi: 10.1093/nar/gkv1270

Parsana, P., Ruberman, C., Jaffe, A., Schatz, M., Battle, A., and Leek, J. (2019). Addressing confounding artifacts in reconstruction of gene co-expression networks. *Genome Biol.* 20:94. doi: 10.1186/s13059-019-1700-9

Piñero, J., Bravo, À., Queralt-Rosinach, N., Gutiérrez-Sacristán, A., Deu-Pons, J., Centeno, E., et al. (2017). DisGeNET: a comprehensive platform integrating information on human disease-associated genes and variants. *Nucleic Acids Res.* 45, D833–D839. doi: 10.1093/nar/gkw943

Pletscher-Frankild, S., Pallejà, A., Tsafou, K., Binder, J., and Jensen, L. (2015). DISEASES: text mining and data integration of disease-gene associations. *Methods* 74, 83–89. doi: 10.1016/j.ymeth.2014.11.020

Qian, C., Li, H., Chang, D., Wei, B., and Wang, Y. (2019). Identification of functional lncRNAs in atrial fibrillation by integrative analysis of the lncRNA-mRNA network based on competing endogenous RNAs hypothesis. *J. Cell. Physiol.* 234, 11620–11630. doi: 10.1002/jcp.27819

Qu, S. L., Chen, L., Wen, X. S., Zuo, J. P., Wang, X. Y., Lu, Z. J., et al. (2020). Suppression of Th17 cell differentiation via sphingosine-1-phosphate receptor 2 by cinnamaldehyde can ameliorate ulcerative colitis. *Biomed. Pharmacother.* 134:111116. doi: 10.1016/j.biopha.2020.111116

Qu, X., Du, Y., Shu, Y., Gao, M., Sun, F., Luo, S., et al. (2017). MIAT is a pro-fibrotic long non-coding RNA governing cardiac fibrosis in post-infarct myocardium. *Sci. Rep.* 7:42657. doi: 10.1038/srep42657

Rappaport, N., Twik, M., Plaschkes, I., Nudel, R., Iny Stein, T., Levitt, J., et al. (2017). MalaCards: an amalgamated human disease compendium with diverse clinical and genetic annotation and structured search. *Nucleic Acids Res.* 45, D877–D887. doi: 10.1093/nar/gkw1012

Ravasz, E., Somera, A., Mongru, D., Oltvai, Z., and Barabási, A. (2002). Hierarchical organization of modularity in metabolic networks. *Science* 297, 1551–1555. doi: 10.1126/science.1073374

Roselli, C., Chaffin, M. D., Weng, L. C., Aeschbacher, S., Ahlberg, G., Albert, C. M., et al. (2018). Multi-ethnic genome-wide association study for atrial fibrillation. *Nat. Genet.* 50, 1225–1233. doi: 10.1038/s41588-018-0133-9

Roselli, C., Rienstra, M., and Ellinor, P. T. (2020). Genetics of atrial fibrillation in 2020: GWAS, genome sequencing, polygenic risk, and beyond. *Circ. Res.* 127, 21–33. doi: 10.1161/CIRCRESAHA.120.316575

Salmena, L., Poliseno, L., Tay, Y., Kats, L., and Pandolfi, P. P. (2011). A ceRNA hypothesis: the Rosetta Stone of a hidden RNA language? *Cell* 146, 353–358. doi: 10.1016/j.cell.2011.07.014

Song, C., Zhang, J., Liu, Y., Pan, H., Qi, H. P., Cao, Y. G., et al. (2016). Construction and analysis of cardiac hypertrophy-associated lncRNA-mRNA network based on competitive endogenous RNA reveal functional lncRNAs in cardiac hypertrophy. *Oncotarget* 7, 10827–10840. doi: 10.18632/oncotarget.7312

Tay, Y., Rinn, J., and Pandolfi, P. P. (2014). The multilayered complexity of ceRNA crosstalk and competition. *Nature* 505, 344–352. doi: 10.1038/nature12986

Valdeolivas, A., Tichit, L., Navarro, C., Perrin, S., Odelin, G., Levy, N., et al. (2019). Random walk with restart on multiplex and heterogeneous biological networks. *Bioinformatics* 35, 497–505. doi: 10.1093/bioinformatics/bty637

Virani, S., Alonso, A., Benjamin, E., Bittencourt, M., Callaway, C., Carson, A., et al. (2020). Heart disease and stroke statistics-2020 update: a report from the American Heart Association. *Circulation* 141, e139–e596. doi: 10.1161/CIR.0000000000000757

Wang, K., Long, B., Zhou, L. Y., Liu, F., Zhou, Q. Y., Liu, C. Y., et al. (2014). CARL lncRNA inhibits anoxia-induced mitochondrial fission and apoptosis in cardiomyocytes by impairing miR-539-dependent PHB2 downregulation. *Nat. Commun.* 5:3596. doi: 10.1038/ncomms4596

Wang, M., Zheng, S., Li, X., Ding, Y., Zhang, M., Lin, L., et al. (2020). Integrated analysis of lncRNA-miRNA-mRNA ceRNA network identified lncRNA EPB41L4A-AS1 as a potential biomarker in non-small cell lung cancer. *Front. Genet.* 11:1130. doi: 10.3389/fgene.2020.511676

Weng, L. C., Choi, S. H., Klarin, D., Smith, J. G., Loh, P. R., Chaffin, M., et al. (2017). Heritability of atrial fibrillation. *Circ. Cardiovasc. Genet.* 10:e001838. doi: 10.1161/CIRCGENETICS.117.001838

Wu, N., Xu, B., Liu, Y., Chen, X., Tang, H., Wu, L., et al. (2016). Elevated plasma levels of Th17-related cytokines are associated with increased risk of atrial fibrillation. *Sci. Rep.* 6:26543. doi: 10.1038/srep26543

Xing, P. C., An, P., Hu, G. Y., Wang, D. L., and Zhou, M. J. (2020). LncRNA MIAT promotes inflammation and oxidative stress in sepsis-induced cardiac injury by targeting miR-330-5p/TRAF6/NF-κB Axis. *Biochem. Genet.* 58, 783–800. doi: 10.1007/s10528-020-09976-9

Xu, L., Wang, N., Liang, Y., Zhou, H., and Yan, J. (2019). Interleukin-17A contributes to atrial fibrillation recurrence and left atrial reservoir function after catheter ablation. *Pol. Arch. Intern. Med.* 129, 432–435. doi: 10.20452/pamw.4489

Yan, B., Yao, J., Liu, J. Y., Li, X. M., Wang, X. Q., Li, Y. J., et al. (2015). lncRNA-MIAT regulates microvascular dysfunction by functioning as a competing endogenous RNA. *Circ. Res.* 116, 1143–1156. doi: 10.1161/CIRCRESAHA.116.305510

Yang, Z., Xiao, Z., Guo, H., Fang, X., Liang, J., Zhu, J., et al. (2019). Novel role of the clustered miR-23b-3p and miR-27b-3p in enhanced expression of fibrosis-associated genes by targeting TGFBR3 in atrial fibroblasts. *J. Cell. Mol. Med.* 23, 3246–3256. doi: 10.1111/jcmm.14211

Yao, L., Zhou, B., You, L., Hu, H., and Xie, R. (2020). LncRNA MIAT/miR-133a-3p axis regulates atrial fibrillation and atrial fibrillation-induced myocardial fibrosis. *Mol. Biol. Rep.* 47, 2605–2617. doi: 10.1007/s11033-020-05347-0

Yeh, Y., Kuo, C., Lee, Y., Lin, Y., Nattel, S., Tsai, F., et al. (2013). Region-specific gene expression profiles in the left atria of patients with valvular atrial fibrillation. *Heart Rhythm* 10, 383–391. doi: 10.1016/j.hrthm.2012.11.013

Yu, G., Wang, L. G., Han, Y., and He, Q. Y. (2012). clusterProfiler: an R package for comparing biological themes among gene clusters. *Omics* 16, 284–287. doi: 10.1089/omi.2011.0118

Zhang, B., and Horvath, S. (2005). A general framework for weighted gene co-expression network analysis. *Stat. Appl. Genet. Mol. Biol.* 4:17. doi: 10.2202/1544-6115.1128

Zhu, X. H., Yuan, Y. X., Rao, S. L., and Wang, P. (2016). LncRNA MIAT enhances cardiac hypertrophy partly through sponging miR-150. *Eur. Rev. Med. Pharmacol. Sci.* 20, 3653–3660.

Zhu, Y., Feng, Z., Cheng, W., and Xiao, Y. (2018). MicroRNA-34a mediates atrial fibrillation through regulation of Ankyrin-B expression. *Mol. Med. Rep.* 17, 8457–8465. doi: 10.3892/mmr.2018.8873

Conflict of Interest: The authors declare that the research was conducted in the absence of any commercial or financial relationships that could be construed as a potential conflict of interest.

frontiers in Genetics

ORIGINAL RESEARCH
published: 03 August 2021
doi: 10.3389/fgene.2021.689916

SNAI2-Induced CircMTO1 Promotes Cell Proliferation and Inhibits Apoptosis Through the miR-320b/MCL1 Axis in Human Granulosa-Like Tumor Cells

Jie Duan[1,2*†], *Hongning Cai*[3,4†], *Yanming Huang*[1,2] *and Liangyan Shi*[1,2]

[1] *Department of Gynecology, Maternal and Child Health Hospital of Hubei Province, Wuhan, China,* [2] *Department of Gynecology, Women and Children's Hospital of Hubei Province, Wuhan, China,* [3] *Department of Gynecology II, Maternal and Child Health Hospital of Hubei Province, Wuhan, China,* [4] *Department of Gynecology II, Women and Children's Hospital of Hubei Province, Wuhan, China*

OPEN ACCESS

Edited by:
Detu Zhu,
Cornell University,
United States

Reviewed by:
Liang-Ting Lin,
Hong Kong Polytechnic University,
China
Elif Pala,
Sanko University, Turkey

***Correspondence:**
Jie Duan
xiaojie5077@126.com

[†]*These authors share first authorship*

Specialty section:
This article was submitted to RNA, a section of the journal Frontiers in Genetics

Received: *01 April 2021*
Accepted: *12 July 2021*
Published: *03 August 2021*

Citation:
Duan J, Cai H, Huang Y and Shi L (2021) SNAI2-Induced CircMTO1 Promotes Cell Proliferation and Inhibits Apoptosis Through the miR-320b/MCL1 Axis in Human Granulosa-Like Tumor Cells. Front. Genet. 12:689916. doi: 10.3389/fgene.2021.689916

Polycystic ovary syndrome (PCOS), one of the most common types of endocrine diseases, is characterized by a high prevalence among women of reproductive-age. However, its pathogenesis and molecular mechanisms remain unclear. CircMTO1 has been reported to participate in numerous biological processes, but, its role in PCOS progression remains unknown. In the current study, we elucidated the expression and circRNA characterization of circMTO1 in human granulosa-like tumor cells. We found that circMTO1 knockdown promoted human granulosa-like tumor cell proliferation and inhibited its apoptosis rate. Next, we explored the underlying molecular mechanisms by using a series of experiments. Our results revealed the effect of the novel circMTO1/miR-320b/MCL1 axis in human granulosa-like tumor cells. Furthermore, we found that the expression of circMTO1 was induced by Snail family transcriptional repressor 2 (SNAI2) in human granulosa-like tumor cells. Our results may provide potential targets for PCOS research and a novel direction for the diagnosis and treatment of PCOS.

Keywords: circular RNA, circMTO1, miR-320b, MCL1, SNAI2, polycystic ovaries syndrome

INTRODUCTION

Polycystic ovary syndrome (PCOS),one of the most common types of endocrine diseases, occurs in about 5–10% of women of reproductive age worldwide (Azziz et al., 2004). Multiple risk factors, such as hyperinsulinemia, polycystic ovaries, and dysfunction of the ovulatory cycle (Azziz et al., 2006; Diamanti-Kandarakis and Dunaif, 2012) lead to its high prevalence and considerable burden for clinical management. However, the pathogenesis and molecular mechanisms of PCOS remain

Abbreviations: cicrRNA, circular RNA; PCOS, Polycystic ovary syndrome; qRT-PCR, quantitative reverse transcription polymerase chain reaction; FISH, Fluorescent *In Situ* Hybridization; RIP, RNA-binding protein immunoprecipitation assay; CCK-8, Cell Counting Kit-8; MCL1, MCL1 Apoptosis Regulator; GAPDH, Glyceraldehyde-3-Phosphate Dehydrogenase; circMTO1, circular RNA Mitochondrial TRNA Translation Optimization 1; SNAI2, Snail Family Transcriptional Repressor 2; siRNA, small interfering RNA.

poorly understood. Therefore, finding new potential targets for understanding the progression of PCOS is urgently needed.

Previous studies have demonstrated that granulosa cells (GCs) may play an essential role in PCOS development. In comparison with GCs from women with normal ovulatory cycles, GCs from PCOS patients have lower proliferation and apoptosis ability than GCs from women with normal ovulatory cycles (Das et al., 2008). Human granulosa-like tumor cells (KGN and SVOG) have similar pathological features to GCs, and could be well-cultured (Nishi et al., 2001); therefore, KGN and SVOG cells have been widely used in PCOS research (Zhang et al., 2010; Han et al., 2018; Li M. et al., 2019; Chen et al., 2020). Indeed, human granulosa-like tumor cells represent a promising research direction for PCOS therapeutic targets.

With the technological innovations in high-throughput sequencing (RNA-seq) over the past two decades, the structure and biological functions of circular RNAs (circRNAs) have been intensely studied (Patop et al., 2019). CircRNA is a covalently closed RNA without polyadenylation (Jeck and Sharpless, 2014) and is abundantly expressed and conserved in eukaryotic organisms (Jeck et al., 2013). Mechanistically, circRNAs are mainly considered as post-transcriptional regulators that act as sponges for microRNAs (miRNAs) and affect the binding capability of messenger RNAs (mRNAs) to downstream factors (Hansen et al., 2013; Memczak et al., 2013). Circular RNAs interact with proteins and even translate proteins (Hentze and Preiss, 2013; Legnini et al., 2017; Yang et al., 2017). Biologically, the essential roles of circRNAs in multiple cellular processes have been widely reported, including proliferation, apoptosis, migration, invasion, and angiogenesis (Bian et al., 2018; Liu et al., 2018; Ouyang et al., 2019; Song et al., 2019; Zhou et al., 2019).

CircRNA expression profiles have been studied in detail in PCOS (Che et al., 2019; Wang et al., 2019; Zhang C. et al., 2019). Lu et al. (2020) found that CiRS-126 acts as a sponge for miR-21 to inhibit ovarian granulosa cell viability. Deng et al. (2020) reported that circPUM1 regulates PCOS development by interacting with miR-760. These studies indicate the crucial role of circRNAs in PCOS progression. CircRNA mitochondrial translation optimization 1 (MTO1 homolog; hsa_circRNA_0007874/hsa_circRNA_104135) has been found to participate in the progression of multiple diseases, including hepatocellular carcinoma, cervical cancer, rectal cancer, and acute kidney injury (Han et al., 2017; Chen et al., 2019; Shi et al., 2020). Several studies have reported the modulation of circMTO1 of cell proliferation behavior (Ge et al., 2018; Zhang X. et al., 2019; Wang N. et al., 2020). However, the involvement of circMTO1 in the cellular progression of human granulosa-like tumor cells remains unclear.

In this study, we aimed to elucidate the function of circMTO1 in human granulosa-like tumor cells. Our study revealed the expression and circRNA characterization of circMTO1 in human granulosa-like tumor cells. We performed CCK8 and flow cytometry to elucidate the cellular effects of circMTO1 on human granulosa-like tumor cells. Further, we explored the underlying molecular mechanisms and subsequently demonstrated a novel snail family transcriptional repressor 2 (SNAI2)/circMTO1/miR-320b/MCL1 axis in PCOS cellular progression.

MATERIALS AND METHODS

Cell Culture and Transfection

Human granulosa-like tumor cell lines (KGN and SVOG cells) and 293T cells were purchased from the Cell Bank of the Chinese Academy of Sciences (Shanghai, China). DMEM high glucose (HyClone, Logan, UT, United States) supplemented with 10% FBS (BI, Israel) was used to culture cells in an environment containing 5% CO_2 at 37°C. All lentiviruses, siRNAs, and plasmids were synthesized by GeneChem (Shanghai, China). Lipofectamine 3,000 (Invitrogen) was used to perform all transfections according to the manufacturer's instructions.

RNA Isolation and Quantitation and RNase R Treatment

We used TRIzol reagent (Invitrogen) was used to harvest RNA from the cells. A superscript RT Kit (TOYOBO) was used to reverse transcribe cDNA following the manufacturer's protocol. For miRNA detection, a TaqMan MicroRNA Assay (Applied Biosystems, United States) using a specific TaqMan miRNA probes hsa-miR-320b (ID 002844) (Applied Biosystems, United States) was applied following the manufacturer's protocols. RNA quality was assessed using a NanoDrop 2,000 spectrophotometer (Thermo Fisher Scientific, United States). GAPDH and U6 were used as the internal controls. RNA levels were detected using a 7,500 Fast PCR instrument (Applied Biosystems, United States). RNA expression fold change level was presented by the $2^{-\Delta\Delta Ct}$ method. For RNase R treatment, 3 U/mg of RNase R (Epicenter, United States) was used to digest 1 μg of RNA for 30 min at 37°C, following the manufacturer's instructions. The stability of mMTO1 and circMTO1 was assessed by RT-PCR assay. Target values were assessed using the 2-ΔΔCT method. The primer sequence information was as follows: circMTO1; 5′-GAGCTGTAGAAGATCTTATTC-3′(F), 5′-CACAGGCCATCCAAGGCATC-3′(R), miR-320b; RT primer: 5′GTCGTATCCAGTGCAGGGTCCGAGGTATTCGCACTGGATACGACTTTTCGAC 3′, 5′ TCCGAAACGGGAGAGTTGG 3′(F), 5′ GTGCAGGGTCCGAGGT 3′ (R); MCL1; 5′-GCTGCATCGAACCATTAGCA-3′(F), 5′-ATGCCAAACCAGCTCCTACT-3′(R), SNAI2; 5′-GTATCTCTATGAGAGTTACTCCATGCCTG-3′ (F), 5′-TTACATCAGAATGGGTCTGCAGATGAGC-3′ (R); GAPDH; 5′ GCACCGTCAAGGCTGAGAAC 3′(F), 5′ TGGTGAAGACGCCAGTGGA 3′(R), U6; 5′ TCCGATCGTGAAGCGTTC 3′(F), 5′ GTGCAGGGTCCGAGGT 3′(R).

Western Blot

Total proteins were isolated using radioimmunoprecipitation assay buffer (Thermo Scientific). Protein quantification was performed using a BCA protein concentration assay kit (Solarbio). Proteins were separated by SDS-PAGE on a 10% gel and transferred onto polyvinylidene fluoride membranes (Millipore, United States). Subsequently, the membranes were subjected to 5% non-fat milk (Sangon, China) for 45 min. The membranes were then incubated with primary antibodies for 12 h at 4°C. The membranes were washed 3 times with TBS-T

and then incubated with secondary antibodies for 1.5 h at 23°C. The experimental results were visualized using an image analysis system (WD-9413B, Liuyi, Beijing, China). The antibodies used in this study were as follows: MCL1 (1:1,000, CST, 94296S), GAPDH (1:1,000, CST, 5174S).

RNA Fluorescence *in situ* Hybridization (FISH) Assay

A fluorescent *in situ* hybridization (FISH) kit (RiboBio, China) was used to conduct our RNA FISH experiment following the manufacturer's protocol. The probes used in this study were purchased from GeneChem (Shanghai, China). The experimental results were visualized using confocal microscopy.

Cell Viability Detection

Cell Counting kit-8 (CCK8, Dojindo, Japan) was used to measure cell viability following the manufacturer's protocol. A 96-well plate was used to seed the cells (2×10^4 cells per well). 2 days later, we added 10 μl CCK-8 solution was added to the culture cells for 120 min. The OD values of the cells were measured at a wavelength of 450 nm.

Cell Apoptosis Measurement

The apoptosis rate of the cells was assessed using flow cytometry (BD Biosciences, United States). First, the cells were collected and resuspended in a binding buffer. Second, cells were cultured with 0.25 mg/ml Annexin V-FITC (Dojindo, Japan) and 10 mg/ml propidium iodide (Dojindo, Japan) in a dark environment at room temperature for 30 min. Finally, the treated cells were subjected to flow cytometry for apoptosis analysis.

Biotinylated RNA Pull-Down

Biotinylated RNA probes were obtained from GenePharma (Shanghai, China). After transfection for 2 days, the cells were

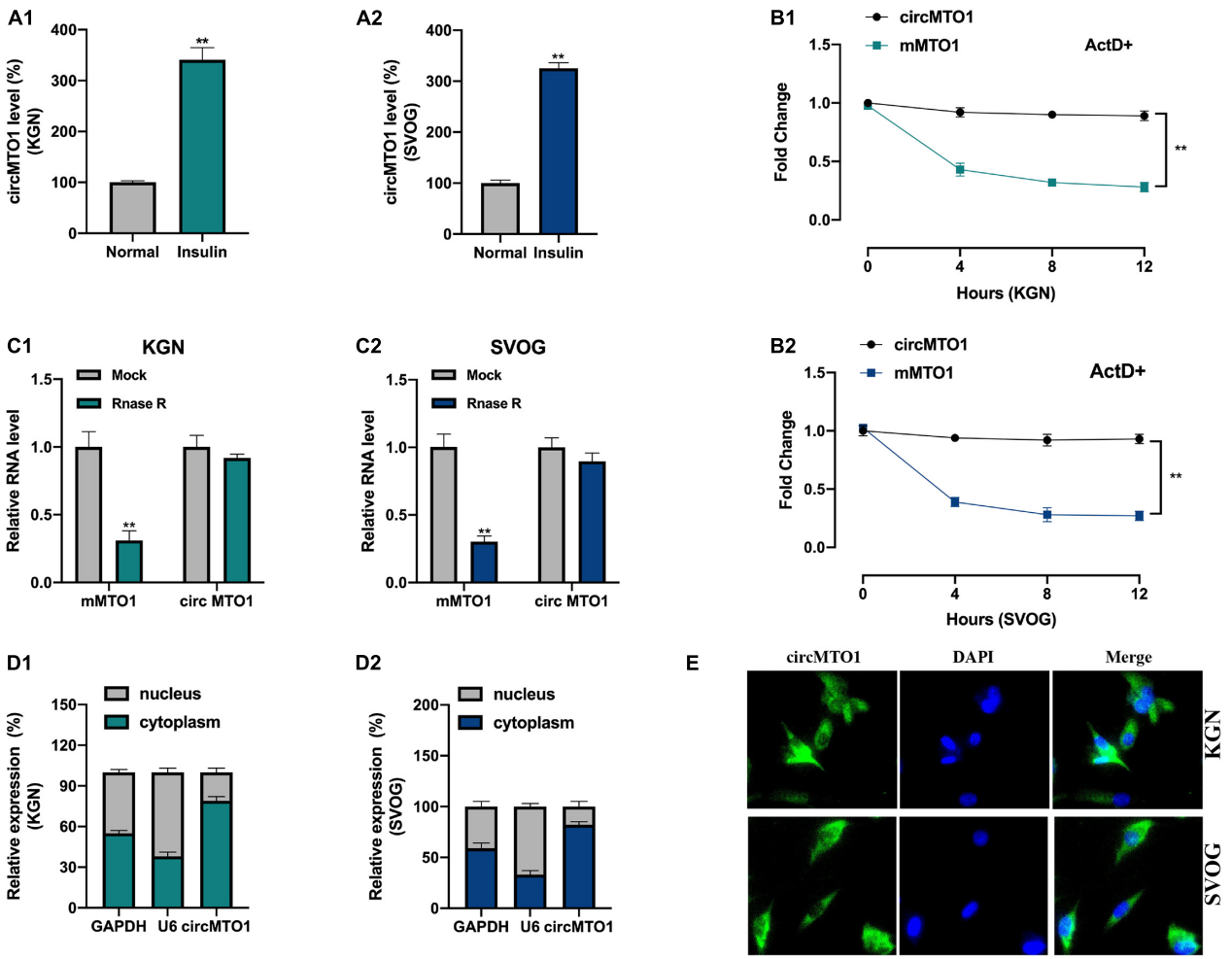

FIGURE 1 | Characterization of circMTO1 in Human granulosa-like tumor cells. **(A1,A2)** Relative circMTO1 expression in insulin-treated Human granulosa-like tumor cells was detected by qRT-PCR. **(B)** Relative expression level of circMTO1 and liner MTO1 (mMTO1) in KGN **(B1)** and SVOG **(B2)** cells after treated with ActD were evaluated by qRT-PCR. **(C)** Relative expression of circMTO1 and mMTO1 in KGN **(C1)** and SVOG **(C2)** after treatment with RNase R were assessed by qRT-PCR. **(D)** The distribution of circMTO1 in KGN **(D1)** and SVOG **(D2)** cells was measured using qRT-PCR. **(E)** The location of circMTO1 in Human granulosa-like tumor cells was detected using the FISH assay. All assays were repeated 3 times, $^*P < 0.01$.

washed with PBS and cultured on ice for 10 min. Total RNA was isolated from the cells pre-transfected with biotinylated RNA. RNA was purified by centrifugation, and 100 ml purified RNA was collected as input. We added M-280 streptavidin magnetic beads (Sigma) to the cell lysates. Trizol was used to purify the bound RNA for analysis.

RNA Immunoprecipitation

We used a Magna RIP^{TM} RNA-Binding Protein Immunoprecipitation Kit (Millipore, Bedford, MA, United States) for the RNA immunoprecipitation assay, following the manufacturer's instructions. AGO2 and IgG antibodies were used. We then conducted a qRT-PCR experiment to analyze the bound RNA.

Dual-Luciferase Reporter Gene Assay

The pmirGLO plasmids harboring the sequences of circMTO1 WT/MUT and MCL1 WT/MUT were synthesized and commercially procured from GenePharma (Shanghai, China). All the transfection processes were performed using Lipofectamine 3,000 (Invitrogen). After transfection, the luciferase activity was measured and recorded.

Statistical Analysis

We used IBM SPSS Statistics for Windows, Version 21.0 (IBM Corp., Armonk, NY) to analyze data from the experiment results. All data are presented as the mean ± standard deviation (SD). For the measurement of data from two groups, we used Student's *t*-test, and for data from three or more groups, we employed a one-way analysis of variance. All experiments were repeated at least 3 times unless otherwise stated. Differences were considered statistically significant at $P < 0.05$.

RESULTS

Characterization and Biological Behavior of CircMTO1 in Human Granulosa-Like Tumor Cells

Initially, we assessed the expression levels of circMTO1 in human granulosa-like tumor cells after insulin treatment. As shown in **Figures 1A1,A2**, the levels of circMTO1 in KGN and SVOG cells were upregulated upon insulin treatment. Next, we verified circRNA characterization of circMTO1 in human granulosa-like tumor cells. Upon ActD treatment, MTO1 mRNA was obviously

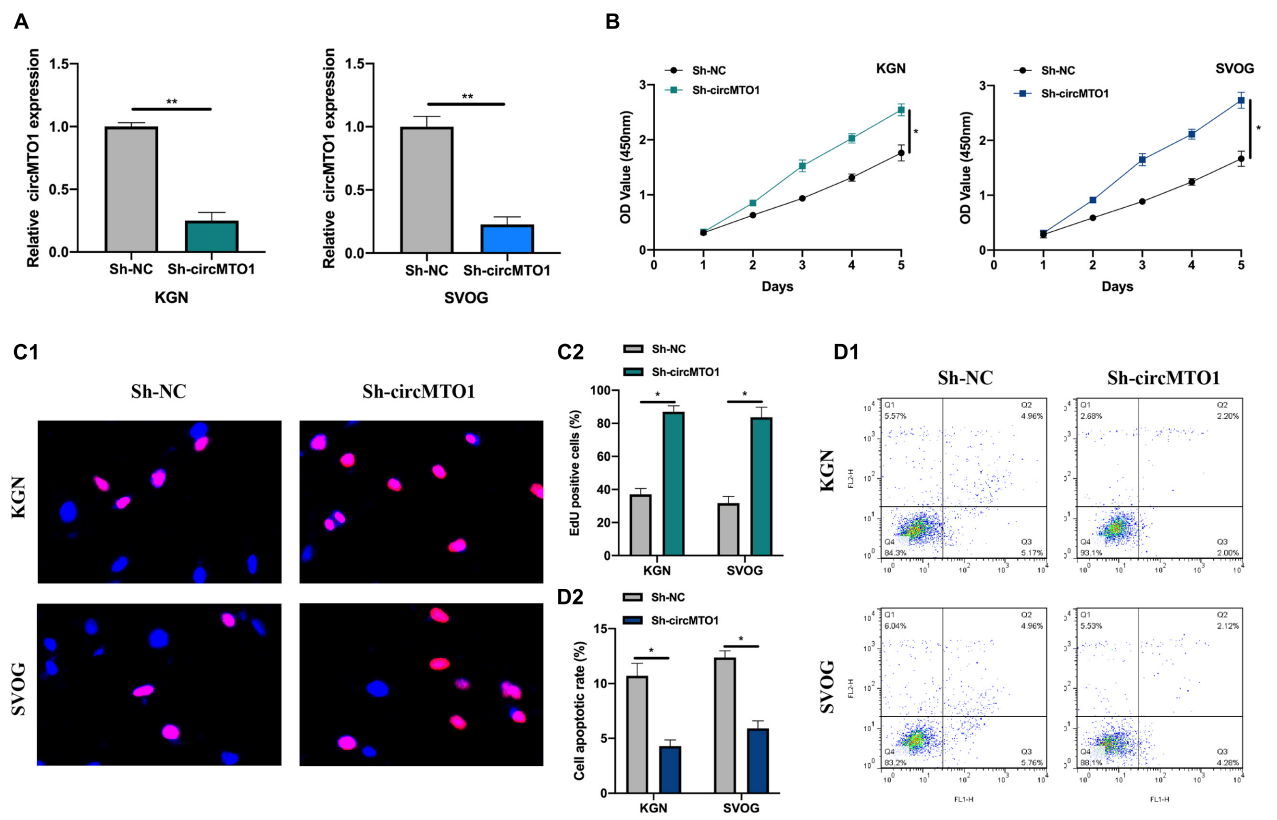

FIGURE 2 | Biological behavior of circMTO1 in Human granulosa-like tumor cells. **(A)** The statistical circMTO1 knockdown cell models were constructed, expression level of circMTO1 in indicated cells was measured by qRT-PCR. **(B)** The proliferation level of circMTO1 knockdown cells was assessed by CCK-8 assay. **(C)** EdU assay was conducted to evaluate the effect of downregulated circMTO1 on the proliferation abilities of human granulosa-like tumor cells **(C1)**; statistical analysis was showed **(C2)**. **(D)** Flow cytometry experiment was conducted to measure cell apoptotic rate of circMTO1 knockdown human granulosa-like tumor cells **(D1)**, statistical results were analyzed **(D2)**. All experiments were conducted 3 times. $^{*}P < 0.05$, $^{**}P < 0.01$.

degraded, but not circMTO1 (**Figures 1B1,B2**). Our results also suggested that the level of MTO1 mRNA, but not its circular form (circRNA), in human granulosa-like tumor cells was significantly decreased by RNase R treatment (**Figures 1C1,C2**). We found that circMTO1 was mainly located in the cytoplasm of human granulosa-like tumor cells (**Figures 1D1,D2,E**).

Subsequently, we evaluated the biological function of circMTO1 in human granulosa-like tumor cells. CircMTO1 knockdown cell models were constructed (**Figure 2A**). Using CCK-8 and EdU assays, we verified that circMTO1 knockdown promoted PCOS cell proliferation (**Figures 2B,C1,C2**). The flow cytometry experiment results indicated that circMTO1 knockdown inhibited the apoptotic rate of human granulosa-like tumor cells (**Figures 2D1,D2**). These results suggest that circMTO1 is involved in the cellular processes of human granulosa-like tumor cells.

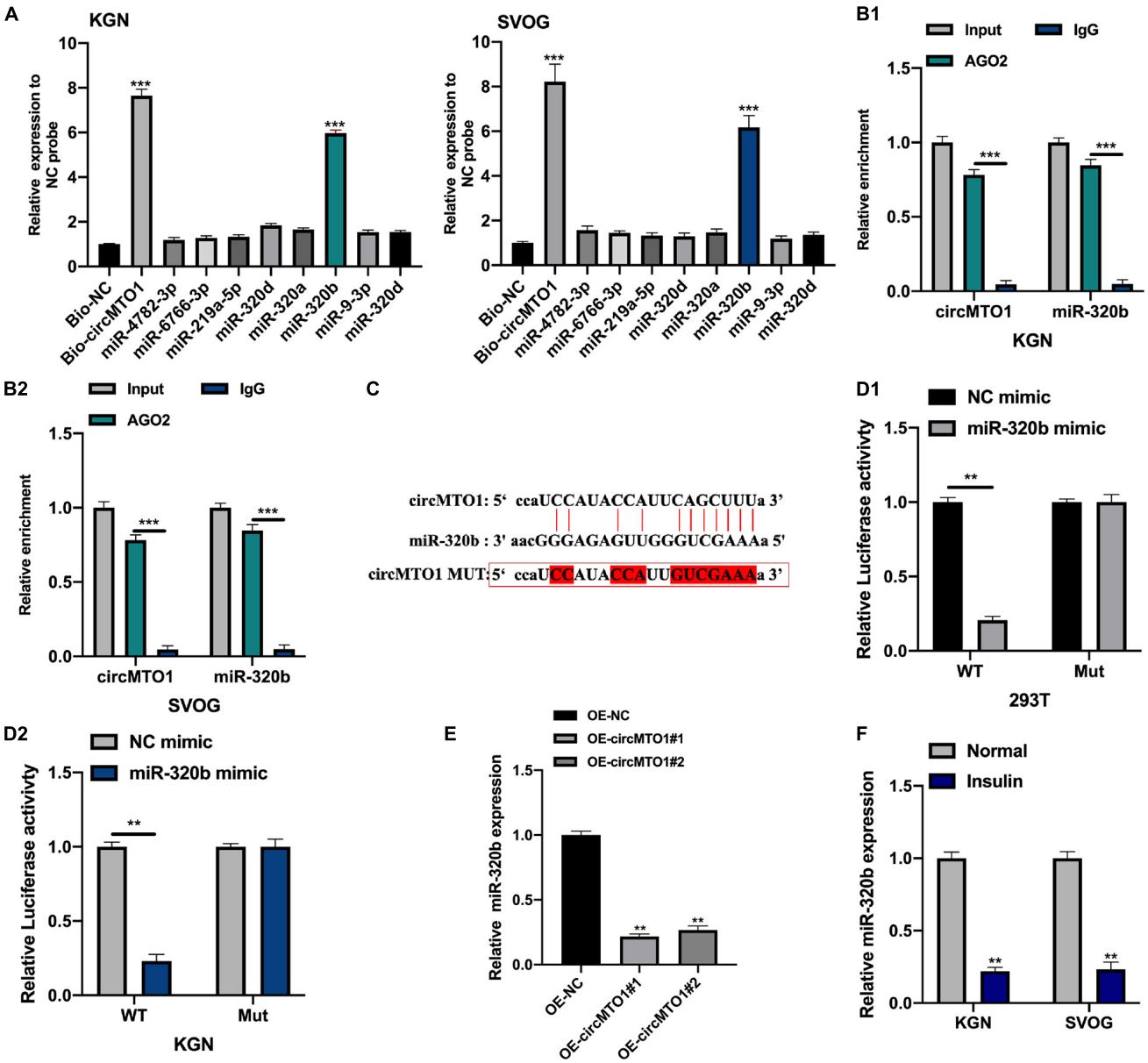

FIGURE 3 | CircMTO1 as an efficient molecular sponge for miR-320b. **(A)** Relative expression of putative miRNAs was measured by qRT-PCR in human granulosa-like tumor cells after biotinylated RNA pull-down. **(B)** Relative enrichment of circMTO1 and miR-320b in anti-IgG and anti-AGO2 incubated KGN **(B1)**, and SVOG **(B2)** cells were assessed by qRT-PCR. **(C)** The binding sites between circMTO1 and miR-320b were presented. **(D)** Relative luciferase activities in 293T **(D1)** and KGN **(D2)** co-transfected with circMTO1 WT or MuT and miR-320b mimics were measured. **(E)** Relative expression of miR-320b in OE-NC and OE-circMTO1 transfected Human granulosa-like tumor cells. **(F)** Relative expression of miR-320b in insulin treated Human granulosa-like tumor cells. All experiments were performed 3 times, $^{**}P < 0.01$, $^{***}P < 0.001$.

CircMTO1 as an Efficient Molecular Sponge for miR-320b

We used the Miranda dataset[1] to predict the downstream targets of circMTO1 (CLIP-seq data: strict stringency ≥ 5). Further, we conducted biotinylated RNA pull-down and qRT-PCR assays to measure the expression of putative miRNAs in biotinylated probes. MiR-320b was found to be highly enriched in Bio-circMTO1 probes in human granulosa-like tumor cells (**Figure 3A**). Subsequently, we found that circMTO1 and miR-320b were abundantly enriched in anti-AGO2 purified complexes compared with anti-IgG (**Figures 3B1,B2**). The predicted binding sites are shown in **Figure 3C**. The luciferase activities in miR-320b mimic and vectors containing circMTO1 WT sequence co-transfected cells were significantly decreased (**Figures 3D1,D2**). Furthermore, circMTO1 suppressed miR-320b expression in human granulosa-like tumor cells (**Figure 3E**). MiR-320b expression in human granulosa-like tumor cells decreased after insulin treatment (**Figure 3F**).

MiR-320b Directly Targeting MCL1

We investigated the mRNA targets of miR-320b using the starBase dataset[2]. We selected 8 potential targets of miR-320b for biotinylated RNA pull-down assays (data were supported by

[1]http://miranda.org.uk/

[2]http://starbase.sysu.edu.cn/

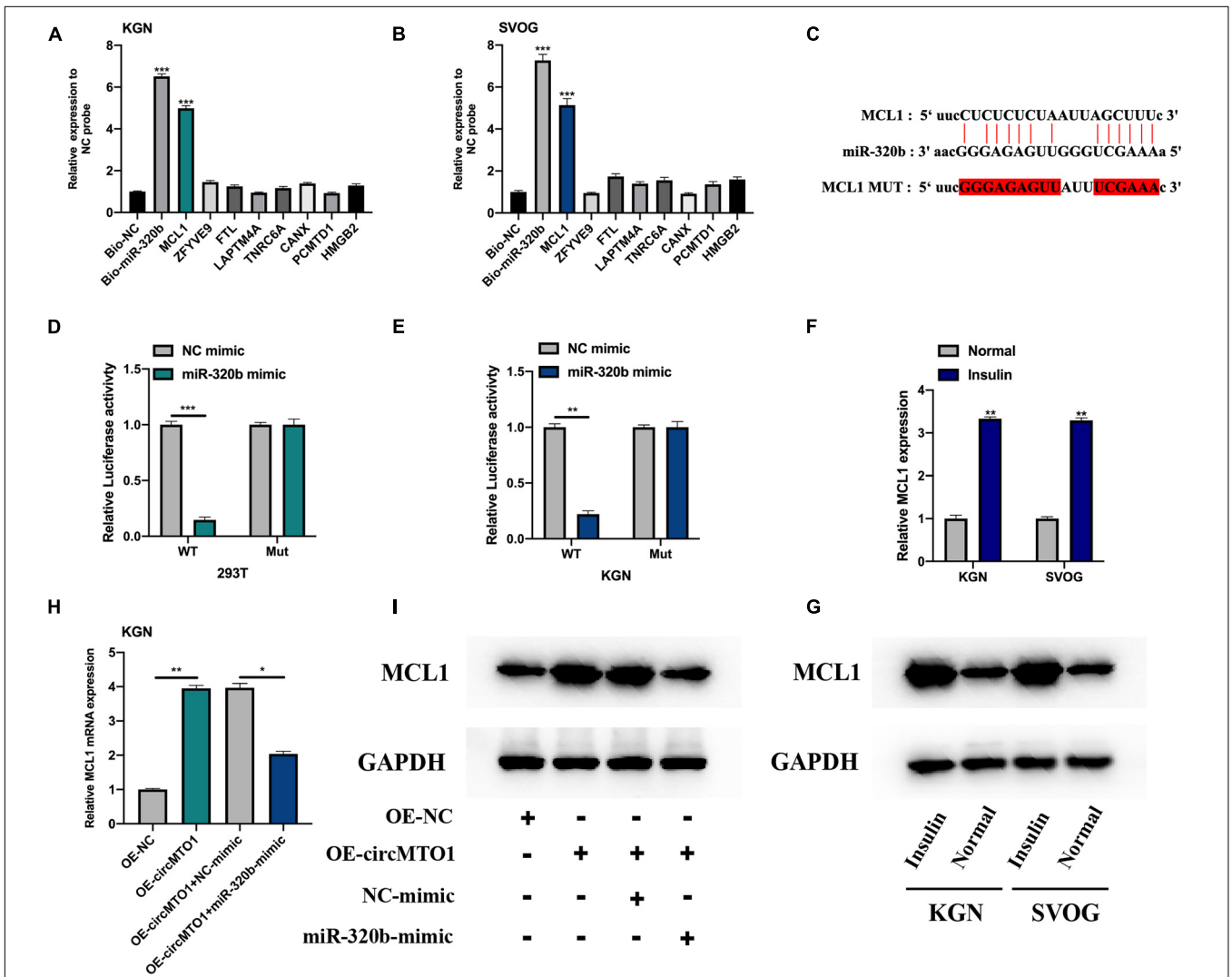

FIGURE 4 | MiR-320b directly targeting MCL1. **(A,B)** Relative expression of putative mRNA targets for miR-320b in biotinylated miR-320b (Bio-miR-320b) and its normal control (Bio-NC) probes infected KGN **(A)**, and SVOG **(B)** cells were evaluated by qRT-PCR. **(C)** The binding sites between miR-320b and MCL1 were showed. **(D,E)** Relative luciferase activities in 293T **(D)** and KGN **(E)** co-transfected with circMTO1 WT or MuT and miR-320b mimics were assessed. **(F,G)** Expression level of MCL1 in insulin-treated human granulosa-like tumor cells was measured by qRT-PCR **(F)** and western blot assays **(G)**. **(H,I)** Expression of MCL1 in OE-NC, OE-circMTO1, OE-circMTO1 + NC-mimic, and OE-circMTO1 + miR-320b-mimic transfected Human granulosa-like tumor cells were measured by qRT-PCR **(H)** and western blot **(I)**. All experiments were applied 3 times, $^{*}P < 0.05$, $^{**}P < 0.01$, $^{***}P < 0.001$.

the maximum number of Ago CLIP-seq). MCL1 was found to be highly enriched in bio-miR-320b probes in human granulosa-like tumor cells (**Figures 4A,B**). The predicted binding sites between miR-320b and MCL1 are shown in **Figure 4C**. Luciferase reporter assays confirmed the association between miR-320b and MCL1 in 293T and KGN cells (**Figures 4D,E**). MCL1 mRNA and protein expression was found to be increased under insulin treatment in human granulosa-like tumor cells (**Figures 4F,G**). CircMTO1 promoted MCL1 expression in human granulosa-like tumor cells and was reversed by the miR-320b mimic (**Figures 4H,I**).

CircMTO1 Regulation of Human Granulosa-Like Tumor Cell Behaviors via miR-320b/MCL1 Axis

Cell models were constructed by transfecting OE-NC, OE-circMTO1, OE-circMTO1 + si-NC, and OE-circMTO1 + si-MCL1 into human granulosa-like tumor cells to elucidate the role of the circMTO1/miR-320b/MCL1 axis. Next, we then evaluated the transfection conditions (**Figure 5A**). The promotive effects of OE-circMTO1 on cell proliferation were rescued by si-MCL1 (**Figures 5B,C1,C2**). Moreover, si-MCL1 reversed the inhibitory effect of OE-circMTO1 on cell apoptosis (**Figures 5D1,D2**). The results showed that circMTO1 facilitated human granulosa-like tumor cell behavior by regulating MCL1 expression via miR-320b.

Induction of CircMTO1 Expression in Human Granulosa-Like Tumor Cells Is Induced by SNAI2

The aforementioned results revealed the novel circMTO1/miR-320b/MCL1 axis in the cellular process of human granulosa-like tumor cells. However, the upstream regulator of circMTO1 requires further investigation. By utilizing the databases of the National Center for Biotechnology Information (NCBI),[3] Genomics Institute at the University of California, Santa Cruz

[3]https://www.ncbi.nlm.nih.gov/

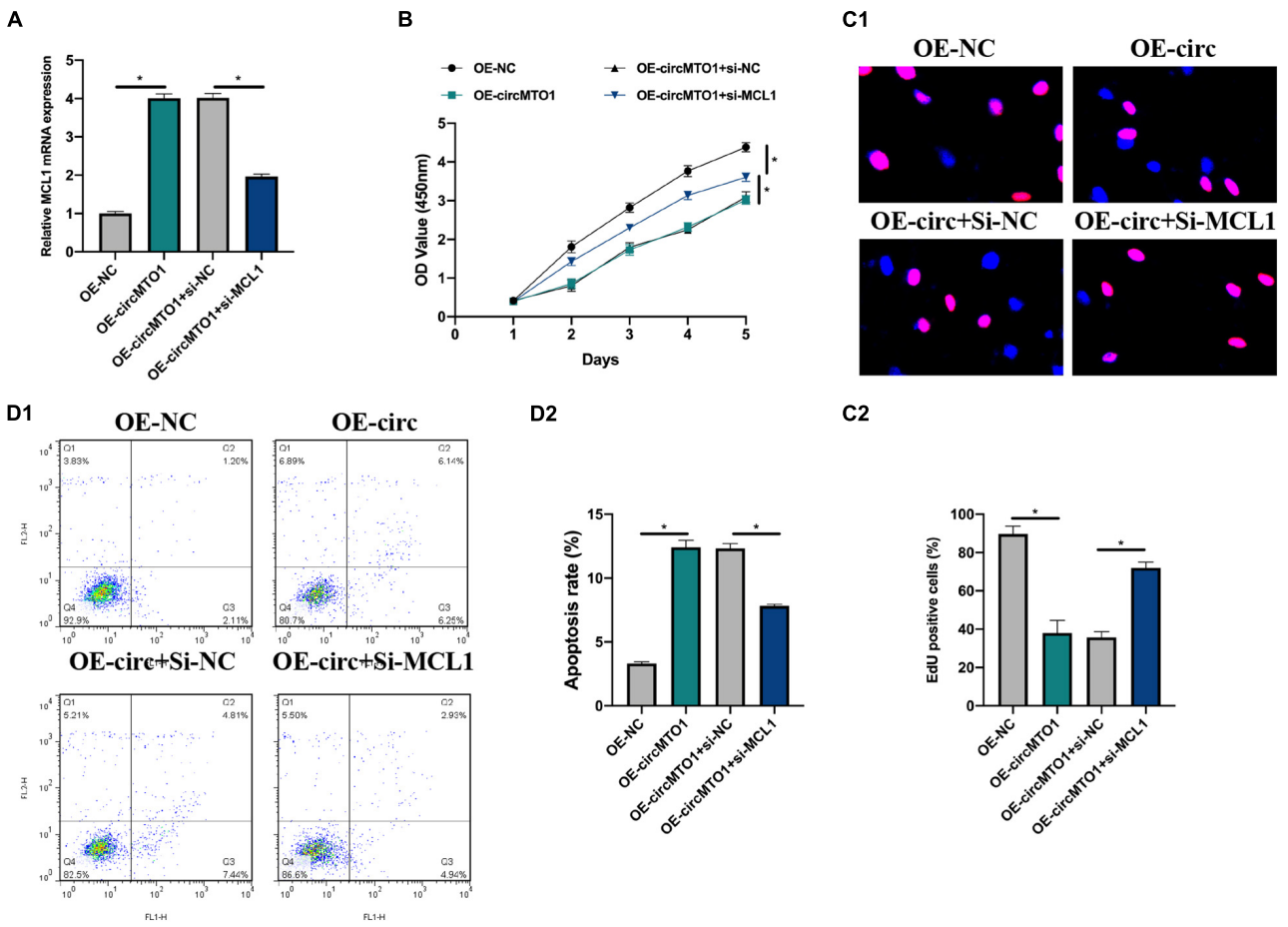

FIGURE 5 | CircMTO1 regulation of human granulosa-like tumor cell behaviors via miR-320b/MCL1 axis. Cell models were generated by infecting OE-NC, OE-circMTO1, OE-circMTO1 + si-NC, OE-circMTO1 + si-MCL1 into KGN cells. **(A)** Relative expression of MCL1 in OE-NC, OE-circMTO1, OE-circMTO1 + si-NC, and OE-circMTO1 + si-MCL1 transfected KGN cells were assessed by qRT-PCR. **(B)** The proliferation of KGN cells under indicated transfections was measured by CCK-8. **(C)** EdU assay was used to evaluate the proliferation level of indicated KGN cells **(C1)**, statistical results were analyzed **(C2)**. **(D)** Cell apoptosis of GCs upon different transfections were detected by flow cytometry **(D1)**, comparative statistics were shown **(D2)**. All assays were performed 3 times, $^{*}P < 0.05$.

(UCSC),[4] and JASPAR,[5] we determined that SNAI2 is a promising putative transcription factor of MTO1.

We generated SNAI2 overexpression and knockdown cell models were generated (**Figure 6A**). SNAI2 positively regulated circMTO1 expression in human granulosa-like tumor cells (**Figure 6B**). Subsequently, the DNA motif of SNAI2 was obtained from the JASPAR dataset (**Figure 6C**). We separated the promoter sequence of MTO1 into five parts (S1–S5) (**Figure 6D**). The predicted binding sites between SNAI2 and MTO1 were located in S2 and S3 fragments (P1-P3) (**Figure 6E**). The association between SNAI2 and the S2 (P1) or S3 (P2/P3) region of the MTO1 promoter was verified using the ChIP assay (**Figure 6F**) and further confirmed by a luciferase reporter

[4]http://genome.ucsc.edu/

[5]http://jaspar.genereg.net/

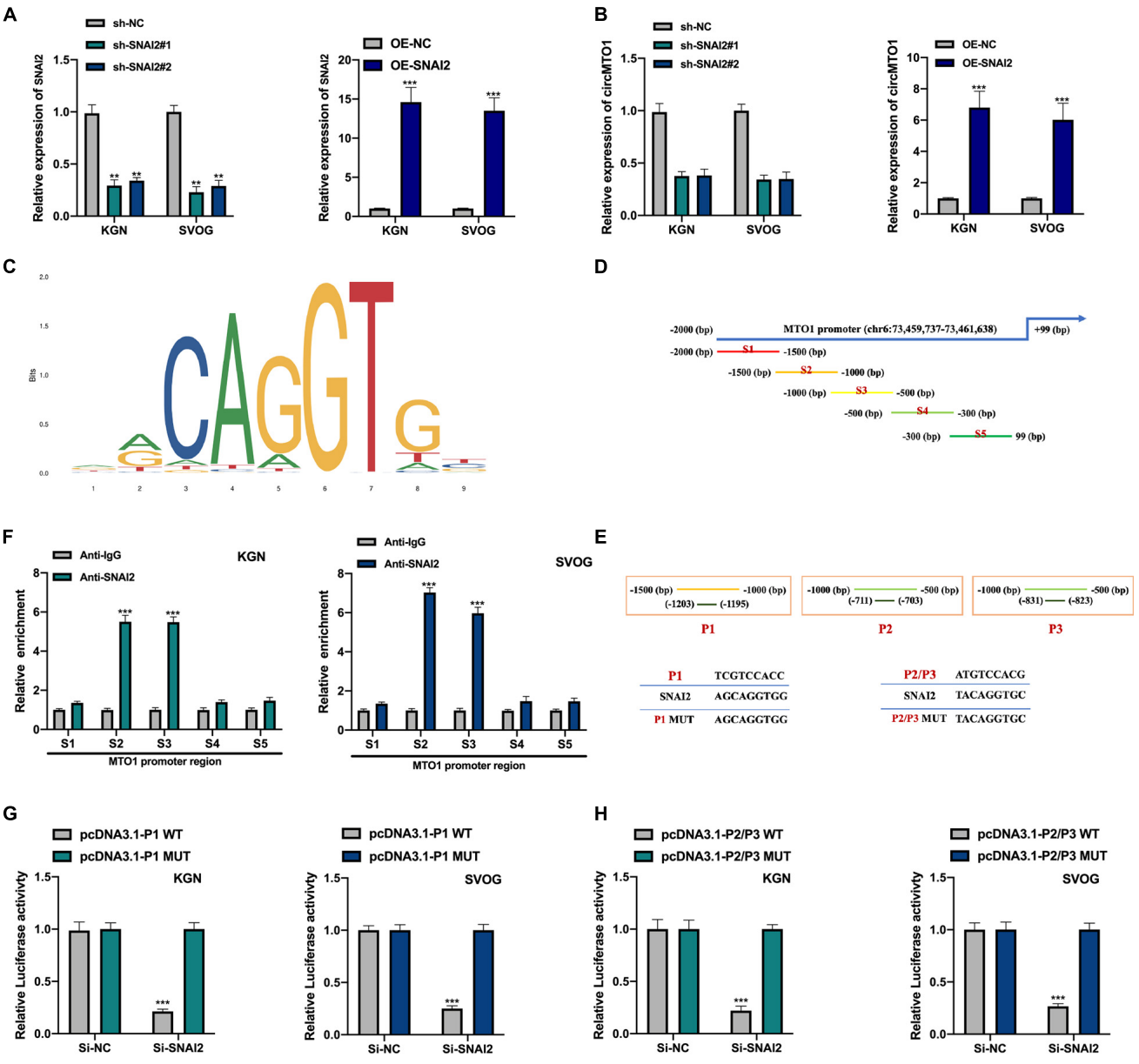

FIGURE 6 | Induction of circMTO1 expression in Human granulosa-like tumor cells is induced by SNAI2. **(A)** Relative expression level of SNAI2 in SNAI2 knockdown or overexpressed Human granulosa-like tumor cells was measured using qRT-PCR. **(B)** Relative expression of circMTO1 in SNAI2 knockdown or overexpressed Human granulosa-like tumor cells was assessed using qRT-PCR. **(C)** The DNA motif of SNAI2 was showed. **(D)** The promoter of MTO1 was fragmented into S1-S5 regions. **(E)** The predicted binding sites between SNAI2 and MTO1 promoter. **(F)** The association between SNAI2 and S2/S3 region of MTO1 promoter was assessed by ChIP assays. **(G)** The association between SNAI2 and predicted P1 binding sites of MTO1 promoter were confirmed by luciferase reporter assays. **(H)** The association between SNAI2 and predicted P2/P3 binding sites of MTO1 promoter was proven by luciferase reporter assays. All experiments were conducted 3 times, $^{**}P < 0.01$, $^{***}P < 0.001$.

gene assay (**Figures 6G,H**) in human granulosa-like tumor cells. Therefore, our results revealed that the expression of circMTO1 in human granulosa-like tumor cells was facilitated by SNAI2.

DISCUSSION

Despite of the fact that PCOS is one of the most common endocrine diseases in women, and with an incidence of 6–12% (Yau et al., 2017), the etiology of PCOS is still poorly understood. On the one hand, the diagnosis and clinical intervention strategies for PCOS are inefficient and poorly improved. On the other hand, PCOS patients suffer varied presentations of PCOS clinical features including hyperandrogenism, oligomenorrhea, ovarian polycystic disorder, anovulation, infertility, and are facing multiple additive risks such as type II diabetes mellitus, metabolic diseases, hypertension and cardiovascular events (Azziz, 2018; Zhang J. et al., 2019). To improve the quality of life of PCOS patients, and reduce the economic burden of the world health care system, novel diagnosis or therapeutic targets for PCOS are urgently needed.

In this study, we verified that the expression and circRNA characterization of circMTO1 in human granulosa-like tumor cells. We also found that circMTO1 knockdown promoted cell proliferation and the inhibited the apoptotic cell rate in human granulosa-like tumor cells. Our results suggest that circMTO1 plays a role in the cellular processes of human granulosa-like tumor cells. Subsequently, the underlying molecular mechanisms are investigated. CircMTO1 sponged miR-320b in 293T cells and human granulosa-like tumor cells and negatively regulated miR-320b expression. We also identified MCL1 as a downstream target of miR-320b. Thus, CircMTO1 mediated human granulosa-like tumor cell progression through the miR-320b/MCL1 axis. Furthermore, we confirmed SNAI2 as an upstream transcription factor of circMTO1 in human granulosa-like tumor cells. We found a novel SNAI2/circMTO1/miR-320b/MCL1 axis in human granulosa-like tumor cell progression.

Evidence has revealed the biological functions of miR-320b in many diseases, such as osteosarcoma, psoriasis, osteoporosis, non-small cell lung cancer, and colorectal cancer (Wang et al., 2015; Lv et al., 2018; Wang Y. et al., 2018; Zhang L. et al., 2019; Zhang S. et al., 2019). Our findings revealed that miR-320b is a downstream factor of circMTO1 in human granulosa-like tumor cells. Its expression is suppressed by circMTO1. A previous study reported decreased miR-320b expression in ovarian cancer tissues, indicating that it might be a useful target for distant metastasis in ovarian carcinoma (Cha et al., 2017). Similarly, our results revealed that circMTO1 significantly downregulated miR-320b expression. However, the dysregulated expression of miR-320b in the ovary has different outcomes. The potential role and molecular mechanisms of miR-320b in ovarian disease require further study.

We also conducted biotinylated RNA pull-down and dual-luciferase gene assays, which confirmed that miR-320b directly targeted to MCL1. MCL1 has been found to be involved in the development of ovarian disorders in multiple ways, such as by deubiquitinating and interacting with miRNAs (Li C. et al., 2019; Wu et al., 2019). In this study, we transfected OE-NC, OE-circMTO1, OE-circMTO1 + si-NC, and OE-circMTO1 + si-MCL1 into human granulosa-like tumor cells, we found that the downregulation of MCL1 reversed the effects of circMTO1 on human granulosa-like tumor cell proliferation and apoptosis. Thus, circMTO1 exerts its functions in PCOS by regulating MCL1 expression.

Several studies have reported that transcriptional factors regulate circRNA expression in multiple cells (Wang R. et al., 2018; Li H. et al., 2019; Wang W. et al., 2020; Liu et al., 2021). Using the UCSC and JASPAR datasets of interest, we found that SNAI2 might be a promising transcription factor for the MTO1 promoter. We assessed and confirmed the association between SNAI2 and MTO1 promoters was assessed and confirmed using ChIP and luciferase reporter gene assays. Additionally, circMTO1 expression in human granulosa-like tumor cells was positively regulated by SNAI2.

CONCLUSION

In conclusion, our findings suggest that circMTO1 could aggravate PCOS progression by upregulating MCL1 expression through interaction with miR-320b. Meanwhile, SNAI2 also induced the expression level of circMTO1 in human granulosa-like tumor cells. Our results provide new insights for human granulosa-like tumor cell research and may be a promising direction for PCOS intervention.

DATA AVAILABILITY STATEMENT

The original contributions presented in the study are included in the article/**Supplementary Material**, further inquiries can be directed to the corresponding author/s.

AUTHOR CONTRIBUTIONS

JD designed the experiments. JD and HC performed the experiments and analyzed the data. YH and LS collected and analyzed the experiments data. All authors read and approved the final manuscript.

FUNDING

This work was supported by the Wuhan Young and Middle-aged Medical Talents Foundation Project of Hubei Province, China (No. 230727010).

SUPPLEMENTARY MATERIAL

The Supplementary Material for this article can be found online at: https://www.frontiersin.org/articles/10.3389/fgene.2021.689916/full#supplementary-material

REFERENCES

Azziz, R. (2018). Polycystic ovary syndrome. *Obstet. Gynecol.* 132, 321–336. doi: 10.1097/AOG.0000000000002698

Azziz, R., Carmina, E., Dewailly, D., Diamanti-Kandarakis, E., Escobar-Morreale, H. F., Futterweit, W., et al. (2006). Positions statement: criteria for defining polycystic ovary syndrome as a predominantly hyperandrogenic syndrome: an androgen excess society guideline. *J. Clin. Endocrinol. Metab.* 91, 4237–4245. doi: 10.1210/jc.2006-0178

Azziz, R., Sanchez, L. A., Knochenhauer, E. S., Moran, C., Lazenby, J., Stephens, K. C., et al. (2004). Androgen excess in women: experience with over 1000 consecutive patients. *J. Clin. Endocrinol. Metab.* 89, 453–462. doi: 10.1210/jc.2003-031122

Bian, L., Zhi, X., Ma, L., Zhang, J., Chen, P., Sun, S., et al. (2018). Hsa_circRNA_103809 regulated the cell proliferation and migration in colorectal cancer via miR-532-3p / FOXO4 axis. *Biochem. Biophys. Res. Commun.* 505, 346–352. doi: 10.1016/j.bbrc.2018.09.073

Cha, S. Y., Choi, Y. H., Hwang, S., Jeong, J. Y., and An, H. J. (2017). Clinical impact of microRNAs associated with cancer stem cells as a prognostic factor in ovarian carcinoma. *J. Cancer* 8, 3538–3547. doi: 10.7150/jca.20348

Che, Q., Liu, M., Xu, J., Liu, Y., Cao, X., Dong, X., et al. (2019). Characterization of circular RNA expression profiles in cumulus cells from patients with polycystic ovary syndrome. *Fertil. Steril.* 111, 1243–1251.e1. doi: 10.1016/j.fertnstert.2019.02.023

Chen, M., Ai, G., Zhou, J., Mao, W., Li, H., and Guo, J. (2019). circMTO1 promotes tumorigenesis and chemoresistance of cervical cancer via regulating miR-6893. *Biomed. Pharmacother.* 117:109064. doi: 10.1016/j.biopha.2019.109064

Chen, Y., Zhang, X., An, Y., Liu, B., and Lu, M. (2020). LncRNA HCP5 promotes cell proliferation and inhibits apoptosis via miR-27a-3p/IGF-1 axis in human granulosa-like tumor cell line KGN. *Mol. Cell Endocrinol.* 503:110697. doi: 10.1016/j.mce.2019.110697

Das, M., Djahanbakhch, O., Hacihanefioglu, B., Saridogan, E., Ikram, M., Ghali, L., et al. (2008). Granulosa cell survival and proliferation are altered in polycystic ovary syndrome. *J. Clin. Endocrinol. Metab.* 93, 881–887. doi: 10.1210/jc.2007-1650

Deng, L., Chen, Q., Xie, J., Wei, W., and Hui, H. (2020). circPUM1 promotes polycystic ovary syndrome progression by sponging to miR-760. *Gene* 754:144903. doi: 10.1016/j.gene.2020.144903

Diamanti-Kandarakis, E., and Dunaif, A. (2012). Insulin resistance and the polycystic ovary syndrome revisited: an update on mechanisms and implications. *Endocr. Rev.* 33, 981–1030. doi: 10.1210/er.2011-1034

Ge, Z., Li, L. F., Wang, C. Y., Wang, Y., and Ma, W. L. (2018). CircMTO1 inhibits cell proliferation and invasion by regulating Wnt/beta-catenin signaling pathway in colorectal cancer. *Eur. Rev. Med. Pharmacol. Sci.* 22, 8203–8209. doi: 10.26355/eurrev_201812_16513

Han, D., Li, J., Wang, H., Su, X., Hou, J., Gu, Y., et al. (2017). Circular RNA circMTO1 acts as the sponge of microRNA-9 to suppress hepatocellular carcinoma progression. *Hepatology* 66, 1151–1164. doi: 10.1002/hep.29270

Han, Q., Zhang, W., Meng, J., Ma, L., and Li, A. (2018). LncRNA-LET inhibits cell viability, migration and EMT while induces apoptosis by up-regulation of TIMP2 in human granulosa-like tumor cell line KGN. *Biomed. Pharmacother.* 100, 250–256. doi: 10.1016/j.biopha.2018.01.162

Hansen, T. B., Jensen, T. I., Clausen, B. H., Bramsen, J. B., Finsen, B., Damgaard, C. K., et al. (2013). Natural RNA circles function as efficient microRNA sponges. *Nature* 495, 384–388. doi: 10.1038/nature11993

Hentze, M. W., and Preiss, T. (2013). Circular RNAs: splicing's enigma variations. *EMBO J.* 32, 923–925. doi: 10.1038/emboj.2013.53

Jeck, W. R., and Sharpless, N. E. (2014). Detecting and characterizing circular RNAs. *Nat. Biotechnol.* 32, 453–461. doi: 10.1038/nbt.2890

Jeck, W. R., Sorrentino, J. A., Wang, K., Slevin, M. K., Burd, C. E., Liu, J., et al. (2013). Circular RNAs are abundant, conserved, and associated with ALU repeats. *RNA* 19, 141–157. doi: 10.1261/rna.035667.112

Legnini, I., Di Timoteo, G., Rossi, F., Morlando, M., Briganti, F., Sthandier, O., et al. (2017). Circ-ZNF609 is a circular RNA that can be translated and functions in myogenesis. *Mol. Cell* 66, 22–37.e29. doi: 10.1016/j.molcel.2017.02.017

Li, C., Zhang, Y., Zhao, W., Cui, S., and Song, Y. (2019). miR-153-3p regulates progression of ovarian carcinoma in vitro and in vivo by targeting MCL1 gene. *J. Cell Biochem.* 120, 19147–19158. doi: 10.1002/jcb.29244

Li, H., Shen, S., Ruan, X., Liu, X., Zheng, J., Liu, Y., et al. (2019). Biosynthetic CircRNA_001160 induced by PTBP1 regulates the permeability of BTB via the CircRNA_001160/miR-195-5p/ETV1 axis. *Cell Death Dis.* 10:960. doi: 10.1038/s41419-019-2191-z

Li, M., Zhao, H., Zhao, S. G., Wei, D. M., Zhao, Y. R., Huang, T., et al. (2019). The HMGA2-IMP2 pathway promotes granulosa cell proliferation in polycystic ovary syndrome. *J. Clin. Endocrinol. Metab.* 104, 1049–1059. doi: 10.1210/jc.2018-00544

Liu, H., Bi, J., Dong, W., Yang, M., Shi, J., Jiang, N., et al. (2018). Invasion-related circular RNA circFNDC3B inhibits bladder cancer progression through the miR-1178-3p/G3BP2/SRC/FAK axis. *Mol. Cancer* 17:161. doi: 10.1186/s12943-018-0908-8

Liu, S., Yang, N., Jiang, X., Wang, J., Dong, J., and Gao, Y. (2021). FUS-induced circular RNA ZNF609 promotes tumorigenesis and progression via sponging miR-142-3p in lung cancer. *J. Cell Physiol.* 236, 79–92. doi: 10.1002/jcp.29481

Lu, J., Xue, Y., Wang, Y., Ding, Y., Zou, Q., Pan, M., et al. (2020). CiRS-126 inhibits proliferation of ovarian granulosa cells through targeting the miR-21-PDCD4-ROS axis in a polycystic ovarian syndrome model. *Cell Tissue Res.* 381, 189–201. doi: 10.1007/s00441-020-03187-9

Lv, G. Y., Miao, J., and Zhang, X. L. (2018). Long noncoding RNA XIST promotes osteosarcoma progression by targeting ras-related protein RAP2B via miR-320b. *Oncol. Res.* 26, 837–846. doi: 10.3727/096504017X14920318811721

Memczak, S., Jens, M., Elefsinioti, A., Torti, F., Krueger, J., Rybak, A., et al. (2013). Circular RNAs are a large class of animal RNAs with regulatory potency. *Nature* 495, 333–338. doi: 10.1038/nature11928

Nishi, Y., Yanase, T., Mu, Y., Oba, K., Ichino, I., Saito, M., et al. (2001). Establishment and characterization of a steroidogenic human granulosa-like tumor cell line, KGN, that expresses functional follicle-stimulating hormone receptor. *Endocrinology* 142, 437–445. doi: 10.1210/endo.142.1.7862

Ouyang, Z., Tan, T., Zhang, X., Wan, J., Zhou, Y., Jiang, G., et al. (2019). CircRNA hsa_circ_0074834 promotes the osteogenesis-angiogenesis coupling process in bone mesenchymal stem cells (BMSCs) by acting as a ceRNA for miR-942-5p. *Cell Death Dis.* 10:932. doi: 10.1038/s41419-019-2161-5

Patop, I. L., Wust, S., and Kadener, S. (2019). Past, present, and future of circRNAs. *EMBO J.* 38:e100836. doi: 10.15252/embj.2018100836

Shi, C. C., Pan, L. Y., Peng, Z. Y., and Li, J. G. (2020). CircMTO1 attenuated acute kidney injury through regulating miR-337. *Inflammation* 43, 1304–1311. doi: 10.1007/s10753-020-01209-w

Song, T., Xu, A., Zhang, Z., Gao, F., Zhao, L., Chen, X., et al. (2019). CircRNA hsa_circRNA_101996 increases cervical cancer proliferation and invasion through activating TPX2 expression by restraining miR-8075. *J. Cell Physiol.* 234, 14296–14305. doi: 10.1002/jcp.28128

Wang, H., Cao, F., Li, X., Miao, H., E, J., Xing, J., et al. (2015). miR-320b suppresses cell proliferation by targeting c-Myc in human colorectal cancer cells. *BMC Cancer* 15:748. doi: 10.1186/s12885-015-1728-5

Wang, L. P., Peng, X. Y., Lv, X. Q., Liu, L., Li, X. L., He, X., et al. (2019). High throughput circRNAs sequencing profile of follicle fluid exosomes of polycystic ovary syndrome patients. *J. Cell Physiol.* Online ahead of print. doi: 10.1002/jcp.28201

Wang, N., Cao, Q. X., Tian, J., Ren, L., Cheng, H. L., and Yang, S. Q. (2020). Circular RNA MTO1 inhibits the proliferation and invasion of ovarian cancer cells through the miR-182-5p/KLF15 axis. *Cell Transplant.* 29:963689720943613. doi: 10.1177/0963689720943613

Wang, R., Zhang, S., Chen, X., Li, N., Li, J., Jia, R., et al. (2018). EIF4A3-induced circular RNA MMP9 (circMMP9) acts as a sponge of miR-124 and promotes glioblastoma multiforme cell tumorigenesis. *Mol. Cancer* 17:166. doi: 10.1186/s12943-018-0911-0

Wang, W., Li, Y., Li, X., Liu, B., Han, S., Li, X., et al. (2020). Circular RNA circFOXP1 induced by SOX9 promotes hepatocellular carcinoma progression via sponging miR-875-3p and miR-421. *Biomed. Pharmacother.* 121:109517. doi: 10.1016/j.biopha.2019.109517

Wang, Y., Yu, X., Wang, L., Ma, W., and Sun, Q. (2018). miR-320b is down-regulated in psoriasis and modulates keratinocyte proliferation by targeting AKT3. *Inflammation* 41, 2160–2170. doi: 10.1007/s10753-018-0859-7

Wu, X., Luo, Q., Zhao, P., Chang, W., Wang, Y., Shu, T., et al. (2019). MGMT-activated DUB3 stabilizes MCL1 and drives chemoresistance in ovarian cancer. *Proc. Natl. Acad. Sci. U.S.A.* 116, 2961–2966. doi: 10.1073/pnas.1814742116

Yang, Y., Fan, X., Mao, M., Song, X., Wu, P., Zhang, Y., et al. (2017). Extensive translation of circular RNAs driven by N(6)-methyladenosine. *Cell Res.* 27, 626–641. doi: 10.1038/cr.2017.31

Yau, T. T., Ng, N. Y., Cheung, L. P., and Ma, R. C. (2017). Polycystic ovary syndrome: a common reproductive syndrome with long-term metabolic consequences. *Hong Kong Med. J.* 23, 622–634. doi: 10.12809/hkmj 176308

Zhang, C., Liu, J., Lai, M., Li, J., Zhan, J., Wen, Q., et al. (2019). Circular RNA expression profiling of granulosa cells in women of reproductive age with polycystic ovary syndrome. *Arch. Gynecol. Obstet.* 300, 431–440. doi: 10.1007/s00404-019-05129-5

Zhang, J., Bao, Y., Zhou, X., and Zheng, L. (2019). Polycystic ovary syndrome and mitochondrial dysfunction. *Reprod. Biol. Endocrinol.* 17:67. doi: 10.1186/s12958-019-0509-4

Zhang, L., Yao, Z., Liu, M., and Liu, Y. (2019). MiR-320b negatively regulates ovariectomy-induced osteoporosis in rats by decreasing RUNX2. *Panminerva Med.* Online ahead of print. doi: 10.23736/S0031-0808.19.03695-4

Zhang, S., Zhang, X., Sun, Q., Zhuang, C., Li, G., Sun, L., et al. (2019). LncRNA NR2F2-AS1 promotes tumourigenesis through modulating BMI1 expression by targeting miR-320b in non-small cell lung cancer. *J. Cell Mol. Med.* 23, 2001–2011. doi: 10.1111/jcmm.14102

Zhang, X., Zhong, B., Zhang, W., Wu, J., and Wang, Y. (2019). Circular RNA CircMTO1 inhibits proliferation of glioblastoma cells via miR-92/WWOX signaling pathway. *Med. Sci. Monit.* 25, 6454–6461. doi: 10.12659/MSM.918676

Zhang, Y., Huang, Q., Cheng, J. C., Nishi, Y., Yanase, T., Huang, H. F., et al. (2010). Homeobox A7 increases cell proliferation by up-regulation of epidermal growth factor receptor expression in human granulosa cells. *Reprod. Biol. Endocrinol.* 8:61. doi: 10.1186/1477-7827-8-61

Zhou, Z. B., Huang, G. X., Fu, Q., Han, B., Lu, J. J., Chen, A. M., et al. (2019). circRNA.33186 contributes to the pathogenesis of osteoarthritis by sponging miR-127-5p. *Mol. Ther.* 27, 531–541. doi: 10.1016/j.ymthe.2019.01.006

Conflict of Interest: The authors declare that the research was conducted in the absence of any commercial or financial relationships that could be construed as a potential conflict of interest.

Publisher's Note: All claims expressed in this article are solely those of the authors and do not necessarily represent those of their affiliated organizations, or those of the publisher, the editors and the reviewers. Any product that may be evaluated in this article, or claim that may be made by its manufacturer, is not guaranteed or endorsed by the publisher.

frontiers in Genetics

ORIGINAL RESEARCH
published: 13 August 2021
doi: 10.3389/fgene.2021.703210

Identification and Validation of a PPP1R12A-Related Five-Gene Signature Associated With Metabolism to Predict the Prognosis of Patients With Prostate Cancer

Zhihao Zou[1,2†], Ren Liu[3†], Yingke Liang[2†], Rui Zhou[2], Qishan Dai[2], Zhaodong Han[2], Minyao Jiang[4], Yangjia Zhuo[2], Yixun Zhang[2], Yuanfa Feng[2], Xuejin Zhu[2], Shanghua Cai[5], Jundong Lin[2], Zhenfeng Tang[5], Weide Zhong[2,3,5,6] and Yuxiang Liang[1,2,7*]*

[1] Department of Geriatrics, The Second Affiliated Hospital of South China University of Technology, Guangzhou, China, [2] Guangdong Key Laboratory of Clinical Molecular Medicine and Diagnostics, Department of Urology, School of Medicine, Guangzhou First People's Hospital, South China University of Technology, Guangzhou, China, [3] Guangdong Provincial Institute of Nephrology, Nanfang Hospital, Southern Medical University, Guangzhou, China, [4] Department of Urology, Huadu District People's Hospital, Southern Medical University, Guangzhou, China, [5] Urology Key Laboratory of Guangdong Province, The First Affiliated Hospital of Guangzhou Medical University, Guangzhou Medical University, Guangzhou, China, [6] State Key Laboratory of Quality Research in Chinese Medicines, Macau University of Science and Technology, Macau, China, [7] Department of Urology, Huizhou Municipal Central Hospital, Huizhou, China

OPEN ACCESS

Edited by:
Detu Zhu,
Cornell University, United States

Reviewed by:
Hai Huang,
Sun Yat-sen Memorial Hospital, China
Kun Tang,
Huazhong University of Science and Technology, China

***Correspondence:**
Weide Zhong
Zhongwd2009@live.cn
Yuxiang Liang
eyliangyx@scut.edu.cn

† These authors have contributed equally to this work

Specialty section:
This article was submitted to RNA, a section of the journal Frontiers in Genetics

Received: 30 April 2021
Accepted: 28 June 2021
Published: 13 August 2021

Citation:
Zou Z, Liu R, Liang Y, Zhou R, Dai Q, Han Z, Jiang M, Zhuo Y, Zhang Y, Feng Y, Zhu X, Cai S, Lin J, Tang Z, Zhong W and Liang Y (2021) Identification and Validation of a PPP1R12A-Related Five-Gene Signature Associated With Metabolism to Predict the Prognosis of Patients With Prostate Cancer. Front. Genet. 12:703210. doi: 10.3389/fgene.2021.703210

Background: Prostate cancer (PCa) is the most common malignant male neoplasm in the American male population. Our prior studies have demonstrated that protein phosphatase 1 regulatory subunit 12A (PPP1R12A) could be an efficient prognostic factor in patients with PCa, promoting further investigation. The present study attempted to construct a gene signature based on PPP1R12A and metabolism-related genes to predict the prognosis of PCa patients.

Methods: The mRNA expression profiles of 499 tumor and 52 normal tissues were extracted from The Cancer Genome Atlas (TCGA) database. We selected differentially expressed PPP1R12A-related genes among these mRNAs. Tandem affinity purification-mass spectrometry was used to identify the proteins that directly interact with PPP1R12A. Gene set enrichment analysis (GSEA) was used to extract metabolism-related genes. Univariate Cox regression analysis and a random survival forest algorithm were used to confirm optimal genes to build a prognostic risk model.

Results: We identified a five-gene signature (*PPP1R12A*, *PTGS2*, *GGCT*, *AOX1*, and *NT5E*) that was associated with PPP1R12A and metabolism in PCa, which effectively predicted disease-free survival (DFS) and biochemical relapse-free survival (BRFS). Moreover, the signature was validated by two internal datasets from TCGA and one external dataset from the Gene Expression Omnibus (GEO).

Conclusion: The five-gene signature is an effective potential factor to predict the prognosis of PCa, classifying PCa patients into high- and low-risk groups, which might provide potential novel treatment strategies for these patients.

Keywords: prostate cancer, protein phosphatase 1 regulatory subunit 12A, metabolism, gene signature, prognostic model

INTRODUCTION

Prostate cancer (PCa) is the most common male malignancy in the developed world and is predicted to account for ∼26% of new cancer diagnoses among US men and 14.1% worldwide in 2021 (Ferlay et al., 2020; Siegel et al., 2021). In cases with early detection, radical prostatectomy (RP), in which local malignant prostate tissue is resected, is the preferred method to treat PCa patients. However, the high recurrence rates of PCa contribute to the risks of progression to castration-resistant PCa (CRPC), giving rise to the second-leading cause of cancer deaths (Ward et al., 2003; Roehl et al., 2004; Ferlay et al., 2018; Matsumoto et al., 2018). Potent diagnostic and prognostic biomarkers are necessary to predict the course of disease and the medical therapeutic efficacy in personalized medicine (Huber et al., 2015). It is demonstrated that the most commonly used clinicopathological factors used to provide important prognostic information for monitoring disease progression in PCa are serum prostate-specific antigen (PSA) level, the Gleason score, the pathological tumor stage, and the surgical margin (Quinn et al., 2001). Nevertheless, because of the great heterogeneity of PCa, the prediction power of these conventional markers is often not satisfactory, and the prognostic markers have not been fully explored yet. Therefore, identification of novel biomarkers for PCa to enhance the accuracy of PCa aggressiveness prediction still is a significant task.

Protein phosphatase 1 regulatory subunit 12a (PPP1R12A), also named myosin phosphatase targeting subunit 1 (MYPT1), is a member of the myosin phosphatase-targeting (MYPT) protein family and participates in the regulation of smooth muscle contraction (Murthy, 2006; Rattan et al., 2010; He et al., 2013; Qiao et al., 2014). In addition, the functions of PPP1R12A in cell development (Weiser et al., 2009), the cell cycle (Yamashiro et al., 2008; Dumitru et al., 2017), and cell adhesion and migration (Joo and Yamada, 2014) have been observed recently in accumulating studies. Importantly, PPP1R12A could inhibit angiogenesis and tumor growth and predict aggressive outcomes in PCa (Lin et al., 2017). Moreover, its expression in PCa, combined with CD31, could be a significant prognostic factor (Liang et al., 2018). Therefore, it is essential to explore more biomarkers that interact with PPP1R12A for the early effective prognosis, and effective treatment of PCa.

After the discovery of the Warburg Effect (Warburg, 1956), metabolic reprogramming drew increased attention in the cancer field and has since become a novel hallmark of cancer (Hanahan and Weinberg, 2011). Anabolic and catabolic metabolism are indispensable to cancer cells in metabolic reprogramming, ensuring that the biomass synthesis and energy supply of cancer cells are adequately supplied (Ward and Thompson, 2012; Pavlova and Thompson, 2016; Sun et al., 2018; Cardoso et al., 2021). Previous studies have revealed a tremendous difference in metabolic statues between tumors and normal tissue due to the unlimited proliferative nature of cancer cells (El Hassouni et al., 2020). However, little is known about the metabolic microenvironment and its prognostic value in PCa. It is particularly significant to recognize biomarkers with high specificities and sensitivities in consideration of the prognosis of PCa at the metabolic level.

In the present study, we extracted five genes related to PPP1R12A interaction and metabolism and developed a robust five-gene signature to predict the prognosis of PCa. Our findings provide a new perspective for the development of therapeutical strategies and personalized treatment approaches.

MATERIALS AND METHODS

Collection of Human Tissue Samples

The patient cohorts and tissue samples in this study were the same as those used in our previous study (Lin et al., 2017; Liang et al., 2018). In total, 225 consecutive PCa patients that underwent radical prostatectomy were included in the human PCa tissue microarrays (TMA). Related clinicopathological data were included.

UALCAN Analysis

The UALCAN database, a publicly accessible web portal that is easy to operate,[1] includes clinical data from 31 cancer types and is commonly used to investigate relative transcriptional expression levels between tumor and normal samples. *PPP1R12A* expression was identified using the "prostate adenocarcinoma" dataset with the "Expression Analysis" module. Expression levels of *PPP1R12A* across PCa and normal samples as well as the relationships between *PPP1R12A* and different Gleason scores were analyzed. $p < 0.05$ was regarded significant.

Direct PPP1R12A Protein Interactor Analysis

The PCa cell line LNCaP, obtained from the American Type Culture Collection (United States), was maintained in RPMI 1640 medium (Hyclone, United States) supplemented with 10% fetal bovine serum (Gibico, United States) and 1% penicillin–streptomycin at 37°C in 5% CO2. LNCaP cells were transfected with a PPP1R12A-encoding vector construct and screened with puromycin. After clone selection, using full-length PPP1R12A protein as bait, we performed tandem affinity purification–mass spectrometry (TAP-MS) (Li et al., 2016) to identify direct PPP1R12A interactors on a proteomic scale. We utilized the Protein Pilot 5.0 software and MASCOT software to identify putative PPP1R12A-binding motifs in interaction partners (Perkins et al., 1999).

Data Processing

The Cancer Genome Atlas (TCGA)[2] contains both sequencing and pathological data for 30 different cancers (Cancer Genome Atlas Network, 2012). We acquired the FPKM data of TCGA RNA-seq datasets for PCa from the UCSC Xena browser.[3] We changed the type of gene expression profiles from $\log_2(\text{FPKM} + 1)$ to $\log_2(\text{TPM} + 1)$ to obtain a more precise data of differentially expressed genes (DEGs). The clinical information for PCa was acquired from cBioPortal.[4] Moreover,

[1] http://ualcan.path.uab.edu/

[2] https://portal.gdc.cancer.gov/

[3] https://xenabrowser.net/

[4] http://www.cbioportal.org/

gene expression profiles from the Taylor (GSE21034) (Taylor et al., 2010) and GSE6956 (Wallace et al., 2008) datasets were retrieved from GEO.[5] The expression profiles data from the Taylor dataset were standardized through RMA and data from the GSE6956 dataset were standardized through MAS5.

Differentially Expressed Gene and Metabolism-Related Genes Analysis

DEGs were identified among the 499 tumor samples and 52 normal prostate gland tissues after normalization. Based on the expression levels of PPP1R12A, the patient samples were ranked from high to low. Thereafter, we used the median expression of PPP1R12A (4.3584) as cut-off value, and the samples data were classified into two groups, the high expression group and the low expression group. We utilized the "Limma" package (Ritchie et al., 2015) in R (version 3.6.0) to screen the DEGs related to PPP1R12A using the screening criteria of adjusted $p < 0.01$ (Benjamini and Hochberg; Madar and Batista, 2016) and $|\log_2(\text{fold change})| \geq 1$. The "pheatmap" package was applied for clustering analyses and heatmaps plotting.

We acquired metabolic pathway gene sets from the Molecular Signatures Database[6] (MSigDB) (Subramanian et al., 2005) and the Kyoto Encyclopedia of Genes and Genomes (KEGG) (Ogata et al., 1999). Using the software of GSEA v4.0.3 for Windows and the "c2.cp.kegg.v7.0.symbols.gmt" gene set, the metabolism-related genes were defined as the genes that were enriched in metabolic pathways by calculating the PCa-related activity levels.

Functional Enrichment Analysis

The elemental biological functions of PPP1R12A-related DEGs in PCa can be assessed by performing Gene Ontology (GO) (The Gene Ontology Consortium, 2019) enrichment analysis in three categories (biological processes, cellular component, and molecular function) and KEGG pathway enrichment analysis, which were conducted using the by R package (version 3.6.0) "clusterProfiler" (Yu et al., 2012; Kanehisa and Sato, 2020) with conditions of adjusted $p < 0.05$.

Prognostic Gene Signature Screening and Generation

We utilized the open source toolkit scikit-learn[7] in Python libraries (version 3.6.0) to select the most promising genes to establish and optimize the predictive random forest model. While constructing the random forest, we conducted sequencing for a total of 10 times, identifying the top five genes of the sequencing results. Subsequently, the genes whose occurrence frequency was greater than or equal to 5 were selected as genes of interest (Hastie et al., 2004).

Construction and Validation of Prognostic Signature

The impact of each promising gene on disease-free survival (DFS) was explored by utilizing the univariate Cox regression analysis. According to the expression levels of screened genes, the risk score (RS) model was developed through Cox univariate analysis as the following formula: RS = (−0.4619 × expression value of *PTGS2*) + (−0.141 × expression value of *PPP1R12A*) + (−0.2915 × expression value of *NT5E*) + (−0.6051 × expression value of *AOX1*) + (0.3527 × expression value of *GGCT*). On the basis of the matching median RS, PCa patients were split into high- or low-risk groups. Using the RS-model formula, we calculated the RS for each patient in the TCGA internal validation cohort and one more external validation cohort to confirm the robustness of the prognostic gene signature. The elementary endpoint was DFS and the secondary endpoint was biochemical relapse-free survival (BRFS). Kaplan–Meier curve analysis was performed in the training set and validation set to assess the relationship between the RS and DFS as well as BRFS. We used receiver operating characteristic (ROC) curves to analyze the specificity and sensitivity of the constructed survival prediction classifier. The area under the ROC curve (AUC) value was calculated and compared to assess the classifier performance. $p < 0.05$ was considered to be statistically significant.

Validation of Expression Levels and Subgroup Analysis of Screened Genes

To validate the expression characteristics of the five promising genes between the PCa and control groups, we analyzed the expression levels of the five genes obtained from the TCGA, Taylor, and GSE6956 datasets and depicted these using boxplots. Subgroup analysis in the TCGA cohort was conducted to validate the predictive superiority of the five-gene signature.

Immunohistochemistry Analysis

Protein expression levels of PPP1R12A protein in PCa and benign tissues were tested by immunohistochemistry (IHC) as previously described.

Statistical Analysis

All statistical analyses used were conducted using R software (version 3.6.0). Differential mRNA expression of PPP1R12A in PCa tissues from the TCGA database was tested using Student's *t*-test. Functional enrichment of PPP1R12A-related DEGs in GO terms or KEGG pathways was analyzed using a hypergeometric test. To establish the risk assessment formula, Cox's regression coefficient was obtained through univariate regression analyses. Survival curves were generated and compared by the log-rank test. $p < 0.05$ was considered statistically significant.

RESULTS

PPP1R12A Expression Was Downregulated in PCa

The overall design of our study is shown in **Figure 1**. In our previous study (Lin et al., 2017; Liang et al., 2018), we demonstrated that the combination of miR-30d/PPP1R12A

[5]https://www.ncbi.nlm.nih.gov/geo/

[6]https://www.gsea-msigdb.org/gsea/index.jsp

[7]https://scikit-learn.org/stable/

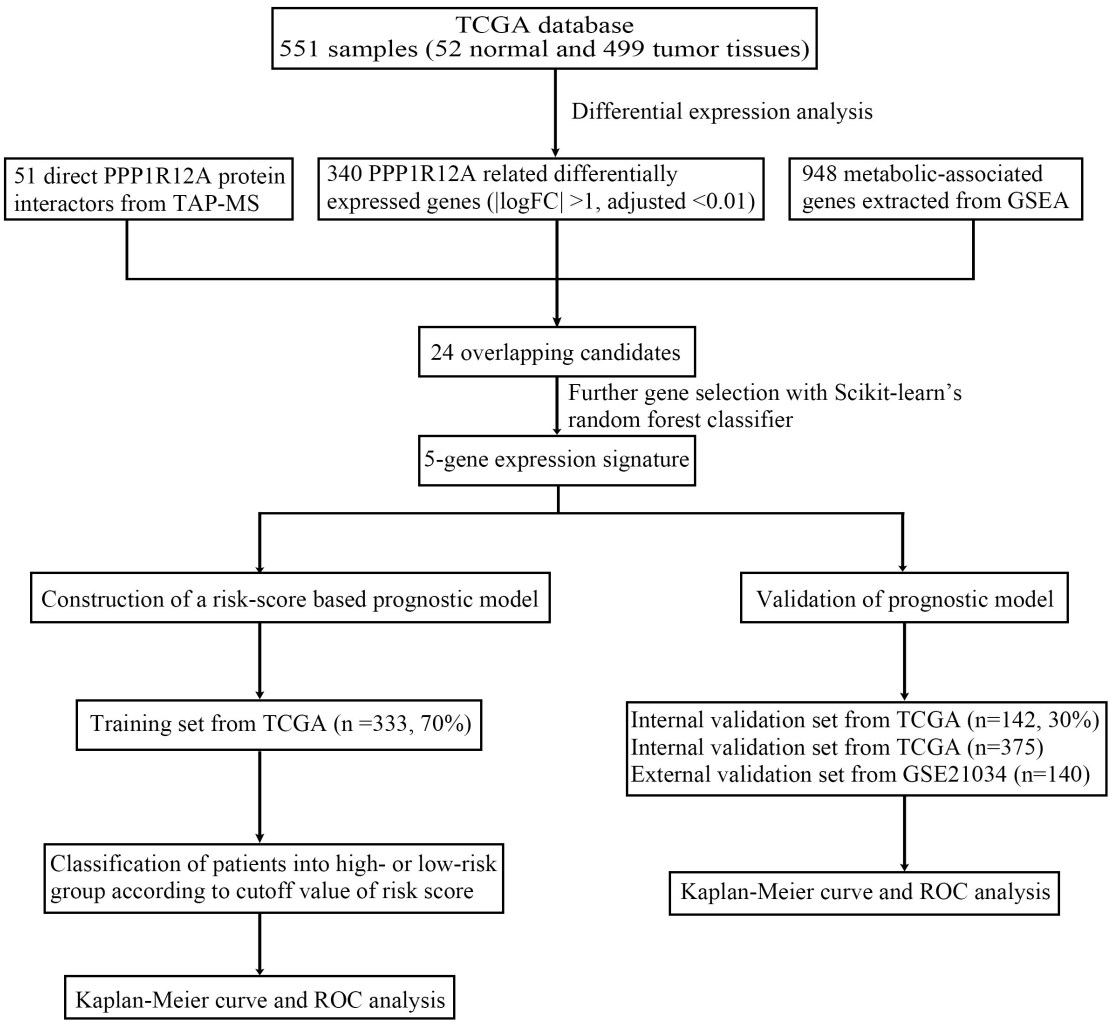

FIGURE 1 | Flow chart of the study.

and the combination of PPP1R12A/CD31 could be effective prognostic factors for human PCa. In order to analyze the expression profiles of PPP1R12A in PCa, mRNA expressions levels of *PPP1R12A* were analyzed by UALCAN, as revealed in 497 PCa samples in TCGA. As shown in **Figure 2A**, mRNA expression levels of *PPP1R12A* were significantly downregulated in PCa tissues compared to normal samples ($p < 0.001$). Furthermore, mRNA levels of *PPP1R12A* in PCa were significantly lower compared to the normal tissues in the subgroup analysis based on the Gleason score (**Figure 2B**). To further validate the level of PPP1R12A in PCa, we conducted IHC to explore the protein expression level of PPP1R12A in PCa and benign tissues. As shown in **Figure 2C**, the immunostaining of PPP1R12A protein in benign prostate tissues was markedly stronger than that in PCa tissues, indicating that the protein expression of PPP1R12A was lower in PCa than in normal prostate tissues. These results suggested that PPP1R12A was significantly downregulated in PCa relative to associated normal tissues.

Identification of Direct PPP1R12A Protein Interactors and PPP1R12A-Related Differentially Expressed Genes

To obtain the direct human PPP1R12A protein interactome, we performed TAP-MS analyses with full-length PPP1R12A protein as bait. We further analyzed our dataset using Protein Pilot 5.0 software and MASCOT software to analyze PPP1R12A interactors, generating a final list of 51 PPP1R12A interactive proteins (**Supplementary Table 1**).

Analysis of PPP1R12A-related DEGs was conducted between the high expression group (higher than median) and low expression group (lower than median) based on the predefined cut-off values (4.3584). With the screening criteria of $p < 0.01$ and $|\log(\text{fold change})| > 1$, we identified 340 PPP1R12A-related DEGs in the TCGA database after screening, which included 338 upregulated genes and two downregulated genes (**Figure 3A**). The heatmaps of these top differentially upregulated

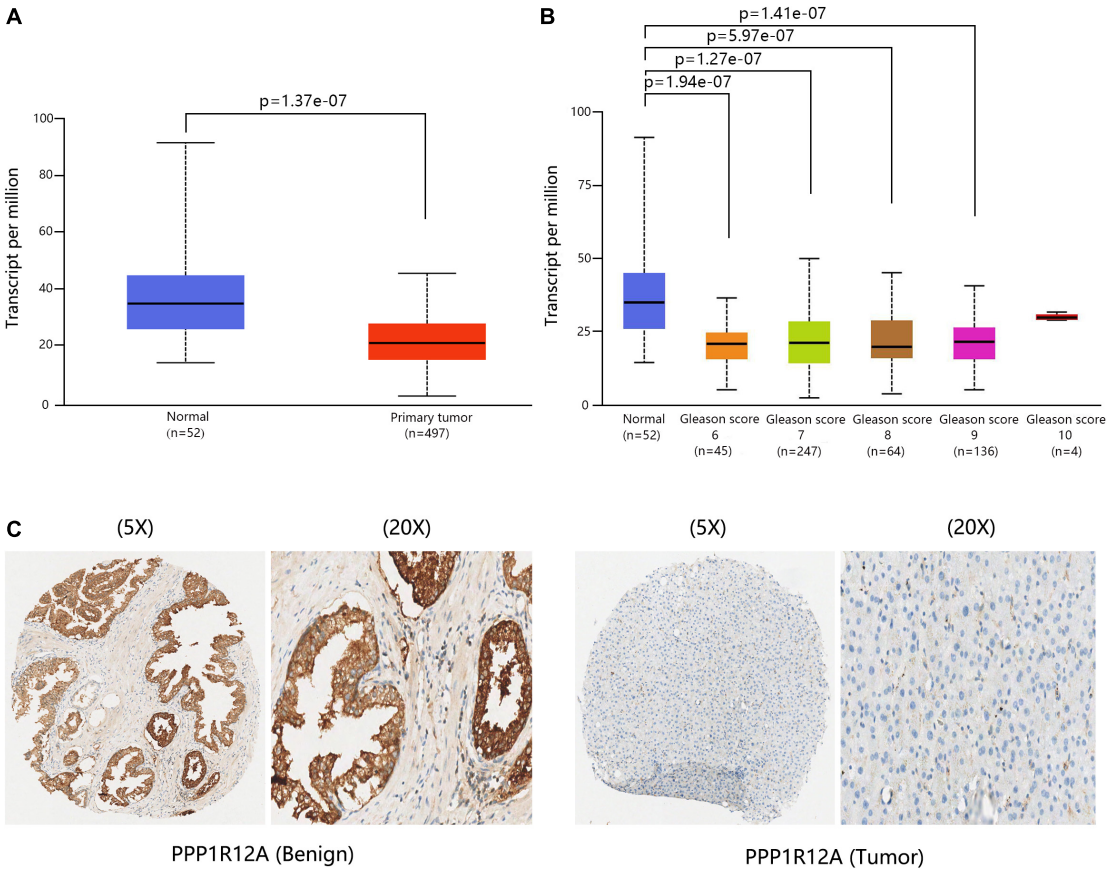

FIGURE 2 | PPP1R12A was downregulated in PCa. **(A)** Relative levels of PPP1R12A in normal prostate and PCa samples based on the UACLAN database. **(B)** Boxplot showing the relative expression of PPP1R12A in healthy controls and PCa patients with different Gleason scores based on the UACLAN database. **(C)** IHC results for MYPT1 in benign and PCa tissues.

and downregulated PPP1R12A-related DEGs are shown in **Figure 3B**.

Gene Functional Enrichment Analysis

GO molecular function enrichment analysis and KEGG pathway enrichment analysis were performed to analyze functional enrichment in PPP1R12A-related DEGs. The top 10 ($^{*}p < 0.05$; $^{**}p < 0.001$) most significant GO terms are shown in **Figure 3C**, which reveals that the most common biological processes among the DEGs were negative regulation of cytosolic calcium ion concentration, positive regulation of fibroblast migration, tumor necrosis factor biosynthesis, endothelial cell morphogenesis, regulation of nitric oxide-mediated signal transduction, prostatic bud formation, prostate glandular acinus development, prostate gland epithelium morphogenesis, bleb assembly, and osteoclast development. Costamere, microfibril, complex of collagen trimers, platelet dense tubular network, integrin complexes, extracellular matrix (ECM) components, protein complexes involved in cell adhesion, basement membrane, fascia adherens, and dystrophin-associated glycoprotein complex were the most significantly enriched cellular components. The most common molecular functions among the DEGs were heparan sulfate proteoglycan binding, intracellular chloride channel activity, intracellular calcium-activated chloride channel activity, proteoglycan binding, EMC structural constituent, transforming growth factor beta binding, nitric-oxide synthase binding, fibronectin binding, ankyrin binding, and calcium-release channel activity.

The results of the KEGG enrichment analysis demonstrated that ECM-receptor interaction, focal adhesion, vascular smooth muscle contraction, proteoglycans in cancer, the cGMP-PKG signaling pathway, the PI3K-Akt signaling pathway, regulation of the actin cytoskeleton, human papillomavirus infection, pathways in cancer, and several other associated KEGG biological pathways were significant to the progression of PCa (**Figure 3D**).

Extraction of Metabolism-Related Genes From the GSEA Website

We acquired 41 metabolic pathway gene sets from MSigDB and KEGG (**Supplementary Table 2**). To identify the metabolism-related genes in PCa, we examined the enrichment scores of 41 metabolic pathway gene sets by using GSEA, extracting 948 metabolism-related genes (**Supplementary Table 3**).

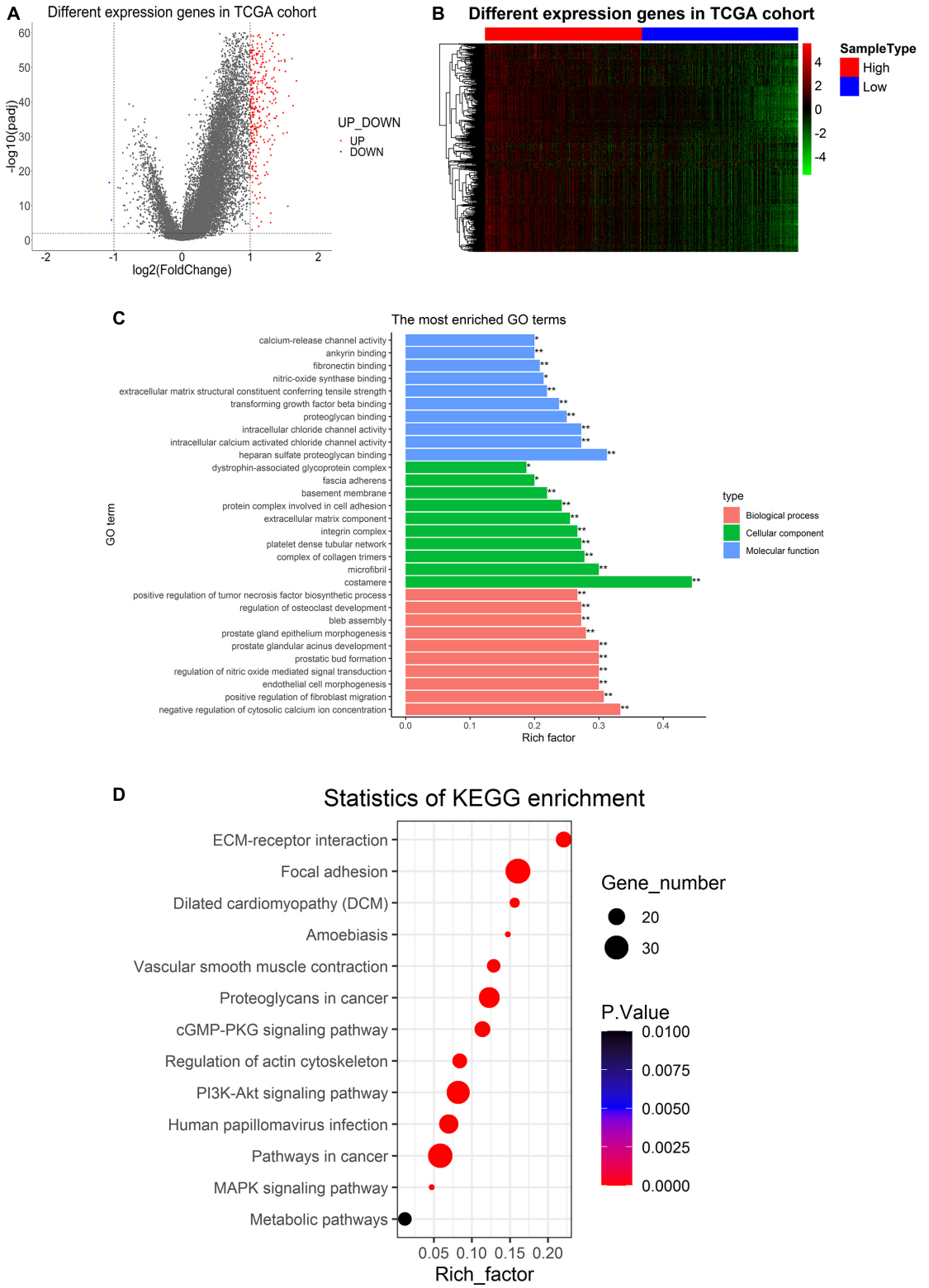

FIGURE 3 | Differentially expressed genes in PCa tissues and GO and KEGG pathway analysis of PPP1R12A-related DEGs. **(A)** Volcano plot for the 340 DEGs from the TCGA PRAD dataset. Red indicates upregulation while blue indicates downregulation. **(B)** Heatmap plot of the top 340 DEGs from the TCGA PRAD dataset. The red shade represents high PPP1R12A expression tissue; the blue shade represents low PPP1R12A expression tissue. **(C,D)** GO functional enrichment analysis **(C)** and KEGG pathway analysis **(D)** of PPP1R12A-related DEGs. *$P < 0.05$, **$P < 0.001$.

Identification of the Candidate Genes and Confirmation of the Five Optimal Genes

To identify common genes among those we extracted above, all three gene groups, including direct PPP1R12A protein interactors, PPP1R12A-related DEGs, and metabolism-related genes, were compared. Although we failed to identify a candidate gene among all three parts of independent gene sets, we selected overlapping candidate genes from the intersection of every two independent gene sets, respectively. In total, 15 overlapping elements in total were identified between the PPP1R12A-related DEGs and the metabolism-related genes (**Supplementary Figure 1A**). In the comparison of the PPP1R12A-related DEGs and the interactive genes, two overlapping genes were identified. Seven overlapping elements were found in the comparison between the metabolism-related genes and the interactive genes (**Supplementary Table 4**). To construct the prognostic signature efficiently, we identified four optimal genes (*PTGS2*, *GGCT*, *AOX1*, and *NT5E*) from the candidate genes we extracted previously through Scikit-learn's random forest classifier (**Supplementary Figure 1B**). These five genes (including *PPP1R12A*) were used to build a predictive signature.

Construction and Verification of the Prognostic Model Based on the Five-Gene Signature

We calculated the RS for each PCa patient in the TCGA training set and ranked them to thoroughly analyze the relevance of the five promising genes in prognosis in these patients. The regression coefficients of the five optimal genes in the Cox regression analysis are shown in **Supplementary Table 5**. Thus, those patients were classified into a low-risk group ($n = 167$) and a high-risk group ($n = 166$) based on median RS (cut-off = –2.7737) (**Figure 4A**, middle). The survival status in the training set is shown in **Figure 4A**, top. Additionally, the five promising genes were differentially expressed in the high- and low-risk groups, as shown in the heatmap in **Figure 4A**, bottom. Utilizing data from the TCGA validation set, the entire TCGA set, and the Taylor database, the RS was calculated in each cohort with the same formula as in the TCGA training set. We confirmed the prognostic value of the five-gene signature by confirming our findings from the TCGA training set (**Figures 4B–D**).

Next, we conducted Kaplan–Meier analysis. In the TCGA training set, patients in the high-risk group exhibited significantly worse DFS than those in the low-risk group (**Figure 5A**) ($p = 0.00507$). Similar analyses of the Kaplan–Meier curve (**Figure 5B**) showed that compared to the high-risk group, patients in the low-risk group exhibited a significantly better DFS in the internal validation set ($p = 0.0454$). In the entire TCGA set of 475 patients, patients in the high-risk group suffered worse DFS than patients in the low-risk group ($p = 0.00059$, **Figure 5C**). Consistently, patients in the low-risk group generally had a better BRFS than patients in the high-risk group in the Taylor external validation cohort ($p = 0.00149$, **Figure 5D**). Time-dependent ROC curve analysis revealed that the five-gene signature had a strong predictive ability in internal and external datasets (**Figures 5E–H**).

Expression Profiles of the Five-Gene Signature and Subgroup Analysis

Utilizing the data concerning different tissues in three databases, we explored the five genes' expression profiles. As shown in **Figure 6A**, *GGCT* expression was significantly upregulated in tumor tissues, while *AOX1*, *NT5E*, *PPP1R12A*, and *PTGS2* were significantly downregulated compared to normal tissues in the TCGA cohort. Similar results were obtained in the Taylor and GSE6956 datasets (**Figures 6B,C**). Subgroup analysis showed that the five-gene signature-based RS had a good predictive ability for DFS in different subgroups, including tumor-free patients ($p = 0.00825$), patients with tumor ($p = 0.0322$), patients aged < 65 years ($p = 0.0238$), patients aged ≥ 65 years ($p = 0.00866$), patients with a Gleason score of < 8 ($p = 0.0173$), patients with a Gleason score of ≥ 8 ($p = 0.0488$), patients with stage T1/T2 PCa ($p = 0.000615$), patients with stage N0 PCa ($p = 0.000604$), and patients with stage M0 PCa ($p = 0.00107$), in the TCGA cohort (**Supplementary Figure 2**).

DISCUSSION

PCa is one of the most common malignant urinary tumors, threatening human health globally. Few effective therapeutic strategies are available for patients with advanced or metastatic diseases, especially CRPC. Consequently, potential biomarkers of PCa that can be used to improve prognostic assessment are urgently needed. We previously identified that PPP1R12A could inhibit angiogenesis and tumor growth, and has been identified as a promising prognostic factor for human PCa. Moreover, previous studies (Dong et al., 2017) showed that cancer metabolism is an essential process in tumorigenesis, while research about the relation between metabolism and the tumor microenvironment in PCa is limited. Therefore, it is important to explore new biomarkers that interact with PPP1R12A for early effective prognosis and personalized treatment of PCa. Thus, we performed a TAP-MS analysis to identify direct PPP1R12A interactors on a proteomic scale, using full-length PPP1R12A protein as bait. We identified 51 direct human PPP1R12A interactors.

First, we conducted an integrated analysis of TCGA datasets to investigate the underlying biomarkers interacting with PPP1R12A in metabolism in PCa. Then, a total of 340 PPP1R12A-related DEGs, including 338 upregulated and 2 downregulated genes, were obtained between 52 normal tissues and 499 PCa tissues. Next, GO analysis and KEGG pathway enrichment analysis were conducted. Calcium-activated chloride channel and chloride channel activity are related to the regulation of cell proliferation, cell migration, and metastasis and are proposed to contribute to tumor growth and invasion in several cancers, including PCa (Lang and Stournaras, 2014; Hu et al., 2019). In addition, EMC (Walker et al., 2018) and cell adhesion (Odero-Marah et al., 2018)

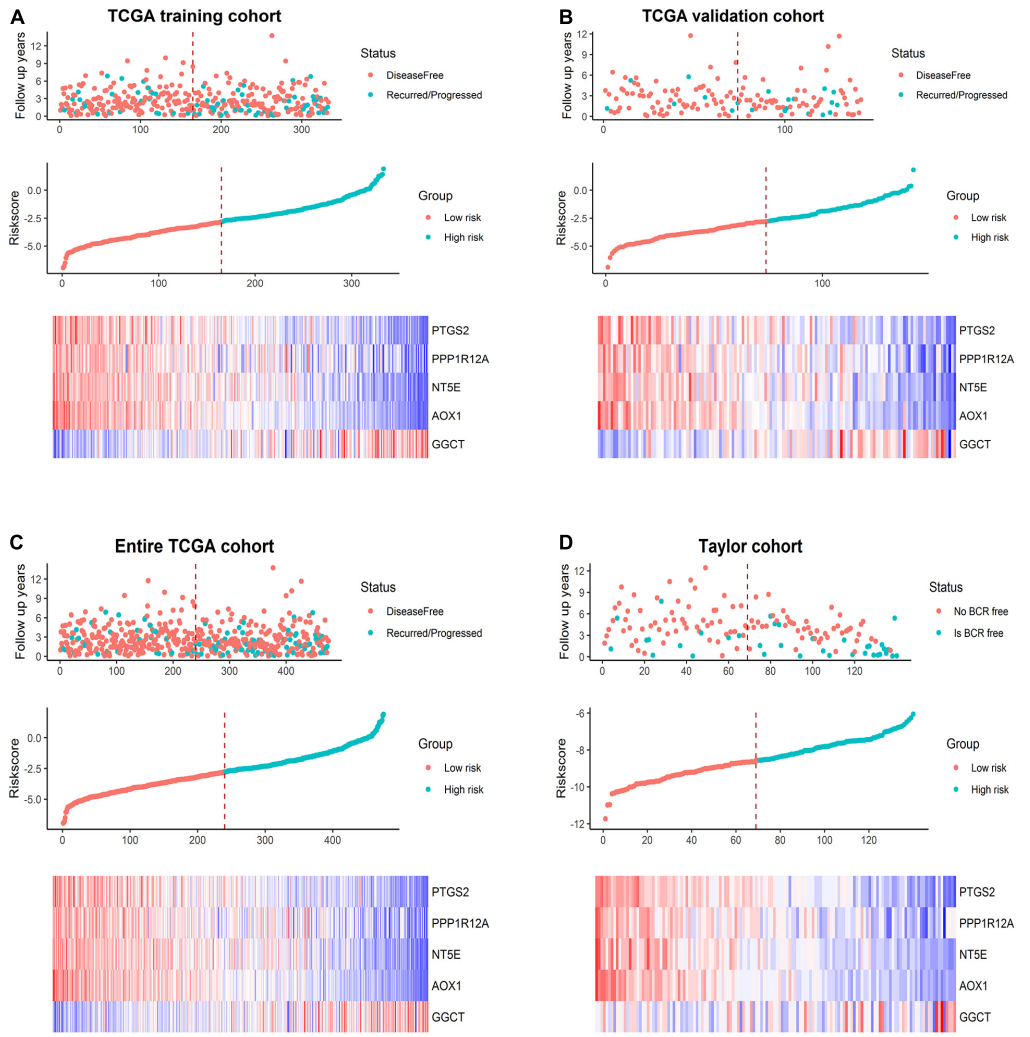

FIGURE 4 | Prognostic model analysis based on the five-gene signature. Analysis of the survival status distribution, risk score, and heatmap based on the five-gene signature in **(A)** the TCGA training set, **(B)** the TCGA validation set, **(C)** the entire TCGA cohort, and **(D)** the Taylor cohort.

are connected to progression and metastasis of PCa. Beyond that, KEGG pathway analysis revealed that these DEGs were primarily involved in vital signaling pathways, including the MAPK signaling pathway, the PI3K-AKT signaling pathway, ECM-receptor interaction, focal adhesion, the cGMP-PKG signaling pathway, and actin cytoskeleton regulation. It was reported that PI3K-AKT signaling is upregulated in PCa, and CRPC is associated with excessive activation of the PI3K-AKT pathway (Carver et al., 2011; Crumbaker et al., 2017). As for the ECM, a vital structural element of the tumor microenvironment, dysregulation of the ECM–receptor interaction signaling pathway was related to the regulation of tumor invasion and metastasis (Zhang et al., 2016; Yeh et al., 2018). Moreover, another study implied that focal adhesion was related to tumor occurrence and metastasis (Eke and Cordes, 2015). Wang et al. (2020) found that the cGMP-PKG signaling pathway also has a tight relationship with proliferation, migration, and invasion in PCa.

After overlapping and Scikit-learn's random forest classifier analysis, *PTGS2*, *GGCT*, *AOX1*, *NT5E*, and *PPP1R12A* were selected as optimal genes. Prostaglandin-endoperoxide synthase 2 (PTGS2), also known as cyclooxygenase-2(COX-2), a crucial enzyme in the process of arachidonic acid conversion to prostaglandins and other eicosanoids, was reported to promote malignant metastasis in colorectal tumor cells (Fenwick et al., 2003). In addition, Guo et al. (2020) demonstrated that PKM2 upregulates COX-2 expression, leading to epithelial-mesenchymal transition (EMT) and metastasis of PCa, by promoting the phosphorylation of ERK1/2. More studies on the role of COX-2 in the regulation of PCa metastasis are required. According to a previous study (Kageyama et al., 2018), γ-glutamylcyclotransferase (GGCT), an indispensable enzyme in connection with glutathione metabolism, is upregulated in most cancers, including PCa. GGCT deficiency leads to the suppression of proliferation, invasion, and migration of cancer cells. It has been demonstrated that downregulation of aldehyde

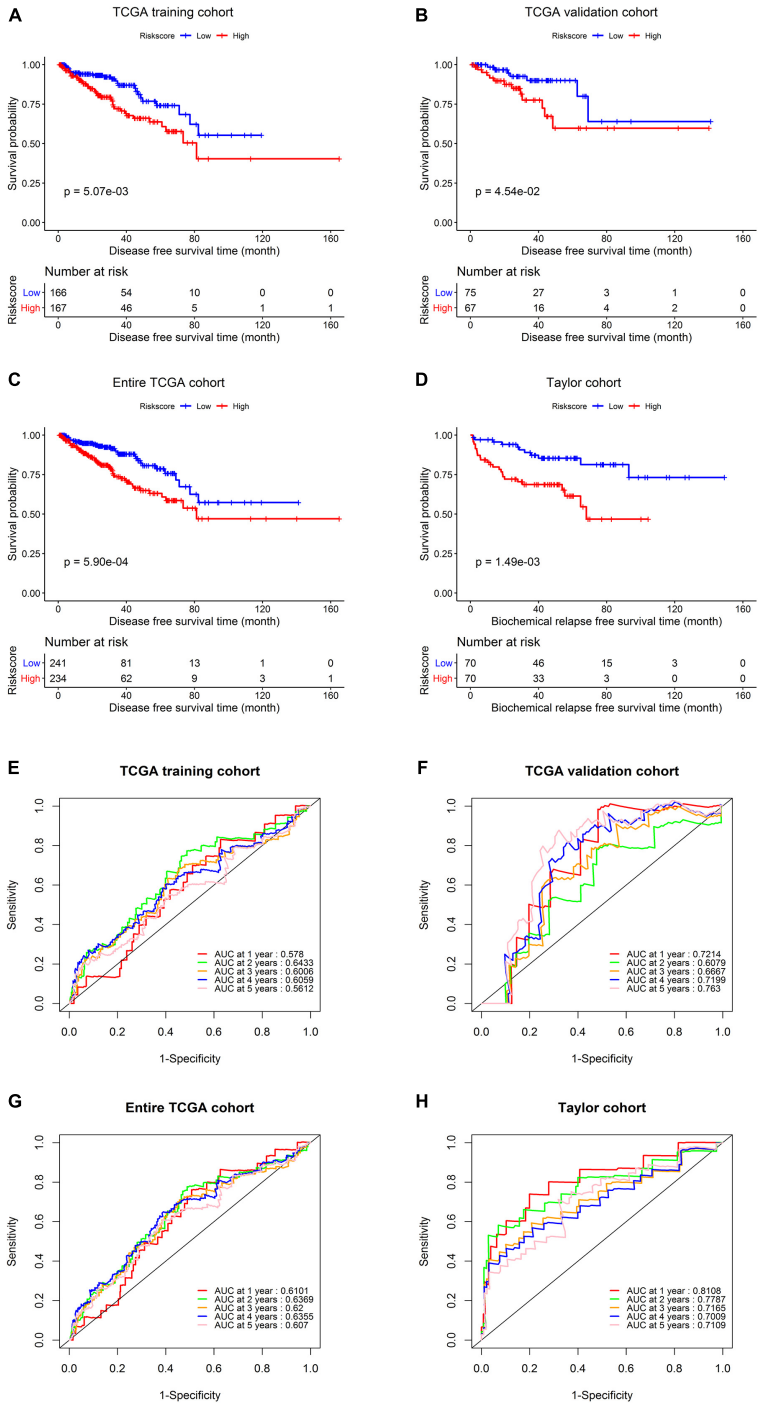

FIGURE 5 | Survival analysis and predictive value validation of the five-gene signature. Comparison of DFS stratified by risk group in the TCGA dataset and comparison of BRFS between the low- and high-risk groups in the Taylor dataset. ROC curves testing the predictive value of the risk score in the following four cohorts: **(A,E)** TCGA training set, **(B,F)** TCGA validation set, **(C,G)** entire TCGA cohort, **(D,H)** Taylor cohort.

oxidase 1 (AOX1) in PCa is related to shorter times until biochemical recurrence (Li et al., 2018). Of note, 5′-nucleotidase ncto (NT5E), also called CD73, whose expression levels can be used to effectively distinguish between aggressive types and indolent forms of PCa, was demonstrated to be a potential independent prognostic marker (Leclerc et al., 2016). The present study provides a direction for further research on the biological functions and clinical characteristics of the five genes in PCa.

Finally, a five-gene prognostic model was established using the TCGA training cohort, and patients were divided into high-risk

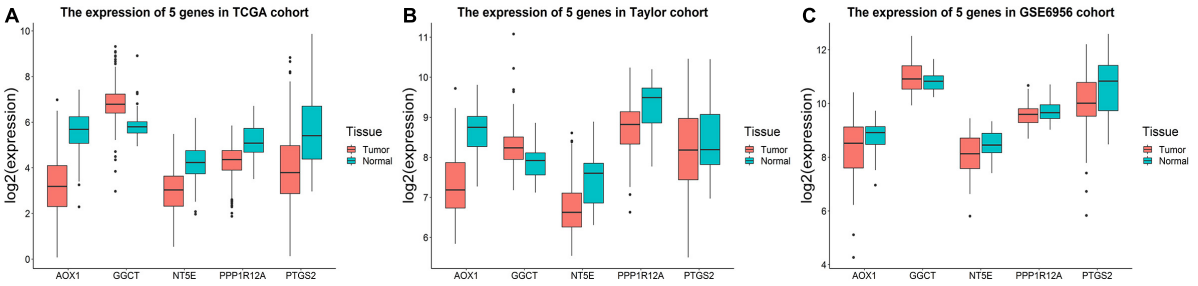

FIGURE 6 | Expression profiles of the five-gene signature. Boxplots presenting the expression levels of the five promising genes (*AOX1*, *GGCT*, *NT5E*, *PPP1R12A*, and *PTGS2*) in the tumor and tumor-free groups from **(A)** the TCGA cohort, **(B)** the Taylor cohort, and **(C)** GSE6956.

and low-risk groups. The AUC values for predicting the 1–, 2–, 3–, 4–, and 5-year DFS rates were 0.578, 0.643, 0.601, 0.606, and 0.561 in the TCGA training cohort, respectively, demonstrating that the model is a reliable predictor of prognosis. We used the data from the TCGA validation cohort and the external Taylor cohort to confirm the prognostic superiority of the five-gene signature. Survival analysis in the validation set confirmed our results from the training set, demonstrating that our five-gene risk model was robust. Additionally, the prognostic significance of the signature was analyzed in different subgroups in the TCGA cohort. The signature also showed a good predictive ability for DFS in different PCa patient subgroups (based on TNM stage, Gleason score, age, or patient status), verifying that the five-gene signature is a functional marker independent of other clinicopathological features.

Despite the merits of the present study, certain limitations should be acknowledged to avoid its overinterpretation. First, it is difficult to fully evaluate the quality of the data used in the study because the number of samples acquired from the databases was relatively low, and part of the gene expression data and clinical data involved were retrieved from open databases. Secondly, further in-depth experimental studies should be conducted to investigate the biological functions and clinical characteristics of the five genes identified in this study.

CONCLUSION

In conclusion, based on publicly available data and our experimental results, we established a robust five-gene signature to predict the prognosis of PCa by stratifying PCa patients into high-risk and low-risk groups. Its prognostic value was validated in an internal cohort from the TCGA database and an external cohort from GEO. Subgroup analysis confirmed that the signature is a functional marker independent of other clinical features. We hope that the signature will guide treatment strategies for PCa patients.

DATA AVAILABILITY STATEMENT

The datasets presented in this study can be found in online repositories. The names of the repository/repositories and accession number(s) can be found in the article/**Supplementary Material**.

ETHICS STATEMENT

The studies involving human participants were reviewed and approved by the Ethics Committee of Guangzhou First People's Hospital. The patients/participants provided their written informed consent to participate in this study.

AUTHOR CONTRIBUTIONS

YuL and WZ conceived, designed the study and revised the manuscript. ZZ, YF, and YiL analyzed the data. RL, QD, YaZ, and ZH contributed to programming. MJ, XZ, SC, and JL collected the clinical samples and data. RZ, ZT, and YiZ performed the experiments. ZZ and YuL wrote and edited the draft. All authors contributed to the article and approved the submitted version.

FUNDING

This work was supported by grants from the National Natural Science Foundation of China (82072813), the Fundamental Research Funds for the Central Universities (2018MS18), the Science and Technology Development Fund (FDCT) of Macau SAR (0031/2021/A and 0049/2021/A1), the Science Foundation of Guangzhou First People's Hospital (Q2019007), and the Natural Science Foundation of Guangdong Province (2020A1515110640 and 2021A1515011088).

ACKNOWLEDGMENTS

We gratefully thank the TCGA database, the GEO database, and the UALCAN database for sharing the data.

SUPPLEMENTARY MATERIAL

The Supplementary Material for this article can be found online at: https://www.frontiersin.org/articles/10.3389/fgene.2021.703210/full#supplementary-material

REFERENCES

Cancer Genome Atlas Network (2012). Comprehensive molecular portraits of human breast tumours. *Nature* 490, 61–70. doi: 10.1038/nature11412

Cardoso, H. J., Carvalho, T. M. A., Fonseca, L. R. S., Figueira, M. I., Vaz, C. V., and Socorro, S. (2021). Revisiting prostate cancer metabolism: from metabolites to disease and therapy. *Med. Res. Rev.* 41, 1499–1538. doi: 10.1002/med.21766

Carver, B. S., Chapinski, C., Wongvipat, J., Hieronymus, H., Chen, Y., Chandarlapaty, S., et al. (2011). Reciprocal feedback regulation of PI3K and androgen receptor signaling in PTEN-deficient prostate cancer. *Cancer Cell* 19, 575–586. doi: 10.1016/j.ccr.2011.04.008

Crumbaker, M., Khoja, L., and Joshua, A. M. (2017). AR Signaling and the PI3K pathway in prostate cancer. *Cancers (Basel)* 9:34 doi: 10.3390/cancers9040034

Dong, W., Keibler, M. A., and Stephanopoulos, G. (2017). Review of metabolic pathways activated in cancer cells as determined through isotopic labeling and network analysis. *Metab. Eng.* 43(Pt B), 113–124. doi: 10.1016/j.ymben.2017.02.002

Dumitru, A. M. G., Rusin, S. F., Clark, A. E. M., Kettenbach, A. N., and Compton, D. A. (2017). Cyclin A/Cdk1 modulates Plk1 activity in prometaphase to regulate kinetochore-microtubule attachment stability. *Elife* 6:e29303. doi: 10.7554/eLife.29303

Eke, I., and Cordes, N. (2015). Focal adhesion signaling and therapy resistance in cancer. *Semin. Cancer Biol.* 31, 65–75. doi: 10.1016/j.semcancer.2014.07.009

El Hassouni, B., Granchi, C., Vallés-Martí, A., Supadmanaba, I. G. P., Bononi, G., Tuccinardi, T., et al. (2020). The dichotomous role of the glycolytic metabolism pathway in cancer metastasis: interplay with the complex tumor microenvironment and novel therapeutic strategies. *Semin. Cancer Biol.* 60, 238–248. doi: 10.1016/j.semcancer.2019.08.025

Fenwick, S. W., Toogood, G. J., Lodge, J. P. A., and Hull, M. A. (2003). The effect of the selective cyclooxygenase-2 inhibitor rofecoxib on human colorectal cancer liver metastases. *Gastroenterology* 125, 716–729.

Ferlay, J., Colombet, M., Soerjomataram, I., Dyba, T., Randi, G., Bettio, M., et al. (2018). Cancer incidence and mortality patterns in Europe: estimates for 40 countries and 25 major cancers in 2018. *Eur. J. Cancer* 103, 356–387. doi: 10.1016/j.ejca.2018.07.005

Ferlay, J., Ervik, M., Lam, F., Colombet, M., Mery, L., Piñeros, M., et al. (2020). *GlobalCancer Observatory: Cancer Today*. Lyon: International Agency for Research on Cancer.

Guo, W., Zhang, Z., Li, G., Lai, X., Gu, R., Xu, W., et al. (2020). Pyruvate kinase M2 promotes prostate cancer metastasis through regulating ERK1/2-COX-2 signaling. *Front. Oncol.* 10:544288. doi: 10.3389/fonc.2020.544288

Hanahan, D., and Weinberg, R. A. (2011). Hallmarks of cancer: the next generation. *Cell* 144, 646–674. doi: 10.1016/j.cell.2011.02.013

Hastie, T., Tibshirani, R., and Friedman, J. (2004). The elements of statistical learning. *J. R. Stat. Soc. Ser. A Stat. Soc.* 167, 192–192.

He, W.-Q., Qiao, Y.-N., Peng, Y.-J., Zha, J.-M., Zhang, C.-H., Chen, C., et al. (2013). Altered contractile phenotypes of intestinal smooth muscle in mice deficient in myosin phosphatase target subunit 1. *Gastroenterology* 144, 1456–1465. doi: 10.1053/j.gastro.2013.02.045

Hu, D., Ansari, D., Bauden, M., Zhou, Q., and Andersson, R. (2019). The emerging role of calcium-activated chloride channel regulator 1 in cancer. *Anticancer Res.* 39, 1661–1666. doi: 10.21873/anticanres.13271

Huber, F., Montani, M., Sulser, T., Jaggi, R., Wild, P., Moch, H., et al. (2015). Comprehensive validation of published immunohistochemical prognostic biomarkers of prostate cancer -what has gone wrong? A blueprint for the way forward in biomarker studies. *Br. J. Cancer* 112, 140–148. doi: 10.1038/bjc.2014.588

Joo, E. E., and Yamada, K. M. (2014). MYPT1 regulates contractility and microtubule acetylation to modulate integrin adhesions and matrix assembly. *Nat. Commun.* 5:3510. doi: 10.1038/ncomms4510

Kageyama, S., Ii, H., Taniguchi, K., Kubota, S., Yoshida, T., Isono, T., et al. (2018). Mechanisms of tumor growth inhibition by depletion of γ-glutamylcyclotransferase (GGCT): a novel molecular target for anticancer therapy. *Int. J. Mol. Sci.* 19:2054 doi: 10.3390/ijms19072054

Kanehisa, M., and Sato, Y. (2020). KEGG Mapper for inferring cellular functions from protein sequences. *Protein Sci.* 29, 28–35. doi: 10.1002/pro.3711

Lang, F., and Stournaras, C. (2014). Ion channels in cancer: future perspectives and clinical potential. *Philos. Trans. R. Soc. Lond. B Biol. Sci.* 369:20130108. doi: 10.1098/rstb.2013.0108

Leclerc, B. G., Charlebois, R., Chouinard, G., Allard, B., Pommey, S., Saad, F., et al. (2016). CD73 expression is an independent prognostic factor in prostate cancer. *Clin. Cancer Res. J. Am. Assoc. Cancer Res.* 22, 158–166. doi: 10.1158/1078-0432.CCR-15-1181

Li, W., Middha, M., Bicak, M., Sjoberg, D. D., Vertosick, E., Dahlin, A., et al. (2018). Genome-wide scan identifies role for AOX1 in prostate cancer survival. *Eur. Urol.* 74, 710–719. doi: 10.1016/j.eururo.2018.06.021

Li, X., Tran, K. M., Aziz, K. E., Sorokin, A. V., Chen, J., and Wang, W. (2016). Defining the protein-protein interaction network of the human protein tyrosine phosphatase family. *Mol. Cell. Proteomics* 15, 3030–3044. doi: 10.1074/mcp.M116.060277

Liang, Y., Zhuo, Y., Lin, Z., Jiang, F., Dai, Q., Lu, J., et al. (2018). Decreased expression of mypt1 contributes to tumor angiogenesis and poor patient prognosis in human prostate cancer. *Curr. Mol. Med.* 18, 100–108. doi: 10.2174/1566524018666180705111342

Lin, Z.-Y., Chen, G., Zhang, Y.-Q., He, H.-C., Liang, Y.-X., Ye, J.-H., et al. (2017). MicroRNA-30d promotes angiogenesis and tumor growth via MYPT1/c-JUN/VEGFA pathway and predicts aggressive outcome in prostate cancer. *Mol. Cancer* 16:48. doi: 10.1186/s12943-017-0615-x

Madar, V., and Batista, S. (2016). FastLSU: a more practical approach for the Benjamini-Hochberg FDR controlling procedure for huge-scale testing problems. *Bioinformatics* 32, 1716–1723. doi: 10.1093/bioinformatics/btw029

Matsumoto, K., Niwa, N., Hattori, S., Takeda, T., Morita, S., Kosaka, T., et al. (2018). Establishment of the optimal follow-up schedule after radical prostatectomy. *Urol. Oncol.* 36, 341.e9–341.e14. doi: 10.1016/j.urolonc.2018.04.003

Murthy, K. S. (2006). Signaling for contraction and relaxation in smooth muscle of the gut. *Annu. Rev. Physiol.* 68, 345–374. doi: 10.1146/annurev.physiol.68.040504.094707

Odero-Marah, V., Hawsawi, O., Henderson, V., and Sweeney, J. (2018). Epithelial-Mesenchymal Transition (EMT) and prostate cancer. *Adv. Exp. Med. Biol.* 1095, 101–110. doi: 10.1007/978-3-319-95693-0_6

Ogata, H., Goto, S., Sato, K., Fujibuchi, W., Bono, H., and Kanehisa, M. (1999). KEGG: kyoto encyclopedia of genes and genomes. *Nucleic Acids Res.* 27, 29–34.

Pavlova, N. N., and Thompson, C. B. (2016). The emerging hallmarks of cancer metabolism. *Cell Metab.* 23, 27–47. doi: 10.1016/j.cmet.2015.12.006

Perkins, D. N., Pappin, D. J., Creasy, D. M., and Cottrell, J. S. (1999). Probability-based protein identification by searching sequence databases using mass spectrometry data. *Electrophoresis* 20, 3551–3567.

Qiao, Y.-N., He, W.-Q., Chen, C.-P., Zhang, C.-H., Zhao, W., Wang, P., et al. (2014). Myosin phosphatase target subunit 1 (MYPT1) regulates the contraction and relaxation of vascular smooth muscle and maintains blood pressure. *J. Biol. Chem.* 289, 22512–22523. doi: 10.1074/jbc.M113.525444

Quinn, D. I., Henshall, S. M., Haynes, A. M., Brenner, P. C., Kooner, R., Golovsky, D., et al. (2001). Prognostic significance of pathologic features in localized prostate cancer treated with radical prostatectomy: implications for staging systems and predictive models. *J. Clin. Oncol.* 19, 3692–3705.

Rattan, S., Phillips, B. R., and Maxwell, P. J. (2010). RhoA/Rho-kinase: pathophysiologic and therapeutic implications in gastrointestinal smooth muscle tone and relaxation. *Gastroenterology* 138, 13–8.e1-3. doi: 10.1053/j.gastro.2009.11.016

Ritchie, M. E., Phipson, B., Wu, D., Hu, Y., Law, C. W., Shi, W., et al. (2015). limma powers differential expression analyses for RNA-sequencing and microarray studies. *Nucleic Acids Res.* 43:e47. doi: 10.1093/nar/gkv007

Roehl, K. A., Han, M., Ramos, C. G., Antenor, J. A. V., and Catalona, W. J. (2004). Cancer progression and survival rates following anatomical radical retropubic prostatectomy in 3,478 consecutive patients: long-term results. *J. Urol.* 172, 910–914.

Siegel, R. L., Miller, K. D., Fuchs, H. E., and Jemal, A. (2021). Cancer statistics, 2021. *CA Cancer J. Clin.* 71, 7–33 doi: 10.3322/caac.21654

Subramanian, A., Tamayo, P., Mootha, V. K., Mukherjee, S., Ebert, B. L., Gillette, M. A., et al. (2005). Gene set enrichment analysis: a knowledge-based approach for interpreting genome-wide expression profiles. *Proc. Natl. Acad. Sci. U.S.A.* 102, 15545–15550.

Sun, L., Suo, C., Li, S.-T., Zhang, H., and Gao, P. (2018). Metabolic reprogramming for cancer cells and their microenvironment: beyond the warburg effect.

Biochim. Biophys. Acta Rev. Cancer 1870, 51–66. doi: 10.1016/j.bbcan.2018.06.005

Taylor, B. S., Schultz, N., Hieronymus, H., Gopalan, A., Xiao, Y., Carver, B. S., et al. (2010). Integrative genomic profiling of human prostate cancer. *Cancer Cell* 18, 11–22. doi: 10.1016/j.ccr.2010.05.026

The Gene Ontology Consortium (2019). The Gene Ontology Resource: 20 years and still GOing strong. *Nucleic Acids Res.* 47, D330–D338. doi: 10.1093/nar/gky1055

Walker, C., Mojares, E., and Del Río Hernández, A. (2018). Role of extracellular matrix in development and cancer progression. *Int. J. Mol. Sci.* 19:3028. doi: 10.3390/ijms19103028

Wallace, T. A., Prueitt, R. L., Yi, M., Howe, T. M., Gillespie, J. W., Yfantis, H. G., et al. (2008). Tumor immunobiological differences in prostate cancer between African-American and European-American men. *Cancer Res.* 68, 927–936. doi: 10.1158/0008-5472.CAN-07-2608

Wang, Z., Zhang, C., Chang, J., Tian, X., Zhu, C., and Xu, W. (2020). LncRNA EMX2OS, regulated by TCF12, interacts with FUS to regulate the proliferation, migration and invasion of prostate cancer cells through the cGMP-PKG signaling pathway. *Onco Targets Ther.* 13, 7045–7056. doi: 10.2147/OTT.S243552

Warburg, O. (1956). On the origin of cancer cells. *Science* 123, 309–314. doi: 10.1126/science.123.3191.309

Ward, J. F., Blute, M. L., Slezak, J., Bergstralh, E. J., and Zincke, H. (2003). The long-term clinical impact of biochemical recurrence of prostate cancer 5 or more years after radical prostatectomy. *J. Urol.* 170, 1872–1876.

Ward, P. S., and Thompson, C. B. (2012). Metabolic reprogramming: a cancer hallmark even warburg did not anticipate. *Cancer Cell* 21, 297–308. doi: 10.1016/j.ccr.2012.02.014

Weiser, D. C., Row, R. H., and Kimelman, D. (2009). Rho-regulated myosin phosphatase establishes the level of protrusive activity required for cell movements during zebrafish gastrulation. *Development* 136, 2375–2384. doi: 10.1242/dev.034892

Yamashiro, S., Yamakita, Y., Totsukawa, G., Goto, H., Kaibuchi, K., Ito, M., et al. (2008). Myosin phosphatase-targeting subunit 1 regulates mitosis by antagonizing polo-like kinase 1. *Dev. Cell* 14, 787–797. doi: 10.1016/j.devcel.2008.02.013

Yeh, M.-H., Tzeng, Y.-J., Fu, T.-Y., You, J.-J., Chang, H.-T., Ger, L.-P., et al. (2018). Extracellular matrix-receptor interaction signaling genes associated with inferior breast cancer survival. *Anticancer Res.* 38, 4593–4605. doi: 10.21873/anticanres.12764

Yu, G., Wang, L.-G., Han, Y., and He, Q.-Y. (2012). clusterProfiler: an R package for comparing biological themes among gene clusters. *OMICS* 16, 284–287. doi: 10.1089/omi.2011.0118

Zhang, H.-J., Tao, J., Sheng, L., Hu, X., Rong, R.-M., Xu, M., et al. (2016). Twist2 promotes kidney cancer cell proliferation and invasion by regulating ITGA6 and CD44 expression in the ECM-receptor interaction pathway. *Onco Targets Ther.* 9, 1801–1812. doi: 10.2147/OTT.S96535

Conflict of Interest: The authors declare that the research was conducted in the absence of any commercial or financial relationships that could be construed as a potential conflict of interest.

Publisher's Note: All claims expressed in this article are solely those of the authors and do not necessarily represent those of their affiliated organizations, or those of the publisher, the editors and the reviewers. Any product that may be evaluated in this article, or claim that may be made by its manufacturer, is not guaranteed or endorsed by the publisher.

frontiers in Genetics

ORIGINAL RESEARCH
published: 27 October 2021
doi: 10.3389/fgene.2021.731278

A Novel Missense Variant of *HOXD13* Caused Atypical Synpolydactyly by Impairing the Downstream Gene Expression and Literature Review for Genotype–Phenotype Correlations

Ruiji Guo[1†], Xia Fang[1†], Hailei Mao[2], Bin Sun[1], Jiateng Zhou[1], Yu An[3] and Bin Wang[1*]*

[1] Department of Plastic and Reconstructive Surgery, Shanghai Ninth People's Hospital, Shanghai Jiao Tong University School of Medicine, Shanghai, China, [2] Department of Anesthesiology and Critical Care Medicine, Zhongshan Hospital, Fudan University, Shanghai, China, [3] Human Phenome Institute, MOE Key Laboratory of Contemporary Anthropology, and School of Life Sciences, Fudan University, Shanghai, China

OPEN ACCESS

Edited by:
Detu Zhu,
Cornell University, United States

Reviewed by:
Antonio Percesepe,
University of Parma, Italy
Tingting Yu,
Shanghai Children's Medical Center, China
Yiping Shen,
Harvard Medical School, United States

***Correspondence:**
Yu An
anyu@fudan.edu.cn
Bin Wang
wangbin1766@163.com

[†] These authors have contributed equally to this work

Specialty section:
This article was submitted to Genetics of Common and Rare Diseases, a section of the journal Frontiers in Genetics

Received: *28 June 2021*
Accepted: *27 August 2021*
Published: *27 October 2021*

Citation:
Guo R, Fang X, Mao H, Sun B, Zhou J, An Y and Wang B (2021) A Novel Missense Variant of HOXD13 Caused Atypical Synpolydactyly by Impairing the Downstream Gene Expression and Literature Review for Genotype–Phenotype Correlations. Front. Genet. 12:731278. doi: 10.3389/fgene.2021.731278

Synpolydactyly (SPD) is a hereditary congenital limb malformation with distinct syndactyly designated as SPD1, SPD2, and SPD3. SPD1 is caused by mutations of *HOXD13*, which is a homeobox transcription factor crucial for limb development. More than 143 SPD patients have been reported to carry *HOXD13* mutations, but there is a lack of genotype–phenotype correlation. We report a novel missense mutation of c. 925A > T (p.I309F) in an individual with atypical synpolydactyly inherited from her father with mild clinodactyly and three other different alanine insertion mutations in *HOXD13* identified by whole exome sequencing (WES) in 12 Chinese SPD families. Unlike polyalanine extension, which tends to form α-helix and causes protein aggregation in the cytoplasm as shown by molecular simulation and immunofluorescence, the c. 925A > T mutation impairs downstream transcription of *EPHA7*. We compiled literature findings and analyzed genotype–phenotype features in 173 SPD individuals of 53 families, including 12 newly identified families. Among the *HOXD13*-related individuals, mutations were distributed in three regions: polyalanine, homeobox, and non-homeobox. Polyalanine extension was the most common variant (45%), followed by missense mutations (32%) mostly in the homeobox compared with the loss-of-function (LOF) variants more likely in non-homeobox. Furthermore, a more severe degree and classic SPD were associated with polyalanine mutations although missense variants were associated with brachydactyly and syndactyly in hands and feet and LOF variants with clinodactyly in hands. Our study broadens the *HOXD13* mutation spectrum and reveals the profile of three different variants and their severity of SPD, the genotype–phenotype correlation related to the *HOXD13* mutation site provides clinical insight, including for genetic counseling.

Keywords: synpolydactyly, *HoxD13*, polyalanine extension, transcription regulation, genotype and phenotype

INTRODUCTION

Synpolydactyly (SPD) is a rare congenital limb deformity characterized by a fusion of adjacent digits and partial or complete digital duplication within the webs. In most patients, synpolydactyly affects the 3/4 fingers and the 4/5 toes (Malik and Grzeschik, 2010). Other features include brachydactyly or camptodactyly of the fifth finger and the fourth–fifth toes, clinodactyly, contraction and flexion of the interphalangeal joint, middle phalanx dysplasia of the second to fifth toes, and syndactyly of the 2/3 finger's etc., (Brison et al., 2012b).

SPD is usually autosomal dominant with variable expressivity (Goodman et al., 1997). Most non-syndromic synpolydactyly cosegregates with a mutation in the *HOXD13* gene on chromosome 2q31 and is categorized as Synpolydactyly type 1 (SPD1, OMIM 186000), which is also known as syndactyly type II (SD II), according to the nomenclature of Temtamy and McKuisck (Temtamy and McKusick, 1978). Other rare genetic synpolydactyly comprises SPD2 (OMIM608180) caused by *FBLN1* gene mutation on chromosome 22q13.31 and SPD3 (OMIM610234), which is mapped to locus 14q11.2-q12 (Malik et al., 2006; Malik and Grzeschik, 2010).

HOXD13 is a member of the *HOX* gene family (Laufer et al., 1994; Deng et al., 2015) expressed in the trunk, limb buds, and genital tubercles. The *HOX* gene cluster encodes a highly conserved transcription factor that plays an important role in morphogenesis during embryonic development (Von Allmen et al., 1996; Goodman, 2002). In humans, there are 39 *HOX* genes arranged in four different gene clusters (*HOXA-HOXD*) on chromosomes 7p14, 17q21, 12q13, and 2q31. The *HOXD13* gene is located at the 5' end of the *HOXD* gene cluster and expressed later than the ones at the 3′ end of the clusters. It is involved in the regulation of distal and posterior regions of the emerging limb bud (Dolle et al., 1991; Brison et al., 2012a,b, 2014; Zhou et al., 2013). The *HOXD13* gene consists of two exons and encodes a protein of 343 amino acids (NM_000523.3). The functional domain of *HOXD13* consists of a 45 bp imperfect trinucleotide repeat, which encodes a 15-residue polyalanine tract within exon 1, a highly conserved 180 bp homeobox in exon 2, and a DNA-binding motif in the protein's C-terminal region. The reported mutations in the *HOXD13* gene comprise three groups: polyalanine tract expansion, truncated mutations, and missense variants. Those mutations have distinct molecular pathogenic mechanisms: (1) polyalanine tract expansion or contraction mutations lead to cytoplasmic retention and aggregation of mutant HOXD13 protein. *In vitro* studies reveal that the mutant protein acts in a dominant-negative manner as it leads to cytoplasmatic aggregates that consist of not only wild-type HOXD13 proteins, but also other polyalanine-containing proteins, such as HOXA13 or RUNX2 (Albrecht et al., 2004). (2) Loss-of-function (LOF) mutations, including frameshift and nonsense mutations, affect the functional domains, including the DNA-binding homeodomain. (3) Missense mutations within the homeobox region affect the transcriptional activation ability of HOXD13 (Dai et al., 2014). Heterozygote and homozygote *HOXD13* mutations are reported, and homozygote carriers manifest severe phenotype with a complex type of SPD (Muragaki et al., 1996; Ibrahim et al., 2016).

Considering the heterogeneous malformations, molecular diagnosis, and treatment need of SPD, we investigate the clinical manifestation of *HOXD13* mutations and their underlying pathogenic mechanisms. We analyzed phenotypes of 53 hereditary SPD families with *HOXD13* mutations, including 12 Chinese non-syndromic SPD families, to explore genotype–phenotype correlation. Furthermore, we investigated the pathogenic mechanisms of aggregate formation within the cells, polymerization-free energy changes, and transcription regulation caused by the *HOXD13* mutations.

MATERIALS AND METHODS

Patient Recruitment and Sample Collection

Patients with non-syndromic SPD and their relatives were recruited. The hands and feet of all probands were radiographed. Phenotypes of family members were acquired by either orthopedist diagnoses or descriptions from the proband's parents (Ni et al., 2018). After informed consent was obtained, peripheral blood samples of patients and their parents were collected for genomic DNA extraction using the DNeasy Blood and Tissue kit (Qiagen, CA 69506, Germany). This study was approved by the ethics committee of the Ninth People's Hospital Affiliated to Shanghai Jiao Tong University (No. SH9H-2018-T50-2).

Trio Whole Exome Sequencing

The genomic DNA samples were processed following the protocol of the SureSelectXT Target Enrichment System for the Illumina Paired-End Sequencing Library (Agilent, CA 95051, United States). Prepared samples were performed by next-generation sequencing (NGS) on a HiSeq system (Illumina). The average coverage was above 20×.

Next-Generation Sequencing Data Analysis

The sequencing data were transformed into Fastq format, and the quality was evaluated by FastQC program. We used the BWA software (0.7.12) for sequence alignment with hg19 genomic reference. The single nucleotide variants and insertions and deletions (InDels) were detected by HaplotypeCaller. The variants were annotated by ANNOVAR software after filtering the variants with AF $\geq$ 1% and intronic and synonymous variants without splicing effects (Ni et al., 2018).

Verification by Sanger Sequencing

The variants of the *HOXD13* gene identified in probands were validated and confirmed in the affected individuals by Sanger sequencing. The PCR system was performed using a PCR kit (Toyobo, CA KFX-101, Japan) in the reaction solution and condition referring to the manufacturer's instructions. The primers were as follows: 1-1F GCGCAGCCAATGGCAC; 1-1R CTTCTCCACGGGAAAGCCTC; 1-2F CCTCTTCTGCCGTTG

TAGCG; 1-2R TTAACCCTGGTCACGTGTGG; 2-1F ACT GTCCTCATGAACGTGCC; 2-1R GGCCTGGAGGGAGAAA CAAA.

Genotype–Phenotype Relationship Analysis

A systematic review of literature and variant databases (ClinVar, Mastermind, HGMD, LOVD, DECIHPER) was conducted to curate the *HOXD13* variations. We selected relevant studies based on the following criteria: (1) having a *HOXD13* mutation site without other gene mutations, (2) having limb malformation phenotypes, (3) having a complete description of the clinical features of malformation. We used "SPD," "polysyndactyly," "synpolydactyly," or "*HOXD13*" as keywords in searching PubMed. A total of 191 studies with *HOXD13* mutations and 84 studies with phenotype and *HOXD13* mutations were retrieved. After excluding 75 duplicates in the two groups and removing those missing photographs of relevant phenotypes, the previously reported mutations and the findings in our study of 12 families were used for statistical analysis (**Supplementary Material 1**).

To evaluate the severity of SPD, we defined an SPD severity score, which is a summary of the frequency of syndactyly, polydactyly, clinodactyly, camptodactyly, and brachydactyly in one patient. One point was assigned to per trait except for synpolydactyly, which was given a score of two points due to its combination of syndactyly and polydactyly. A higher SPD severity score means more limb defects. The statistical analysis was performed on the relationship between the SPD severity score and the *HOXD13* variant type and location.

Plasmid Construction and Transfection

HOXD13 wild type and c.925A > T (p.I309F) DNA fragments were amplified by PCR and cloned into pcDNA3.1(+) using the LIC ligase system (NEB system). *HOXD13* poly-Ala mutant plasmid with + 7A, + 8A, and + 9A (p.A65_A71dup, p.A64_A71dup, p.A63_A71dup) were constructed by inserting synthesized oligo nucleotides encoding the additional alanines (Generay Biotech Co., Ltd., Shanghai) and confirmed by Sanger sequencing. A 660bp fragment of *EPHA7* gene promoter containing a HOXD13 binding site (from −580 to + 80) was obtained from human genomic DNA by PCR and inserted into the *Xho*I and *Hin*dIII sites of a pGL3-basic vector (Promega, E1751, United States) to generate a pGL3-EPHA7 reporter construct (Zhao et al., 2007; Dai et al., 2014). COS-7 cells were cultured in DMEM/high-glucose medium (Hyclone, CA SH30022.01, United States) supplemented with 1% penicillin/streptomycin and 10% fetal bovine serum (6×10^5 cells per well in a six-well plate, 1×10^5 cells per well in a 24-well plate). After the cells were incubated at 37°C for 24 h, 50 μL of DNA-lipid complex (DNA: Lipofectamine® 2000 Reagent, 250ng: 1μL) (Invitrogen, Lipofectamine® 2000 Reagent, United States) was added per well in a 24-well plate for immunofluorescence detection, and 250 μL DNA-lipid complex was added per well in a six-well plate for luciferase assay.

Immunofluorescence Assay

COS-7 cells transfected with pcDNA3.1-HOXD13^{WT}, pcDNA3.1-HOXD13^{I309F}, pcDNA3.1-HOXD13^{+7A}, pcDNA3.1-HOXD13^{+8A}, or pcDNA3.1- HOXD13^{+9A} were incubated for 1 day at 37°C. Cells were treated as follows: washed with PBS and fixed with 4% paraformaldehyde for 10 min, permeabilizied with 0.2% Triton X for 10 min, and blocked with 1% bovine serum albumin for 0.5 h; the cells were incubated with anti-HOXD13 primary antibody for 1 h at 37°C (Abcam, CA ab19866, United States) (1:100 dilution) and FITC conjugated secondary antibody for half an hour at 37°C (Abcam, CA ab6717, United States) (1:200 dilution). The nuclei were stained by DAPI and observed under the fluorescent microscope in the darkroom after mounting.

Luciferase Assay

PcDNA3.1-HOXD13^{WT} and pcDNA3.1-HOXD13^{I309F} were cotransfected with Renilla and pGL3-EPHA7 luciferase reporter plasmid into 293T cells and incubated for 24 h at 37°C. The cells were lysed following the protocol of the Dual-Luciferase® Reporter Assay (Promega, CA E1960, United States): 100 μl of LAR II was predispensed into the luminometer tube before programming the GloMax 20/20 single tube luminometer, 20 μl of PLB lysate was transferred into a tube, and firefly luciferase activity was measured. Then, 100 μl of Stop and Glo® Reagent was dispensed, and renilla luciferase activity was measured. The assay was repeated three times.

Protein Structure Prediction and Molecular Simulation

I-TASSER online software[1] was used to simulate the 3-D structure of HOXD13 homeodomain. The amino acid residues between 276 and 335 were entered to cover the location of the I309F mutation. In addition, we performed molecular dynamics (MD) simulation of the + 0A, + 7A, + 8A, and + 9A monomer using the Gromacs (V5.1.2) software with Charmm36 force field parameter and TIP3P model to figure out the binding energy between two dimers.[2] The initial structure model of dimer and steered molecular dynamics (SMD) simulation were carried out based on the stable conformation of MD simulation equilibrium. Umbrella sampling following SMD simulation and the weighted histogram analysis method were employed to obtain the potential mean force (PMF) during the depolymerization of the polyalanine dimer, which was used to indicate the polymerization-free energy.

Statistical Analyses

Statistical analyses were performed with the GraphPad Prism 8 software. The differences in the relative luciferase activity were assessed by unpaired *t*-test, which was also applied to analyze the differences in severity scores between polyA and homeobox, offspring and parents, among different expansion sizes of polyalanine tract. The statistical differences in severity

[1]https://zhanglab.ccmb.med.umich.edu/I-TASSER/

[2]https://www.gromacs.org/

scores between homeobox and non-homeobox and between polyA and non-homeobox were assessed by Mann–Whitney test due to the unequal variances. $P < 0.05$ was considered statistically significant.

RESULTS

Clinical Features and *HOXD13* Mutations

A total of 12 families with *HOXD13* variants were collected from our clinical center. The pedigree investigation and imaging or X-ray of hands or feet are described in **Figures 1**, **2**, including one pedigree (No 32 in **Supplementary Table 1**), which was reported previously (Ni et al., 2018). Besides synpolydactyly as the typical manifestation, the patients were often accompanied with other phenotypes, including syndactyly (3/4 fingers, 1/2 or 2/3 or 4/5 toes), polydactyly (1/2 fingers, 1/2 or 5/6 toes), clinodactyly (2nd or 4th or 5th finger, 1st or 2nd or 4th or 5th toe), camptodactyly (all five fingers, 1st or 3rd or 4th toe), and brachydactyly (all five fingers, 1st or 2nd or 3rd or 4th toe). Syndactyly presented in an SPD patient was cutaneous or bony. The well-developed duplicated toe could be found at the tibial or fibular side. Clinodactyly can be represented as delta or trapezoidal phalanx.

The major mutations of *HOXD13* observed in this study were polyalanine expansions in exon 1. We identified c.192_212 alanine insertion mutation of *HOXD13* in five families (Family A/B/C/D/E), c.189_212 alanine insertion mutation in Family F and c.186_212 alanine insertion mutation in four families (Family H/I/J/K) (**Supplementary Material 1**). We also found a frameshift mutation of c.610delC inherited from the affected father, which led to a truncated protein (p.P204fs*61) reported previously (Ni et al., 2018). Another novel missense mutation of c.925A > T (p.I309F) was identified in the proband of Family K (**Figure 2**), which was inherited from her father with mild camptodactyly of the fifth digit of right foot.

Genotype–Phenotype Relationship Analysis

To expand our genotype–phenotype analysis, we compiled literature findings and included 53 families with *HOXD13* mutations in this study. Of these *HOXD13* mutations, polyalanine tract expansion was observed in 11 reports, missense mutations in 12 reports, nonsense mutations in 13 reports, and deletion and insertion mutations in five reports. Among the 53 families, polyalanine extension was the most common form of mutation (24/53, 45%) in *HOXD13*. The second most common form of variants was missense mutation (17/53, 32%). The loss of function variants was identified in 10 families (10/53, 19%). Of 10 variants located in the homeobox domain of *HOXD13*, eight of them (8/10, 80%) were missense mutations, and of 12 variants located in the non-homeobox domain of HOXD13, eight of them (8/12, 67%) were truncating mutations.

The 27 curated variants from our expanded data set were mapped to different regions of the *HOXD13* gene (**Figure 3A**). In patients with *HOXD13* polyA mutations, synpolydactyly was observed in 155 affected hands and feet (**Figure 3B**) and especially in feet (> 35%) (**Figure 3C**). We further compared the clinical features of patients with variants in three functional regions of *HOXD13* (polyA, homeobox, and non-homeobox). We observed that the patients with *HOXD13* mutations in the homeobox region had the tendency to present brachydactyly, especially in hands. The patients with non-homeobox mutations in *HOXD13* mostly presented clinodactyly in hands (**Figures 3B,C**). Due to anatomical differences between hand and foot, clinodactyly was often observed in fingers with a greater range of motion and less often in toes.

Statistical analysis was performed on the correlation between the SPD severity scores and *HOXD13* variation types. A statistically significant difference in severity scores between polyA mutation and the variants in homeobox ($P < 0.001$) or non-homeobox ($P < 0.05$) was observed, and no significant difference was found between homeobox and non-homeobox variations (**Figure 3D**). The severity scores between polyalanine tract with + 7A expansion and + 8A or + 9A were statistically different ($P < 0.001$) although the difference between + 8A and + 9A was insignificant (**Figure 3E**). When we examined the transmission effect of poly-Ala expansion, there was no statistically significant difference in severity scores between the offspring and their parents ($p > 0.05$) (**Figure 3F**), suggesting that their clinical manifestation severity remains the same.

Cytoplasmic Aggregation Effect of HOXD13 Variants

To investigate the effect of *HOXD13* mutation on protein aggregation in the cytoplasm, we transfected COS-7 cells with plasmids carrying the wild type, polyalanine extension (+ 7A, + 8A, + 9A), or I309F variation of the *HOXD13* gene. We found the polyalanine expansion mutant (+ 7A, + 8A, + 9A) was partially localized in the cytoplasm, and the wild type and I309F mutant were localized in the nucleus. This indicates that I309F mutant protein did not interfere with nuclear transport of the protein, but the polyalanine extension mutant proteins resulted in cytoplasmic aggregates (**Figure 4**).

Polyalanine Extension Led to Structural Change

Molecular simulation shows that the dimer with alanine insertion mutations (+ 7A, + 8A, + 9A) had conformation changes at the distances of 1.0, 3.0, and 5.5 nm, respectively, and presented varying degrees of α-helix (**Figure 5A**) compared with the one without alanine insertion (+ 0A), which remained free as β-sheet or random coil structure. The polymerization energy of polyalanine dimer with alanine insertion mutation was higher than the wild type, suggesting that proteins with alanine insertion could not depolymerize easily and tended to aggregate (**Figure 5B**).

I309F Reduced the Transcriptional Activation of HOXD13

Based on the computed 3-D structure of HOXD13, I309F is located in the second α-helix of the homeobox domain, which is directly involved in DNA binding (**Figure 5C**).

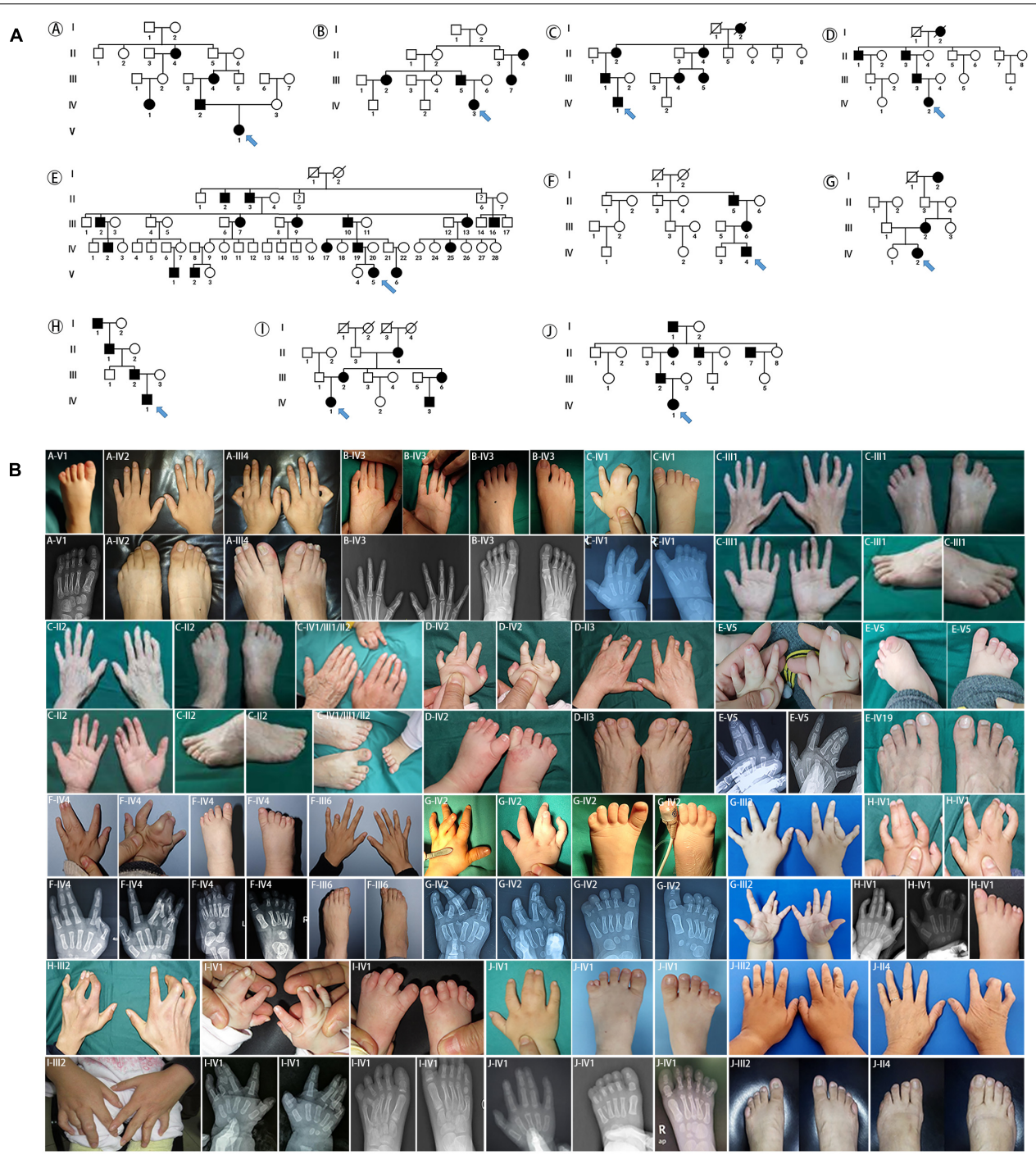

FIGURE 1 | Pedigrees and clinical phenotypes in SPD families with *HOXD13* polyalanine extension. **(A)** The relationship charts of 10 families with synpolydactyly. **(B)** Clinical manifestations of the limbs in affected individuals, including synpolydactyly, syndactyly, syndactyly, clinodactyly, camptodactyly, brachydactyly.

Because the parallel localization of the first and second α-helices is important for DNA binding to the third helix and N-terminal tail (**Figure 5D**), the replacement of isoleucine with a larger phenylalanine residue may disrupt its interaction with the L291 residue of the second α-helix, which results in dysfunction of HOXD13.

We performed luciferase assays of the luciferase reporter gene driven by the promoter of *EPHA7*, which is a downstream gene of HOXD13. The transcriptional activation ability of HOXD13 was examined to understand the regulation effect of the HOXD13 I309F variation. In comparison with the wild-type HOXD13, we observed that the luciferin signal of EPHA7 was significantly

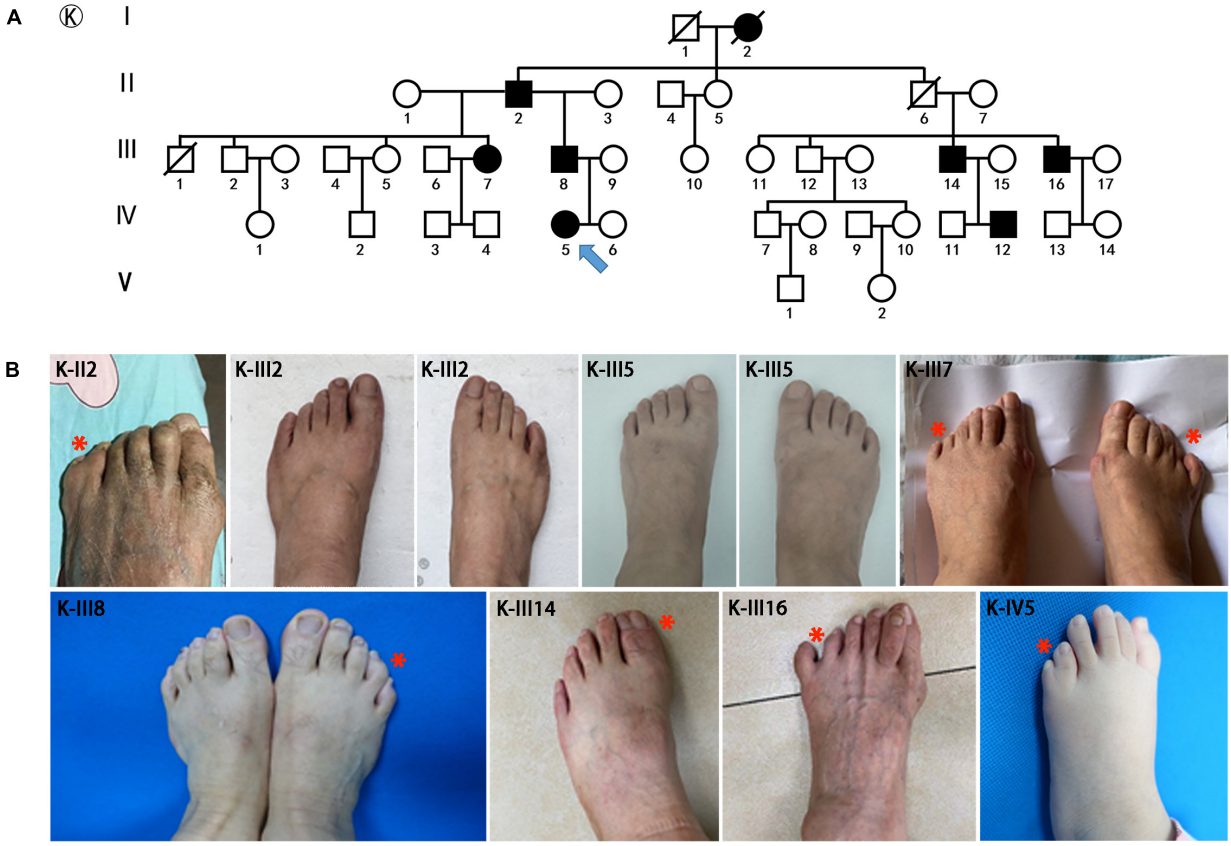

FIGURE 2 | Pedigrees and clinical phenotypes in SPD families with *HOXD13* c.925A > T mutation. **(A)** The relationship chart of the family with atypical synpolydactyly. **(B)** Clinical manifestations of the limbs in affected individuals, including postaxial and preaxial polydactyly, camptodactyly.

decreased in the I309F transfectants. This indicates an impaired transcription factor activity of I309F mutant on the downstream target gene *EPHA7* (**Figure 5E**).

DISCUSSION

SPD is a rare limb deformity showing a special combination of polydactyly and syndactyly (Malik and Grzeschik, 2010). *HOXD13* is an important genetic factor of SPD. There is variable and asymmetrical expressivity of clinical phenotypes caused by *HOXD13* mutations (Malik and Grzeschik, 2010; Al-Qattan, 2020) and studies on genotype–phenotype correlation are limited.

The alanine insertion mutations at c.192_212, c.189_212, and c.186_212 identified in this study are located in the protein-coding region of the first exon of *HOXD13*. So far, a total of nine kinds of human diseases were reported to be associated with alanine repeat mutations, including SPD (*HOXD13*) (Goff and Tabin, 1997), blepharophimosis syndrome (*FOXL2*) (Baere et al., 2003), cleidocranial dysplasia (*RUNX2*) (Mundlos et al., 1997), congenital central hypoventilation syndrome (*PHOX2b*) (Jeanne et al., 2003), holoprosencephaly type 5 (*ZIC2*) (Brown et al., 2001), hand-foot-genital syndrome (*HOXA13*) (Boris et al., 2002), growth hormone deficiency (*SOX3*) (Laumonnier et al., 2002), Paddington syndrome (*ARX*) (Petter et al., 2002), and oculopharyngeal muscular dystrophy (*OPMD*, *PABPN1*) (Brais et al., 1998). All polyalanine repeats are believed to disrupt protein folding, leading to intracellular aggregation (Albrecht et al., 2004). The alanine expansion in HOXA13, RUNX2, and SOX3 resulted in the accumulation of protein in the cytoplasm with interaction with heat shock proteins (Albrecht et al., 2004; Villavicencio-Lorini et al., 2010). Therefore, the protein aggregation due to the alanine extension mutation could prevent the translocation of transcription factor HOXD13 protein into the nucleus resulting in the dysregulation of downstream genes. The length of Ala expansions was previously reported to correlate with the HOXD13 aggregation, and the mutant protein with + 14 Ala and + 21 Ala were exclusively found in the cytoplasm (Albrecht et al., 2004). The alanine repeat expansions resulted in reduced HOXD13-dependent transcriptional activity without affecting DNA binding (Basu et al., 2020). We observed that the alanine extension mutant HOXD13 proteins (+ 7A, + 8A, + 9A) were partially localized in the cytoplasm (**Figure 4**). Furthermore, the molecular simulation of the alanine fragment dimer showed that the molecular structure and polymerization energy were changed when the extra alanine residues were inserted to the 15 alanine

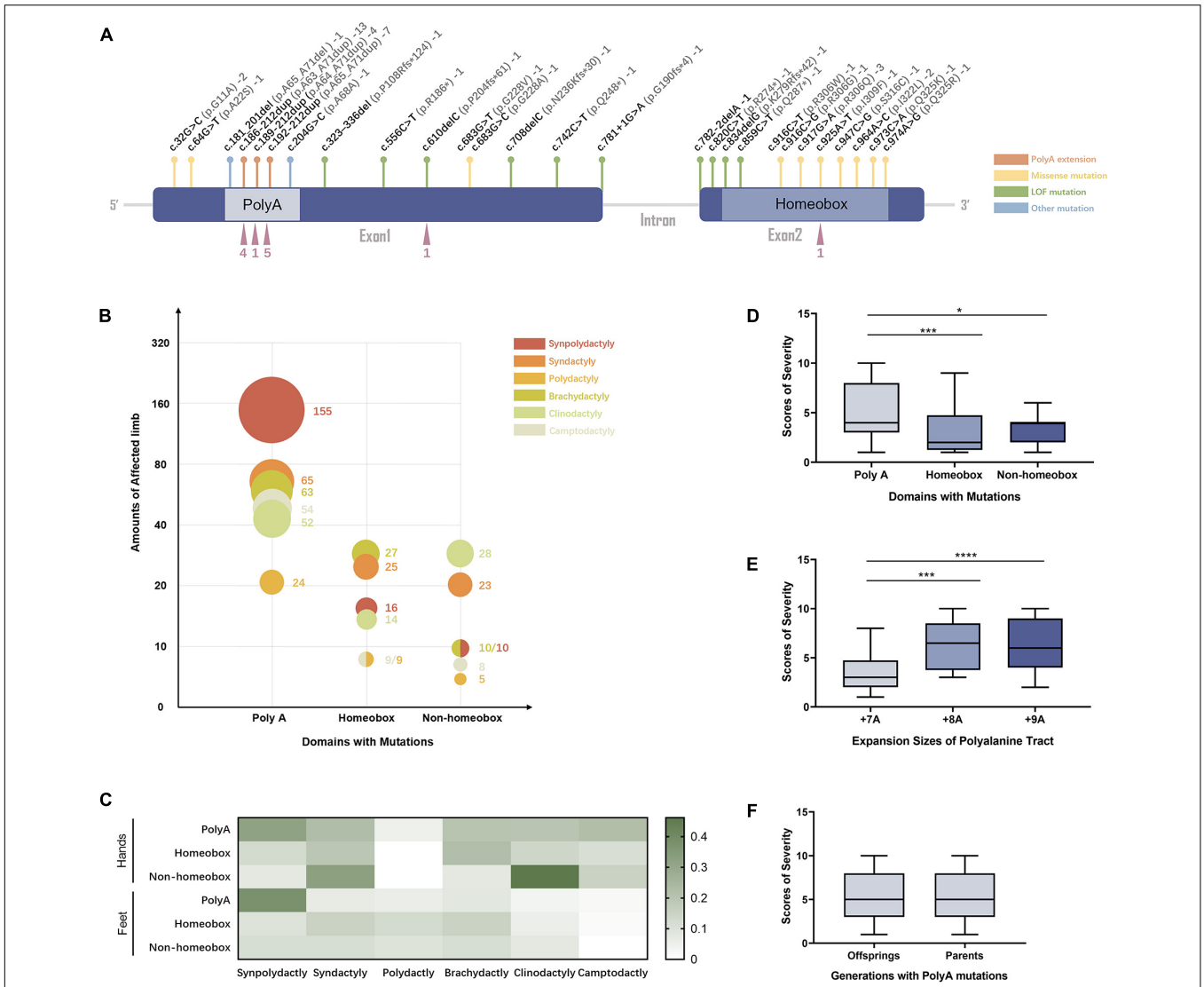

FIGURE 3 | The genotype–phenotype relationship in SPD patients with *HOXD13* mutation. **(A)** The mutation sites in *HOXD13*. **(B)** The number of affected limbs with different phenotypes in different domains with *HOXD13* mutation. **(C)** Heat map of the phenotype:genotype ratios in different *HOXD13* mutation regions in hands and feet separately. **(D)** The scores of severity in different domains with *HOXD13* mutation. **(E)** The scores of severity with different *HOXD13* expansion sizes of polyalanine tract. **(F)** The scores of severity in the offsprings and parents who both have polyA mutations in the *HOXD13* gene. $^{*}P < 0.05$, $^{***}P < 0.001$, and $^{****}P < 0.0001$.

polypeptides, and the dimer was more likely to form α-helical structures and aggregation (**Figures 5A–D**). This indicates that the repeat expansion changed the biophysical properties of HOXD13 protein.

We identified a novel missense mutation c. 925A > T (p.I309F) in the homeodomain of *HOXD13*. The mutant protein was localized in the nucleus with no aggregation in the cytoplasm. The homeobox domain contains 60 residues and is the key region for HOXD13 to bind to DNA as a transcription factor (Scott et al., 1989; Johnson et al., 2003; Burglin and Affolter, 2016). The amino acid sequence of the homeobox domain is highly conserved among different genes in many organisms (Scott et al., 1989; Kissinger et al., 1990). We investigated the effect of a I309F mutation on the transcription activation of the EPHA7 gene, which is one of the downstream genes of HOXD13 and plays an important role in limb development (Valentina and Vincenzo, 2006). Reduced transcription activation of EPHA7 was observed in cells transfected with c. 925A > T *HOXD13*, indicating that the I309F mutation in the homeobox region resulted in impaired transcriptional activation (**Figure 5E**). This is consistent with other studies that report the effect of other missense mutations in the homeobox domain, such as c.940A > C (p.I314L) and c.893G > A (p. R298Q) (Johnson et al., 2003; Wang et al., 2012). In this study, the girl who carried the c. 925A > T mutation had polydactyly L5/6 toes, and this was inherited from the affected father who had a mild phenotype with camptodactyly at his right

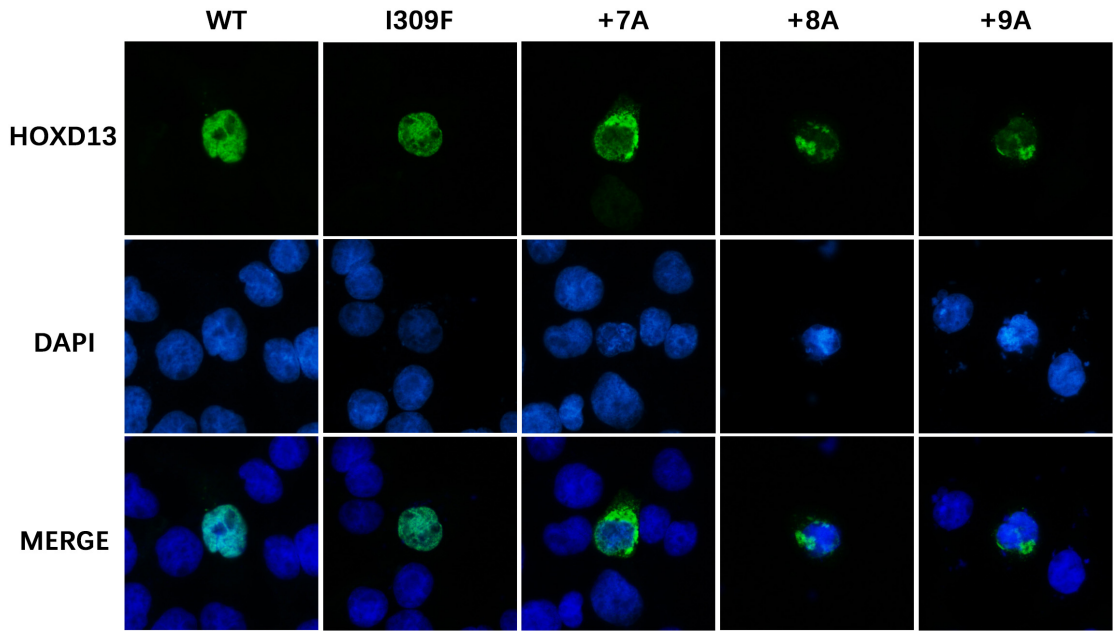

FIGURE 4 | Subcellular location of HOXD13 protein. The blue color in the nucleus shows DAPI staining, and the green color shows HOXD13 staining. WT and I309F mutated HOXD13 protein are localized in nucleus only. Mutants with + 7A, + 8A, + 9A inserted in the polyalanine fragment partially entered the nucleus.

foot. In this four-generation family, there were seven affected individuals who had variable expressivity of atypical SPD at B5/6 or L5/6 toe in feet with HOXD13 c. 925A > T mutation. Considering the segregation evidence of the family (**Figure 2**), the variant c. 925A > T (p.I309F) is pathogenic according to ACMG Guidelines [PM2_P, PS3_M (reduce the transcription of EPHA7), PP1_M (6 affected segregations), PM1 (in homeodomain), PP3 (REVEL score 0.95)].

It is shown that the mutations of *HOXD13* led to variable expressivity and a broad spectrum of clinical features (Brison et al., 2014). We summarized the phenotypes of affected individuals in 53 families with the *HOXD13* mutation spectrum to understand the potential correlation (**Supplementary Table 1**). Although the variable phenotypes were observed in the individuals with *HOXD13* heterozygous mutations, the defects were only related to limbs, a single organ system, and seldom syndrome although *HOXA13* mutations were associated with hand-foot-genital syndrome (Mortlock and Innis, 1997). Among all the clinical features, six of them were common limb abnormalities (synpolydactyly, syndactyly, polydactyly, clinodactyly, camptodactyly, and brachydactyly), and synpolydactyly in the 3/4 fingers and the 4/5 toes were the primary phenotypes. In addition, abnormal flexion crease, stiff joint, broad halluce, symphalangism, oligodactyly, and other features are also described. The cortical bone morphology was abnormal in the individuals with *HOXD13* mutations (Villavicencio-Lorini et al., 2010), resulting in the irregular shape of the long bones in the hand and foot.

The 27 variants from our compiled data set were mapped to the *HOXD13* gene (**Figure 3A**) and categorized into three types of mutations based on the molecular pathogenic mechanisms: polyananine extension, missense mutation, and LOF mutation. The most common mutations, i.e., the polyalanine extension, were frequently associated with classic SPD (Zhao et al., 2007). According to the severity evaluation in this study, patients with polyalanine tract expansion mutations had more severe manifestations than the ones with LOF or missense mutations. In patients with *HOXD13* polyalanine tract expansion mutations, synpolydactyly was observed in 155 affected hands and feet (**Figure 3B**) and especially in feet (> 35%) (**Figure 3C**). Meanwhile, they were also likely to present with syndactyly, brachydactyly, and camptodactyly in hands (> 20%). The misfolding and cytoplasmic aggregation of polyalanine expansion mutants were conferred as dominant negative phenotypes. The missense mutants tend to localize in the homeobox region although the LOF (frameshift or nonsense) mutants usually reside in the non-homeobox region. The patients with LOF mutations in the non-homeobox region had *a priori* clinodactyly (> 40%) in hands as joints have a wider range of motion than feet. The LOF mutations in the homeobox region could be dominant LOF of transcription activity of HOXD13 owing to the truncated proteins produced. The missense mutations in the homeobox region were often presented as brachydactyly and syndactyly in hands and feet. The missense mutations, such as the c. 925A > T (p.I309F) mutation, had a deleterious effect on the transcriptional activation of the human *EPHA7* promoter without forming aggregates in the cytoplasm. For missense variants outside the homeobox region of *HOXD13*, the expression of the HOXD13 G220V mutant was studied in chick limb by Fantini et al. and also presented LOF with the impaired capability to bind DNA and to activate the downstream target of HOXD13 (Fantini et al., 2009). Another G11A missense mutation at the position 32 of the

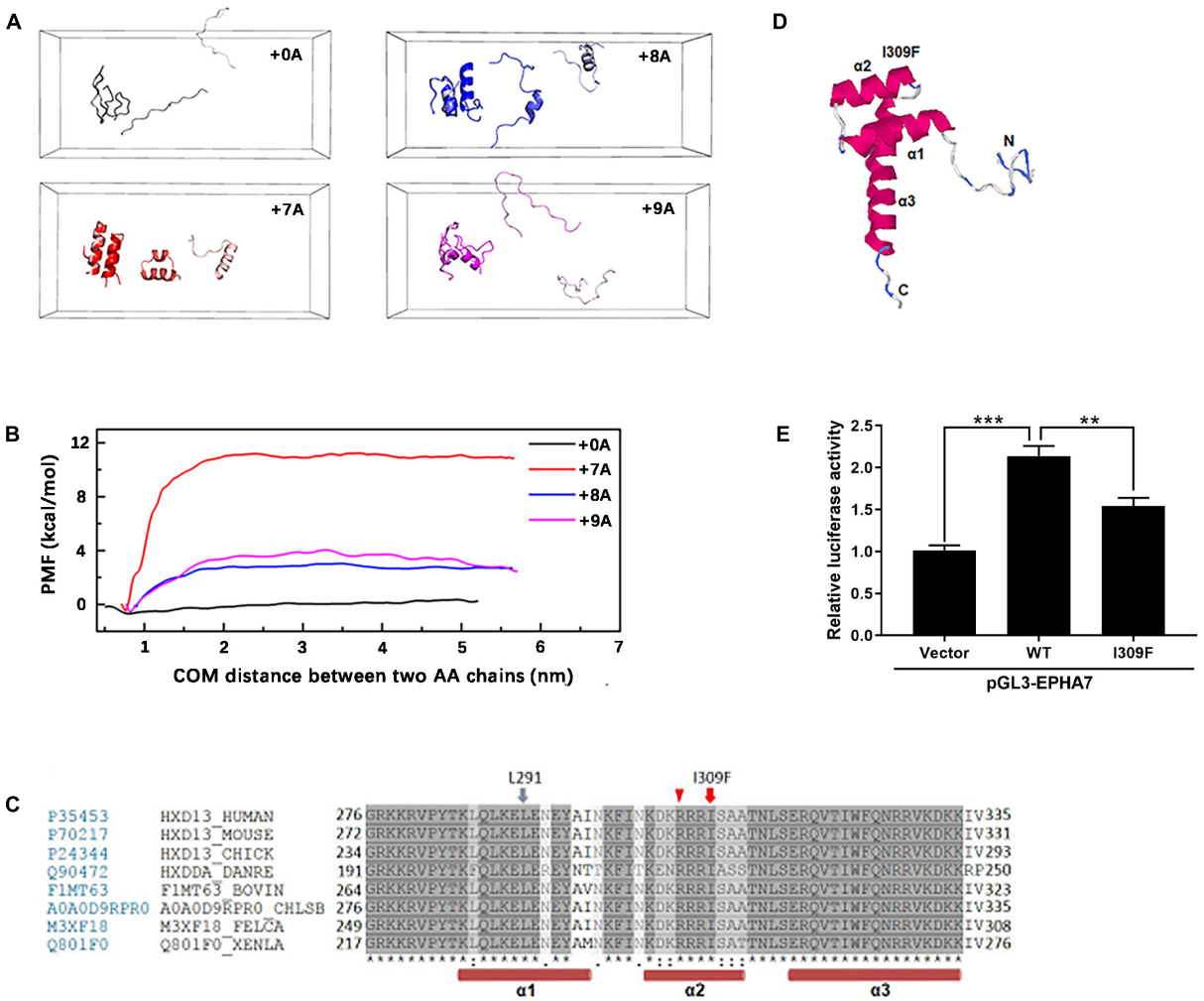

FIGURE 5 | Molecular simulation of mutant HOXD13 and the transcriptional activity of I309F. **(A)** The simulated conformation of the polyalanine fragment dimer. Gray: 15 alanine (+ 0A), Red: 22 alanine (+ 7A). Blue: 23 alanine (+ 8A). Purple: 24 alanine (+ 9A). **(B)** The polymerization energy of alanine dimer. The PMF of 15, 22, 23, 24 alanine was 1.15, 11.71, 3.15, 4.58 kcal/mol, respectively. **(C)** I309 is located in the second α-helix of the homeobox domain. **(D)** The computed 3-D structure of the HOXD13 homeobox domain was generated by the I-TASSER online software. **(E)** Transactivation activity of the pGL3-EPHA renilla luciferase reporter plasmid by HOXD13 I309F mutants and WT. The results of the luciferase assay are presented as relative luciferase activity.

coding region where HOXD13 binds with *GLI3R* resulted in the same phenotype as the depletion of *GLI3R* (Chen et al., 2004), suggesting a new molecular mechanism of *HOXD13*.

We thoroughly evaluated the correlation of SPD phenotype with genotype of *HOXD13* in this study. Previous reports show that homozygous patients may present severe phenotypes but not all (Ibrahim et al., 2016). We created a severity score for the evaluation of synpolydactyly. By comparing the clinical features in the SPD patients with different *HOXD13* mutations (PolyA, homeobox, and non-homeobox), we found a statistically significant difference in the severity scores between polyA mutation and homeobox or non-homeobox ($P < 0.05$) although no significant difference was observed between the variants in homeobox and non-homeobox (**Figure 3D**). In addition, a difference was statistically significant between the polyalanine tract with + 8A or + 9A expansion or + 7A ($P < 0.001$) (**Figure 3E**). It suggests that the individuals with polyA mutations, especially + 8A or + 9A expansion, might have more severe phenotypes, and the ones carrying the missense mutations might have atypical SPD. Penetrance of these variants could not be evaluated due to the lack of genotype in the unaffected.

Our study analyzed the clinical characteristics and inheritance of SPD caused by *HOXD13* mutations and confirmed that the HOXD13 abnormality plays an important role in SPD. We first revealed correlations between the location and types of mutations of HOXD13 and severities of the phenotypes by the overview of 173 affected individuals with *HOXD13* mutations. We compared the mechanism of different types of mutations in *HOXD13* and indicate that the alanine insertion mutations lead to protein aggregation in the cytoplasm, and the mutations in the homeobox decreased downstream transcriptional activity. The finding is of

value for a better understanding of the variable phenotypes and clinical utility of HOXD13-related disease.

DATA AVAILABILITY STATEMENT

The datasets presented in this study can be found in online repositories. The names of the repository/repositories and accession number(s) can be found in the article/ **Supplementary Material**.

ETHICS STATEMENT

The studies involving human participants were reviewed and approved by the Independent Ethics Committee, the Ninth People's Hospital Affiliated to Shanghai Jiao Tong University School of medicine. Written informed consent to participate in this study was provided by the participants' legal guardian/next of kin.

AUTHOR CONTRIBUTIONS

BW, YA, and RG: conceptualization. RG, XF, YA, and BW: data curation. RG and YA: formal Analysis. BW, YA, and HM: funding acquisition. RG, XF, HM, BS, JZ, and YA: methodology. RG, XF, and HM: software. RG and HM: visualization. RG: writing – original draft. BW and YA: writing – review and editing. All authors contributed to the article and approved the submitted version.

FUNDING

This study was supported by the National Natural Science Foundation of China (81772115, 51973041, and 52173118), Shanghai Municipal Science and Technology Major Project (2017SHZDZX01), Shanghai Natural Science Foundation (19ZR1408800), the Shanghai Municipal Key Clinical Specialty (shslczdzk00901), and the Project of Biobank (YBKB202108) from the Shanghai Ninth People's Hospital, Shanghai Jiao Tong University School of Medicine.

ACKNOWLEDGMENTS

We thank Limeng Dai from Department of Medical Genetics, College of Basic Medicine, Army Medical University (Third Military Medical University) for providing the pGL3 plasmid. And we also thank Dr. Xiaomei Lu from Dongguan Children's Hospital for collecting clinical information of families and the Fulgene Genetics for shipping samples.

SUPPLEMENTARY MATERIAL

The Supplementary Material for this article can be found online at: https://www.frontiersin.org/articles/10.3389/fgene.2021.731278/full#supplementary-material

Supplementary Material 1 | *HOXD13* mutation sites in SPD patients. **(A)** Sanger sequencing results in patients with polyalanine extension (c.192_212dup, c.189_212dup, and c.186_212dup). **(B)** Sanger sequencing results in the family members with c.925A > T mutation.

REFERENCES

Albrecht, A. N., Kornak, U., Boddrich, A., Suring, K., Robinson, P. N., Stiege, A. C., et al. (2004). A molecular pathogenesis for transcription factor associated poly-alanine tract expansions. *Hum. Mole. Genet.* 13, 2351–2359. doi: 10.1093/hmg/ddh277

Al-Qattan, M. M. (2020). A Review of the Phenotype of Synpolydactyly Type 1 in Homozygous Patients: Defining the Relatively Long and Medially Deviated Big Toe with/without Cupping of the Forefoot as a Pathognomonic Feature in the Phenotype. *BioMed. Res. Int.* 2020:2067186. doi: 10.1155/2020/2067186

Baere, E. D., Beysen, D., Oley, C., Lorenz, B., Cocquet, J., Sutter, P. D., et al. (2003). FOXL2 and BPES: Mutational Hotspots, Phenotypic Variability, and Revision of the Genotype-Phenotype Correlation. *Am. J. Hum. Genet.* 72, 478–487. doi: 10.1086/346118

Basu, S., Mackowiak, S. D., Niskanen, H., Knezevic, D., Asimi, V., Grosswendt, S., et al. (2020). Unblending of Transcriptional Condensates in Human Repeat Expansion Disease. *Cell* 181, 1062–1079.e1030. doi: 10.1016/j.cell.2020.04.018

Boris, U., Karl, B., Detlef, B., Lentze, M. J., Frank, B., and Michael, L. (2002). A novel stable polyalanine [poly(A)] expansion in the HOXA13 gene associated with hand-foot-genital syndrome: proper function of poly(A)-harbouring transcription factors depends on a critical repeat length? *Hum. Genet.* 110:488. doi: 10.1007/s00439-002-0712-8

Brais, B., Bouchard, J. P., Xie, Y. G., Rochefort, D. L., Chrétien, N., Tomé, F. M. S., et al. (1998). Short GCG expansions in the PABP2 gene cause oculopharyngeal muscular dystrophy. *Nat. Genet.* 121, 164–167. doi: 10.1038/ng0298-164

Brison, N., Debeer, P., Fantini, S., Oley, C., Zappavigna, V., Luyten, F. P., et al. (2012a). An N-terminal G11A mutation in HOXD13 causes synpolydactyly and interferes with Gli3R function during limb pre-patterning. *Hum. Mole. Genet.* 21, 2464–2475. doi: 10.1093/hmg/dds060

Brison, N., Tylzanowski, P., and Debeer, P. (2012b). Limb skeletal malformations - what the HOX is going on? *Eur. J. Med. Genet.* 55, 1–7. doi: 10.1016/j.ejmg.2011.06.003

Brison, N., Debeer, P., and Tylzanowski, P. (2014). Joining the fingers: a HOXD13 Story. *Devel. Dyn.* 243, 37–48. doi: 10.1002/dvdy.24037

Brown, L. Y., Odent, S., David, V., Blayau, M., Dubourg, C., Apacik, C., et al. (2001). Holoprosencephaly due to mutations in ZIC2: alanine tract expansion mutations may be caused by parental somatic recombination. *Hum. Mole. Genet.* 10, 791–796. doi: 10.1093/hmg/10.8.791

Burglin, T. R., and Affolter, M. (2016). Homeodomain proteins: an update. *Chromosoma* 125, 497–521. doi: 10.1007/s00412-015-0543-8

Chen, Y., Knezevic, V., Ervin, V., Hutson, R., and Mackem, S. (2004). Direct interaction with Hoxd proteins reverses Gli3-repressor function to promote digit formation downstream of Shh. *Development* 131:2339. doi: 10.1242/dev.01115

Dai, L., Liu, D., Song, M., Xu, X., Xiong, G., Yang, K., et al. (2014). Mutations in the homeodomain of HOXD13 cause syndactyly type 1-c in two Chinese families. *PLoS One* 9:e96192. doi: 10.1371/journal.pone.0096192

Deng, H., Tan, T., and Yuan, L. (2015). Advances in the molecular genetics of non-syndromic polydactyly. *Exp. Rev. Mole. Med.* 17:e18. doi: 10.1017/erm.2015.18

Dolle, P., Izpisua-Belmonte, J. C., Boncinelli, E., and Duboule, D. (1991). The Hox-4.8 gene is localized at the 5' extremity of the Hox-4 complex and is expressed in the most posterior parts of the body during development. *Mechan. Devel.* 36, 3–13. doi: 10.1016/0925-4773(91)90067-g

Fantini, S., Vaccari, G., Brison, N., Debeer, P., Tylzanowski, P., and Zappavigna, V. (2009). A G220V substitution within the N-terminal transcription regulating domain of HOXD13 causes a variant synpolydactyly phenotype. *Hum. Mole. Genet.* 18, 847–860. doi: 10.1093/hmg/ddn410

Goff, D. J., and Tabin, C. J. (1997). Analysis of Hoxd-13 and Hoxd-11 misexpression in chick limb buds reveals that Hox genes affect both bone condensation and growth. *Development* 124, 627–636. doi: 10.1007/s004290050040

Goodman, F. R. (2002). Limb malformations and the human HOX genes. *Am. J. Med. Genet.* 112, 256–265. doi: 10.1002/ajmg.10776

Goodman, F. R., Mundlos, S., Muragaki, Y., Donnai, D., Giovannucci-Uzielli, M. L., Lapi, E., et al. (1997). Synpolydactyly phenotypes correlate with size of expansions in HOXD13 polyalanine tract. *Proc. Natl. Acad. Sci. U.S.A.* 94, 7458–7463. doi: 10.1073/pnas.94.14.7458

Ibrahim, D. M., Tayebi, N., Knaus, A., Stiege, A. C., Sahebzamani, A., Hecht, J., et al. (2016). A homozygous HOXD13 missense mutation causes a severe form of synpolydactyly with metacarpal to carpal transformation. *Am. J. Med. Genet. Part A* 170, 615–621. doi: 10.1002/ajmg.a.37464

Jeanne, A., Béatrice, L., Tania, A. B., Ha, T., LoïC, D. P., Blanca, G., et al. (2003). Polyalanine expansion and frameshift mutations of the paired-like homeobox gene PHOX2B in congenital central hypoventilation syndrome. *Nat. Genet.* 33, 459–461. doi: 10.1038/ng1130

Johnson, D., Kan, S. H., Oldridge, M., Trembath, R. C., Roche, P., Esnouf, R. M., et al. (2003). Missense mutations in the homeodomain of HOXD13 are associated with brachydactyly types D and E. *Am. J. Hum. Genet.* 72, 984–997. doi: 10.1086/374721

Kissinger, C. R., Liu, B. S., Martin-Blanco, E., Kornberg, T. B., and Pabo, C. O. (1990). Crystal structure of an engrailed homeodomain-DNA complex at 2.8 A resolution: a framework for understanding homeodomain-DNA interactions. *Cell* 63, 579–590. doi: 10.1016/0092-8674(90)90453-l

Laufer, E., Nelson, C. E., Johnson, R. L., Morgan, B. A., and Tabin, C. (1994). Sonic hedgehog and Fgf-4 act through a signaling cascade and feedback loop to integrate growth and patterning of the developing limb bud. *Cell* 79, 993–1003. doi: 10.1016/0092-8674(94)90030-2

Laumonnier, F., Ronce, N., Hamel, B. C. J., Thomas, P., Lespinasse, J., Raynaud, M., et al. (2002). Transcription Factor SOX3 Is Involved in X-Linked Mental Retardation with Growth Hormone Deficiency. *Am. J. Hum. Genet.* 71, 1450–1455. doi: 10.1086/344661

Malik, S., Abbasi, A. A., Ansar, M., Ahmad, W., Koch, M. C., and Grzeschik, K. H. (2006). Genetic heterogeneity of synpolydactyly: a novel locus SPD3 maps to chromosome 14q11.2-q12. *Clin. Genet.* 69, 518–524. doi: 10.1111/j.1399-0004.2006.00620.x

Malik, S., and Grzeschik, K.-H. (2010). Synpolydactyly: clinical and molecular advances. *Clin. Genet.* 73, 113–120. doi: 10.1111/j.1399-0004.2007.00935.x

Mortlock, D. P., and Innis, J. W. (1997). Mutation of HOXA13 in hand-foot-genital syndrome. *Nat. Genet.* 15, 179–180. doi: 10.1038/ng0297-179

Mundlos, S., Otto, F., Mundlos, C., Mulliken, J. B., Aylsworth, A. S., Albright, S., et al. (1997). Mutations involving the transcription factor CBFA1 cause cleidocranial dysplasia. *Cell* 89, 773–779. doi: 10.1016/s0092-8674(00)80260-3

Muragaki, Y., Mundlos, S., Upton, J., and Olsen, B. R. (1996). Altered growth and branching patterns in synpolydactyly caused by mutations in HOXD13. *Science* 272, 548–551. doi: 10.1126/science.272.5261.548

Ni, F., Han, G., Guo, R., An, Y., and Wang, B. (2018). Novel HOXD13 frameshift mutation causes synpolydactyly and clinodactyly. *Int. J. Clin. Exp. Med.* 11, 10988–10994.

Petter, S., Mangelsdorf, M. E., Shaw, M. A., Lower, K. M., Lewis, S. M. E., Helene, B., et al. (2002). Mutations in the human ortholog of Aristaless cause X-linked mental retardation and epilepsy. *Nat. Genet.* 30, 441–445. doi: 10.1038/ng862

Scott, M. P., Tamkun, J. W., and Iii, G. W. H. (1989). The structure and function of the homeodomain. *Biochem. Boiophys. Acta* 989, 25–48. doi: 10.1016/0304-419x(89)90033-4

Temtamy, S. A., and McKusick, V. A. (1978). The genetics of hand malformations. *Birth Defects Orig. Artic. Ser.* 14, 1–619.

Valentina, S., and Vincenzo, Z. (2006). Hoxd13 and Hoxa13 directly control the expression of the EphA7 Ephrin tyrosine kinase receptor in developing limbs. *J. Biol. Chem.* 281, 1992–1999.

Villavicencio-Lorini, P., Kuss, P., Friedrich, J., Haupt, J., Farooq, M., Turkmen, S., et al. (2010). Homeobox genes d11-d13 and a13 control mouse autopod cortical bone and joint formation. *J. Clin. Investig.* 120, 1994–2004. doi: 10.1172/JCI41554

Von Allmen, G., Hogga, I., Spierer, A., Karch, F., Bender, W., Gyurkovics, H., et al. (1996). Splits in fruitfly Hox gene complexes. *Nature* 380, 116. doi: 10.1038/380116a0

Wang, B., Xu, B., Cheng, Z., Zhou, X., Wang, J., Yang, G., et al. (2012). A novel non-synonymous mutation in the homeodomain of HOXD13 causes synpolydactyly in a Chinese family. *Clin. Chim. Acta* 413, 1049–1052. doi: 10.1016/j.cca.2012.02.015

Zhao, X., Sun, M., Zhao, J., Leyva, J. A., Zhu, H., Yang, W., et al. (2007). Mutations in HOXD13 underlie syndactyly type V and a novel brachydactyly-syndactyly syndrome. *Am. J. Hum. Genet.* 80, 361–371. doi: 10.1086/511387

Zhou, X., Zheng, C., He, B., Zhu, Z., Li, P., He, X., et al. (2013). A novel mutation outside homeodomain of HOXD13 causes synpolydactyly in a Chinese family. *Bone* 57, 237–241. doi: 10.1016/j.bone.2013.07.039

Conflict of Interest: The authors declare that the research was conducted in the absence of any commercial or financial relationships that could be construed as a potential conflict of interest.

The reviewer TY declared a shared affiliation with several of the authors, RG, JZ, XF, BS, and BW, to the handling editor at the time of review.

Publisher's Note: All claims expressed in this article are solely those of the authors and do not necessarily represent those of their affiliated organizations, or those of the publisher, the editors and the reviewers. Any product that may be evaluated in this article, or claim that may be made by its manufacturer, is not guaranteed or endorsed by the publisher.

frontiers in Genetics

ORIGINAL RESEARCH
published: 06 December 2021
doi: 10.3389/fgene.2021.774155

Construction and Analysis of Immune Infiltration-Related ceRNA Network for Kidney Stones

Yuqi Xia†, Xiangjun Zhou†, Zehua Ye, Weimin Yu, Jinzhuo Ning, Yuan Ruan, Run Yuan, Fangyou Lin, Peng Ye, Di Zheng, Ting Rao and Fan Cheng**

Department of Urology, Renmin Hospital of Wuhan University, Wuhan, China

Purpose: Kidney stones is a common medical issue that mediates kidney injury and even kidney function loss. However, the exact pathogenesis still remains unclear. This study aimed to explore the potential competing endogenous RNA (ceRNA)-related pathogenesis of kidney stones and identify the corresponding immune infiltration signature.

Methods: One mRNA and one long non-coding RNA (lncRNA) microarray dataset was obtained from the GEO database. Subsequently, we compared differentially expressed mRNAs (DE-mRNAs) and lncRNAs between Randall's plaques in patients with calcium oxalate (CaOx) stones and controls with normal papillary tissues. lncRNA-targeted miRNAs and miRNA–mRNA pairs were predicted using the online databases. lncRNA-related DE-mRNAs were identified using the Venn method, and GO and KEGG enrichment analyses were subsequently performed. The immune-related lncRNA–miRNA–mRNA ceRNA network was developed. The CIBERSORT algorithm was used to estimate the rate of immune cell infiltration in Randall's plaques. The ceRNA network and immune infiltration were validated in the glyoxylate-induced hyperoxaluric mouse model and oxalate-treated HK-2 cells.

Results: We identified 2,340 DE-mRNAs and 929 DE-lncRNAs between Randall's plaques in patients with CaOx stones and controls with normal papillary tissues. lncRNA-related DE-mRNAs were significantly enriched in extracellular matrix organization and collagen-containing extracellular matrix, which were associated with kidney interstitial fibrosis. The immune-related ceRNA network included 10 lncRNAs, 23 miRNAs, and 20 mRNAs. Moreover, we found that M2 macrophages and resting mast cells were differentially expressed between Randall's plaques and normal tissues. Throughout kidney stone development, kidney tubular injury, crystal deposition, collagen fiber deposition, TGF-β expression, infiltration of M1 macrophages, and activation of mast cells were more frequent in glyoxylate-induced hyperoxaluric mice compared with control mice. Nevertheless, M2 macrophage infiltration increased in early stages (day 6) and decreased as kidney stones progressed (day 12). Furthermore, treatment with 0.25 and 0.5 mM of oxalate for 48 h significantly upregulated NEAT1, PVT1, CCL7, and ROBO2 expression levels and downregulated hsa-miR-23b-3p, hsa-miR-429, and hsa-miR-139-5p expression levels in the HK-2 cell line in a dose-dependent manner.

OPEN ACCESS

Edited by:
Detu Zhu,
Cornell University, United States

Reviewed by:
Malgorzata Kloc,
Houston Methodist Research Institute, United States
Udayan Bhattacharya,
NewYork-Presbyterian, United States

****Correspondence:***
Ting Rao
tinart@126.com
Fan Cheng
Urology1969@aliyun.com

†These authors have contributed equally to this work

Specialty section:
This article was submitted to RNA, a section of the journal Frontiers in Genetics

Received: *11 September 2021*
Accepted: *17 November 2021*
Published: *06 December 2021*

Citation:
Xia Y, Zhou X, Ye Z, Yu W, Ning J, Ruan Y, Yuan R, Lin F, Ye P, Zheng D, Rao T and Cheng F (2021) Construction and Analysis of Immune Infiltration-Related ceRNA Network for Kidney Stones. Front. Genet. 12:774155. doi: 10.3389/fgene.2021.774155

Conclusion: We found that significant expressions of ceRNAs (NEAT1, PVT1, hsa-miR-23b-3p, hsa-miR-429, hsa-miR-139-5p, CCL7, and ROBO2) and infiltrating immune cells (macrophages and mast cells) may be involved in kidney stone pathogenesis. These findings provide novel potential therapeutic targets for kidney stones.

Keywords: kidney stones, ceRNA, immune cell infiltration, calcium oxalate, glyoxylate

INTRODUCTION

Kidney stones are common and have high incidence and recurrence rates. Kidney stone prevalence in China is 6.4% and increases annually worldwide (Zeng et al., 2017; Kittanamongkolchai et al., 2018), inducing a heavy burden on the healthcare system. Calcium oxalate (CaOx) kidney stones, the most common type of kidney stone, can induce urinary tract obstruction, renal tubular injury, interstitium inflammation and fibrosis, and even chronic renal disease (Rule et al., 2011). However, the process of kidney stone formation is complex, and the exact mechanism remains unclear. Currently, Randall's plaque (RP), the calcium phosphate crystal deposition at the tip of the renal papillae, is considered to be the origin of kidney stones (Daudon et al., 2015). Crystals in supersaturated urine nucleates deposit in the renal papillae and grow gradually, eventually forming kidney stones (Khan and Canales, 2015). Evidence from endoscopic images demonstrated that stones attach to RP, which appeared in approximately half of patients with kidney stones (Pless et al., 2019). Moreover, renal papillae biopsies have shown that RP formation was associated with high urinary calcium levels, acidic urine, and metabolic diseases (Marien and Miller, 2016). Thus, studying RP to explore the potential pathogenesis of kidney stones and effective therapeutic targets is essential.

Non-coding RNAs (ncRNAs) include long non-coding RNAs (lncRNAs), microRNAs (miRNAs), and circular RNAs, which regulate gene expression at transcriptional and post-transcriptional levels without coding proteins (Beermann et al., 2016). Accumulating evidence has shown that the regulation of mRNAs and ncRNAs is essential for kidney stone-induced renal injury, including apoptosis, oxidative stress, inflammation, and interstitial fibrosis (Liu et al., 2019; Li et al., 2020; Zhu et al., 2020). In recent years, a competing endogenous RNAs (ceRNAs) network hypothesis has been proposed. This hypothesis states that RNAs communicate with each other using miRNA response elements (MREs). LncRNAs regulate the function of mRNAs by competitively binding to the corresponding miRNAs through MREs (Salmena et al., 2011). Given their complexity, the dysregulation of lncRNA–miRNA–mRNA networks is closely related to the pathogenesis of acute and chronic kidney injuries, including ischemia-reperfusion injury and unilateral ureteral obstruction (Cheng et al., 2019; Ren et al., 2019). Nevertheless, few studies have concentrated on the ceRNA regulatory network in patients with kidney stones.

Conventionally, the immune system plays a crucial role in the formation and pathogenesis of kidney stones. Throughout kidney stone development, CaOx crystals promote the secretion of inflammatory cytokines and chemokines, possibly recruiting various immune cells to renal interstitium, including neutrophils, macrophages, and T cells (Zhu et al., 2019; Taguchi et al., 2021). The dysfunction of the immune microenvironment in the kidney could not only initiate adverse factors, but also further exacerbate kidney stone formation (Khan et al., 2021). Previous studies have revealed that M2 macrophages can phagocytize and degrade crystals to suppress stone formation and prevent CaOx inflammatory damage (Taguchi et al., 2021). However, the polarization of M1 macrophages induces cell damage and increases stone burden (Taguchi et al., 2021). In this context, another study has shown that aberrant γδT cells were activated and accumulated in CaOx kidney stones in a mouse model (Zhu et al., 2019). Despite the importance of maintaining immune microenvironmental homeostasis, in patients with kidney stones, the landscape of immune cell infiltration has not been fully clarified.

In this study, we compared differentially expressed (DE) mRNAs and lncRNAs between RPs in patients with CaOx stones and controls with normal papillary tissues based on the Gene Expression Omnibus (GEO) database and constructed an immune-related ceRNA network. Subsequently, to the best of our knowledge, we were the first to estimate the rate of immune cell infiltration in RPs. Moreover, we validated the ceRNA network and immune infiltration *in vivo* and *in vitro*. This study aimed to explore the potential ceRNA-related pathogenesis of kidney stones and identify its corresponding immune infiltration signature.

MATERIALS AND METHODS

Data Acquisition and Differential Expression Analysis

The mRNA microarray dataset GSE73680 (Taguchi et al., 2017) and lncRNA microarray dataset GSE117518 (Zhu et al., 2021) were obtained from the GEO database (https://www.ncbi.nlm.nih.gov/geo/). The GSE73680 dataset included 24 RPs from patients with CaOx stones and six controls with normal papillary tissues. The GSE117518 dataset included three RPs from patients with CaOx stones and three controls with normal papillary tissues. The details of both datasets are presented in **Table 1**. Probe names were transformed into gene symbols according to platform annotation information. Moreover, immune-related genes were obtained from the Immunology Database and Analysis Portal (IMMPORT) database (http://www.immport.org/) (Bhattacharya et al., 2014).

Subsequently, DE-mRNAs and lncRNAs were analyzed and compared between RPs and normal–papillary tissue controls

TABLE 1 | Details of lncRNA and mRNA datasets of patients with calcium oxalate kidney stones.

Type	GEO accession	Platform	Sample organism	Samples (kidney tissues), *n*		Contributors. (Year)
				Randall's plaque	Normal papillary	
mRNA	GSE73680	GPL17077	*Homo sapiens*	24	6	Taguchi et al. (2015)
lncRNA	GSE117518	GPL21827	*Homo sapiens*	3	3	Cui et al. (2016)

using the "limma" package (Ritchie et al., 2015) in the R software (http://www.r-project.org). mRNAs that met the criteria of $|\log_2FC|>1$ and $p < 0.01$ were considered as DE-mRNAs, and lncRNAs that met the criteria of $|\log_2FC|>0.58$ and $p < 0.01$ were considered as DE-lncRNA. The "ggplot2" package was used to draw heatmaps and volcano plots for data visualization.

Prediction of lncRNA–miRNA and miRNA–mRNA Interactions

Potential DE-lncRNA-targeted miRNAs were predicted using the miRcode database (http://mircode.org/) (Jeggari et al., 2012). Subsequently, miRNA–mRNA pairs were analyzed using TargetScan (http://www.targetscan.org/vert_72/) (Agarwal et al., 2015), miRTarBase (https://mirtarbase.cuhk.edu.cn/php/index.php) (Huang et al., 2020), and miRDB (http://mirdb.org/) (Chen and Wang, 2020) databases. mRNAs that were found in at least two databases were considered as candidate targets of miRNAs.

Venn Method

The Venn method was used to analyze overlapping genes. Intersections between DE-mRNA and DE-lncRNA-targeted mRNAs, as well as lncRNA-related DE-mRNAs and immune-related genes were identified using the Venny version 2.1 online tool (https://bioinfogp.cnb.csic.es/tools/venny/index.html).

Functional Enrichment and Protein–Protein Interaction Analysis

To explore the functions of lncRNA-related DE-mRNAs, gene ontology (GO) and Kyoto Encyclopedia of Genes and Genomes (KEGG) enrichment analyses were conducted using the "org.Hs.eg.db" and "ClusterProfiler" packages (Yu et al., 2012) in the R software. An adjusted $p < 0.05$ was considered statistically significant. Subsequently, the STRING database (https://string-db.org/) (Szklarczyk et al., 2019) was used to determine the relationship between the DE-mRNAs, and Cytoscape software (https://cytoscape.org) was used to develop the PPI network.

Construction of the Immune-Related ceRNA Network

After identifying immune-related and lncRNA-related DE-mRNAs, the interaction between lncRNAs, miRNAs, and mRNAs was confirmed as described in item 3.2. Subsequently, the immune-related lncRNA–miRNA–mRNA ceRNA network was developed using the R software. The "ggalluvial" package was used to draw a sankey diagram for data visualization.

Analysis of Immune Cell Infiltration

To estimate the abundance of 22 types of immune cell types in Randall's plaques and normal–papillary tissue controls, the mRNA microarray dataset GSE73680 was uploaded to the platform of CIBERSORT (http://cibersort.stanford.edu/) (Newman et al., 2015). Only samples that had a CIBERSORT algorithm output of $p < 0.05$ were considered for further analysis. Histograms and heatmaps were drawn to show the rate of immune cell infiltration in different samples. Co-expression patterns in immune-related DE-mRNAs and infiltrating immune cells were analyzed using Pearson's correlation coefficient. Subsequently, the Wilcoxon rank-sum test was performed to compare differentially infiltrating immune cells between RPs in patients with CaOx stones and controls with normal papillary tissues. The relationship between DE-mRNA expression and the fractions of macrophages and mast cells was also investigated using the Wilcoxon test. Results were visualized using the "heatmap" and "vioplot" packages in the R software.

Animal Experiments

Thirty male C57BL/6J mice weighing 22–25 g and aging 6–8 weeks were acquired from the Center of Experimental Animals at the Renmin hospital of Wuhan University, Hubei, China. The mice were acclimatized in the animal house of our institution at a steady temperature of 22 ± 2°C and humidity of 40–70% on a 12/12-h light–dark cycle and with free access to water and feed. The animal experiments were conducted according to the Guide for the Care and Use of Laboratory Animals, and the study protocol was approved by the Laboratory Animal Welfare and Ethics Committee of the Renmin hospital of Wuhan University (approval number: WDRM-20200604).

According to previous publications (Okada et al., 2007; Usami et al., 2018), the mice were intraperitoneally injected with 80 or 120 mg/kg of glyoxylate (Sigma–Aldrich; St. Louis, MO, United States) daily for 6 or 12 days to establish a CaOx kidney stone model. Mice were randomly assigned to the five following dosage groups ($n = 6$): control, 80 mg/kg of glyoxylate for 6 days, 120 of mg/kg glyoxylate for 6 days, 80 mg/kg of glyoxylate for 12 days, and 120 mg/kg of glyoxylate for 12 days groups. After 6 or 12 days, the mice were sacrificed, and kidneys were removed for analyses.

Cell Culture and Treatment

Human renal tubular epithelial cell line (HK-2) cells were provided by Stem Cell Bank, Chinese Academy of Sciences, Shanghai, China. HK-2 cells were cultured in an MEM medium supplemented with 10% fetal bovine serum (Gibco, Waltham, MA, United States) and 1% antibiotics

(penicillin/streptomycin). The cells were maintained at 37°C under a humidified atmosphere with 5% CO_2. Oxalate was purchased from Sigma–Aldrich and dissolved in the culture medium. Subsequently, the cells were cultured in six-well plates, and 0.25 mM or 0.5 mM of oxalate were added for 48 h.

Hematoxylin and Eosin, Von Kossal, and Masson Staining

After fixation in 4% paraformaldehyde, kidneys were imbedded in paraffin and were cut into 5-μm slices. HE staining was performed to assess the histopathological kidney tubular injuries as previously described (Dong et al., 2019). Injuries were scored as follows: 0, no tubular injury; 1, <10% tubular damage; 2, 10–25% tubular damage; 3, 25–50% tubular damage; 4, 50–74% tubular damage; and 5, >75% tubular damage. Subsequently, crystals were detected using Von Kossal staining, as previously described (Wang et al., 2019). The crystal deposition area was quantified using Image J software. Renal fibrosis was verified using Masson trichrome staining, and the collagen fiber deposition area on kidney sections was quantified using Image J software.

Immunohistochemistry and Immunofluorescence Staining

The protein expression levels of TGF-β, iNOS, and CD206 were analyzed using immunohistochemical and immunofluorescence staining. Antibodies (i.e., TGF-β [21898-1-AP], iNOS [18985-1-AP], and CD206 [60143-1-Ig]) were purchased from Proteintech (Chicago, IL, United States). All procedures were conducted according to the recommendations of the manufacturer. By comparing the positive area between groups using microscopy, figures were analyzed using Image J software.

Toluidine Blue Staining

Mast cells were detected using Toluidine blue staining as previously described (Zhang et al., 2017). Mast cells were identified using purple granules, and activated mast cells were characterized by disgorged and loosely packed granules. Activated mast cells per field were counted at a magnification of 400 ×.

Quantitative Real-Time PCR

Total RNA was extracted from HK-2 cells using TRIzol reagent (Invitrogen Life Technologies, Carlsbad, CA, United States), and RNA purity was measured using spectrophotometry. RNAs were reverse transcribed into cDNAs using the Takara RNA PCR kit (Takara Biotechnology, Shiga, Japan) according to the instructions of the manufacturer. Subsequently, cDNA was amplified by RT-qPCR using an Applied Biosystems SYBR Green mix kit (Applied Biosystems, Foster City, CA, United States). GAPDH was used as an internal reference for lncRNAs and mRNAs, while U6 was used as a reference for miRNA. The primers used for these reactions are shown in **Supplementary Table S1**. The reactions were measured on the ABI 7900 Real-Time PCR system (Applied Biosystems Life Technologies), and the $2^{-\Delta\Delta CT}$ method was used for analysis.

Statistical Analysis

All data are presented as the mean ± SD. Statistical analysis was conducted using SPSS version 19.0 (SPSS Inc., Chicago, IL, United States). Student's t-test was used to compare differences between groups. A p-value of <0.05 was considered statistically significant. All experiments were performed at least three times.

RESULTS

Identification of DE mRNAs and lncRNAs

To clarify the process of this research, a schematic representation is presented in **Figure 1**. Original data were downloaded from the GSE73680 and GSE117518 datasets in the GEO database. In the GSE73680 dataset, RNA-seq data of 24 RPs from patients with CaOx stones and from six controls with normal papillary tissues were analyzed using criteria of $|\log_2 FC|>1$ and $p < 0.01$. A total of 2,340 DE-mRNAs (2,098 upregulated and 242 downregulated) were compared between RPs and normal papillary tissues. In the GSE117518 dataset, the RNA-seq data of three RPs from patients with CaOx stones and three normal papillary tissues were analyzed using criteria of $|\log_2 FC|>0.58$ and $p < 0.01$. A total of 929 DE-lncRNAs (587 upregulated and 342 downregulated) were identified. Corresponding heatmaps and volcano plots are shown in **Figure 2**. Details of datasets are presented in **Table 1**.

Function Enrichment Analysis of lncRNA-Related DE-mRNAs

To establish the ceRNA network, DE-lncRNAs were further analyzed. Potential DE-lncRNA-targeted miRNAs were predicted using the miRcode database. Subsequently, miRNA–mRNA pairs were analyzed using the TargetScan, miRTarBase, and miRDB databases. A total of 197 miRNAs and 8,457 mRNAs were predicted. Subsequently, the Venn method was used to analyze the intersection between DE-mRNA and DE-lncRNA-targeted mRNAs (**Figure 3A**). Consequently, 278 overlapping lncRNA-related DE-mRNAs were identified. To determine the functions of lncRNA-related DE-mRNAs, GO and KEGG enrichment analyses were conducted (**Figures 3B,C**). A biological process analysis showed that lncRNA-related DE-mRNAs were significantly enriched in extracellular matrix organization, cellular calcium ion homeostasis, and regulation of cellular response to growth factor stimulus. A cellular component analysis showed that lncRNA-related DE-mRNAs were mostly enriched in collagen-containing extracellular matrix and endoplasmic reticulum lumen. A molecular function (MF) analysis showed that lncRNA-related DE-mRNAs were mostly enriched in channel activity and extracellular matrix structural constituent. The KEGG pathway enrichment analysis showed that lncRNA-related DE-mRNAs were significantly enriched in PI3K-Akt

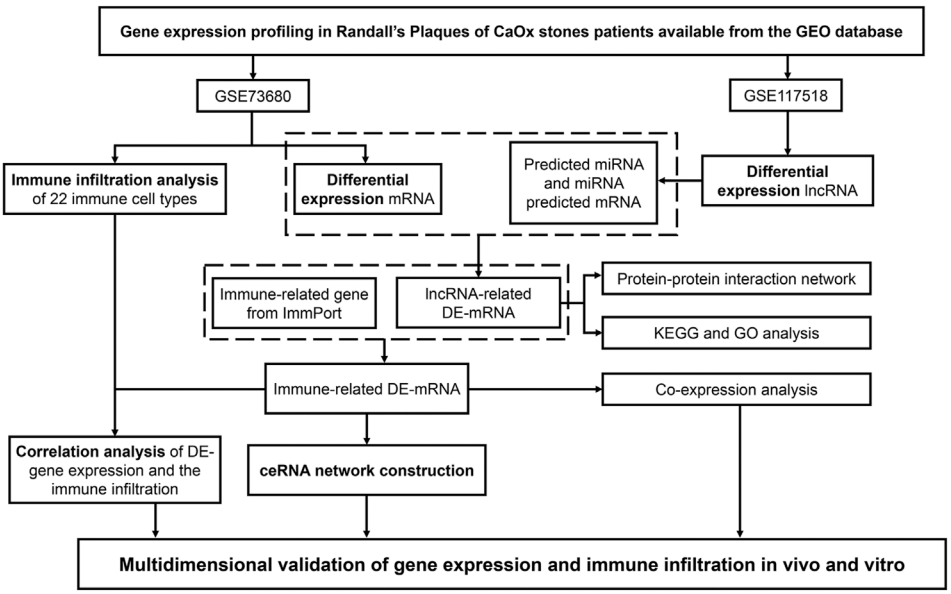

FIGURE 1 | Schematic representation of our analytic process.

signaling pathway, focal adhesion, and extracellular matrix-receptor interaction. Details of GO and KEGG enrichment analyses are presented in **Tables 2**, **3**. The PPI network of lncRNA-related DE-mRNAs is shown in **Supplementary Figure S1**.

Construction of the Immune-Related ceRNA Network

To construct the immune-related ceRNA network, the Venn method was used to analyze the intersection between lncRNA-related DE-mRNAs and immune-related genes obtained from the IMMPORT database. Consequently, 20 overlapping immune-related DE-mRNAs (12 upregulated and eight downregulated) were identified (**Figure 4A**). A co-expression analysis of immune-related DE-mRNAs was performed (**Figure 4B**). Subsequently, immune-related DE-mRNAs and their paired miRNAs and lncRNAs were chosen to develop the ceRNA regulatory network (**Figure 4C**). In total, the immune-related ceRNA network contained 10 lncRNAs, 23 miRNAs, and 20 mRNAs.

Composition of Infiltrating Immune Cells

The composition of 22 infiltrating immune cells in RPs in patients with CaOx stones and controls with normal papillary tissues were estimated using the CIBERSORT algorithm (**Figures 5A,B**). The relationships among these 22 immune cells are presented in **Figure 5C**. M1 macrophages were positively correlated with resting dendritic cells (R = 0.70). M2 macrophages were positively correlated with eosinophils (R = 0.52). Activated mast cells activated were positively correlated with neutrophils (R = 0.59). Resting mast cells were positively correlated with activated NK cells (R = 0.55) and negatively correlated with resting dendritic cells (R = –0.45). The differential proportion of infiltrating immune cells between RPs in patients with CaOx stones and in controls with normal papillary tissues was analyzed. As shown in **Figure 5D**, compared with the RPs in controls, M2 macrophages (p = 0.038) and resting mast cells (p = 0.019) were significantly downregulated and M1 macrophages (p = 0.49) and activated mast cells (p = 0.296) were significantly upregulated in the RPs in patients with kidney stones.

Co-Expression Patterns of Infiltrating Immune Cells and DE-mRNAs

For further analysis, DE-mRNAs were divided to the high expression and low expression groups. The correlation between infiltrating immune cells and DE-mRNAs expression was estimated using the Wilcoxon test, and significantly correlated pairs with $p < 0.05$ are shown in **Figure 6**. Results indicated that the expression of IL-13, OGN, and VEGFC was significantly negatively correlated with the proportion of M1 macrophages (p = 0.011, p = 0.002, and p = 0.05, respectively), whereas the expression of VAV2 was significantly positively correlated with proportion of M1 macrophages (p = 0.038). The expression of ADM2, CCL7, FGF18, FGF21, CCR9, LEP, ROBO2, and VAV2 was significantly negatively correlated with the proportion of resting mast cells (p = 0.011, p = 0.049, p = 0.001, p = 0.002, $p < 0.001$, p = 0.016, p = 0.007, p = 0.02, and p = 0.002, respectively).

Validation in a Glyoxylate-Induced Hyperoxaluric Mouse Model

To validate the aforementioned pathway and differentially infiltrating immune cells, kidney tubular injury, crystal

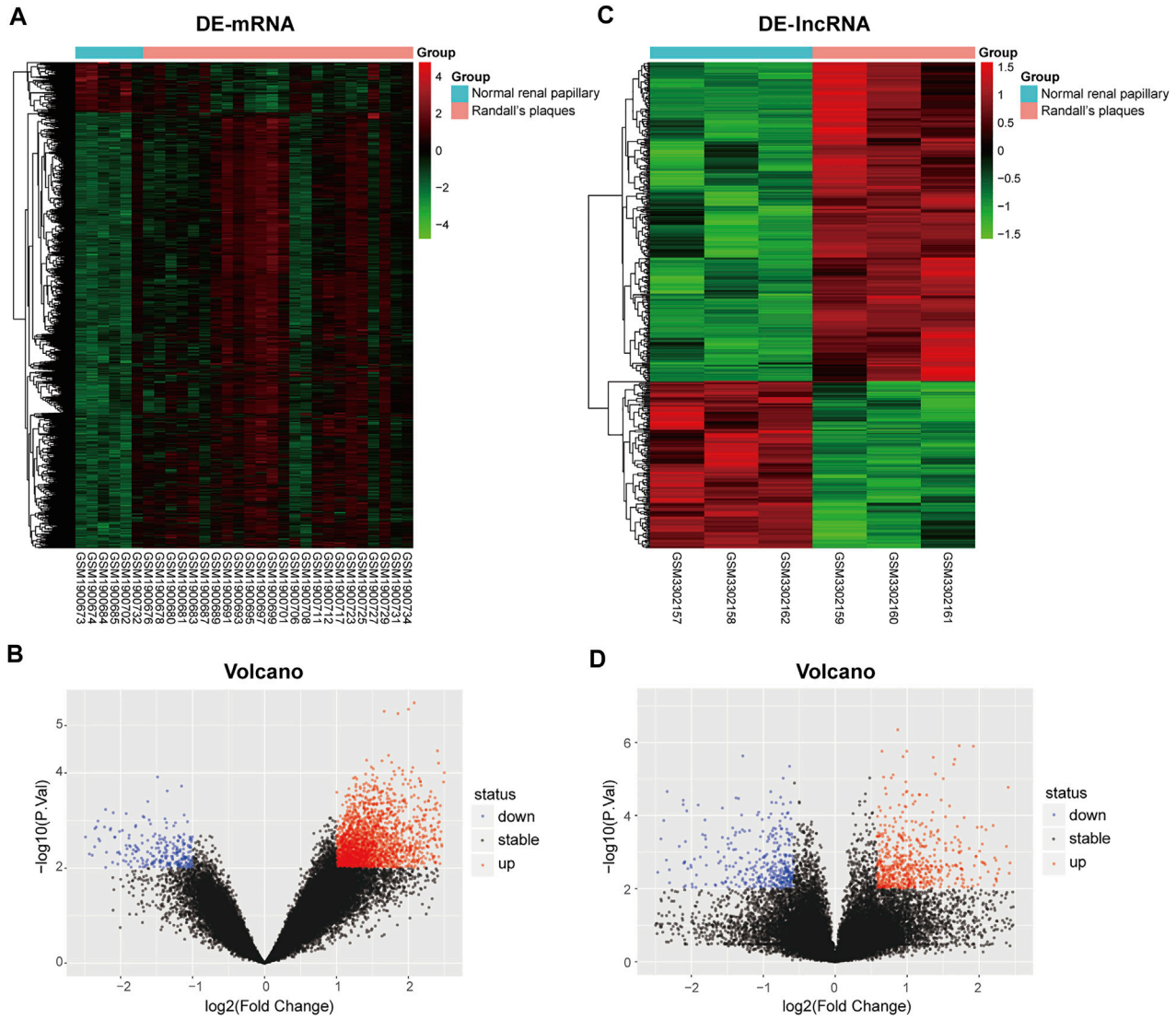

FIGURE 2 | Heatmaps and volcano plots of differentially expressed genes between the Randall's plaques of patients with CaOx kidney stones and normal–renal papillary tissue controls: **(A,B)** mRNA and **(C,D)** lncRNA.

deposition, fibrosis level, and macrophage and mast cell infiltration were evaluated in a glyoxylate (Gly)-induced hyperoxaluric mouse model. As shown in **Figure 7**, kidney tubular injury and crystal deposition were aggravated as treatment concentration and time of glyoxylate increased. Tubular injury and crystals were markedly worse in the day–12 Gly-treated groups than in the day–6 Gly-treated groups. Moreover, tubular injury and crystals were markedly worse in the 120–mg/kg Gly-treated mice than in the 80–mg/kg Gly-treated mice in both day-6 and day-12 groups. Fibrosis and collagen fiber deposition were evaluated using Masson staining and immunohistochemical staining of TGF-β. Results have shown that collagen fiber depositions and TGF-β-positive areas were significantly more frequent in the Gly-treated groups than in the control group in a dose- and time-dependent manner; these results are consistent with those shown in **Figure 3B**.

Subsequently, the immunofluorescence staining of macrophage-related molecules iNOS (M1) and CD206 (M2) showed that M1 macrophage infiltration significantly increased as kidney stones aggravated, whereas M2 macrophage infiltration increased in the early stages (day 6) and decreased as kidney stones progressed (day 12). Toluidine blue staining showed that activated mast cell infiltration significantly increased in the kidneys of mice with stone formation. As treatment concentration and time of Gly increased, activated mast cells

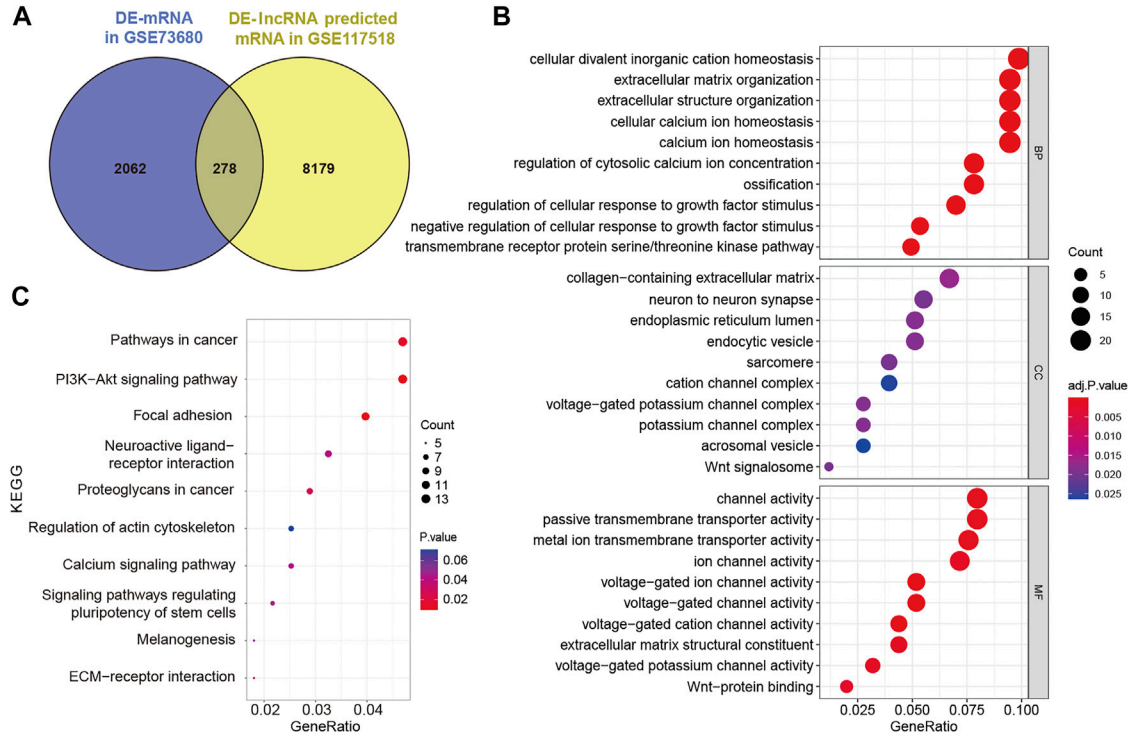

FIGURE 3 | Identification and analysis of lncRNA-related DE-mRNAs. **(A)** Intersection between DE-mRNAs and DE-lncRNAs predicted mRNAs. **(B)** GO enrichment analysis of lncRNA-related DE-mRNAs. **(C)** KEGG enrichment analysis of lncRNA-related DE-mRNAs. DE-mRNAs, differentially expressed mRNAs; DE-lncRNAs, differentially expressed lncRNAs; GO, gene ontology; and KEGG, Kyoto Encyclopedia of Genes and Genomes.

concomitantly increased. These immune cell infiltration results are consistent with our findings shown in **Figure 5**.

Construction of Immune-Related hub ceRNA Network and Validation in HK-2 Cells Stimulated With Oxalate

Through literature review and co-expression analysis of infiltrating immune cells, we established the immune-related hub ceRNA network, comprising 2 lncRNAs, 3 miRNAs, and 2 mRNAs (**Figure 8A**). Details of the immune-related hub ceRNA network developed from the GSE73680 and GSE117518 datasets are presented in **Table 4**. To validate the immune-related hub ceRNA network in kidney stones, RT-qPCR was used to detect the expression levels of the hub genes. As shown in **Figure 8B**, treatment with 0.25 and 0.5 mM oxalate for 48 h significantly upregulated the expression levels of NEAT1, PVT1, CCL7, and ROBO2 but downregulated the expression levels of hsa-miR-23b-3p, hsa-miR-429, and hsa-miR-139-5p in the HK-2 cell line in a dose-dependent manner. These results are consistent with the findings of GEO datasets.

DISCUSSION

Kidney stones are among the most common urological diseases and have a high recurrence rate. In the GEO database, several datasets assessed gene expression profiling by RNA-sequencing in kidney stones. However, most experiments were based on animal models (GSE72135, GSE36446, and GSE75543 datasets) or cell lines (GSE110509, GSE75111, and GSE56934 datasets), rather than patient samples. RPs are considered as the origin of kidney stones (Daudon et al., 2015). Thus, analysis based on the gene expression profiling of RPs may provide more convincing results to reveal kidney stone pathogenesis. In this study, for the first time, an immune-related ceRNA network was constructed and the composition of infiltrating immune cells was estimated based on gene expression profiling in RPs from patients with CaOx kidney stones.

Kidney stones mediate kidney injury and even kidney function loss (Rule et al., 2011). A recent study has found that symptomatic patients with kidney stones have an increased risk off chronic kidney disease compared with the risk of normal individuals (Rule et al., 2009). A retrospective clinical study has demonstrated that 6.01% of patients with kidney stones experience renal atrophy 2 years after percutaneous nephrolithotomy; kidney stones lasting more than 12 months and multiple calyces stone are independent risk factors (Xiangrui et al., 2020), indicating the serious outcomes of kidney stones. The underlying mechanisms may be associated with urinary tract obstruction, infection, and crystal-induced injury and fibrosis (Uribarri, 2020). Convento et al. (2017) demonstrated that the expression levels of TGF-β and epithelial-mesenchymal transition-associated proteins increased in hyperoxaluric mice and HK-2 cells treated with oxalate and CaOx, accompanied by progressive renal failure. In this study, we found that lncRNA-related DE-mRNAs are significantly enriched

TABLE 2 | Top 10 GO enrichment terms of differential expression genes.

GO term ID	Term description	GeneRatio	adj.p.val
Biological process			
GO:0072503	Cellular divalent inorganic cation homeostasis	24/243	2.30E-05
GO:0030198	Extracellular matrix organization	23/243	3.25E-06
GO:0043062	Extracellular structure organization	23/243	3.25E-06
GO:0006874	Cellular calcium ion homeostasis	23/243	2.30E-05
GO:0055074	Calcium ion homeostasis	23/243	2.96E-05
GO:0051480	Regulation of cytosolic calcium ion concentration	19/243	9.83E-05
GO:0001503	Ossification	19/243	0.00055
GO:0090287	Regulation of cellular response to growth factor stimulus	17/243	0.00025
GO:0090288	Negative regulation of cellular response to growth factor stimulus	13/243	0.00026
GO:0090101	Negative regulation of transmembrane receptor protein serine/threonine kinase signaling pathway	12/243	8.63E-05
Cellular component			
GO:0062023	Collagen-containing extracellular matrix	17/254	0.01691
GO:0098984	Neuron to neuron synapse	14/254	0.01987
GO:0005788	Endoplasmic reticulum lumen	13/254	0.01863
GO:0030139	Endocytic vesicle	13/254	0.01863
GO:0030017	Sarcomere	10/254	0.01987
GO:0034703	Cation channel complex	10/254	0.02633
GO:0008076	Voltage-gated potassium channel complex	7/254	0.01863
GO:0034705	Potassium channel complex	7/254	0.01863
GO:0001669	Acrosomal vesicle	7/254	0.02647
GO:1990909	Wnt signalosome	3/254	0.01987
Molecular function			
GO:0015267	Channel activity	20/251	0.00085
GO:0022803	Passive transmembrane transporter activity	20/251	0.00085
GO:0046873	Metal ion transmembrane transporter activity	19/251	0.00085
GO:0005216	Ion channel activity	18/251	0.00153
GO:0005244	Voltage-gated ion channel activity	13/251	0.00057
GO:0022832	Voltage-gated channel activity	13/251	0.00057
GO:0022843	Voltage-gated cation channel activity	11/251	0.00057
GO:0005201	Extracellular matrix structural constituent	11/251	0.00148
GO:0005249	Voltage-gated potassium channel activity	8/251	0.00153
GO:0017147	Wnt-protein binding	5/251	0.00236

TABLE 3 | KEGG pathway enrichment analysis of differentially expressed genes.

KEGG term ID	Term description	Count	p.val
hsa05200	Pathways in cancer	13	0.00692
hsa04151	PI3K-Akt signaling pathway	13	0.00243
hsa04510	Focal adhesion	11	4.70E-04
hsa04080	Neuroactive ligand-receptor interaction	9	0.03502
hsa05205	Proteoglycans in cancer	8	0.01920
hsa04810	Regulation of actin cytoskeleton	7	0.06697
hsa04020	Calcium signaling pathway	7	0.03532
hsa04550	Signaling pathways regulating pluripotency of stem cells	6	0.04222
hsa04916	Melanogenesis	5	0.04751
hsa04512	Extracellular matrix-receptor interaction	5	0.03078

in extracellular matrix organization, regulation of cellular response to growth factor stimulus, and collagen-containing extracellular matrix, which were associated with kidney interstitial fibrosis. Moreover, we revealed that, throughout kidney stone development, collagen fiber deposition and TGF-β expression were significantly increased in glyoxylate-induced hyperoxaluric mice in a dose- and time-dependent manner. Hence, we speculated that more attention should be paid to kidney stone-induced fibrosis and that lncRNAs may play a crucial role on the corresponding process.

miRNAs, as transcription regulators, are essential in various physiological and pathological processes, including kidney stone-induced renal injury (Jiang et al., 2020; Su et al., 2020). Su et al. (2020) indicated that miR-21 expression increased in hyperoxaluric mice, which promoted CaOx-induced renal tubular injury by PPARA. Jiang demonstrated that miR-155-5p upregulated and promoted oxalate and that CaOx induced oxidative stress injury in HK-2 cells (Jiang et al., 2020). In recent years, the lncRNA–miRNA–mRNA ceRNA network has been proved to be involved in various kidney diseases, including

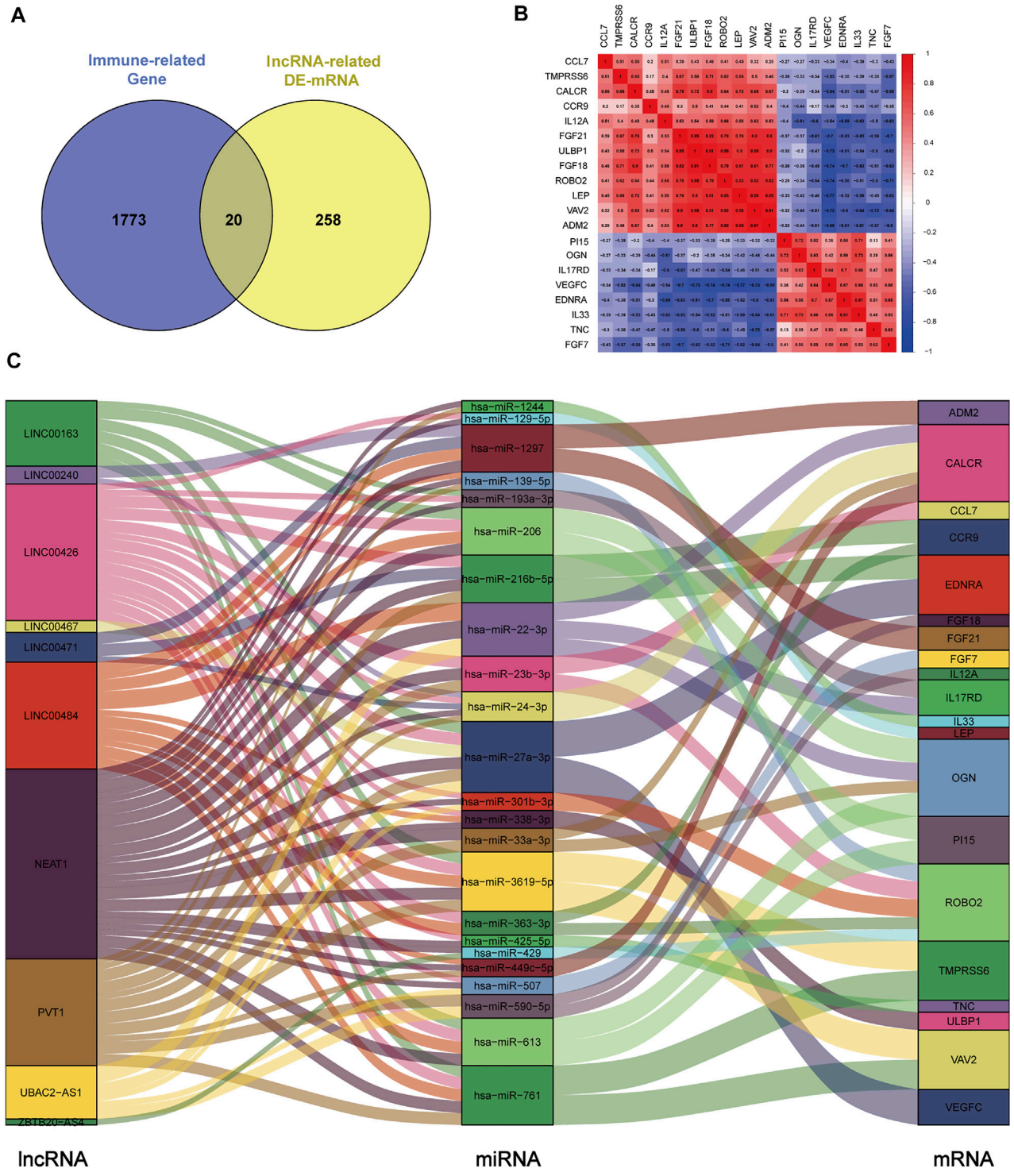

FIGURE 4 | Construction of immune-related ceRNA network in kidney stones. **(A)** Intersection between lncRNA-related DE-mRNAs and immune-related genes. **(B)** Co-expression analysis of immune-related DE-mRNAs. **(C)** Immune-related ceRNA regulatory network.

kidney stones (Liang et al., 2019; Liu et al., 2019; Ren et al., 2019). Liu et al. (2019) determined that the interaction between lncRNA H19 and miR-216b facilitated CaOx-induced kidney injury *via* the HMGB1/TLR4/NF-κB pathway. Moreover, Liang et al. (2019) identified the lncRNA–miRNA–mRNA expression variation profile in the urine of patients with CaOx stones. In this study, we constructed an immune-related ceRNA network based on gene expression profiling in RPs, including 10

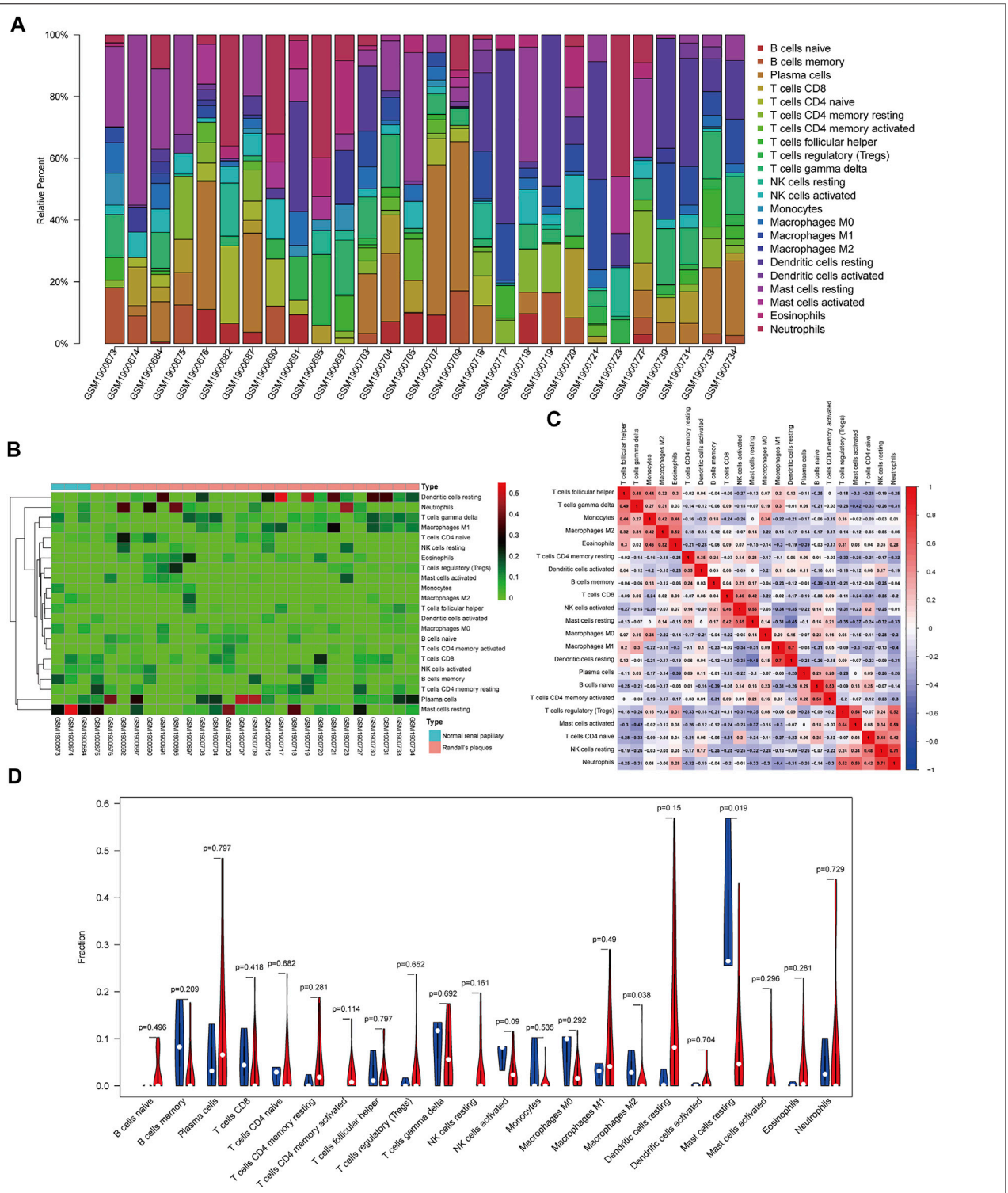

FIGURE 5 | Composition of infiltrating immune cells assessed using the CIBERSORT algorithm in kidney tissues. **(A)** Distribution of immune cell infiltration in each sample. **(B)** Heatmap of immune cell types. **(C)** The correlation among infiltrating immune cells. **(D)** Violin plot of infiltrating immune cells.

lncRNAs, 23 miRNAs, and 20 mRNAs, which are potential therapeutic targets. Subsequently, the immune-related hub ceRNA network was established and validated *in vitro*. Treatment with 0.25 and 0.5 mM of oxalate significantly upregulated NEAT1 and PVT1 expression levels and downregulated hsa-miR-23b-3p, hsa-miR-429, and hsa-miR-

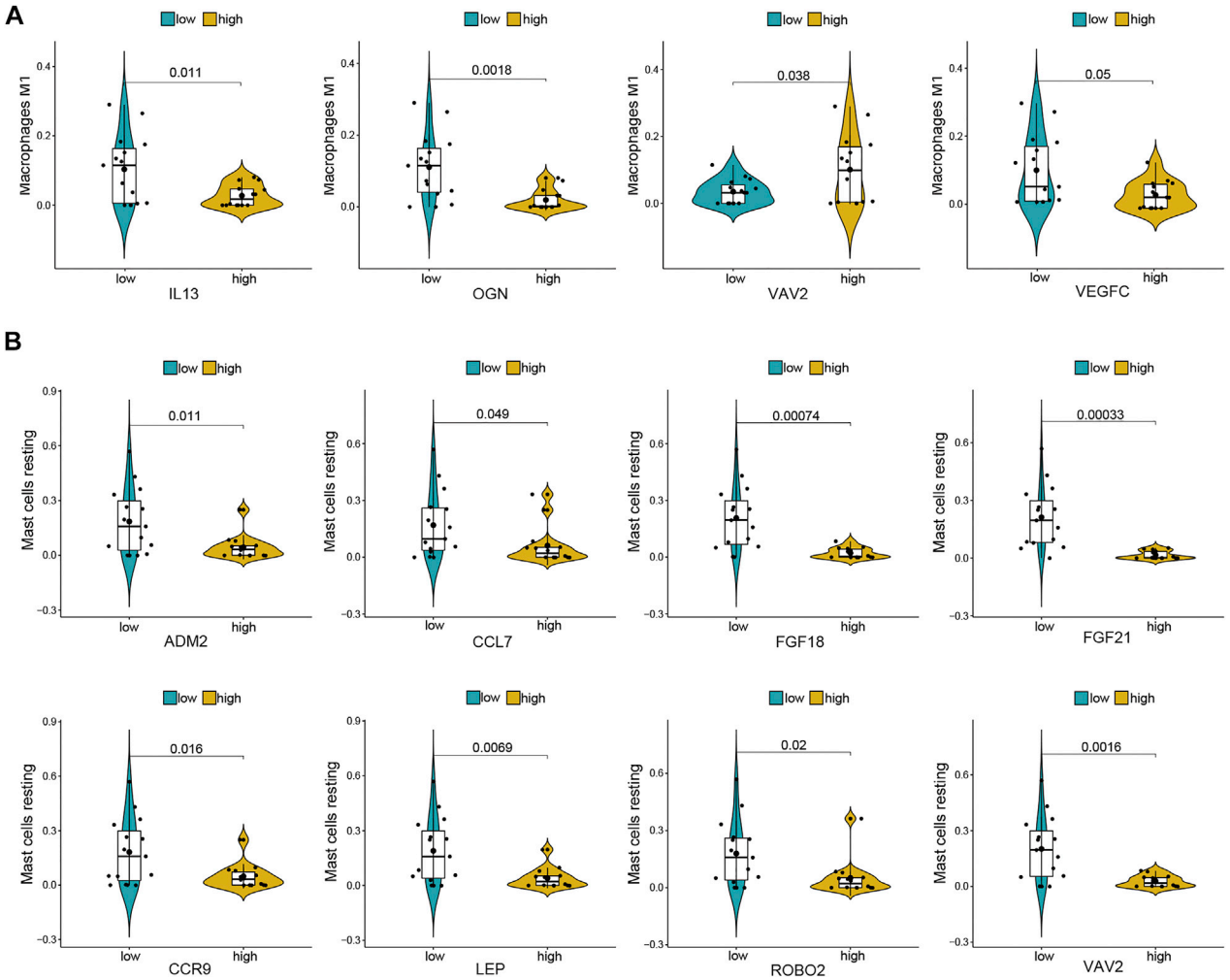

FIGURE 6 | Co-expression patterns of differential infiltrating immune cells and DE-mRNAs. **(A)** Significantly correlated pairs between M1 macrophages and DE-mRNAs. **(B)** Significantly correlated pairs between mast cell resting and DE-mRNAs.

139-5p expression levels in the HK-2 cell line in a dose-dependent manner. The interaction between NEAT1, PVT1, miR-429, miR-139-5p, and miR-23b-3p may regulate CaOx-induced kidney injury via CCL7 and ROBO2.

The CCL7 gene encodes C-C motif chemokine 7, which can attract monocytes to meditate inflammation and fibrosis (Klein et al., 2009). Inaba et al. (2020) demonstrated that CCL7 increased in a murine model of folic acid-induced acute kidney injury and that the blockade of CCL7 expression reduced monocyte recruitment and ameliorated injury. Sun et al. (2018) reported that CCL7 expression increased in the papillary and urine of patients with nephrolithiasis. The ROBO2 gene encodes the roundabout homolog 2, which is a receptor of slit homolog proteins (SLITs) and is associated with cellular migration guidance (Daehn and Duffield, 2021). ROBO2 dysfunction has been considered to cause congenital kidney and urinary tract abnormalities (Daehn and Duffield, 2021). Moreover, the SLITs/ROBO2 pathway was found to meditate inflammation and acute kidney injury (Chaturvedi and Robinson, 2015). In this study, treatment with 0.25 and 0.5 mM of oxalate significantly upregulated the expression levels of CCL7 and ROBO2 in the HK-2 cell line in a dose-dependent manner, yet the underlying mechanism still needed further investigation.

The polarization of macrophages has been recognized to be involved in the pathogenesis of kidney stones (Taguchi et al., 2021). Taguchi et al. (2016) found that M1-macrophage transfusion promoted kidney stone formation in hyperoxaluric mice and that M2-macrophage transfusion suppressed stone formation. Moreover, Xi et al. (2019) demonstrated that Sirtuin 3-overexpression suppressed crystal deposition through the promotion of the polarization of M2 macrophages. Mast cells have been considered as important components in kidney disease development (Vibhushan et al., 2020). Summers et al. (2012) demonstrated that mast cell activation and degranulation promoted renal fibrosis in mice with unilateral ureteric obstruction, while mast cell-deficient mice showed decreased collagen deposition. Moreover, it has been reported that mast cells can mediate cisplastin-induced acute kidney injury through

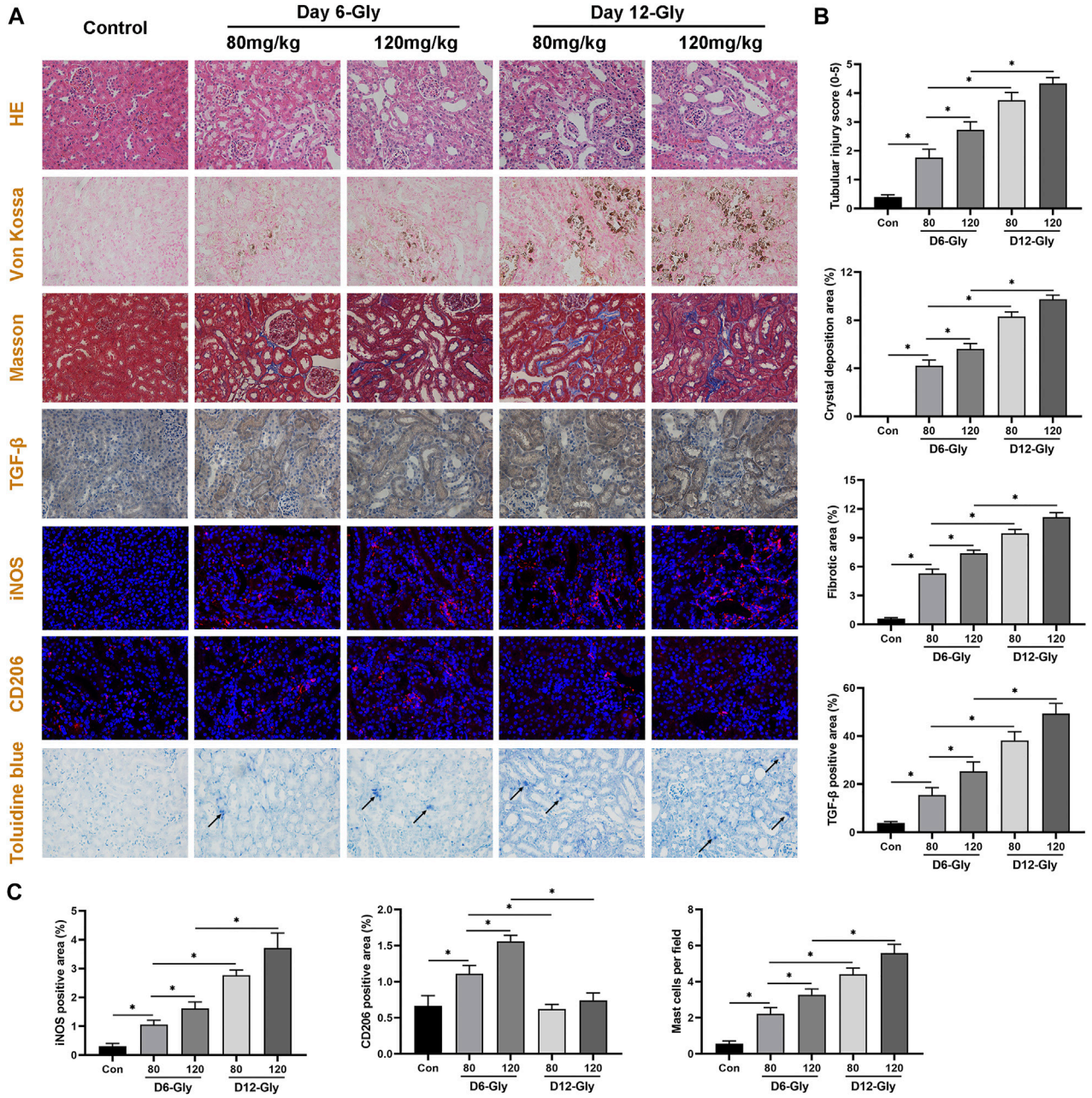

FIGURE 7 | Evaluation of kidney tubular injury, crystal deposition, fibrosis level, macrophage, and mast cell infiltration in a glyoxylate-induced hyperoxaluric mouse model. **(A)** Representative pictures of HE staining, Von Kossal staining, Masson staining, immunohistochemical staining, immunofluorescence staining, and Toluidine blue staining (magnification, 400×). **(B)** Quantification of kidney tubular injury score, CaOx crystal deposition area, collagen fiber deposition area, and TGF-β positive area. **(C)** Quantification of macrophage-related molecules in the iNOS (M1) and CD206 (M2) positive areas, and quantification of activated mast cell per field. Gly, glyoxylate. The arrow indicates activated mast cells. *$p < 0.05$.

the recruitment of leukocytes and secretion of TNF (Summers et al., 2011). However, the role of mast cells in the development of kidney stones has not been reported. Consistent with the aforementioned studies, we found that the proportion of M2 macrophages and resting mast cells decreased in the RPs of patients with CaOx stones. Furthermore, throughout kidney stone development, the infiltration of M1 macrophages and activated mast cells increased in mice with glyoxylate-induced hyperoxaluria. M2-macrophage infiltration increased in the early stage and decreased as kidney stones progressed. Together, these results indicate that the polarization of macrophages and recruitment of mast cells may play crucial roles in the development of kidney stones.

This study has several limitations. First, although we analyzed two microarray datasets of kidney stones, the sample size was still

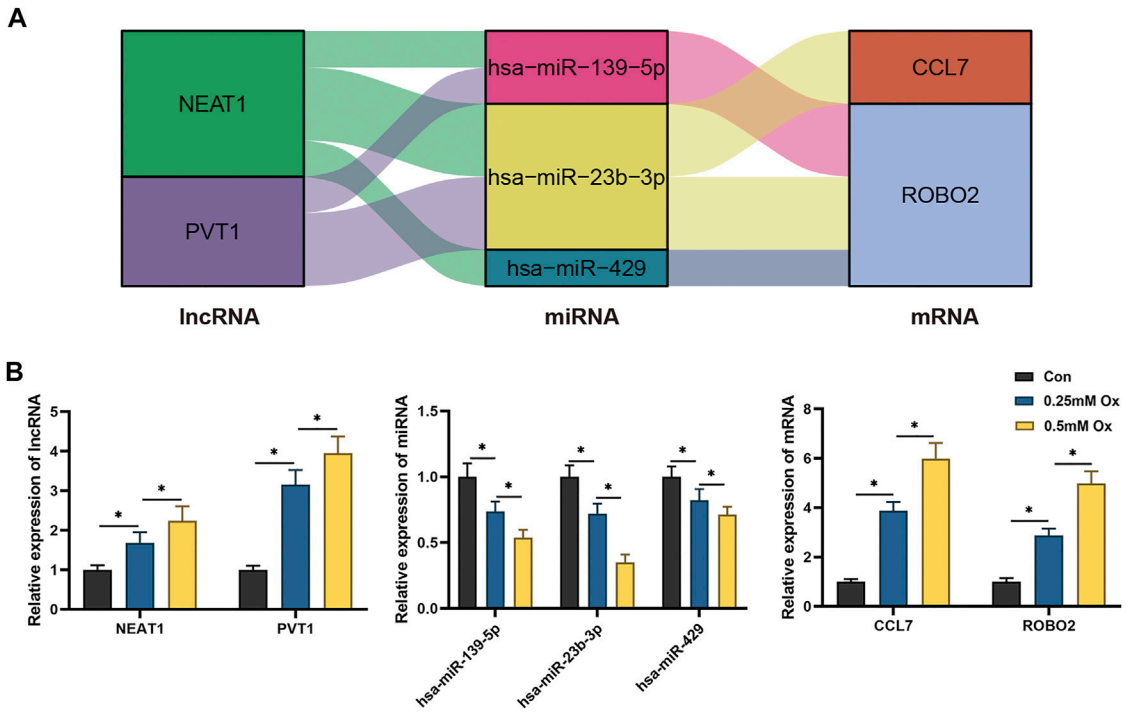

FIGURE 8 | RT-qPCR validation of the immune-related hub ceRNA network in HK-2 cells treated with oxalate. **(A)** The immune-related hub ceRNA network. **(B)** Quantification of the relative expression levels of NEAT1, PVT1, hsa-miR-23b-3p, hsa-miR-429, hsa-miR-139-5p, CCL7, and ROBO2 using RT-qPCR. *$p < 0.05$.

TABLE 4 | The details of hub ceRNA network from GEO datasets.

LncRNA				microRNA	mRNA			
Name	**Fold change**	**p.val**	**Status**	**Name**	**Name**	**Fold change**	**p.val**	**Status**
NEAT1	1.58	0.00053	up	hsa-miR-23b-3p	CCL7	2.96	0.00013	up
					ROBO2	2.27	0.00607	up
				hsa-miR-429	ROBO2	2.27	0.00607	up
PVT1	2.70	0.00043	up	hsa-miR-23b-3p	CCL7	2.96	0.00013	up
					ROBO2	2.27	0.00607	up
				hsa-miR-139-5p	ROBO2	2.27	0.00607	up

limited; this was partly due to the low biopsy rate and low morbidity of kidney stones. Second, no miRNA microarray dataset of patients with kidney stones was available from an open database, thus potential target miRNAs were predicted by online tools. Third, the analysis of infiltrating immune cells only included 22 types; accordingly, the subtypes of macrophages and mast cells require further investigation. Fourth, HK-2 cell line was the only cell line for *in vitro* validation, other renal tubular epithelial cell lines should be studied in the further research. Finally, further functional experiments are needed to demonstrate the mechanisms of the immune-related ceRNA network and their relationship with immune cell infiltration.

In conclusion, in this comprehensive study, we construct an immune-related ceRNA regulatory network and estimate the composition of immune cell infiltration in the RPs of patients with kidney stones. Based on one mRNA and one lncRNA microarray datasets, we identified the DE-mRNA and DE-lncRNA present in RPs and normal papillary tissues and used them for the construction of the ceRNA network. Subsequently, we estimated DE infiltrating immune cells between RPs and normal papillary tissues and their correlation with immune-related DE-mRNAs. Among these cells, macrophages and mast cells were considered to be important immune cells associated with kidney stone formation. Moreover, we validated the ceRNA

network and immune infiltration *in vivo* and *in vitro*. These findings provide new insights on the pathogenesis of kidney stones and novel potential therapeutic targets.

DATA AVAILABILITY STATEMENT

The datasets analyzed for this study can be found in the Gene expression Omnibus (GEO) database (https://www.ncbi.nlm.nih.gov/geo/) (Accession: GSE73680 and GSE117518).

ETHICS STATEMENT

The animal study was reviewed and approved by the Laboratory Animal Welfare and Ethics Committee of the Renmin hospital of Wuhan University (approval number: WDRM-20200604).

AUTHOR CONTRIBUTIONS

FC, TR, and YX designed the study. YX, TR, XZ, ZY, WY, and JN performed the experiments and collected the data. YR, RY, FL, PY, and DZ analyzed the data. YX, XZ, and ZY wrote the manuscript.

FUNDING

This research was supported by the grants from National Natural Science Foundation of China (81870471, 82170775, and 82100806), Science and Technology Major Project of Hubei Province (2019AEA170) and Key Research and Development Project of Hubei Province (2020BCB017).

ACKNOWLEDGMENTS

We would like to thank the staffs of the central laboratory, Renmin Hospital of Wuhan University, for their full support.

SUPPLEMENTARY MATERIAL

The Supplementary Material for this article can be found online at: https://www.frontiersin.org/articles/10.3389/fgene.2021.774155/full#supplementary-material

Supplementary Figure 1 | PPI network of lncRNA-related differentially expressed mRNAs.

Supplementary Table S1 | Sequence of primers used for RT-qPCR.

REFERENCES

Agarwal, V., Bell, G. W., Nam, J.-W., and Bartel, D. P. (2015). Predicting Effective microRNA Target Sites in Mammalian mRNAs. *Elife* 4, e05005. doi:10.7554/eLife.05005

Beermann, J., Piccoli, M.-T., Viereck, J., and Thum, T. (2016). Non-coding RNAs in Development and Disease: Background, Mechanisms, and Therapeutic Approaches. *Physiol. Rev.* 96 (4), 1297–1325. doi:10.1152/physrev.00041.2015

Bhattacharya, S., Andorf, S., Gomes, L., Dunn, P., Schaefer, H., Pontius, J., et al. (2014). ImmPort: Disseminating Data to the Public for the Future of Immunology. *Immunol. Res.* 58 (2-3), 234–239. doi:10.1007/s12026-014-8516-1

Chaturvedi, S., and Robinson, L. A. (2015). Slit2-Robo Signaling in Inflammation and Kidney Injury. *Pediatr. Nephrol.* 30 (4), 561–566. doi:10.1007/s00467-014-2825-4

Chen, Y., and Wang, X. (2020). miRDB: an Online Database for Prediction of Functional microRNA Targets. *Nucleic Acids Res.* 48 (D1), D127–D131. doi:10.1093/nar/gkz757

Cheng, W., Li, X.-W., Xiao, Y.-Q., and Duan, S.-B. (2019). Non-coding RNA-Associated ceRNA Networks in a New Contrast-Induced Acute Kidney Injury Rat Model. *Mol. Ther. - Nucleic Acids* 17, 102–112. doi:10.1016/j.omtn.2019.05.011

Convento, M. B., Pessoa, E. A., Cruz, E., da Glória, M. A., Schor, N., and Borges, F. T. (2017). Calcium Oxalate Crystals and Oxalate Induce an Epithelial-To-Mesenchymal Transition in the Proximal Tubular Epithelial Cells: Contribution to Oxalate Kidney Injury. *Sci. Rep.* 7, 45740. doi:10.1038/srep45740

Daehn, I. S., and Duffield, J. S. (2021). The Glomerular Filtration Barrier: a Structural Target for Novel Kidney Therapies. *Nat. Rev. Drug Discov.* 20, 770–788. doi:10.1038/s41573-021-00242-0

Daudon, M., Bazin, D., and Letavernier, E. (2015). Randall's Plaque as the Origin of Calcium Oxalate Kidney Stones. *Urolithiasis* 43 (Suppl. 1), 5–11. doi:10.1007/s00240-014-0703-y

Dong, Y., Zhang, Q., Wen, J., Chen, T., He, L., Wang, Y., et al. (2019). Ischemic Duration and Frequency Determines AKI-To-CKD Progression Monitored by Dynamic Changes of Tubular Biomarkers in IRI Mice. *Front. Physiol.* 10, 153. doi:10.3389/fphys.2019.00153

Huang, H.-Y., Lin, Y.-C. -D., Li, J., Huang, K.-Y., Shrestha, S., Hong, H.-C., et al. (2020). miRTarBase 2020: Updates to the Experimentally Validated microRNA-Target Interaction Database. *Nucleic Acids Res.* 48 (D1), D148–D154. doi:10.1093/nar/gkz896

Inaba, A., Tuong, Z. K., Riding, A. M., Mathews, R. J., Martin, J. L., Saeb-Parsy, K., et al. (2020). B Lymphocyte-Derived CCL7 Augments Neutrophil and Monocyte Recruitment, Exacerbating Acute Kidney Injury. *J.I.* 205 (5), 1376–1384. doi:10.4049/jimmunol.2000454

Jeggari, A., Marks, D. S., and Larsson, E. (2012). miRcode: a Map of Putative microRNA Target Sites in the Long Non-coding Transcriptome. *Bioinformatics* 28 (15), 2062–2063. doi:10.1093/bioinformatics/bts344

Jiang, K., Hu, J., Luo, G., Song, D., Zhang, P., Zhu, J., et al. (2020). Promotes Oxalate- and Calcium-Induced Kidney Oxidative Stress Injury by Suppressing MGP Expression. *Oxidative Med. Cell Longevity* 2020 (5863617), 1–14. doi:10.1155/2020/5863617

Khan, S. R., Canales, B. K., and Dominguez-Gutierrez, P. R. (2021). Randall's Plaque and Calcium Oxalate Stone Formation: Role for Immunity and Inflammation. *Nat. Rev. Nephrol.* 17 (6), 417–433. doi:10.1038/s41581-020-00392-1

Khan, S. R., and Canales, B. K. (2015). Unified Theory on the Pathogenesis of Randall's Plaques and Plugs. *Urolithiasis* 43 (Suppl. 10 1), 109–123. doi:10.1007/s00240-014-0705-9

Kittanamongkolchai, W., Vaughan, L. E., Enders, F. T., Dhondup, T., Mehta, R. A., Krambeck, A. E., et al. (2018). The Changing Incidence and Presentation of Urinary Stones over 3 Decades. *Mayo Clinic Proc.* 93 (3), 291–299. doi:10.1016/j.mayocp.2017.11.018

Klein, J., Gonzalez, J., Duchene, J., Esposito, L., Pradere, J. P., Neau, E., et al. (2009). Delayed Blockade of the Kinin B1 Receptor Reduces Renal Inflammation and Fibrosis in Obstructive Nephropathy. *FASEB j.* 23 (1), 134–142. doi:10.1096/fj.08-115600

Li, Y., Yan, G., Zhang, J., Chen, W., Ding, T., Yin, Y., et al. (2020). LncRNA HOXA11-AS Regulates Calcium Oxalate crystal-induced Renal Inflammation via miR-124-3p/MCP-1. *J. Cel Mol Med.* 24 (1), 238–249. doi:10.1111/jcmm.14706

Liang, X., Lai, Y., Wu, W., Chen, D., Zhong, F., Huang, J., et al. (2019). LncRNA-miRNA-mRNA Expression Variation Profile in the Urine of Calcium Oxalate Stone Patients. *BMC Med. Genomics* 12 (1), 57. doi:10.1186/s12920-019-0502-y

Liu, H., Ye, T., Yang, X., Liu, J., Jiang, K., Lu, H., et al. (2019). H19 Promote Calcium Oxalate Nephrocalcinosis-Induced Renal Tubular Epithelial Cell Injury via a ceRNA Pathway. *EBioMedicine* 50, 366–378. doi:10.1016/j.ebiom.2019.10.059

Marien, T. P., and Miller, N. L. (2016). Characteristics of Renal Papillae in Kidney Stone Formers. *Minerva Urol. Nefrol* 68 (6), 496–515.

Newman, A. M., Liu, C. L., Green, M. R., Gentles, A. J., Feng, W., Xu, Y., et al. (2015). Robust Enumeration of Cell Subsets from Tissue Expression Profiles. *Nat. Methods* 12 (5), 453–457. doi:10.1038/nmeth.3337

Okada, A., Nomura, S., Higashibata, Y., Hirose, M., Gao, B., Yoshimura, M., et al. (2007). Successful Formation of Calcium Oxalate crystal Deposition in Mouse Kidney by Intraabdominal Glyoxylate Injection. *Urol. Res.* 35 (2), 89–99. doi:10.1007/s00240-007-0082-8

Pless, M. S., Williams, J. C., Jr, Andreassen, K. H., Jung, H. U., Osther, S. S., Christensen, D. R., et al. (2019). Endoscopic Observations as a Tool to Define Underlying Pathology in Kidney Stone Formers. *World J. Urol.* 37 (10), 2207–2215. doi:10.1007/s00345-018-02616-3

Ren, G. L., Zhu, J., Li, J., and Meng, X. M. (2019). Noncoding RNAs in Acute Kidney Injury. *J. Cel Physiol* 234 (3), 2266–2276. doi:10.1002/jcp.27203

Ritchie, M. E., Phipson, B., Wu, D., Hu, Y., Law, C. W., Shi, W., et al. (2015). Limma powers Differential Expression Analyses for RNA-Sequencing and Microarray Studies. *Nucleic Acids Res.* 43 (7), e47. doi:10.1093/nar/gkv007

Rule, A. D., Bergstralh, E. J., Melton, L. J., 3rd, Li, X., Weaver, A. L., and Lieske, J. C. (2009). Kidney Stones and the Risk for Chronic Kidney Disease. *Cjasn* 4 (4), 804–811. doi:10.2215/CJN.05811108

Rule, A. D., Krambeck, A. E., and Lieske, J. C. (2011). Chronic Kidney Disease in Kidney Stone Formers. *Cjasn* 6 (8), 2069–2075. doi:10.2215/CJN.10651110

Salmena, L., Poliseno, L., Tay, Y., Kats, L., and Pandolfi, P. P. (2011). A ceRNA Hypothesis: the Rosetta Stone of a Hidden RNA Language? *Cell* 146 (3), 353–358. doi:10.1016/j.cell.2011.07.014

Su, B., Han, H., Ji, C., Hu, W., Yao, J., Yang, J., et al. (2020). MiR-21 Promotes Calcium Oxalate-Induced Renal Tubular Cell Injury by Targeting PPARA. *Am. J. Physiology-Renal Physiol.* 319 (2), F202–F214. doi:10.1152/ajprenal.00132.2020

Summers, S. A., Chan, J., Gan, P.-Y., Dewage, L., Nozaki, Y., Steinmetz, O. M., et al. (2011). Mast Cells Mediate Acute Kidney Injury through the Production of TNF. *Jasn* 22 (12), 2226–2236. doi:10.1681/ASN.2011020182

Summers, S. A., Gan, P.-y., Dewage, L., Ma, F. T., Ooi, J. D., O'Sullivan, K. M., et al. (2012). Mast Cell Activation and Degranulation Promotes Renal Fibrosis in Experimental Unilateral Ureteric Obstruction. *Kidney Int.* 82 (6), 676–685. doi:10.1038/ki.2012.211

Sun, A. Y., Hinck, B., Cohen, B. R., Keslar, K., Fairchild, R. L., and Monga, M. (2018). Inflammatory Cytokines in the Papillary Tips and Urine of Nephrolithiasis Patients. *J. Endourology* 32 (3), 236–244. doi:10.1089/end.2017.0699

Szklarczyk, D., Gable, A. L., Lyon, D., Junge, A., Wyder, S., Huerta-Cepas, J., et al. (2019). STRING V11: Protein-Protein Association Networks with Increased Coverage, Supporting Functional Discovery in Genome-wide Experimental Datasets. *Nucleic Acids Res.* 47 (D1), D607–D613. doi:10.1093/nar/gky1131

Taguchi, K., Hamamoto, S., Okada, A., Unno, R., Kamisawa, H., Naiki, T., et al. (2017). Genome-Wide Gene Expression Profiling of Randall's Plaques in Calcium Oxalate Stone Formers. *Jasn* 28 (1), 333–347. doi:10.1681/ASN.2015111271

Taguchi, K., Okada, A., Hamamoto, S., Unno, R., Moritoki, Y., Ando, R., et al. (2016). M1/M2-macrophage Phenotypes Regulate Renal Calcium Oxalate crystal Development. *Sci. Rep.* 6, 35167. doi:10.1038/srep35167

Taguchi, K., Okada, A., Unno, R., Hamamoto, S., and Yasui, T. (2021). Macrophage Function in Calcium Oxalate Kidney Stone Formation: A Systematic Review of Literature. *Front. Immunol.* 12, 673690. doi:10.3389/fimmu.2021.673690

Uribarri, J. (2020). Chronic Kidney Disease and Kidney Stones. *Curr. Opin. Nephrol. Hypertens.* 29 (2), 237–242. doi:10.1097/mnh.0000000000000582

Usami, M., Okada, A., Taguchi, K., Hamamoto, S., Kohri, K., and Yasui, T. (2018). Genetic Differences in C57BL/6 Mouse Substrains Affect Kidney crystal Deposition. *Urolithiasis* 46 (6), 515–522. doi:10.1007/s00240-018-1040-3

Vibhushan, S., Bratti, M., Montero-Hernández, J. E., El Ghoneimi, A., Benhamou, M., Charles, N., et al. (2020). Mast Cell Chymase and Kidney Disease. *Ijms* 22 (1), 302. doi:10.3390/ijms22010302

Wang, X. F., Zhang, B. H., Lu, X. Q., and Wang, R. Q. (2019). Gastrin-releasing Peptide Receptor Gene Silencing Inhibits the Development of the Epithelial-Mesenchymal Transition and Formation of a Calcium Oxalate crystal in Renal Tubular Epithelial Cells in Mice with Kidney Stones via the PI3K/Akt Signaling Pathway. *J. Cel Physiol* 234 (2), 1567–1577. doi:10.1002/jcp.27023

Xi, J., Chen, Y., Jing, J., Zhang, Y., Liang, C., Hao, Z., et al. (2019). Sirtuin 3 Suppresses the Formation of Renal Calcium Oxalate Crystals through Promoting M2 Polarization of Macrophages. *J. Cel Physiol* 234 (7), 11463–11473. doi:10.1002/jcp.27803

Xiangrui, Y., Xiong, W., Xi, W., Yuanbing, J., Shenqiang, Q., and Yu, G. (2020). Clinical Assessment of Risk Factors for Renal Atrophy after Percutaneous Nephrolithotomy. *Med. Sci. Monit.* 26, e919970. doi:10.12659/MSM.919970

Yu, G., Wang, L.-G., Han, Y., and He, Q.-Y. (2012). clusterProfiler: an R Package for Comparing Biological Themes Among Gene Clusters. *OMICS: A J. Integr. Biol.* 16 (5), 284–287. doi:10.1089/omi.2011.0118

Zeng, G., Mai, Z., Xia, S., Wang, Z., Zhang, K., Wang, L., et al. (2017). Prevalence of Kidney Stones in China: an Ultrasonography Based Cross-Sectional Study. *BJU Int.* 120 (1), 109–116. doi:10.1111/bju.13828

Zhang, L., Wu, J.-H., Otto, J. C., Gurley, S. B., Hauser, E. R., Shenoy, S. K., et al. (2017). Interleukin-9 Mediates Chronic Kidney Disease-dependent Vein Graft Disease: a Role for Mast Cells. *Cardiovasc. Res.* 113 (13), 1551–1559. doi:10.1093/cvr/cvx177

Zhu, C., Liang, Q., Liu, Y., Kong, D., Zhang, J., Wang, H., et al. (2019). Kidney Injury in Response to Crystallization of Calcium Oxalate Leads to Rearrangement of the Intrarenal T Cell Receptor delta Immune Repertoire. *J. Transl Med.* 17 (1), 278. doi:10.1186/s12967-019-2022-0

Zhu, Z., Cui, Y., Huang, F., Zeng, H., Xia, W., Zeng, F., et al. (2020). Long Non-coding RNA H19 Promotes Osteogenic Differentiation of Renal Interstitial Fibroblasts through Wnt-β-Catenin Pathway. *Mol. Cel Biochem* 470 (1-2), 145–155. doi:10.1007/s11010-020-03753-3

Zhu, Z., Huang, F., Xia, W., Zeng, H., Gao, M., Li, Y., et al. (2021). Osteogenic Differentiation of Renal Interstitial Fibroblasts Promoted by lncRNA MALAT1 May Partially Contribute to Randall's Plaque Formation. *Front. Cel Dev. Biol.* 8, 596363. doi:10.3389/fcell.2020.596363

Conflict of Interest: The authors declare that the research was conducted in the absence of any commercial or financial relationships that could be construed as a potential conflict of interest.

Publisher's Note: All claims expressed in this article are solely those of the authors and do not necessarily represent those of their affiliated organizations, or those of the publisher, the editors and the reviewers. Any product that may be evaluated in this article, or claim that may be made by its manufacturer, is not guaranteed or endorsed by the publisher.

frontiers in Genetics

ORIGINAL RESEARCH
published: 17 December 2021
doi: 10.3389/fgene.2021.779195

Downregulation of hsa_circRNA_0001400 Helps to Promote Cell Apoptosis Through Disruption of the circRNA_0001400–miR-326 Sponge in Cervical Cancer Cells

Yantao Cai[1†], Chuyu Li[2†], Fang Peng[3†], Shuanghong Yin[4], Huiyi Liang[1], Jiyan Su[1], Lin Li[2,4], Anping Yang[5], Hui Liu[5], Chuansheng Yang[6], Dixian Luo[7]* and Chenglai Xia[1,4]**

[1]Affiliated Foshan Maternity and Chlid Healthcare Hospital, Southern Medical University, Foshan, China, [2]Department of Pharmacology, Guangdong Medical University, Zhanjiang, China, [3]Guangdong Second Provincial General Hospital, Guangzhou, China, [4]School of Pharmaceutical Sciences, Southern Medical University, Guangzhou, China, [5]School of Medicine, Foshan University, Foshan, China, [6]Department of Head-Neck and Breast Surgery, Yuebei People's Hospital of Shantou University, Shaoguan, China, [7]Department of Laboratory Medicine, Huazhong University of Science and Technology Union Shenzhen Hospital (Nanshan Hospital), Shenzhen, China

Background: In recent years, circular RNAs (circRNAs) have been reported to serve as essential regulators in several human cancers. Nevertheless, the function and mechanism of circRNAs in cervical cancer remain elusive.

Methods: Flow cytometry assays were performed to measure cell apoptosis and cell cycle. Colony Formation and transwell chamber were performed to measure cell migration and invasion. Double luciferase reporter for gene analysis was used to detect the interaction between hsa-circRNA_0001400, miR-326, and Akt. Relative protein levels were determined by immunoblotting and relative gene levels were determined by quantitative real-time PCR. Tumor Xenograft Modeling was used to evaluate the effect of hsa_circRNA_0001400_siRNA *in vivo*.

Results: In the present study, we showed that hsa_circRNA_0001400 was highly expressed in cervical cancer tissues relative to in matched normal tissue. We found that hsa_circRNA_0001400_siRNA significantly promoted the apoptosis of cervical cancer cells and arrested the cell cycle and migration of cervical cancer cells. We showed that hsa_circRNA_0001400_siRNA can inhibit the protein expression of Akt and that the inhibition of miR-326 could rescue the inhibition of Akt in cervical cancer cells. We found that has-miR-326 was downregulated in cervical cancer tissues and hsa_circRNA_0001400_siRNA could increase the gene expression of has-miR-326. We also observed that hsa_circRNA_0001400_siRNA inhibited the growth and angiogenesis of SiHa xenografts in nude mice.

Abbreviations: circRNAs, circular RNAs; HPV, human papillomavirus; miRNA, microRNA; mRNA, messenger RNA; siRNA, small interfering RNA; KEGG, Kyoto Encyclopedia of Genes and Genomes.

OPEN ACCESS

Edited by:
Jian-Hong Fang,
Sun Yat-sen University, China

Reviewed by:
Fei Yu,
Hebei Agricultural University, China
Li Qin,
Hunan University of Chinese Medicine, China
Chengfeng Qiu,
Huaihua First People's Hospital, China

***Correspondence:**
Dixian Luo
luodixian_2@163.com
Chuansheng Yang
ychssmile@163.com
Chenglai Xia
xiachenglai@126.com

†These authors have contributed equally to this work

Specialty section:
This article was submitted to RNA, a section of the journal Frontiers in Genetics

Received: 18 September 2021
Accepted: 18 November 2021
Published: 17 December 2021

Citation:
Cai Y, Li C, Peng F, Yin S, Liang H, Su J, Li L, Yang A, Liu H, Yang C, Luo D and Xia C (2021) Downregulation of hsa_circRNA_0001400 Helps to Promote Cell Apoptosis Through Disruption of the circRNA_0001400–miR-326 Sponge in Cervical Cancer Cells. Front. Genet. 12:779195. doi: 10.3389/fgene.2021.779195

Conclusion: In conclusion, this study provides evidence that the hsa_circRNA_0001400–miR-326–Akt network promotes cervical cancer progression. Notably, our findings demonstrate the novel antitumor effects of hsa_circRNA_0001400_siRNA in cervical cancer.

Keywords: circRNA, cervical cancer, apoptosis, phosphatidylinositol-3 kinase, Akt

BACKGROUND

Cervical cancer is the fourth leading cause of cancer death in women worldwide and is second only to lung cancer in developed regions (Small Jr et al., 2017). The 2017 American Cancer Society Guidelines noted that 12,820 women in the United States were diagnosed with invasive cervical cancer in 2016 and predicted that 4,210 of those women would die from the disease (Sawaya et al., 2019). Infection by human papillomavirus (HPV) is a major cause of cervical cancer in women. However, though HPV vaccines exist for the prevention of cervical cancer in women, they are still not widely available in developing countries and, as a result of the persistent lack of screening, a large number of cervical cancer cases in the next 50 years can be expected (Wang et al., 2020). For early cancer patients, the 5-year survival rate is 100% with surgery and, in recent years, the incidence of cervical cancer has trended toward affecting women of youngers age, making the need to retain fertility a concern. In addition, statistics show that 10–15% of patients with cervical cancer after treatment experience recurrence or metastasis, which is the main reason for the failure of cervical cancer treatment. Therefore, there is an urgent need to clarify the mechanism of cervical cancer metastasis, develop new antitumor drugs, improve the quality of life of patients with cervical cancer, and improve the 5-year survival rate (Canfell, 2019).

Circular RNAs (circRNAs) are noncoding RNAs that covalently join the 5' and 3' ends of linear RNA precursors via reverse splicing and play a regulatory role in many biological processes, such as cell proliferation, senescence, and apoptosis (Visci et al., 2020). CircRNAs may play an important role in tumorigenesis and development (Zhou et al., 2018). Several reports have demonstrated that the circRNA–microRNA (miRNA)–messenger RNA (mRNA) signaling pathway is involved in tumorigenesis (Zhou et al., 2018; Xu et al., 2020). In a study of tumor metastasis, circRNA had unique advantages and its ring structure was shown to determine its stability, which can greatly reduce the possibility of a mistargeting effect in clinical treatment. At the same time, many studies have also found that there are many kinds of circRNA in human body fluid, suggesting that circRNAs may be a new target for noninvasive disease diagnosis and prognosis (Zhang et al., 2018; Lu et al., 2020). Several studies to date have evaluated the roles of circRNAs and their possible mechanisms in cervical cancer andavailable research findings have indicated that circRNAs are involved in cervical tumor progression by various mechanisms, among which miRNA sponging is the most important (Kristensen et al., 2018). The study of circRNAs potentially represents a new promising strategy for diagnosis and treatment of cervical cancer.

In this study, we used RNA sequencing to analyze the differential expression of circRNA in human cervical cancer and found that hsa_circRNA_0001400 exhibited high expression in cervical cancer tissue. By silencing circRNAs with small interfering RNA (siRNA) interference, the molecular mechanism of hsa_circRNA_0001400–miR-326–Akt sponge in cervical cancer migration was elucidated from the cytological and zoological levels.

MATERIALS AND METHODS

Cell, Reagents, and Antibodies

Human cervical cancer SiHa cells, HeLa cells, and VK2/E6E7 cells were obtained from our laboratory. Fetal bovine serum and Dulbecco's modified Eagle's medium culture medium were purchased from Gibco Laboratories (Gaithersburg, MD, United States). Additionally, Transwell Cell (8.0 μM; Corning, Corning, NY, United States); Crystal Violet (Beijing Regan Biotechnology Co., Ltd. Beijing, China); and primary antibodies including glyceraldehyde 3-phosphate dehydrogenase (GAPDH) (cat.#5174), Akt (cat.#4691), Phospho-Akt (Ser473) (cat. #4060), Phospho-PI3 Kinase p85 (Tyr458) (cat.#17366)and PI3K (cat.#4249) as well as the second antibody (Anti-rabbit IgG, cat.#7074) were purchased from Cell Signaling Technology (Danvers, MA, United States). Lipofectamine 2000 was purchased from Invitrogen Corporation (Carlsbad, CA, United States). We designed hsa_circRNA_0001400 primer and siRNA according to the has_circRNA_0001400 sequence listed in the CircRNA database using the methods described in a previous study (Dalmer and Clugston, 2019). The primers of hsa_circRNA_0001400, miR-326, and hsa_circRNA_0001400_siRNA were synthesized by Genecfps Corporation (Shanghai, China). Finally, the microRNA kit used to analyze microRNAs was purchased from FulenGene Biology Co., Ltd. (Shanghai, China). The sequences of the primers were as follows:

hsa_circRNA_0001400-F:ATGTCTGTTAGTGGGGCTGA;
hsa_circRNA_0001400-R:TATCTGCTACCATCGCCTTT;
miR-326 mimic: CCUCUGGGCCCUUCCAG;
miR-326 inhibitor: CTGGAGGAAGGGCCCAGAGG
has-miR-326-F: CCTCTGGGCCCTTCCTCAG;
has-Akt2-F:CTCAGCATCAACTGGCAGGA;
hsa-Akt2-R: GTGATGGACTGGGCGGTAAA;
hsa_circRNA_0001400_siRNA-F:5′-AGUAGCAGCGAAUGCUGAUGUUU-3';
hsa_circRNA_0001400_siRNA-R: 5′-ACAUCAGCAUUCGCUGCUACUUU-3'

CircRNA Sequencing

In this study, six cervical cancer tissue samples were collected from January 2019 to December 2019 at Foshan Maternity and Child Healthcare Hospital. All samples were collected after receiving signed informed consent forms from patients and their families and the approval of the Ethics Committee of Foshan Maternity and Child Healthcare Hospital (No. FSFY-MEC-2018-061). Specimens from patients were diagnosed by pathological examination with carcinoma *in situ* of the cervix. The patient did not receive any radiation, chemotherapy, or other anticancer treatment prior to the operation. The tumor tissue was removed and transferred to the laboratory in an icebox at a low temperature. After cleaning three times with phosphate-buffered saline (PBS), the tumor tissue was stored in liquid nitrogen for further extraction of total RNA. Additionally, specimens collected from 2 cm away from the edge of tumor tissue were confirmed to be normal tissue by pathological examination. There was no atypical hyperplasia or infiltration of cancer tissue.

The sample library was built an ILUMIMA kit (Illumina, Inc. San Diego, CA, United States) and the original data were sequenced using HiSeq 4000 (Illumina, Inc. San Diego, CA, United States). The simple procedure used was as follows: the sample RNA was reverse-transcribed into complementary DNA; then, poly-A was added at the 3' end, then the sample was connected to the sequencing connector of the kit, and polymerase chain reaction (PCR) amplification was performed. Finally, HiSeq 4000 was used to detect the fault. The original image files of Illumina high-throughput sequencing were base-called and transformed into original sequence sequences (sequenced reads) for subsequent analysis—that is, a collection of original sequences, called raw data. The analysis results are presented in FASTQ files (FQs for short). Based on the long noncoding RNA length threshold, potential assembled transcripts shorter than 200 bp were filtered out. For the assembled transcripts with only one exon, the transcripts with FPKM values of at least 2, and those with multiple exons, the transcripts with FPKM values of at least 0.5 were kept. When more than three samples were present, at least two samples were required to meet the screening criteria. The unknown transcripts were assembled by the Stringtie software for further coding ability filtering and the CPC, CNCI, and HMMER software programs were used for coding ability prediction, while FASTQC (version 0.11.2), fastp (version 0.14.0), Top Hat (version 2.0.13), Lemma (version 3.32.10) and Edger (version 3.18.1) were used for quality-control analysis.

Kyoto Encyclopedia of Genes and Genomes (KEGG) Analysis

Cluster analysis based on the functional enrichment of varying groups of differentially expressed circRNA was performed to investigate the potential associations and differences in specific functions (KEGG pathway) (Xia et al., 2020a). We first collected functional classification information enriched by circRNA grouping and the corresponding enriched *p*-values, then filtered out functional classifications that were significantly enriched ($p < 0.05$) in at least one circRNA grouping. First, the *p*-value data matrix was transformed using the log10 logarithm; then, the transformed data matrix was transformed by Z transformation for each function classification. Finally, hierarchical clustering (Euclidean distance, average join clustering) was used to analyze the data set after Z transformation. Clustering relationships were visualized using heat maps drawn by the function heatmap 2 in the R language package gplots (R Foundation for Statistical Computing, Vienna, Austria).

Cell Cycle

According to the methods described in a previous study (Xia et al., 2020b), when the cell density of HeLa and Siha cells was up to 70%, fresh medium was used. In preparing for transfection, 10 μL of siRNA (10 μL of negative control or 5 μL of siRNA + 5 μL of inhibitor) was diluted in 250 μL of Opti-MEM, while 10 μL of Lipofectamine 2000 transfection reagent was diluted in another 250 μL of Opti-MEM, with the transfection reagent left to rest for 5 min. The mixed solution was added into the holes for transfection and the complete medium was changed after 12 h. After being cultured for 48 h, the cells were removed from the incubator, the medium was discarded, the cells were rinsed with PBS, 0.25% trypsin was added, and the cells were digested at 37°C for 1–2 min. Then, 1–2 ml of medium was added to complete digestion and the cells were blown down with a pipette gun, transferred to a 15-ml centrifuge tube at 1,000 rpm, and centrifuged for 5 min and the supernatant was discarded. The cells were then resuspended and transferred to a sterile Eppendorf enzyme-free tube at 1.5 ml, then centrifuged for 2 min at 4°C and 500 g, and the supernatant was discarded. Precooled PBS was added again, under the same conditions of centrifugation, and the supernatant was discarded. We added 250 μL of precooled PBS, then 750 μL of precooled anhydrous ethanol, which were gently blown on and mixed at 4°C overnight, then fixed. Cells were centrifuged at 4°C and 500 g for 2 min, and then, the supernatant was discarded and washed with precooled PBS. Cells were centrifuged again at 4°C and 500 g for 2 min; then, the supernatant was discarded and cells were washed again. After washing, the cells were resuspended by PBS with 300–500 μL of supernatant; the final concentration of propidium iodide (PI) and RNaseA was 50 g/ml. Finally, the cells were warmed at 37°C for 30 min and cell-cycle distribution was measured and analyzed by flow cytometry. The flowcytometry in our laboratory is FACS Canto^{TM} II (Becton, Dickinson and Company, United States). The software we applied to process apoptotic data is called DIVA (Version 8.0).

Cell Apoptosis

As described in the methods of a previous study (Xia et al., 2018), HeLa and Siha cells (1×10^6) were planted in six-well plates. When the cell density was 70%, the fresh medium was changed. In preparing for transfection, 10 μL of siRNA (10 μL of negative control or 5 μL of siRNA + 5 μL of inhibitor) was diluted in 250 μL of Opti-MEM, while 10 μL of Lipofectamine 2000 transfection reagent was diluted in another 250 μL of Opti-MEM, with the transfection reagent left to rest for 5 min. The mixed solution was added into the holes for transfection and the

complete medium was changed after 12 h. The cells were incubated for 48 h, then digested with trypsin free of EDTA, gently beaten and transferred to a 1.5-ml Eppendorf tube, and centrifuged for 5 min at 1,000 rpm. We used Dead Cell Apoptosis Kit with Annexin V FITC and PI (ThermoFish, V13242) to measure cell apoptosis. FITC-Annexin V was Soluted in 25 mM HEPES, 140 mM NaCl, 1 mM EDTA, pH 7.4, 0.1% bovine serum albumin (BSA). The supernatant was discarded and cells were rinsed gently with an appropriate amount of PBS for 5 min at 1,000 rpm three times, then gently stirred with 500 μL of binding buffer and mixed with 5 μL of annexin V-FITC and incubated at room temperature under light for 15 min. Finally, they were mixed with 1 μL of the 100 μg/ml PI under light for 5 min and apoptosis was detected by flow cytometry.

Cell Migration

According to the methods described in a previous study (Abere et al., 2020), when the cell density of HeLa and Siha cells was 70%, the fresh medium was changed. In preparing for transfection, 10 μL of siRNA (10 μL of negative control or 5 μL of siRNA + 5 μL of inhibitor) was diluted in 250 μL of Opti-MEM, while 10 μL of Lipofectamine 2000 transfection reagent was diluted in another 250 μL of Opti-MEM, with the transfection reagent left to rest for 5 min. The mixed solution was added into the holes for transfection and the complete medium was changed after 12 h. After 24 h, the supernatant was discarded, cells were rinsed again with 2 ml of PBS and digested with 1 ml of trypsin for 2 min. Next, 1 ml of complete medium was added to stop digestion, cells were transferred to an Eppendorf tube and centrifuged at 500 g at room temperature for 2 min, and the supernatant was discarded. Then, we added 2 ml of basic medium, blew with spearhead, prepared the cell suspension, and counted the cells. Next, 500 μL of basal medium was added into a Transwell pore plate (Corning Inc. Corning, NY, United States) and the membrane was soaked for 30 min, then activated. After activation, the basal medium was discarded, and 400 μL of complete medium was added in the lower chamber, gently placed into the upper chamber, and 1×10^5 cells were added. We cultured the cells for 36 h, discarded the plate of upper-chamber culture medium, and rinsed it gently twice with PBS. The medium in the lower chamber was also discarded, 600 μL of formaldehyde was added, 200 μL was added in the upper chamber and fixed at room temperature for 15 min. After fixation, the formaldehyde was discarded, washed gently three times with PBS, and then dyed with 1% crystal violet.

Colony Formation

Cell suspension was prepared according to a previous study (Abere et al., 2020), where the concentration of cells was adjusted by the cell culture medium. A total of 1,000 cells were placed into the cell culture medium and inoculated with 5 ml of cell culture medium; then, hsa_circ_0001400_siRNA and its control siRNA were added and incubated at 37°C and 5% CO_2 for10 days, withthe medium replaced with fresh medium followingany pH changes. When visible clones appeared in the dish, we discarded the culture medium and used PBS solution to carefully soak and wash the cells twice. The colony was fixed with methanol for 20 min. Then the methanol was discarded and the colony was allowed to air-dry. Only then were the counts performed. Then, Giemsa solution was used to dye the colony for 30 min beforebeing washed off slowly with running water. The percentage of colony formation was calculated according to the following equation: % colony = (the number of colonies/total cells number) × 100%.

RNA Extraction and Quantitative Real-Time PCR

We discarded the cell culture solution, washed with PBS twice, added 1 ml of TRIzol reagent, blew gently until the cells fell off, inhale a 1.5-ml Eppendorf tube, and rested for 5 min. Then, we added 200 μL of chloroform, shook vigorously by hand for 15 s, left at room temperature for 23 min, and centrifuged at 4°C and 12,000 g for 15 min. We carefully transferred the upper aqueous phase to a new Eppendorf tube, without excessive volume (about 400–500 μL). We added isopropanol of equal volume into the upper aqueous phase mixture, gently mixedisopropanol and the upper aqueous phase mixture five times, and left the mixture at room temperature for 10 min. After 12,000 g of centrifugation at 4°C for 10 min, and 1 ml of 75% ethanol (0.75 ml of anhydrous ethanol + 0.25 ml of diethylpyrocarbonate water, now mixed) were added, then cells were washed twice, swirled, and mixed completely. Finally, we removed the supernatant, air-dried the RNA for 10 min, added 20 μL of diethylpyrocarbonate water, blew several times, and measured the concentration.

The all-in-one miRNA qRT-PCR kit (no. AOMD-Q020; GeneCopoeia, Guangzhou, China) was used. The reaction conditions were set according to the standard procedure given by the kit. The specific procedures were as follows: the components were mixed according to the configuration table, followed by instant centrifugation, incubation at 37°C for 60 min, incubation at 85°C for 5 min, reverse transcription, predenaturation at 95°C for 1 minute, denaturation at 95°C for 10 s, annealing at 53°C for 10 s, and acceptance at 72°C for 10 s, then repeat for 40 cycles, with analysis using the Roche LC96 default melting curve (Roche Holding, Basel, Switzerland). The amplification specificity of the miRNA in each sample was analyzed by the melting curve. The comparative cycle threshold ($2^{-\Delta\Delta T}$) was used to evaluate the miRNA expression of the target. For mRNA detection, qRT-PCR was reverse-transcribed using the Bestar qPCR RT Kit (No. 2220, DBI Bioscience) and Bestar SYBR Green qPCR Mix Master (No. 2043, DBI Bioscience) for gene detection. The reaction conditions were set according to the standard procedure given by the kit as follows: the components were mixed according to the configuration table, followed by instant centrifugation, incubation at 37°C for 15 min, incubation at 98°C for 5 min, reverse transcription, predenaturation at 95°C for 2 min, denaturation at 95°C for 10 s, annealing at 53°C for 30 s, and acceptance at 72°C for 30 s, then repeat for 40 cycles, with analysis using the Roche LC96 default melting curve. The

specificity of the mRNA amplification in each sample was analyzed by the melting curve. The comparative period threshold (2−ΔΔCt) was used to assess target mRNA expression.

Double Luciferase Reporter for Gene Analysis

According to the methods described in a previous study (Abere et al., 2020), 293T cells (37°C, 5% CO_2) were inoculated into a 24-well plate with 1.5×10^5 cells per well for a total volume of each well of 500 ml, then cultured in a 37°C incubator for 24 h. Dilution of 1.5 μL of miR-Mimic (inhibitor, negative control) with 25 ml of Opti-MEM medium diluted with 0.6 μg of the target gene 3'UTR double-report gene vector (50 ml) was performed. Also, Opti-MEM medium was diluted with 2 ml of Lipofectamine 2000 reagent and the mixture was mixed for 5 min, shaken gently, and left to rest for 20 min. Before the transfection mixture was added into cells, 100 μL of medium was sucked out per hole; then, the 100 ml mixture was added and, finally, the total volume of each hole was 500 ml, with three double holes in each group. The fresh medium of 500 μL was changed after 8 h. After the lysate of reporter cells had been thoroughly thawed and mixed, 200 μL of lysate of reporter cells was added to lyse the cells. Next, centrifugation at 4°C and 10,000 g for 1 minute was performed, keeping the supernatant. For each sample, 100 μL of serum was taken from the top of the sample and 100 μL of Firefly luciferin was added to the mixture to determine the relative light unit. Reporter gene cell lysate was used as a blank control. After completion of the above Firefly luciferin procedure, the relative light unit value was determined by adding 100 μL of harennin luciferase detection working fluid and mixing it in. The relative fluorescence expression of each group was calculated.

Western Blotting

According to the methods described in a previous study (Abere et al., 2020), the samples were taken from −80°C, and 4× volume cracking buffer solution (8 m urea, 1% protease inhibitor) was added to the samples. RIPA containing protease inhibitors was used to extract protein and cells were lysed for 30 min. Centrifugation was performed at 4°C and 12,000 g for 10 min, the cell fragments were removed, the supernatant was transferred to a new centrifuge tube, and the protein concentration was determined by bicinchoninic acid (BCA) protein assay kit (Novagen, Madison, WI, United States). The prepared buffer was poured into the electrophoresis tank and the precooled protein sample and protein maker were slowly added into the gel pore. We ran the gel at 80 volts (V), then switched to 110 V until the bromophenol blue dye moved to the bottom of the gel and stopped electrophoresis. The sandwich splint was placed in the electrophoresis tank at 4°C and 250 mA of constant current was applied for 60 min; then, 5% skimmed milk powder was sealed at room temperature for 2 h, the first reactant was added and incubated overnight at 4°C, and the second reactant was incubated at room temperature for 1.5 h. The PVDG membrane was incubated with electro-chemiluminescence for 3 min at room temperature and imaged using the Bio-Rad gel system. We use ImageJ to analyze immunoblot lane intensity. Calculation results from each independent experiment were presented by folds to control group.

Tumor Xenograft Modeling and *In Vivo* Experiments

BALB/C nude mice (3–4 weeks old) were purchased from the Laboratory Animal Center of Guangdong Province. Weighing about 15–17 g, the mice were injected with 0.1 ml of Siha single-cell suspension (containing about 5×10^6 cells) in serum-free medium to disinfect the skin near the armpit of the left forelimb. When a rice-size nodule appeared (1–2 mm^3) in nude mice (about 1 week after injection), the xenograft model of cervical cancer was believed to be successfully established. The subcutaneous tumors of the left forelimb of nude mice were measured with electronic Vernier calipers. When the diameter of the tumor was about 0.3–0.5 cm, the nude mice were numbered using a random number table method and randomly divided into five groups (model group, negative control group, high-dose group, medium-dose group, and low-dose group), with six mice in each group. The growth of nude mice and their tumors were closely observed every day, focusing on whether the tumors were inflamed or ulcerated, whether the skin of nude mice had luster, and whether their mental state was good were observed. The maximum and minimum diameters of subcutaneous tumors in nude mice were measured with the Vernier scale every 2 days and the tumor volume was calculated according to the following: $V = 0.5 \times A \times B^2$ (where V = tumor volume, A = tumor maximum diameter, and B = tumor minimum diameter). In this experiment, the hsa_circRNA_0001400_siRNA was given once a day for 4 days. After drug treatment, the nude mice were killed by cervical dislocation and the subcutaneous tumor was quickly peeled off on ice. The weight of each tumor was weighed by electronic balance and some tumor tissue was cut and placed into a cryopreservation tube and stored in liquid nitrogen for subsequent experimental analysis.

Statistical Analysis

Using the Statistical Package for the Social Sciences version 16.0 statistical software (IBM Corporation, Armonk, NY, United States) for data analysis, data were compared between two groups using an independent *t*-test, while comparisons between more groups were made using multifactor analysis of variance. $p < 0.05$ indicated a significant difference, while $p < 0.01$ suggested a very significant difference.

RESULTS

The Differential Expression of circRNA in Cervical Cancer

In order to explore the role of circRNA in the pathogenesis of cervical cancer, we used an RNA sequencing method to search for differential circRNA. Specifically, we used the differential

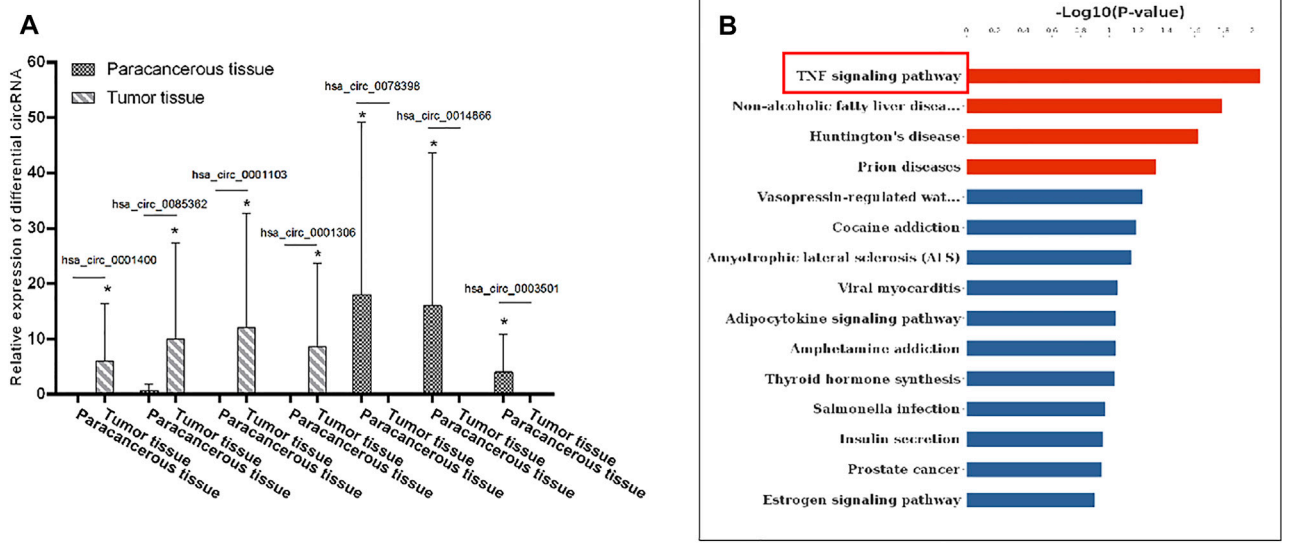

FIGURE 1 | Differential expression levels of circRNA in cervical cancer: **(A)** The expression levels of hsa_circRNA_0001400, hsa_circRNA_0085362, hsa_circRNA_0001103, and hsa_circRNA_0001306 were significantly increased and those of hsa_circRNA_0078398, hsa_circRNA_0014866, and hsa_circRNA_0003501 were significantly decreased. B) KEGG was used to analyze the signal pathway involved in the differential expression of circRNA. Data are expressed as mean ± standard deviation, $n = 3$, $^{*}p < 0.05$ and $^{**}p < 0.01$ vs. control group.

expression multiple of more than 1.2-fold as the standard for screening and found that, as compared with the adjacent tissues, a total of 48 circular RNAs were expressed, of which 28 were upregulated and 20 were downregulated. Notably, hsa_circRNA_0001400, hsa_circ_0085362, hsa_circ_0001103, and hsa_circ_0001306 were significantly increased, while hsa_circ_0078398, hsa_circ_0014866, hsa_circ_0003501 were significantly decreased (**Figure 1A**).

We first used bioinformatics to analyze the results of RNA sequencing. GO is an important bioinformatics analysis method and tool used to express the attributes of genes and gene products. GO notes can be divided into three categories: biological process, cellular components, and molecular function, which explain the biological function of proteins from different perspectives. We analyzed the distribution of differentially expressed circRNA in GO secondary annotation. According to the classification results of biological processing, we found that these circRNAs are mainly involved in the apoptosis signal pathway through death receptors (**Supplementary Figure S1A**); according to the classification results of cellular components, these circRNAs mainly belong to the interleukin complex and protein kinase complex (**Supplementary Figure S1B**), while, according to the classification results from molecular function, these circRNAs mainly have binding functions (**Supplementary Figure S1C**). KEGG is an information network connecting known molecular interactions, such as metabolic pathways, complexes, and biochemical reactions. The KEGG pathway mainly includes metabolism, genetic information processing, environmental information processing, cell processes, human diseases, drug development, and so on. Protein domain refers to some components that appear repeatedly in different protein molecules. The similar sequence, structure, and function of proteins is the unit in evolution. The length of the domain is usually between 25 and 500 amino acids. From the enrichment of the KEGG pathway, we found that the differentially expressed circRNA mainly regulates the tumor necrosis factor signaling pathway (**Figure 1B**). These results suggest that circRNA can regulate the apoptosis signaling pathway and combine with downstream signaling molecules to participate in the pathogenesis of cervical cancer.

Hsa-circRNA_0001400_siRNA promotes cervical cancer cell apoptosis and arrest of thecell cyclein the G2 phase.

Our sequencing results showed that hsa_circRNA_0001400 is a highly expressed circRNA in tumor tissues. Previous studies showed that hsa_circ_0001400 was up-regulated upon Kaposi's sarcoma herpesvirus (KSHV) infection in the microarray expression profiling (Takanobu Tagawa, et al., 2018). Thus, we selected hsa_circRNA_0001400 for follow-up study. We confirmed hsa_circRNA_0001400 to be highly expressed in cervical cancer cell lines (**Figure 2A**). Unlimited proliferation and permanent cell division are the characteristics of tumor cells. Therefore, it is an important strategy to inhibit tumor growth by inhibiting tumor cell proliferation, promoting tumor cell apoptosis, and blocking tumor cell division. We used hsa_circRNA_0001400_siRNA to trigger interference expression of hsa_circRNA_0001400 by flow cytometry. We found that hsa_circRNA_0001400_siRNA can significantly promote the apoptosis of SiHa and HeLa cells and arrest the division of both cell types in the G2 phase (**Figures 2B,C**). We also analyzed the colony formation of

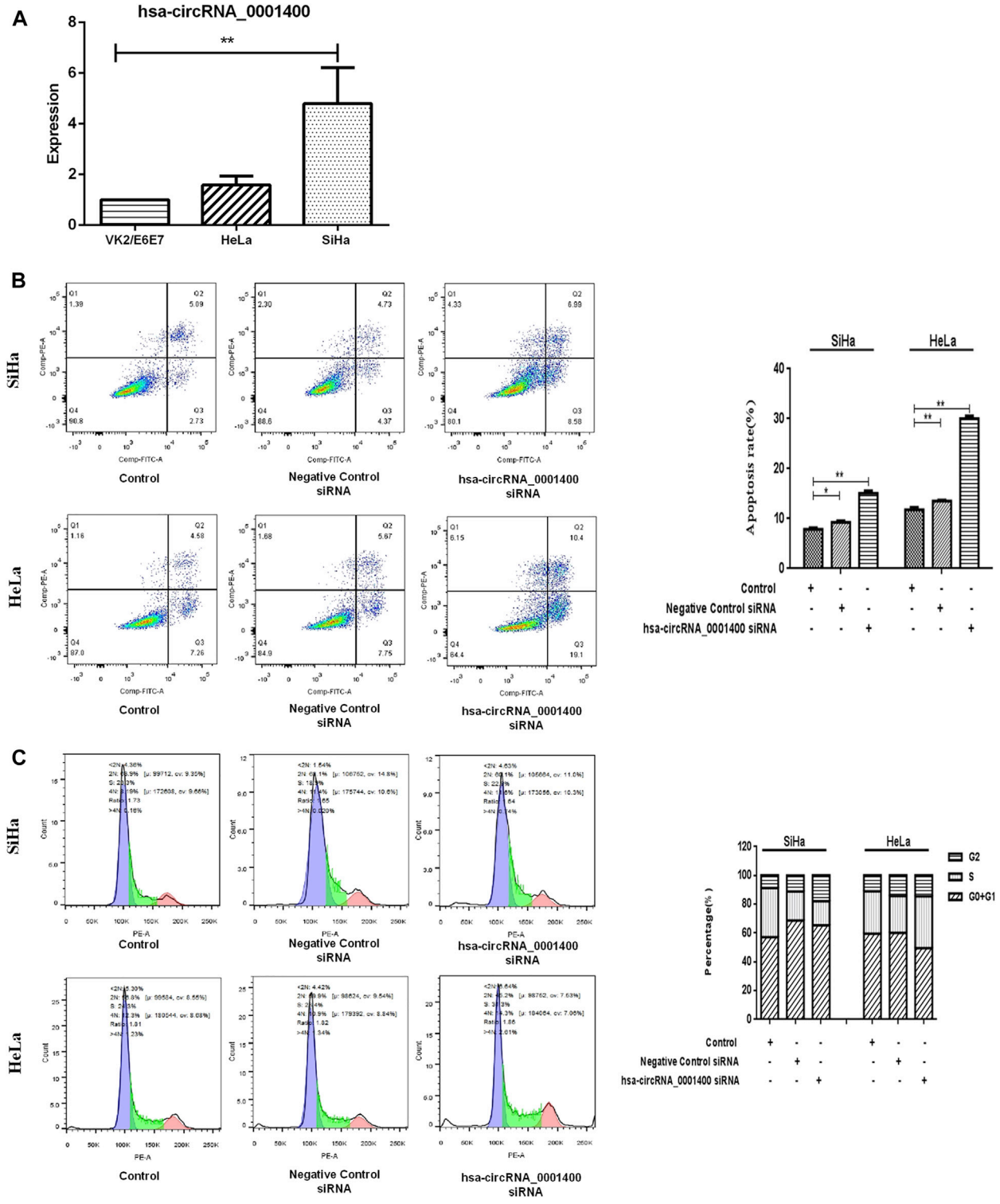

FIGURE 2 | Hsa-circRNA_0001400_siRNA promotes the apoptosis of cervical cancer cells and causes G1-phase arrest of the cell cycle. **(A)** hsa_circRNA_0001400 in human vaginal epithelial, cervical cancer SiHa, and HeLa cell lines. **(B)** The effect of hsa_circRNA_0001400_siRNA on the apoptosis of cervical cancer cells. **(C)** The effect of hsa_circRNA_0001400_siRNA on the cell cycle of cervical cancer cells. **(D)** The effect of hsa_circRNA_0001400_siRNA on cervical cancer colony formation. **(E)** The effects of hsa_circRNA_0001400_siRNA on Akt, Phospho-Akt (Ser473), PI3K, and Phospho-PI3 Kinase p85 (Tyr458) protein expression in cervical cancer cells. Data are expressed as mean ± standard deviation, $n = 3$, $^{*}p < 0.05$ and $^{**}p < 0.01$ vs. control group.

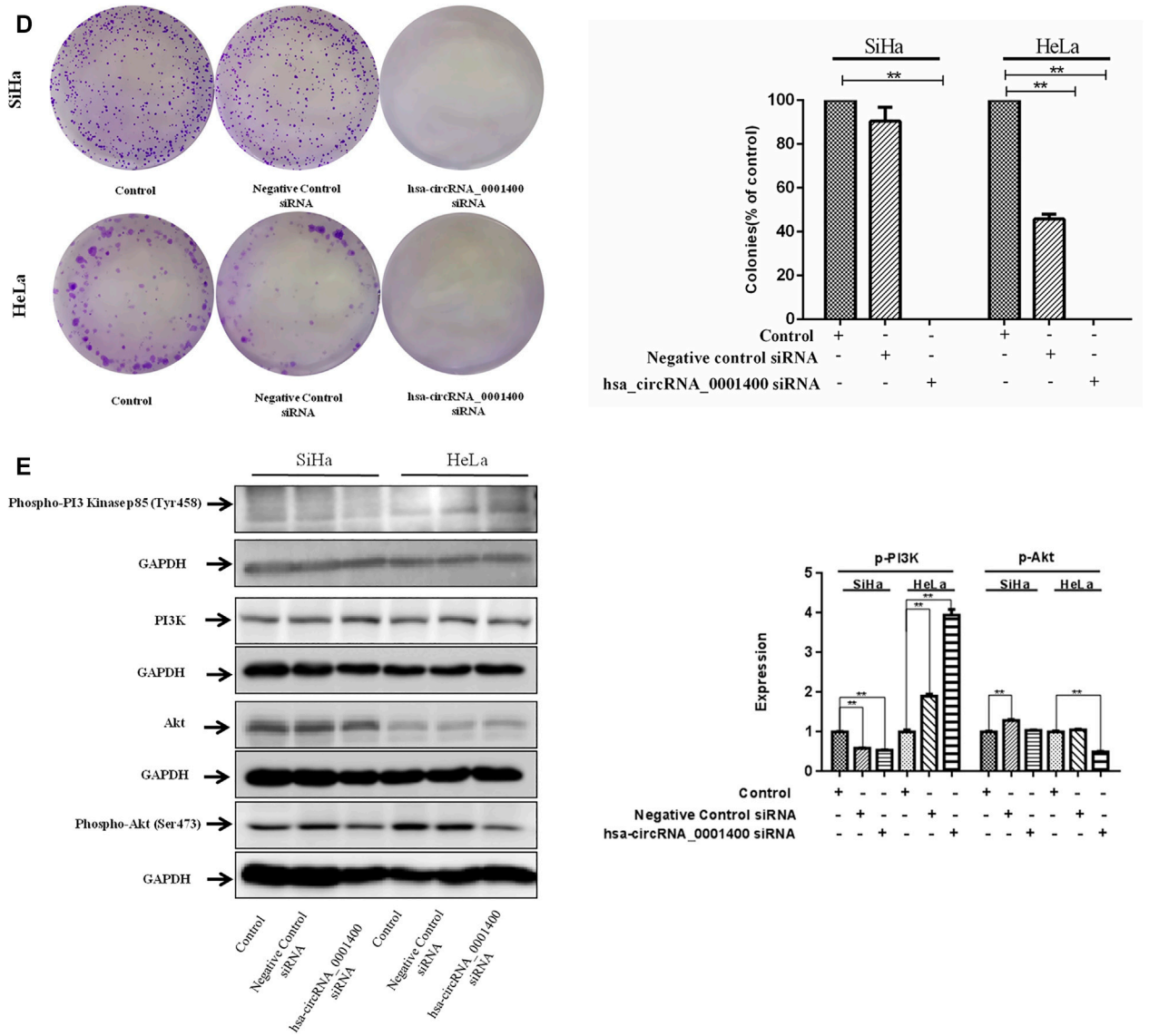

FIGURE 2 | (Continued)

cervical cancer cells under the presence of hsa_circRNA_0001400_siRNA. We found that hsa_circRNA_0001400_siRNA can significantly suppressthe colony formation of SiHa and HeLa cells (**Figure 2D**). The PI3K-Akt signaling pathway is an important signal pathway of tumor proliferation. Akt is at the center of the signal pathway network, responsible for a variety of signal transduction functions, and is a key molecule in the PI3K–Akt signaling pathway. We analyzed the effect of hsa_circRNA_0001400_siRNA on PI3K, Phospho-PI3 Kinase p85 (Tyr458), Akt and Phospho-Akt (Ser473) in cervical cancer cells. Our results showed that hsa_circRNA_0001400_siRNA can inhibit the expression of p-Akt in SiHa and HeLa cells. The expression of p-PI3K was not affected by hsa_circRNA_0001400_siRNA. Interestingly, these results showed that the target gene of microRNA adsorbed by hsa_circRNA_0001400 might be Akt and not to be PI3K (**Figure 2E**).

The Direct Interaction Between hsa-circRNA_0001400, miR-326, and Akt

Because of its spongy function, circRNA can adsorb microRNA and regulate the function of microRNA target genes (Liu et al., 2019; Zhou et al., 2019; Yang et al., 2021). We first predicted the binding sites of miR-326, Akt, and hsa_circRNA_0001400 by bioinformatics. Our prediction results showed that the binding sites of hsa_circRNA_0001400 and miR-326 were located at 241 to 247 of the 5′ end of the circular RNA, while the binding target of mir-326 with AKT2 was located at positions 2,224 to 2,234 in

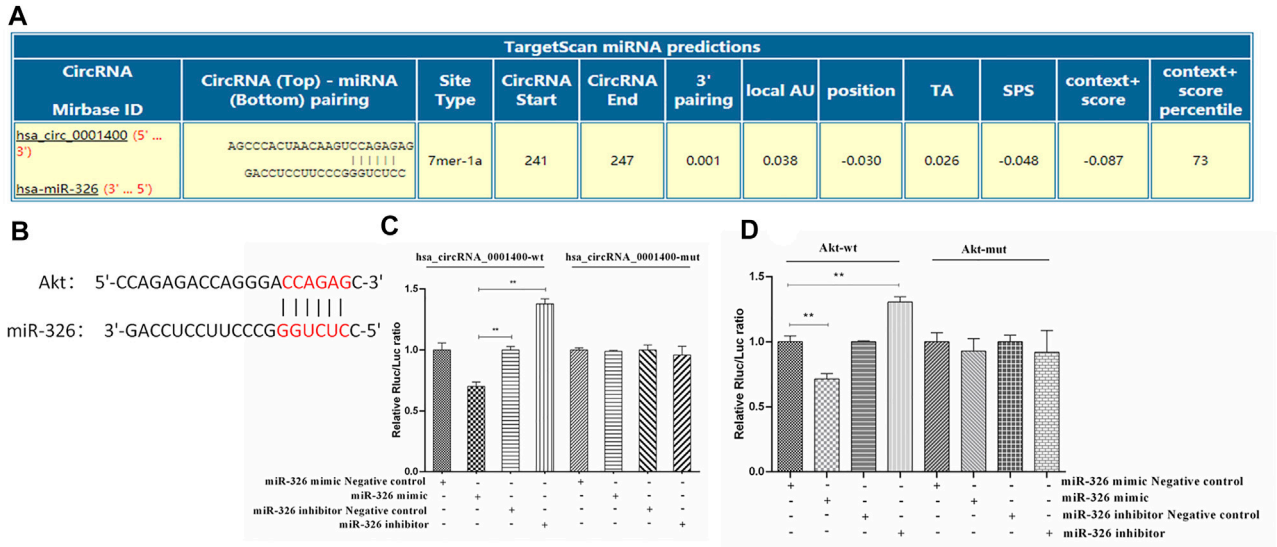

FIGURE 3 | Direct interaction of hsa-circRNA_0001400, miR-326, and Akt. **(A)** Bioinformatics prediction of the direct interaction sites of hsa_circRNA_0001400 and miR-326. **(B)** Bioinformatics prediction of the direct interaction of miR-326 and Akt. **(C)** The direct interaction between hsa_circRNA_0001400 and miR-326 was analyzed by double luciferase reporter gene analysis. **(D)** The direct interaction between miR-326 and Akt was analyzed by double luciferase reporter gene analysis. Data are expressed as mean ± standard deviation, $n = 3$, $^{*}p < 0.05$ and $^{**}p < 0.01$ vs. control group.

the AKT2 mRNA 3′UTR region (www.https://circinteractome.nia.nih.gov/) (**Figures 3A,B**). We then verified the direct interaction between hsa_circRNA_0001400 and miR-326, miR-326 and Akt by luciferase reporter gene analysis. In addition, we mutated the region from position 241 to 247 at the 5′ end of the circular RNA and position 2,224 to 2,234 at the AKT2 3′UTR region in 293T cells. Our results showed that direct interaction between hsa_circRNA_0001400 and miR-326, as well as miR-326 and Akt, has disappeared (**Figures 3C,D**).

miR-326 Rescues the Action of hsa-circRNA_0001400_siRNA

CircRNAs have a variety of biological characteristics (Hong et al., 2019). The mechanism of action of circRNAs is mainly focused on the sponge adsorption of miRNA. The results show that there are miRNA binding sites on circRNAs, which act as miRNA sponges by adsorbing miRNAs (Stanley et al., 2014; An et al., 2017). CircRNA contains a large number of miRNA response elements, which can bind miRNAs competitively to prevent complementary pairing with the 3′UTR region of downstream target mRNA and regulate mRNA gene expression (Tsikouras et al., 2016). We next verified that hsa_circRNA_0001400 was able to adsorb miR-326 on the sponge. When hsa_circRNA_0001400 was silenced by hsa_circRNA_0001400_siRNA, the sponge of hsa_circRNA_0001400–miR-326 was destroyed and miR-326 was transformed from hsa_circRNA_0001400–miR-326 sponge and was released. Also, the target of miR-326 was inhibited, the apoptosis of tumor cells increased (**Figure 4A**), migration was inhibited (**Figure 4B**), the number of G1-phase cells increased, and the cell division rate was slowed down (**Figure 4C**). When we used miR-326 inhibitor at the same time, the antitumor effect of free miR-326 released from the sponge was inhibited and tumor cell apoptosis decreased again (**Figure 4A**), cell migration increased (**Figure 4B**), the number of G1-phase cells decreased, and cells entered a rapid division and proliferation phase (**Figure 4C**). We also detected the protein expression of Akt and found that Akt expression decreased when hsa_circRNA_0001400 was silenced alone by hsa_circRNA_0001400_siRNA. Once miR-326 inhibition was combined with hsa_circRNA_0001400_siRNA, the Akt expression increased, which was consistent with the conclusion of flow cytometry (**Figure 4D**). Furthermore, we measured the expression of hsa_circRNA_0001400 under the condition of hsa_circRNA_0001400_siRNA or miR-326 inhibition. Our results showed that the expression of hsa_circRNA_0001400 decreased when hsa_circRNA_0001400_siRNA was used alone. The expression of hsa_circRNA_0001400 increased when hsa_circRNA_0001400_siRNA was combined with miR-326 inhibition (**Figure 4E**). We also tested the expression of miR-326 under the condition of hsa_circRNA_0001400_siRNA or miR-326 inhibition. Our results showed that the expression of miR-326 increased when hsa_circRNA_0001400_siRNA was used alone. The expression of miR-326 decreased when hsa_circRNA_0001400_siRNA was combined with miR-326 inhibition (**Figure 4F**). These results suggest that hsa_circRNA_0001400_siRNA could destroy the sponge of hsa_circRNA_0001400–miR-326. When the hsa_circRNA_0001400–miR-326 sponge was damaged, miR-326 was released from the sponge and suppressed the expression of Akt following the inhibition of p-Akt.

Hsa-circRNA_0001400_siRNA suppresses the growth of cervical cancer cell xenograft, decoying the hsa-circRNA_0001400–miR-326 sponge.

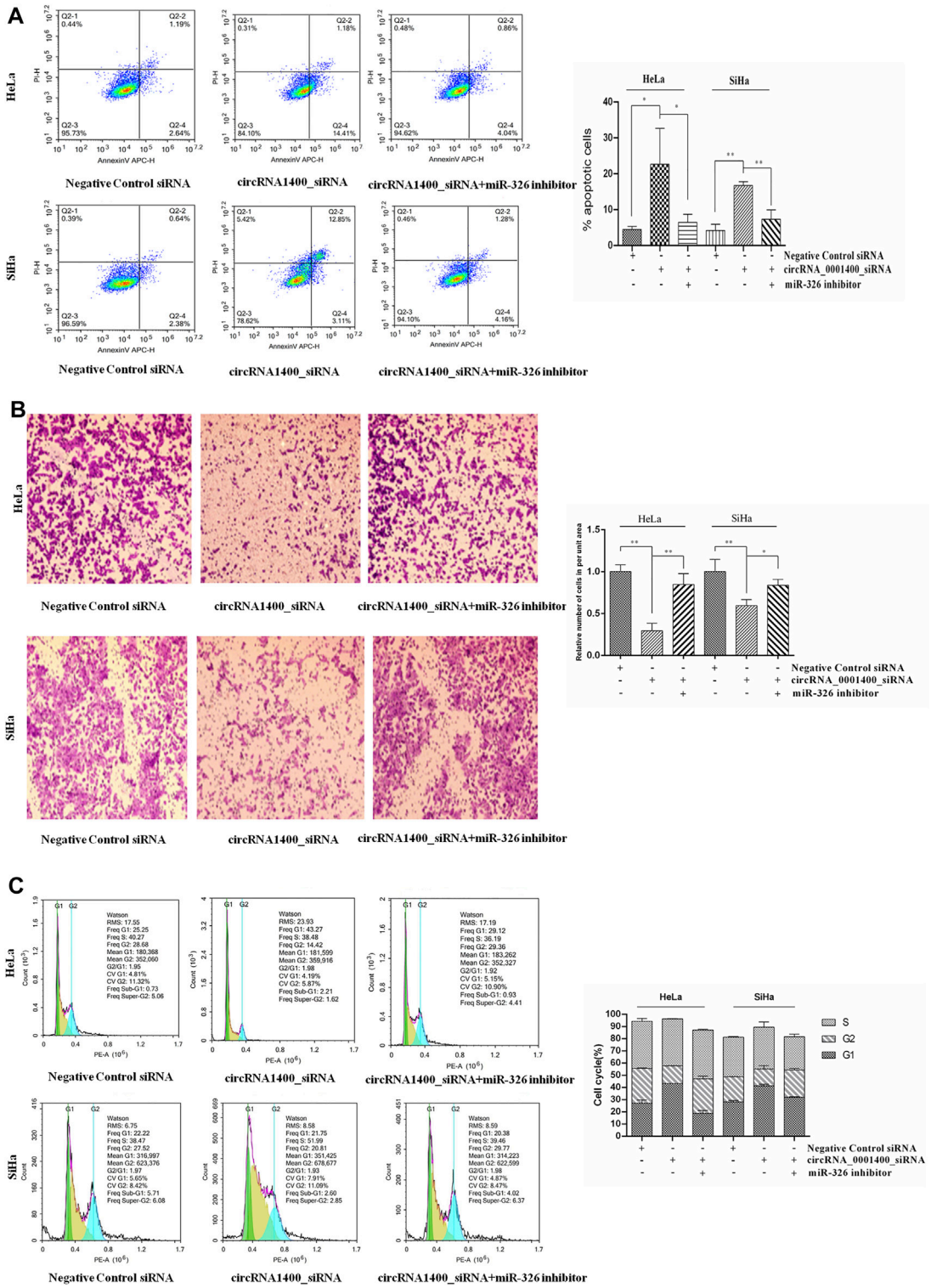

FIGURE 4 | Hsa_circRNA_0001400 targeting miR-326 rescue experiment. **(A)** Apoptosis recovery test; **(B)** cell migration recovery test; **(C)** cell cycle recovery test; and **(D)** Akt and Phospho-Akt (Ser473) expression. **(E)** The effect of miR-326 inhibitor rescue of hsa_circRNA_0001400_siRNA on hsa_circRNA_0001400. **(F)** The effect of miR-326 inhibitor rescue of hsa_circRNA_0001400_siRNA on miR-326. Data are expressed as mean ± standard deviation, $n = 3$, $^{*}p < 0.05$ and $^{**}p < 0.01$ vs. control group.

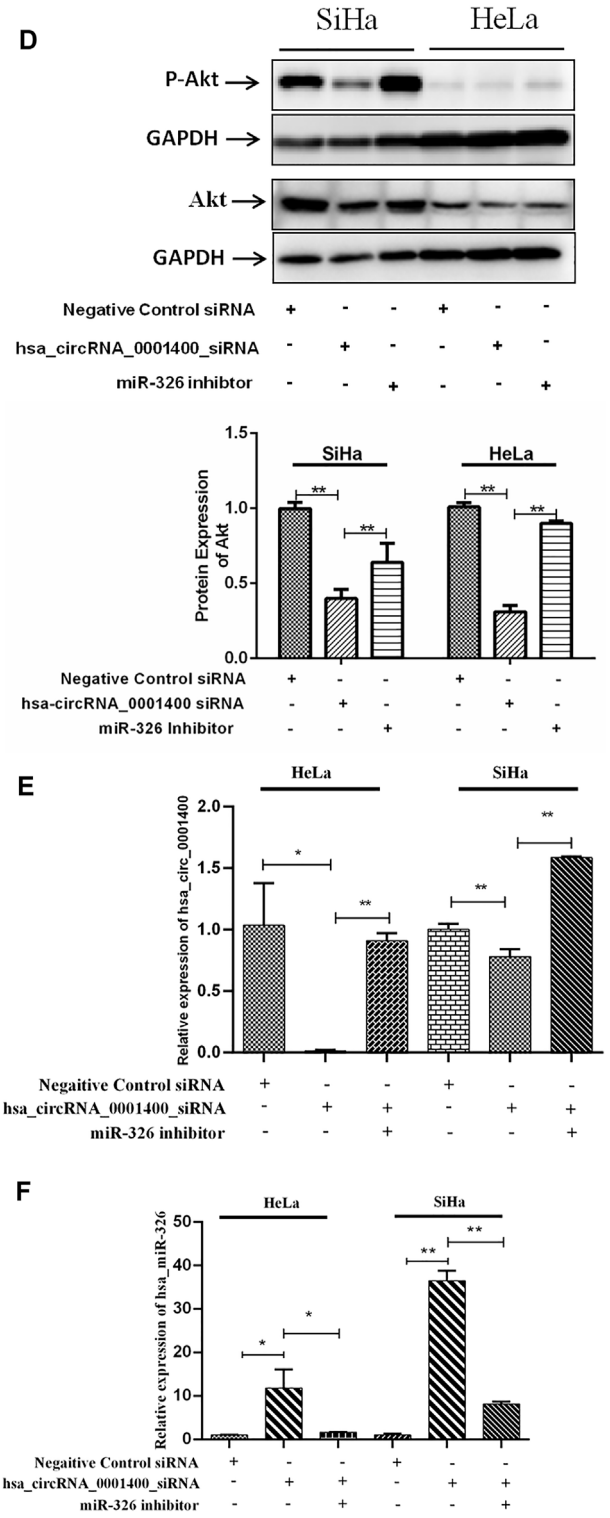

FIGURE 4 | (Continued)

The animal model of xenotransplantation of tumor cells has been widely used in the screening and evaluation of antitumor drugs because of its easy construction, high tumor formation rate, and short experimental cycle (Xia et al., 2020a). To study the effect of hsa_circRNA_0001400_siRNA on tumors *in vivo*, we established a BALB/C nude mouse model of heterotopic tumor

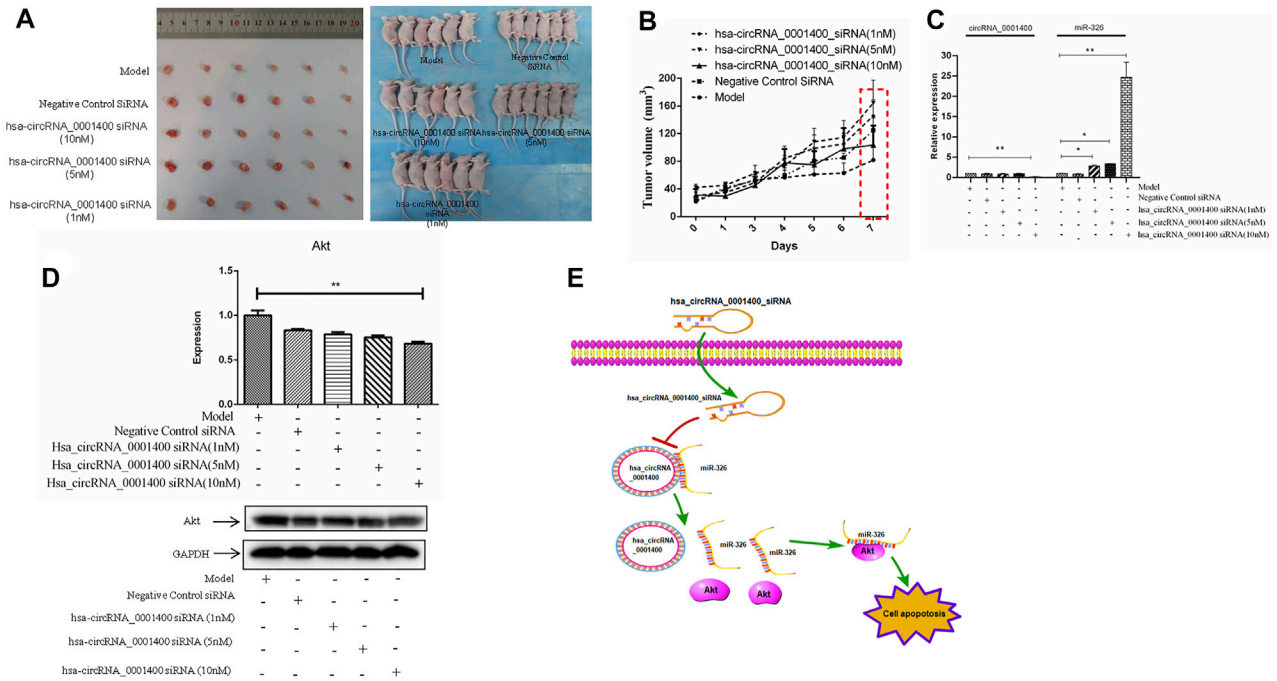

FIGURE 5 | Hsa-circRNA_0001400_siRNA inhibits the growth of cervical xenograft tumors. **(A)** Tumor volume; **(B)** tumor growth curve; **(C)** the expression levels of hsa-circRNA_0001400 and miR-326; **(D)** the expression of Akt in tumor tissue; and **(E)** the pattern of action. Data are expressed as mean ± standard deviation, $n = 3$, $^{*}p < 0.05$ and $^{**}p < 0.01$ vs. control group.

using SiHa cells. After successful modeling, 1, 5, and 10 nm of hsa_circRNA_0001400_siRNA were used in tumor mice. As compared with the model group, 10 nm of hsa_circRNA_0001400_siRNA was injected into the tumor-bearing mice for 7 days. The growth of tumors in the siRNA group was slower than that in the control group (**Figures 5A,B**). The expression of hsa_circRNA_0001400 and Akt decreased, while the expression of miR-326 increased (**Figures 5C,D**). These results suggest that hsa_circRNA_0001400_siRNA destroyed the hsa_circRNA_0001400–miR-326 sponge and may have inhibited the growth of cervical cancer xenograft in BALB/C nude mice (**Figure 5E**).

DISCUSSION

We found the expression levels of hsa_circRNA_0001400, hsa_circRNA_0085362, hsa_circRNA_0001103, and hsa_circRNA_0001306 were significantly increased in tumor tissues by RNA sequencing. We chose hsa_circRNA_0001400 to study further and found that hsa_circRNA_0001400_siRNA can promote the apoptosis of SiHa and HeLa cells and arrest the division of SiHa and HeLa cells in the G2 phase. Hsa_circRNA_0001400–miR-326–Akt sponge plays an important role in cervical cancer metastasis. Hsa_circRNA_0001400_siRNA destroys hsa_circRNA_0001400–miR-326 sponge, inhibiting Akt, promoting tumor cell apoptosis, and suppressing cervical cancer metastasis.

Although the main cause of cervical cancer is HPV infection, the availability of HPV vaccines can bring good news to patients with cervical cancer. At present, however, the HPV vaccine is mainly used to prevent tumors and a therapeutic vaccine has not yet come onto the market (Hu and Ma, 2018). At present, surgery and chemotherapy are still the main treatments. However, 10–15% of patients with cervical cancer relapse or experience metastasis after treatment, which are the primary reasons for the failure of cervical cancer treatment (Moldovan et al., 2019; Xu et al., 2019). With the development of high-throughput sequencing technology, a large number of circRNAs have been discovered and confirmed to have functions of posttranscriptional regulation (Arnaiz et al., 2019; Yu C. et al., 2019). CircRNAs have gradually attracted attention. Studies have confirmed that circRNAs affect the occurrence, development, invasion, and metastasis of tumors mainly through escaping growth inhibition and apoptosis; activating invasion, metastasis, and angiogenesis processes; and maintaining proliferation signals (Verduci et al., 2019; Vo et al., 2019). In this study, we first analyzed the differentially expressed circRNA in cervical cancer by RNA sequencing. We found that hsa_circRNA_0001400 was highly expressed in cervical cancer tissues and cervical cancer cells. It has been reported that hsa_circRNA_0001400 expression can be induced by viral infection. Therefore, we used hsa_circRNA_0001400_siRNA to interrupt the expression of hsa_circRNA. The cell apoptosis was tested by using flow cytometry. Hsa_circRNA_0001400_siRNA can

significantly promote the apoptosis of SiHa and HeLa cells. In SiHa cells, when treated with hsa_circRNA_0001400_siRNA, the apoptosis rate increased from 2.01 to 8.71%, while, in HeLa cells, the apoptosis rate increased from 4.48 to 23.26%. We also analyzed the percentage of cells in each cell cycle. We found that among SiHa cells treated with hsa_circRNA_0001400_siRNA, the cell cycle of G2-phase cells decreased from 5.4 to 4.71%, while in HeLa cells, that of G2-phase cells decreased from 4.9 to 4.6%. In other words, Hsa_circRNA_0001400_siRNA arrested the division of SiHa and HeLa in the G2 phase. Moreover, we identified that hsa_circRNA_0001400_siRNA inhibited the expression of Akt in SiHa and HeLa cells. However, hsa_circRNA_0001400_siRNA did not affect the expression of *PI3K*. These results suggested that the target gene of miRNA adsorbed by hsa_circRNA_0001400 was not *PI3K*.

It is generally believed that one of the important functions of circRNA is to negatively regulate the corresponding miRNA through its binding site, thus affecting its downstream target molecules—namely, to provoke a spongy effect (Weng et al., 2017; Li et al., 2018; Xia et al., 2020b). Among them, the most representative is human circRNA cerebellar degeneration–associated protein 1 transcript (cdr1as)/cirs-7. As an miR-7 sponge, it contains more than 70 miR-7 binding sites, which bind to and regulate the function of miR-7 (Yao et al., 2019; Yin et al., 2019). This study is the first to prove that circRNA has the function of miRNA sponge. However, until 2017, only a few kinds of circRNAs had been proven to be spongy (Yu T. et al., 2019). To verify our hypothesis, we used bioinformatics tools to predict that hsa_circrRNA_0001400 and miR-326 have a sponge effect and we have confirmed the binding sites of hsa_circRNA_0001400 and mir-326 were located at 241 to 247 of the 5′ end of the circular RNA, while the binding target of miR-326 with AKT2 was located at positions 2,224 to 2,234 of AKT2 3′UTR region by luciferase reporter gene analysis. We further verified hsa_circRNA_0001400–miR-326–Akt by means of reversibility experimentation. When we first inhibited hsa_circRNA_0001400 by hsa_circRNA_0001400_siRNA, miR-326 was transformed from the hsa_circRNA_0001400–miR-326 sponge. Specifically, the target gene *Akt* of miR-326 was inhibited, the apoptosis rate of HeLa tumor cells increased from 3.83 to 15.59%, and the number of G1-phase cells decreased from 5.41 to 4.44%. When we used miR-326 inhibitor in combination with hsa_circRNA_0001400_siRNA, the antitumor effect of free miR-326 released from sponge was inhibited, the apoptosis rate of tumor cells decreased from 15.59 to 4.9%, and the number of G2-phase cells increased from 4.44%% to 5.16%. We also detected the protein expression of Akt in SiHa cells and found that, after hsa_circRNA_0001400 was silenced by hsa_circRNA_0001400_siRNA, the expression of Akt decreased, yet it increased when miR-326 inhibitor was added. MiR-326 inhibition can ameliorate the hsa_circRNA_0001400 reduction induced by hsa_circRNA_0001400_siRNA. However after hsa_circRNA_0001400 was silenced by hsa_circRNA_0001400_siRNA in HeLa cells, the expression of Akt increased, yet it decreased when miR-326 inhibitor was added. We did not explain this phenomenon. We also verified the inhibitory effect of hsa_circRNA_0001400_siRNA on the growth of cervical xenograft tumors. In conclusion, we found hsa_circRNA_0001400–miR-326–Akt to be a novel circular RNA sponge, which is involved in tumor metastasis. Hsa_circRNA_0001400_siRNA may be a new treatment for cervical cancer.

At present, most of our research on the role of circRNAs in tumorigenesis and development has been focused on the adsorption function of miRNA sponge by circRNA (Zang et al., 2020). In fact, the mechanism of circRNA in tumor progression is not only one or two aspects. CircRNAs can bind to both mRNA and proteins. Can they act as an intermediary bridge to bring mRNA or protein close to each other and promote the interaction between them, or do they have biological functions as a whole? What are the main components of this complex? The expression level of circRNAs is not high and how circRNAs can effectively compete to bind miRNAs or proteins is a problem that needs to be considered. Although a lot of circRNAs related to tumor metastasis have been identified, most existing studies are limited to including small sample groups or tumor phenotypes and long-term follow-up investigation of clinical information is urgently needed. Therefore, the in-depth and accurate study of circRNA will provide new ideas for researchers to comprehensively explain the molecular mechanism of tumor metastasis and then put forward related methods of tumor-metastasis prevention and treatment. To summarize, circRNAs have unique characteristics, which have significant research value for studying the pathogenesis of diseases, regardless of whether they can be used as diagnostic biomarkers or as therapeutic targets. We need to deepen our understanding of circRNAs and their important functions and mechanisms need to be discovered.

CONCLUSION

This study provides evidence that the hsa_circRNA_0001400–miR-326–Akt network promotes cervical cancer progression. Notably, our findings demonstrate the novel antitumor effects of hsa_circRNA_0001400_siRNA in cervical cancer. Since hsa_circRNA_0001400_siRNA play key roles in cervical cancer development and that hsa_circRNA_0001400 might be used as novel diagnostic and prognostic biomarkers as well as for targeted therapies. Furthermore, many studies which establishing circRNAs significance as biomarkers of early disease and clinical outcome indicators are on the way.

DATA AVAILABILITY STATEMENT

Publicly available datasets were analyzed in this study. This data can be found here: https://www.jianguoyun.com/p/DV5rq5UQi4zqCRjB6o0E Account: xiachenglai@126.com password: Xiacl998.

ETHICS STATEMENT

The studies involving human participants were reviewed and approved by the Ethics Committee of Foshan Maternity and Child Healthcare Hospital. The patients/participants provided their written informed consent to participate in this study. The animal study was reviewed and approved by the Ethics Committee of Foshan Maternity and Child Healthcare Hospital.

AUTHOR CONTRIBUTIONS

All other authors declare no competing interests. CX supervised the entire work and performed the cell cultures. YC, CL, FP, SY, and HL performed all experiments. YC, CL, AY, and HL performed all the figures and legends. LL, JS, CY, DL, and CX analyzed the data. CX conceived and designed the experiments and critically revised the manuscript. All authors discussed the results and contributed to manuscript writing.

FUNDING

This study was supported by grants from the Science and Technology Bureau of Foshan (No. FS0AA-KJ218-1301-0008 and no. FS0AA-KJ819-4,901-0082) awarded to CX a grant from the Guangdong Medical Science (No. A2019009) awarded to YC and the Foshan Medicine Dengfeng Project of China (2019–2021).

SUPPLEMENTARY MATERIAL

The Supplementary Material for this article can be found online at: https://www.frontiersin.org/articles/10.3389/fgene.2021.779195/full#supplementary-material

Supplementary Figure S1 | GO analysis was used to analyze **(A)** the biological process of differential expression of circRNA, **(B)** the cell composition of differentially expressed circRNA, and **(C)** the molecular function of differentially expressed circRNA.

REFERENCES

Abere, B., Zhou, H., Li, J., Cao, S., Toptan, T., Grundhoff, A., et al. (2020). Merkel Cell Polyomavirus Encodes Circular RNAs (circRNAs) Enabling a Dynamic circRNA/microRNA/mRNA Regulatory Network. *MBio* 11, e03059-20. doi:10.1128/mBio.03059-20

An, Y., Furber, K. L., and Ji, S. (2017). Pseudogenes Regulate Parental Gene expressionviaceRNA Network. *J. Cel. Mol. Med.* 21, 185–192. doi:10.1111/jcmm.12952

Arnaiz, E., Sole, C., Manterola, L., Iparraguirre, L., Otaegui, D., and Lawrie, C. H. (2019). CircRNAs and Cancer: Biomarkers and Master Regulators. *Semin. Cancer Biol.* 58, 90–99. doi:10.1016/j.semcancer.2018.12.002

Canfell, K. (2019). Towards the Global Elimination of Cervical Cancer. *Papillomavirus Res.* 8, 100170. doi:10.1016/j.pvr.2019.100170

Dalmer, T. R. A., and Clugston, R. D. (2019). Gene Ontology Enrichment Analysis of Congenital Diaphragmatic Hernia-Associated Genes. *Pediatr. Res.* 85, 13–19. doi:10.1038/s41390-018-0192-8

Hong, H., Zhu, H., Zhao, S., Wang, K., Zhang, N., Tian, Y., et al. (2019). The Novel circCLK3/miR-320a/FoxM1 axis Promotes Cervical Cancer Progression. *Cell Death Dis* 10, 950. doi:10.1038/s41419-019-2183-z

Hu, Z., and Ma, D. (2018). The Precision Prevention and Therapy of HPV-Related Cervical Cancer: New Concepts and Clinical Implications. *Cancer Med.* 7, 5217–5236. doi:10.1002/cam4.1501

Kristensen, L. S., Hansen, T. B., Venø, M. T., and Kjems, J. (2018). Circular RNAs in Cancer: Opportunities and Challenges in the Field. *Oncogene* 37, 555–565. doi:10.1038/onc.2017.361

Li, R.-c., Ke, S., Meng, F.-k., Lu, J., Zou, X.-j., He, Z.-g., et al. (2018). CiRS-7 Promotes Growth and Metastasis of Esophageal Squamous Cell Carcinoma via Regulation of miR-7/HOXB13. *Cel Death Dis* 9, 838. doi:10.1038/s41419-018-0852-y

Liu, Z., Yu, Y., Huang, Z., Kong, Y., Hu, X., Xiao, W., et al. (2019). CircRNA-5692 Inhibits the Progression of Hepatocellular Carcinoma by Sponging miR-328-5p to Enhance DAB2IP Expression. *Cel Death Dis* 10, 900. doi:10.1038/s41419-019-2089-9

Lu, H.-c., Yao, J.-q., Yang, X., Han, J., Wang, J.-z., Xu, K., et al. (2020). Identification of a Potentially Functional circRNA-miRNA-mRNA Regulatory Network for Investigating Pathogenesis and Providing Possible Biomarkers of Bladder Cancer. *Cancer Cel Int* 20, 31. doi:10.1186/s12935-020-1108-3

Moldovan, L.-I., Hansen, T. B., Venø, M. T., Okholm, T. L. H., Andersen, T. L., Hager, H., et al. (2019). High-throughput RNA Sequencing from Paired Lesional- and Non-lesional Skin Reveals Major Alterations in the Psoriasis circRNAome. *BMC Med. Genomics* 12, 174. doi:10.1186/s12920-019-0616-2

Sawaya, G. F., Smith-McCune, K., and Kuppermann, M. (2019). Cervical Cancer Screening. *JAMA* 321, 2018–2019. doi:10.1001/jama.2019.4595

Small, W., Jr, Bacon, M. A., Bajaj, A., Chuang, L. T., Fisher, B. J., Harkenrider, M. M., et al. (2017). Cervical Cancer: A Global Health Crisis. *Cancer* 123, 2404–2412. doi:10.1002/cncr.30667

Stanley, M. A., Sudenga, S. L., and Giuliano, A. R. (2014). Alternative Dosage Schedules with HPV Virus-like Particle Vaccines. *Expert Rev. Vaccin.* 13, 1027–1038. doi:10.1586/14760584.2014.935767

Tagawa, T., Gao, S., Koparde, V. N., Gonzalez, M., Spouge, J. L., Serquiña, A. P., et al. (2018). Discovery of Kaposi's Sarcoma Herpesvirus-Encoded Circular RNAs and a Human Antiviral Circular RNA. *Proc. Natl. Acad. Sci. USA* 115, 12805–12810. doi:10.1073/pnas.1816183115

Tsikouras, P., Zervoudis, S., Manav, B., Tomara, E., Iatrakis, G., Romanidis, C., et al. (2016). Cervical Cancer: Screening, Diagnosis and Staging. *J. BUON* 21, 320–325.

Verduci, L., Strano, S., Yarden, Y., and Blandino, G. (2019). The Circ RNA -micro RNA Code: Emerging Implications for Cancer Diagnosis and Treatment. *Mol. Oncol.* 13, 669–680. doi:10.1002/1878-0261.12468

Visci, G., Tolomeo, D., Agostini, A., Traversa, D., Macchia, G., and Storlazzi, C. T. (2020). CircRNAs and Fusion-circRNAs in Cancer: New Players in an Old Game. *Cell Signal.* 75, 109747. doi:10.1016/j.cellsig.2020.109747

Vo, J. N., Cieslik, M., Zhang, Y., Shukla, S., Xiao, L., Zhang, Y., et al. (2019). The Landscape of Circular RNA in Cancer. *Cell* 176, 869–881. e13. doi:10.1016/j.cell.2018.12.021

Wang, R., Pan, W., Jin, L., Huang, W., Li, Y., Wu, D., et al. (2020). Human Papillomavirus Vaccine against Cervical Cancer: Opportunity and challenge. *Cancer Lett.* 471, 88–102. doi:10.1016/j.canlet.2019.11.039

Weng, W., Wei, Q., Toden, S., Yoshida, K., Nagasaka, T., Fujiwara, T., et al. (2017). Circular RNA ciRS-7-A Promising Prognostic Biomarker and a Potential Therapeutic Target in Colorectal Cancer. *Clin. Cancer Res.* 23, 3918–3928. doi:10.1158/1078-0432.CCR-16-2541

Xia, C., He, Z., Cai, Y., and Liang, S. (2020a). Vorinostat Upregulates MICA via the PI3K/Akt Pathway to Enhance the Ability of Natural Killer Cells to Kill Tumor Cells. *Eur. J. Pharmacol.* 875, 173057. doi:10.1016/j.ejphar.2020.173057

Xia, C., Liang, S., He, Z., Zhu, X., Chen, R., and Chen, J. (2018). Metformin, a First-Line Drug for Type 2 Diabetes Mellitus, Disrupts the MALAT1/miR-142-3p Sponge to Decrease Invasion and Migration in Cervical Cancer Cells. *Eur. J. Pharmacol.* 830, 59–67. doi:10.1016/j.ejphar.2018.04.027

Xia, C., Liu, C., He, Z., Cai, Y., and Chen, J. (2020b). Metformin Inhibits Cervical Cancer Cell Proliferation by Modulating PI3K/Akt-Induced Major Histocompatibility Complex Class I-Related Chain A Gene Expression. *J. Exp. Clin. Cancer Res.* 39, 127. doi:10.1186/s13046-020-01627-6

Xu, D., Wu, Y., Wang, X., Hu, X., Qin, W., Li, Y., et al. (2020b). Identification of Functional circRNA/miRNA/mRNA Regulatory Network for Exploring

Prospective Therapy Strategy of Colorectal Cancer. *J. Cel. Biochem.* 121, 4785–4797. doi:10.1002/jcb.29703

Xu, Z., Shen, J., Hua, S., Wan, D., Chen, Q., Han, Y., et al. (2019). High-throughput Sequencing of circRNAs Reveals Novel Insights into Mechanisms of Nigericin in Pancreatic Cancer. *BMC Genomics* 20, 716. doi:10.1186/s12864-019-6032-3

Yang, X., Ye, T., Liu, H., Lv, P., Duan, C., Wu, X., et al. (2021). Expression Profiles, Biological Functions and Clinical Significance of circRNAs in Bladder Cancer. *Mol. Cancer* 20, 4. doi:10.1186/s12943-020-01300-8

Yao, Y., Hua, Q., and Zhou, Y. (2019). CircRNA Has_circ_0006427 Suppresses the Progression of Lung Adenocarcinoma by Regulating miR-6783-3p/DKK1 axis and Inactivating Wnt/β-Catenin Signaling Pathway. *Biochem. Biophysical Res. Commun.* 508, 37–45. doi:10.1016/j.bbrc.2018.11.079

Yin, Y., Long, J., He, Q., Li, Y., Liao, Y., He, P., et al. (2019). Emerging Roles of circRNA in Formation and Progression of Cancer. *J. Cancer* 10, 5015–5021. doi:10.7150/jca.30828

Yu, C., Tian, F., Liu, J., Su, M., Wu, M., Zhu, X., et al. (2019a). Circular RNA cMras Inhibits Lung Adenocarcinoma Progression via Modulating miR-567/PTPRG Regulatory Pathway. *Cell Prolif* 52, e12610. doi:10.1111/cpr.12610

Yu, T., Wang, Y., Fan, Y., Fang, N., Wang, T., Xu, T., et al. (2019b). CircRNAs in Cancer Metabolism: a Review. *J. Hematol. Oncol.* 12, 90. doi:10.1186/s13045-019-0776-8

Zang, J., Lu, D., and Xu, A. (2020). The Interaction of circRNAs and RNA Binding Proteins: An Important Part of circRNA Maintenance and Function. *J. Neurosci. Res.* 98, 87–97. doi:10.1002/jnr.24356

Zhang, H.-d., Jiang, L.-h., Sun, D.-w., Hou, J.-c., and Ji, Z.-l. (2018). CircRNA: a Novel Type of Biomarker for Cancer. *Breast Cancer* 25, 1–7. doi:10.1007/s12282-017-0793-9

Zhou, R., Wu, Y., Wang, W., Su, W., Liu, Y., Wang, Y., et al. (2018). Circular RNAs (circRNAs) in Cancer. *Cancer Lett.* 425, 134–142. doi:10.1016/j.canlet.2018.03.035

Zhou, Z.-b., Huang, G.-x., Fu, Q., Han, B., Lu, J.-j., Chen, A.-m., et al. (2019). circRNA.33186 Contributes to the Pathogenesis of Osteoarthritis by Sponging miR-127-5p. *Mol. Ther.* 27, 531–541. doi:10.1016/j.ymthe.2019.01.006

Conflict of Interest: The authors declare that the research was conducted in the absence of any commercial or financial relationships that could be construed as a potential conflict of interest.

Publisher's Note: All claims expressed in this article are solely those of the authors and do not necessarily represent those of their affiliated organizations, or those of the publisher, the editors and the reviewers. Any product that may be evaluated in this article, or claim that may be made by its manufacturer, is not guaranteed or endorsed by the publisher.

frontiers in Genetics

ORIGINAL RESEARCH
published: 29 March 2022
doi: 10.3389/fgene.2022.853529

Identification of Ion Channel-Related Genes and miRNA-mRNA Networks in Mesial Temporal Lobe Epilepsy

Zhengwei Su[1,2†], Yinchao Li[1†], Shuda Chen[1†], Xianyue Liu[1], Ke Zhao[1], Ying Peng[2] and Liemin Zhou[1*]*

[1]Department of Neurology, The Seven Affiliated Hospital, Sun Yat-sen University, Shenzhen, China, [2]Department of Neurology, Sun Yat-sen Memorial Hospital, Sun Yat-sen University, Guangzhou, China

Objective: It aimed to construct the miRNA-mRNA regulatory network related to ion channel genes in mesial temporal lobe epilepsy (mTLE), and further identify the vital node in the network.

Methods: Firstly, we identified ion channel-related differentially expressed genes (DEGs) in mTLE using the IUPHAR/BPS Guide to Pharmacology (GTP) database, neXtProt database, GeneCards database, and the high-throughput sequencing dataset. Then the STRING online database was used to construct a protein-protein interaction (PPI) network of DEGs, and the hub module in the PPI network was identified using the cytoHubba plug-in of Cytoscape software. In addition, the Single Cell Portal database was used to distinguish genes expression in different cell types. Based on the TarBase database, EpimiRBase database and the high-throughput sequencing dataset GSE99455, miRNA-mRNA regulatory network was constructed from selected miRNAs and their corresponding target genes from the identified DEGs. Finally, the rats were selected to construct chronic li-pilocarpine epilepsy model for the next stage experimental verification, and the miR-27a-3p mimic was used to regulate the miRNA expression level in PC12 cells. The relative expression of miR-27a-3p and its targeting mRNAs were determined by RT-qPCR.

Results: 80 mTLE ion channel-related DEGs had been screened. The functional enrichment analysis results of these genes were highly enriched in voltage-gated channel activation and ion transport across membranes. In addition, the hub module, consisting of the Top20 genes in the protein-protein interaction (PPI) network, was identified, which was mainly enriched in excitatory neurons in the CA3 region of the hippocampus. Besides, 14 miRNAs targeting hub module genes were screened, especially the miR-27a-3p deserving particular attention. miR-27a-3p was capable of regulating multiple mTLE ion channel-related DEGs. Moreover, in Li–pilocarpine-induced epilepsy models, the expression level of miR-27a-3p was increased and the mRNAs expression level of *KCNB1*, *SCN1B* and *KCNQ2* was decreased significantly. The mRNAs expression level of *KCNB1* and *KCNQ2* was decreased significantly following PC12 cells transfection with miR-27a-3p mimics.

Conclusion: The hub ion channel-related DEGs in mTLE and the miRNA-mRNA regulatory networks had been identified. Moreover, the network of miR-27a-3p regulating ion channel genes will be of great value in mTLE.

OPEN ACCESS

Edited by:
Yumei Luo,
The Third Affiliated Hospital of Guangzhou Medical University, China

Reviewed by:
Xiaorong Liu,
Guangzhou Medical University, China
Estela Maria Bruxel,
State University of Campinas, Brazil

***Correspondence:**
Ying Peng
pengy2@mail.sysu.edu.cn
Liemin Zhou
lmzhou56@163.com

†These authors have contributed equally to this work

Specialty section:
This article was submitted to RNA, a section of the journal Frontiers in Genetics

Received: *12 January 2022*
Accepted: *14 March 2022*
Published: *29 March 2022*

Citation:
Su Z, Li Y, Chen S, Liu X, Zhao K, Peng Y and Zhou L (2022) Identification of Ion Channel-Related Genes and miRNA-mRNA Networks in Mesial Temporal Lobe Epilepsy. Front. Genet. 13:853529. doi: 10.3389/fgene.2022.853529

Keywords: temporal lobe epilepsy, ion channel, microRNA, MiR-27a-3p, bioinformatics

INTRODUCTION

There were currently about 65 million patients affected by epilepsy worldwide. More than 80% of the patients with epilepsy occurred in low- and middle-income countries, about 15 per 1,000 people (GBD 2016 Epilepsy Collaborators, 2019). Temporal lobe epilepsy (TLE) was the most common type of adult epilepsy, and its prevalence rate was about 1.7 in 1000 (Englot et al., 2020). Although most TLE patients were treated with regular medication, about 40% of seizures cannot be controlled, which significantly decreased the quality of life for patients and placed a heavy burden on society (Englot et al., 2020). The pathogenesis of epilepsy was very complex. With the improvement of genetic screening techniques, the construction of large-scale genetic databases, and the popularization of gene sequencing, multiple genes closely related to brain network remodeling, neuronal death, inflammation, changes in the function of ionic channels and neurogenesis were identified for epileptogenesis (Henshall et al., 2016).

A systematic review summarized 977 epilepsy-related genes, in which ion channels and receptors occupied the major part (Wang et al., 2017). Furthermore, disruption of ion channels could cause a wide spectrum of human diseases, known as channelopathies (Palleria et al., 2015). Ion channels were not only the basis for generating and regulating the excitability of neurons but also involved in maintaining cellular ion homeostasis and membrane potential. Various ion channels associated with epilepsy had been identified, including voltage-gated ion channels, ligand-gated ion channels and other ion channels. Some of them were the molecular targets of antiepileptic drugs.

MicroRNA (miRNA) is one of the non-coding RNAs that are capable of regulating gene expression by affecting mRNA stability and inhibiting translation. Its role in epilepsy was becoming more prominent due to its ability to regulate multiple mRNAs simultaneously. In addition, miRNA may not only be involved in the pathological processes of epilepsy but also be considered a potential new therapeutic target to override drug resistance (Brennan and Henshall, 2018; Gross and Tiwari, 2018; Almeida Silva et al., 2020). Prior studies had also reported that miRNAs could alter the excitability of the neuron and effectively influence the incidence of epilepsy (Henshall et al., 2016). Over 1,000 miRNAs expression alterations in the hippocampus and other epileptic focus had been described in human epilepsy and models of epilepsy (Mooney et al., 2016). Manipulation of miRNAs may have powerful effects on seizures and epilepsy-induced neuronal cell death (Dogini et al., 2013). MiRNAs may affect epileptogenesis by altering the silencing and translation of ion channels.

In recent years, research on the molecular regulation mechanism of miRNA in mTLE-related genes had made tremendous progress. However, the details of the mechanism of ion channel-related genes that are mediated by miRNA are worthy of further analysis and investigation. Therefore, this study initially identified the key miRNAs and mRNAs and construct the miRNA-mRNA regulatory network related to ion channels genes in mTLE.

MATERIALS AND METHODS

Data Sources

The workflow of our study was shown in **Figure 1**. To identify ion channel-related genes associated with mTLE, including ligand-gated ion channel genes, voltage-gated ion channels genes and other ion channel genes, the IUPHAR/BPS Guide to Pharmacology (GTP) database (https://www.guidetopharmacology.org/) and neXtProt database (https://www.nextprot.org/) were searched. Then, the medical subject headings (MeSH) of epilepsy and its text words related to epilepsy were searched in GeneCards database: The Human Gene Database (https://www.genecards.org/), a comprehensive resource for gene-related information, which contains a total of gene-centric data from 150 web sources. Finally, we combined the results with the published high-throughput sequencing results of mTLE in the journal of Brain (Guelfi S et al., 2019) to screen expression profiles of mTLE-related ion genes. The study included temporal lobe cortical tissue samples from 85 patients who were neuropathologically confirmed as definite mTLE + HS and 75 neurologically healthy controls for whole-gene and exon-level transcriptome analysis. The data adjustment was performed using the residual method, and the false discovery rate (FDR) was set to less than 5% (Guelfi et al., 2019).

DEGs Functional and Signaling Pathway Enrichment Analysis

The mTLE ion channel-related genes were extracted for GO functional enrichment and KEGG pathway enrichment analysis. The analysis method was based on the R clusterProfiler and pathview packages. The results were visually displayed by the online bioinformatics tool.

Construction of PPI Network and Identification of Hub Module

The PPI networks were produced by STRING (http://string-db.org/). The hub modules were then identified by the cytoHubba plug-in in Cytoscape software. CytoHubba was a topological network algorithm that assigned a value to each gene and sequentially discovered its hub genes and sub-network.

Single Cell Analysis of Hub Module Genes

Single cell analysis was done using the Single Cell Portal database (https://singlecell.broadinstitute.org/single_cell). The database collected the results of 390 single-cell

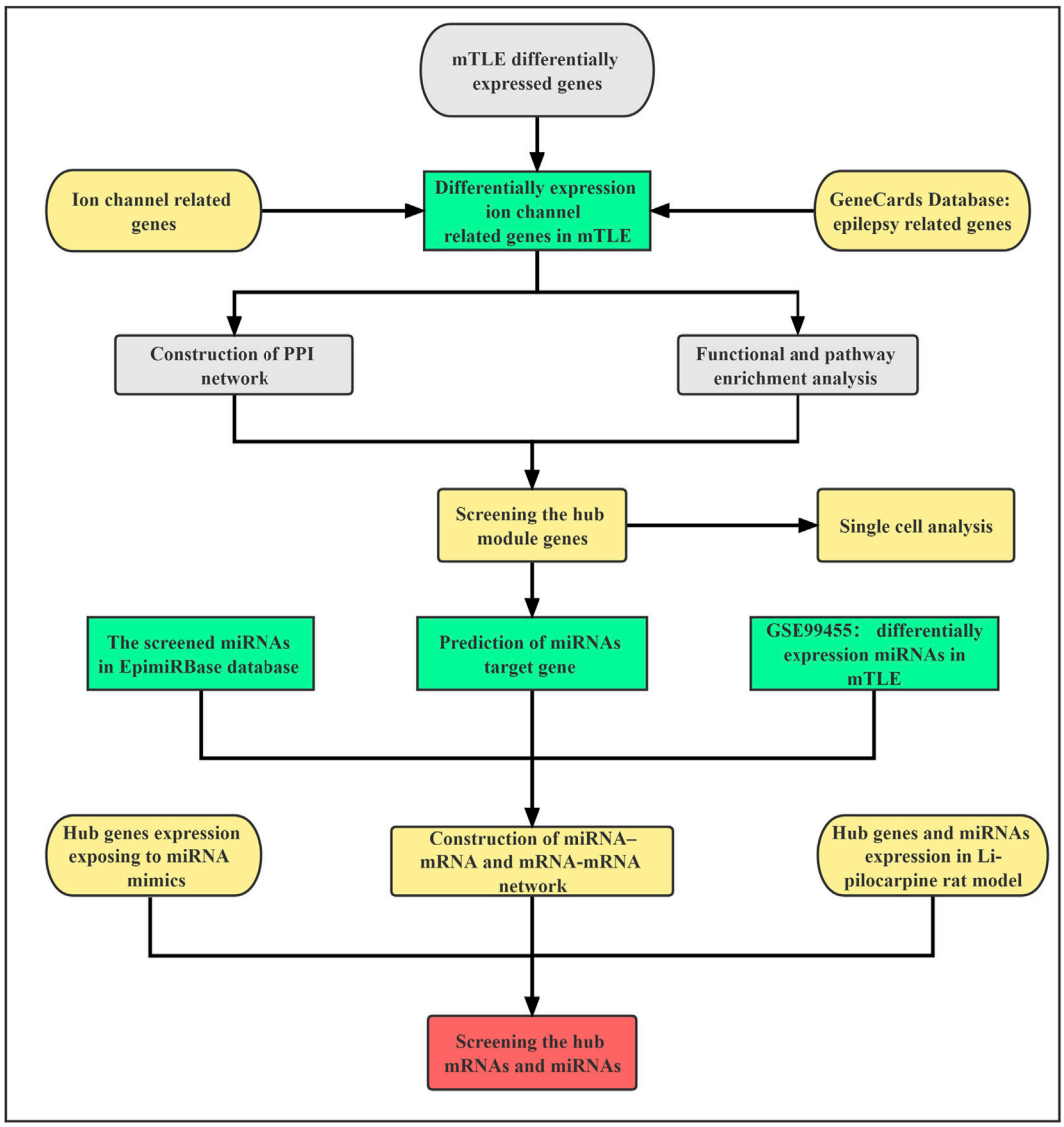

FIGURE 1 | The flow chart.

sequencing studies and contained sequencing data for a total of 17061708 cells. Single-cell raw RNA sequencing data were retrieved under accession of brain tissue. The distribution of hub module genes in normal hippocampal tissue and their expression in different cell types were analyzed.

Prediction of miRNA-Targeting Hub Module Genes

Visualization and functional annotation of potential ion channels mRNA-miRNA interactions were performed using the miRNet website online tool (https://www.mirnet.ca/). Its miRNA-mRNA target pairs prediction was from the TarBase database, which is based on experimental validation (Chang et al., 2020).

Screening of Differentially Expressed miRNAs in mTLE

To screen for differentially expressed miRNAs in mTLE, we searched the NCBI Gene Expression Omnibus (GEO) database to retrieve any appropriate dataset associated with epilepsy. The inclusion criteria were 1) the specimens were from brain tissue; 2) the specimens included mTLE patients and normal control; 3) the species were limited to *Homo sapiens*; 4) the raw data or processed data were public and accessible. The GSE99455 dataset was selected as a candidate to study ultimately. The detailed information of GSE99455 was shown in **Supplementary Table S1**. We processed the Bioconductor software package Deseq2 to identify differentially expressed miRNAs. We selected those miRNAs using selection with $|\log2FC| > 0.5$ and FDR<0.05.

Identification of the Regulatory Network of miRNA With Hub Module Genes

The miRNAs in the regulatory network were identified from differentially expressed miRNAs in mTLE, prediction result of miRNA targeting hub module genes and the EpimiRBase database. The EpimiRBase database (https://www.epimirbase.eu/epimirbase/), which contains differentially expressed miRNAs associated with epilepsy, including results from experimental studies in *Homo sapiens*, rats and mice. The miRNA with the most regulatory targets were selected for the next step of the study.

Establishment of the Lithium-Pilocarpine Chronic Epilepsy Model

Sixteen healthy male Sprague-Dawley (SD) rats, aged 8–9 weeks and weighing 150–180 g, were purchased from Beijing Vital Lihua Experimental Animals Co., Ltd.

All animals were raised in SPF level environment (circadian rhythm: 12 h/12 h, temperature: 22 ± 2°C; humidity: 50 ± 10%) and were allowed free access to food and water. Prior to initiation of experimental procedures, rats were acclimatized for at least a 3-day period. All procedures were in accordance with the Regulations of Experimental Animal Administration issued by the Ministry of Science and Technology of the People's Republic of China (http://www.most.gov.cn). The rats were injected intraperitoneally with lithium chloride (127 mg/kg, Sigma L9650) on day 1 and administered scopolamine methyl bromide (1 mg/kg, Macklin S835305) injection 24 h later, Intraperitoneal injected of pilocarpine (TargetMol T0804) 30 min later. The first dose of pilocarpine was 30 mg/kg intraperitoneally. If there was no grade IV or above seizure grade after 30 min, an additional dose of 10 mg/kg would be given intraperitoneally at 30 min interval until there was grade IV or above Status epileptics (SE)-like seizure without obvious interval, and the extreme dose was 60 mg/kg. SE was terminated after 2 h by injecting diazepam (10 mg/kg). The rat seizure symptoms were graded based on the Racine grading criteria. Animals were video-monitored 8 h a day for general behavior and occurrence of spontaneous seizures by 2 weeks after SE. Rats showing spontaneous recurrent seizures were used as chronic epilepsy animals, which were randomly chosen for EEG recording.

Cell Culture and Transfection

PC12 cells were ordered from Zixiao Biological Technology Co., Ltd. (Wuxi, China). The above cells were grown in RPMI-1640 complete medium (Thermo Fisher Scientific, Shanghai, China) comprising 10% fetal bovine serum and 1% penicillin/streptomycin. They were then maintained at 37°C with 5% CO_2 and saturated humidity, with the medium substituted once every 2–3 days. During the cells' logarithmic growth phase, 0.25% trypsin (Thermo Fisher HyClone, Utah, United States) was adopted for trypsinization and passage. Afterward, the cells were trypsinized with 0.25% trypsin for subsequent experiments. The above cell lines were inoculated into 6-well plates and further cultured in an incubator. When the cells reached more than 80% confluence, they were transfected with miR-27a-3p mimics and miR-27a-3p negative controls, followed by 24 h of culturing. After trypsinization with 0.25% trypsin, the cells were used for subsequent experiments Real-time fluorescent quantitative PCR (RT-qPCR).

RT-qPCR

The hippocampus of brain tissue was removed after rapid decapitation of SD rats, and the tissue was isolated on ice. Total RNA was extracted using the miRcute miRNA Isolation Kit (DP501, Tiangen, China) and subsequently reversed transcribed using the miRcute Plus miRNA First-Strand cDNA Kit (KR211, Tiangen, China) and FastKing gDNA Dispelling RT SuperMix Kit (KR118, Tiangen, China). RT-qPCR was performed on the ABI QuantStudio5 System using miRcute Plus miRNA qPCR Kit (SYBR Green) (FP411, Tiangen, China) and Talent qPCR PreMix Kit (SYBR Green) (FP209, Tiangen, China). The primer design was completed by Sangon Biotech, and the primer list was shown in **Supplementary Table S2**.

Statistical Analysis

Most of the statistical results were completed through R software, log2FC > 0.5 and p-value <0.05 were considered statistically significant when performing gene expression differential analysis. GraphPad Prism 9 software was used for the t-test and the visual display was mainly based on Cytoscape software.

RESULTS

Genes Associated With Ion Channels in mTLE

A total of 405 ion channel-related genes were taken into account. These genes were classified into three types: ligand-gated ion channels, voltage-gated ion channels, and other ion channels. 3732 genes related to epilepsy were screened in the GeneCards database. Subsequently, a total of 80 differentially expressed mTLE-related ion genes were screened out with 20 high-expressed genes and 60 low-expressed genes. The results were shown in **Figures 2A,B**. For details, see **Supplementary Table S3**.

Functional and Pathway Enrichment Analysis

80 DEGs related to mTLE were analyzed further by GO term and KEGG pathway analysis. The biological processes were concentrated in regulating membrane potential, regulation of ion transmembrane transport, and potassium ion transmembrane transport. The analysis result of the cellular component focused on ion channel complex, transmembrane transporter complex, transporter complex, and cation channel complex. Passive transmembrane transporter activity and ion channel activity were mainly enriched in molecular function. The result of the KEEG pathway analysis focused on neuroactive ligand-receptor interaction, GnRH secretion, GABAergic synapse and oxytocin signaling pathways. The functional enrichment analysis results of these genes mainly focused on a variety of voltage-gated channel activation, ion

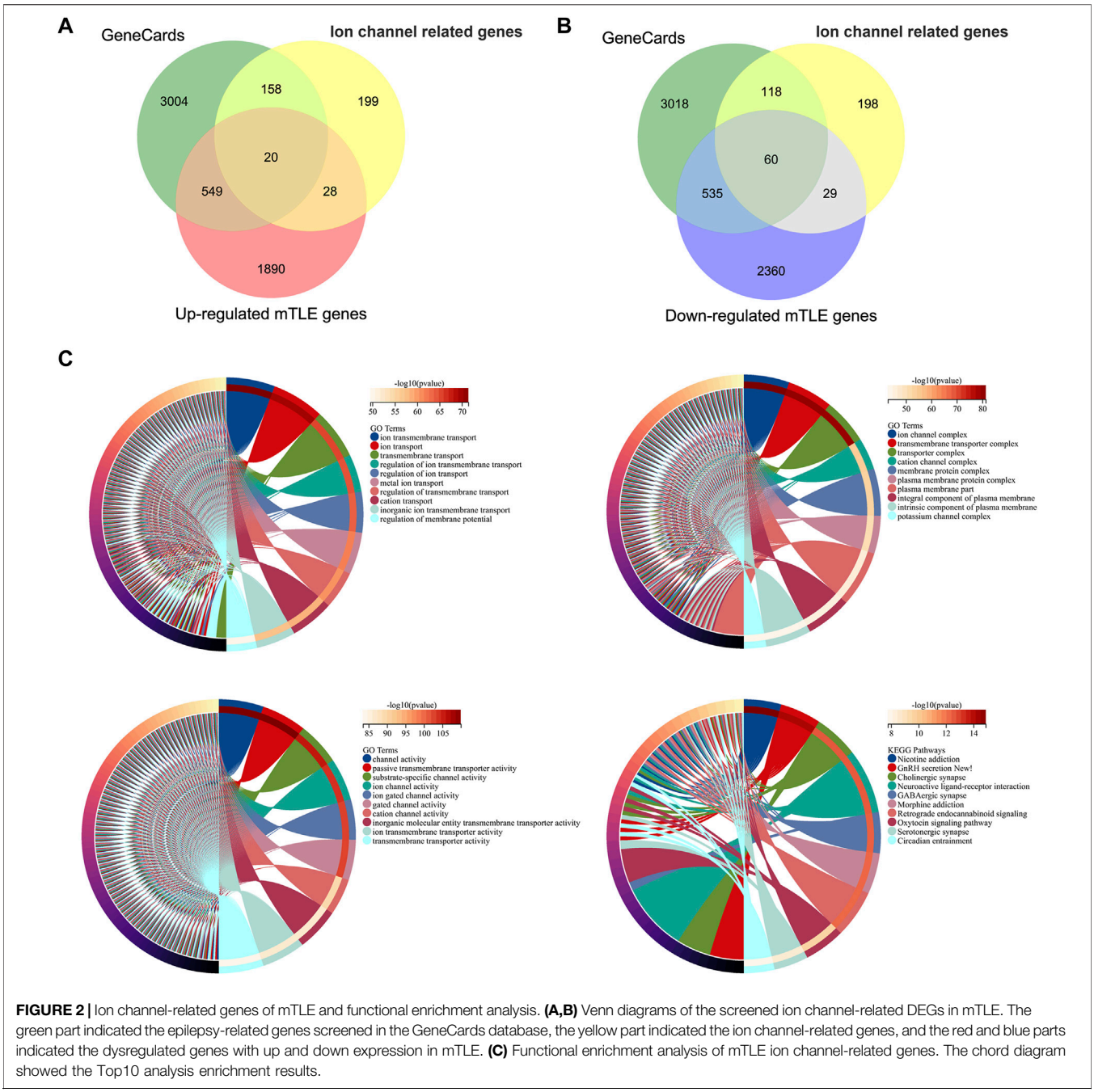

FIGURE 2 | Ion channel-related genes of mTLE and functional enrichment analysis. **(A,B)** Venn diagrams of the screened ion channel-related DEGs in mTLE. The green part indicated the epilepsy-related genes screened in the GeneCards database, the yellow part indicated the ion channel-related genes, and the red and blue parts indicated the dysregulated genes with up and down expression in mTLE. **(C)** Functional enrichment analysis of mTLE ion channel-related genes. The chord diagram showed the Top10 analysis enrichment results.

transport across the membrane, and other critical biological processes (**Figure 2C**).

Hub Module of mTLE Ion Channel-Related Genes

The PPI network was constructed based on the STRING database for ion channel-related genes in mTLE, which were broken down into four main modules (**Figures 3A,B**). The hub module (20 genes) had been screened in the PPI network (**Figure 3C**), which had higher linkage in the whole PPI network and might play a more important role in physiological processes. Information about the hub module genes were shown in **Table 1**.

Single Cell Analysis of Hub Module Genes

Three studies were used to perform single-cell RNA-seq analysis (Habib et al., 2016; Ximerakis et al., 2019; Ding et al., 2020). In our study, we identified nine main clusters (**Figure 4A**). Based on the expression of ion channel markers, which were strongly and specifically marked regarding each major cell population, we noticed that most of the hub module genes were highly

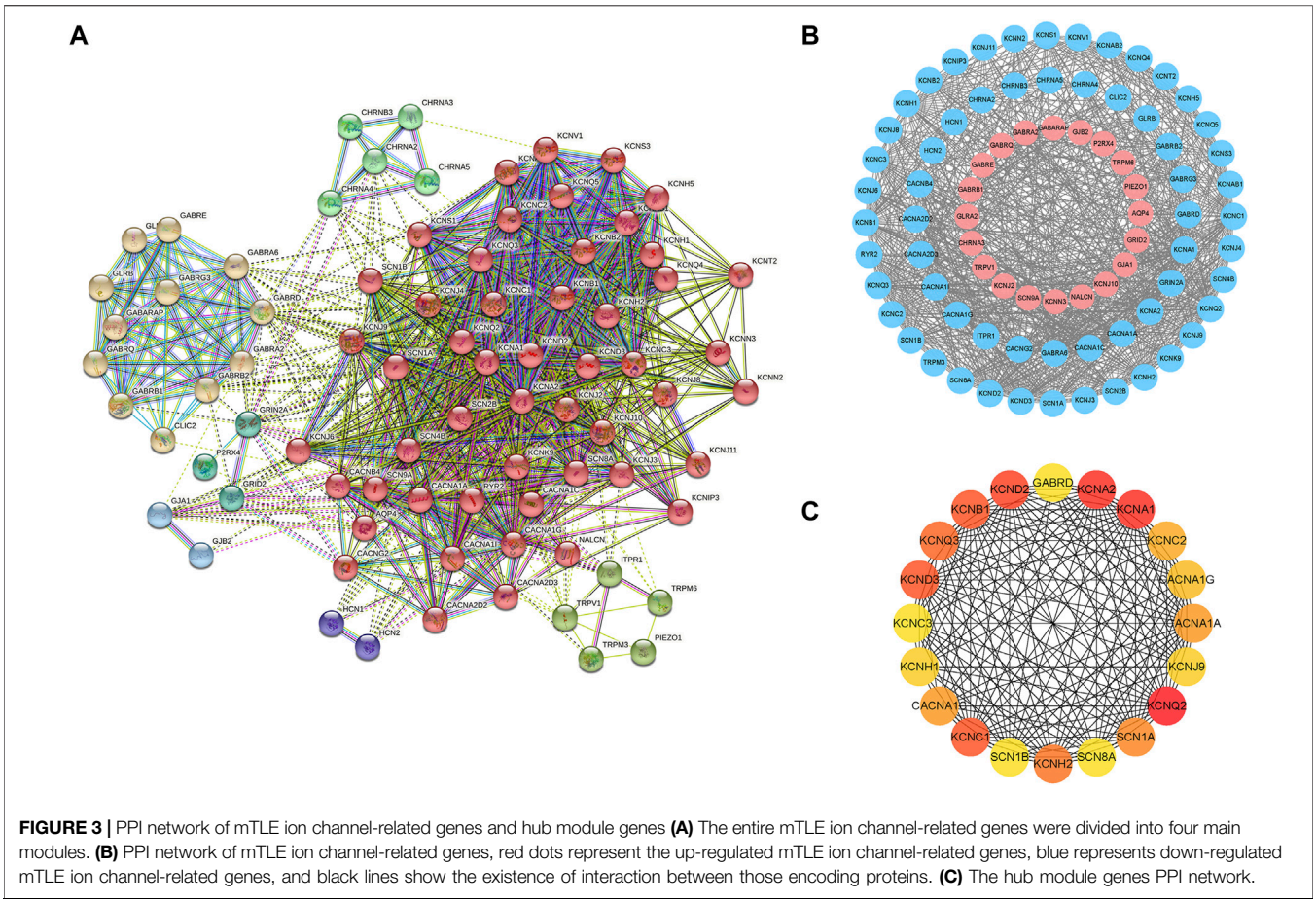

FIGURE 3 | PPI network of mTLE ion channel-related genes and hub module genes **(A)** The entire mTLE ion channel-related genes were divided into four main modules. **(B)** PPI network of mTLE ion channel-related genes, red dots represent the up-regulated mTLE ion channel-related genes, blue represents down-regulated mTLE ion channel-related genes, and black lines show the existence of interaction between those encoding proteins. **(C)** The hub module genes PPI network.

expressed in excitatory neurons, such as *KCNQ3, KCNQ2, KCND3, KCNA2, CACNA1C, KCNJ9, KCND2, KCNB1, CACNA1G*; Genes of *KCNC1, SCN1A, KCNH2, CACNA1C, KCNC2, KCNC3,* and *GABRD* were relatively abundantly expressed in inhibitory neurons; *KCNH1* and *KCNH2* were mainly expressed in cardiac progenitor cells (CPC), and *KCNA1* was mainly located in oligodendrocytes (OLG) (**Figures 4A,B**). Moreover, we found that the distribution of most hub module genes in the hippocampus, such as *SCN8A, SCN1B, SCN1A, KCNQ3, KCNQ2, KCNH2, KCNH1, KCND3, KCNC2, KCNC1, KCNA1, KCNA2, CACNA1C, CACNA1A*, were enriched in CA3 region of the hippocampus; The expression of *KCNJ9, KCND2, KCNC3, KCNB1, GABRD* were relatively high in DG region; *KCNB1, CACNA1G* were mainly enriched in CA1 region (**Figure 4C**). Those revealed that the hub genes were mainly located in the CA3 region.

TABLE 1 | The hub module genes.

Genes	Type	*p* value	LogFC	Expression
CACNA1A	vgic	0.0004	−1.1127	Down
CACNA1C	vgic	0.0168	−1.0732	Down
CACNA1G	vgic	0.0001	−1.1708	Down
GABRD	lgic	0.0000	−1.2457	Down
KCNA1	vgic	0.0000	−1.4105	Down
KCNA2	vgic	0.0000	−1.2605	Down
KCNB1	vgic	0.0000	−1.2777	Down
KCNC1	vgic	0.0001	−1.1897	Down
KCNC2	vgic	0.0101	−1.1167	Down
KCNC3	vgic	0.0000	−1.1720	Down
KCND2	vgic	0.0001	−1.1699	Down
KCND3	vgic	0.0082	−1.0765	Down
KCNH1	vgic	0.0001	−1.1568	Down
KCNH2	vgic	0.0003	−1.0774	Down
KCNJ9	vgic	0.0000	−1.1927	Down
KCNQ2	vgic	0.0017	−1.0869	Down
KCNQ3	vgic	0.0007	−1.0994	Down
SCN1A	vgic	0.0000	−1.4172	Down
SCN1B	vgic	0.0000	−1.5477	Down
SCN8A	vgic	0.0002	−1.1585	Down

Differentially Expressed miRNAs and miRNAs Targeting of the Hub Module Genes

The prediction of miRNAs targeting the hub module genes based on the TarBase database. 451 miRNAs with possible regulatory relationships of hub module genes were predicted (**Figure 5A**). A total of 103 differentially expressed miRNAs were found in dataset GSE99455 (63 upregulated and 40 down regulated miRNAs) (**Figure 5B**). Differentially expressed miRNAs information was shown in **Supplementary Table S4**.

miRNA-mRNA Regulatory Network

14 miRNAs with a significant regulatory relationship with hub module genes were found, which were proved to be up-regulated expression in mTLE in humans and animal models, the results shown in **Figure 5C**; **Table 2**. **Figure 5D** showed the visualization of the miRNA-mRNA regulatory network which contained 14 miRNAs and 20 mRNAs.

The Network and Expression of miR-27a-3p With Targeted mRNA

The prediction regulated network of miR-27a-3p and mRNAs showed in **Figure 6A**. In the study, 62.5% (10/16) of rats displayed spontaneous seizures 60 days after SE. According to the Racine grading standard, epileptic seizures in rats reached grade III -V with obvious epileptic discharge in the hippocampus. The

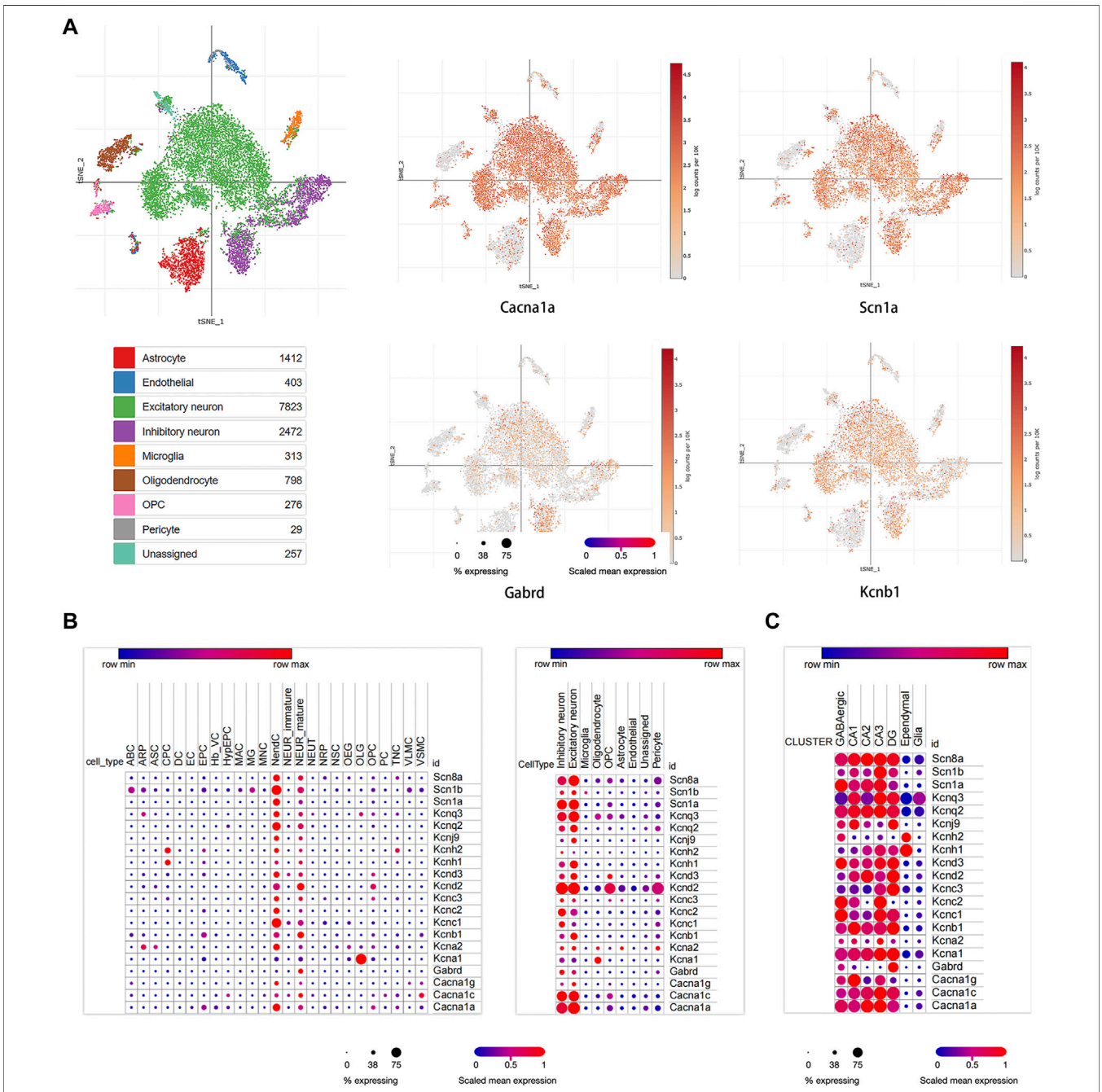

FIGURE 4 | Single cell analysis results of hub module genes. **(A)** The proportion of diverse cell types across hub module genes in the brain; **(B)** the distribution of some ion channel genes in different cell types. **(C)** The expression of hub module genes in different areas of the hippocampus.

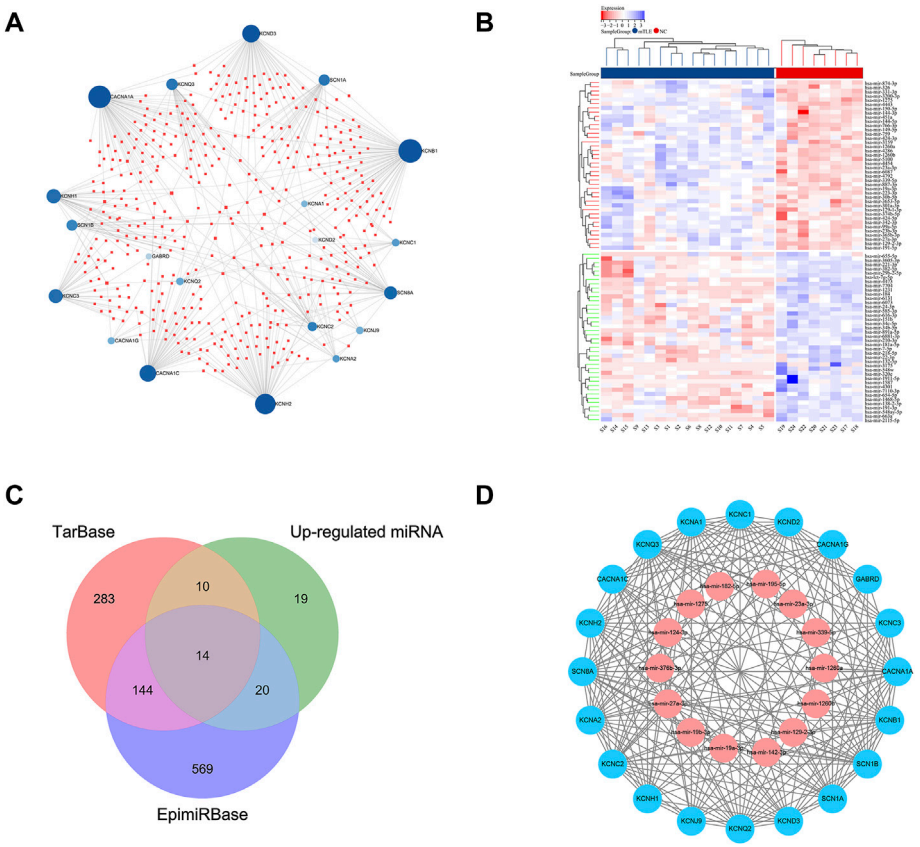

FIGURE 5 | miRNA-mRNA regulatory network of hub module genes. **(A)** Predicted results of target-binding miRNAs based on the TarBase database for the screened hub module genes. Blue dots represented hub module genes in mTLE, red squares represented miRNAs with regulatory relationships. **(B)** The heat map of dataset GSE99455 differentially expressed miRNAs. The horizontal axis showed the sample information (mTLE group and the NC group), and the vertical axis showed the differentially expressed miRNAs. The red color represented the up-regulated miRNAs, and the blue color represented the down-regulated miRNAs. **(C)** Venn diagram of up-regulated expression miRNAs in dataset GSE99455, TarBase prediction results and EpimiRBase database. **(D)** The screened mTLE hub module genes and their target-binding miRNAs; the red color represented the up-regulated genes and the blue color represented the down-regulated genes.

TABLE 2 | Hub module genes-targeting miRNAs.

miRNA	logFC	*p* value	FDR	Exprssion
hsa-miR-1275	2.7125	0.0000	0.0000	Up
hsa-miR-376b-3p	1.9484	0.0006	0.0100	Up
hsa-miR-23a-3p	0.7900	0.0000	0.0007	Up
hsa-miR-142-3p	1.8311	0.0000	0.0008	Up
hsa-miR-129-2-3p	1.7577	0.0000	0.0000	Up
hsa-miR-182-5p	1.5401	0.0010	0.0128	Up
hsa-miR-19b-3p	1.4601	0.0001	0.0028	Up
hsa-miR-1260b	1.4220	0.0000	0.0000	Up
hsa-miR-19a-3p	1.3845	0.0002	0.0036	Up
hsa-miR-1260a	1.2250	0.0000	0.0000	Up
hsa-miR-27a-3p	0.5830	0.0017	0.0194	Up
hsa-miR-124-3p	0.5721	0.0041	0.0406	Up
hsa-miR-195-5p	1.1019	0.0003	0.0052	Up
hsa-miR-339-5p	1.0530	0.0000	0.0000	Up

mortality rate was 25% (4/16). Then, it showed that the expression level of miR-27a-3p was increased and the mRNAs expression level of *KCNB1*, *SCN1B* and *KCNQ2* were decreased in lithium–pilocarpine-induced epilepsy models compared with that in the control group (**Figure 6B**). The mRNAs expression level of *KCNB1* and *KCNQ2* were decreased using RT-qPCR following PC12 cells transfection with miR-27a-3p mimics (**Figure 6C**).

DISCUSSION

A growing body of research suggested that large-scale alterations in the expression of genes that controlled ion channels, dendritic remodeling, neuroinflammation and neuronal death were involved in the pathogenesis of epilepsy (Thom, 2014; Srivastava et al., 2017; Bruxel et al., 2021). Ion channels were the basis of excitability regulation, and many human idiopathic epilepsies were currently considered to be ion channel-related disorders (Oyrer et al., 2018). With the gradual deepening of gene research, the role of regulatory networks involving multiple genes in disease has received increasing attention. In the study of temporal lobe epilepsy, genes related to ion channels, inflammation, gliosis, and synaptic structure were involved in the process of seizure and recurrence, and such alterations in differential gene expression affect the whole network

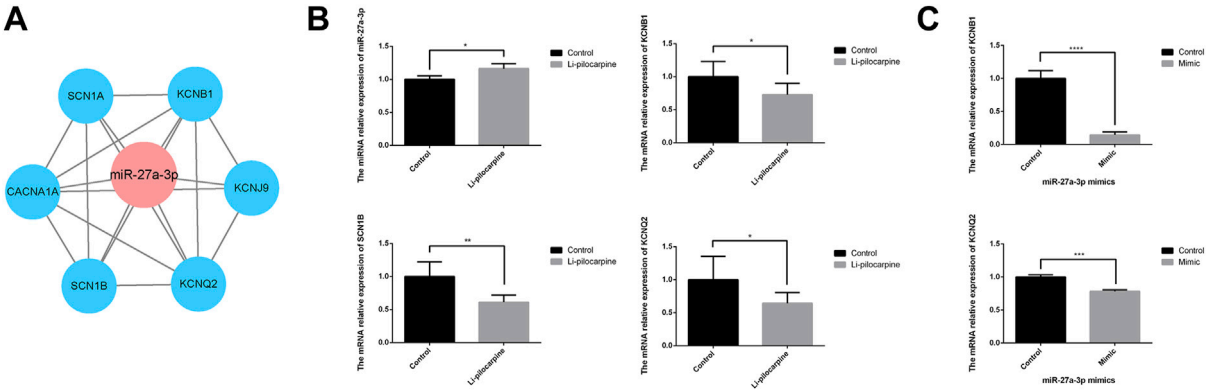

FIGURE 6 | The network and expression of miR-27a-3p with targeted mRNA. **(A)** The miR-27a-3p with targeted mRNA regulatory network. **(B)** Relative expression of miR-27a-3p and mRNA in the hippocampus of lithium-pilocarpine rat epilepsy model. **(C)** Relative expression of *KCNB1* and *KCNQ2* in the PC12 cells after treating with miR-27a-3p mimics. *p value < 0.05, **p value < 0.01, ****p value < 0.0001.

(Johnson et al., 2015). The different ion channels were interconnected in time and space to work together. For example, Na^+ channels worked dynamically in concert with K^+ channels to generate action potentials (Smith and Walsh, 2020). Therefore, when studying the role of ion channels in temporal lobe epilepsy, we should not only focus on individual channel or a single gene but also the role of multiple channels or multiple genes in epilepsy together as a network are noteworthy and a concern. In this study, we identified 80 ion channel-related genes in mTLE, including 20 high-expressed genes and 60 low-expressed genes, which represented the possible interrelationship among those genes, and performed systematically investigating the contribution of ion channels in the development and formation of epilepsy.

MiRNA was a small non-coding, single-stranded small RNA, which was found in most eukaryotes and was an important mode of epigenetic modification. After processing, mature miRNAs mainly enter the complex by binding to the RNA-induced silencing complex (RISC), which in turn bind specifically to the 3′UTR region of the target gene mRNA in full or partial complementary pairing, thereby enabling regulation of the target gene expression, thus exerting their gene silencing function and ultimately leading to a reduction in the expression of the gene (Lu and Rothenberg, 2018). The miRNA can negatively regulate multiple target genes, and the same target gene can be regulated by multiple miRNAs. It was because miRNAs acted by regulating the expression of target genes, and miRNAs mediate interactions between genes and form complex miRNA-mRNA regulatory networks. Through the study of miRNAs, we can better reveal the important mechanisms of epileptogenesis and find a possible diagnostic marker for early stages and new safe and effective therapeutic targets for epilepsy. In this research, we identified 103 differentially expressed miRNAs with 63 up-regulation and 40 down-regulation in mTLE. miR-27a-3p deserve some attention. This miRNA was shown to regulate multiple ion channels genes. Raoof et al. suggested that miR-27a-3p may be potential diagnostic biomarkers for TLE, and the findings were further confirmed in animal models of epilepsy (Raoof et al., 2018). They found that inhibition of miR-27a-3p could inhibit hippocampal neuronal apoptosis, promote *Bcl2* expression, and decrease *Bax* and *Caspase 3* expression in the kainic acid-induced rat model of epilepsy, meanwhile effectively reducing the expression levels of interleukin-1β (*IL-1β*), *IL-6*, and tumor necrosis factor-α (*TNF-α*) in hippocampal tissues. Previous preliminary experiment data and other research results showed that miR-27a-3p inhibitors prevented epilepsy-induced inflammatory responses and hippocampal neuronal apoptosis by targeting *MAP2K4* (Lu et al., 2019).

In recent years, an increasing number of studies have shown that miRNA played an important role in regulating ion channel silencing. MiRNAs regulated the intrinsic excitability of neurons by targeting ion channels, thereby affecting the entire brain network. A microRNA that regulated voltage-gated potassium channels in the brain was first reported by Raab-Graham et al. They found that miR-129-5p inhibited the expression of the shaker-like potassium channel *Kv1.1* (Sosanya et al., 2013). In the subsequent studies, miRNA-regulated ion channels attracted much attention (Zhang et al., 2018; Tiwari et al., 2019). In our study, we found that the expression level of miR-27a-3p was increased and the mRNAs expression level of *KCNB1, SCN1B* and *KCNQ2* were decreased significantly in epilepsy models. In addition, miR-27a-3p could down-regulate mRNAs expression levels of *KCNB1* and *KCNQ2*, which showed that miR-27a-3p could regulate multiple ion channel genes. Moreover, Single cell analysis results also revealed that *KCNB1* and *KCNQ2* were highly expressed in excitatory neurons. Potassium channels were the largest family of ion channel proteins that regulated changes in cell membrane currents. Their main function was to maintain the resting potential of the cell membrane and to control cell excitability by mediating the repolarization of the cell membrane through the outflow of potassium ions. The *KCNB1* gene encoded the *Kv2.1* channel protein, a major component of the somatodendritic delayed rectifier-type potassium channel in hippocampal and cortical neurons, with a high density of distribution in hippocampal neurons. Its physiological functions included mediating the efflux of potassium currents, being essential for apoptotic signaling

cascades as well as maintaining membrane potential, and regulating the electrical excitability of neurons and muscles (Zhang et al., 2018). Torkamani et al. identified three different *de novo* heterozygous missense mutations in the *KCNB1* gene in three unrelated patients with developmental and epileptic encephalopathies. All mutations affected the pore domain of the channel, and *in vitro* expression studies in CHO-K1 cells had shown that these mutations result in a loss of potassium ion selectivity while gaining depolarized cation inward conductivity (Torkamani et al., 2014). In animal models, *KCNB1* knockout mice were found to be more excitable than normal mice, as well as to promote the development of epilepsy, thus reinforcing the important role of *KCNB1* in epileptogenesis (Speca et al., 2014). The *KCNQ2* gene encodes the *Kv7.2* protein, together with its homologue *KCNQ3,* forms homo- and heterotetrameric ion channels in the neuronal plasma membrane, and is responsible for the M-current, thereby preventing neuronal hyperexcitability (Li et al., 2021). Abnormalities of *KCNQ2* ion channel proteins may lead to benign familial neonatal epileps (Singh et al., 1998). Abnormalities in this channel could also cause epileptic encephalopathy. Many patients usually present with recurrent seizures. They have the characteristics of long seizure-free periods, and followed by seizure recurrences, along with severe intellectual impairment and language dysfunctions (Boets et al., 2021). *KCNQ2* was also a very crucial target for antiepileptic drug research, and retigabine was an antiepileptic drug developed specifically for the *KCNQ* channel, but its treatment was sub-optimal, and miRNA may be a better therapeutic option.

Previous studies on the regulation of ion channel gene expression by miRNAs had focused on the effect of a particular miRNA on one ion channel gene, but there was growing evidence to support the involvement of numerous ion channel genes in the pathogenesis of epilepsy. In this study, to further investigate the regulatory network of ion channel genes and miRNAs in mTLE, we identified miRNAs that can regulate multiple important ion channels. Therefore, establishing the network of miRNAs regulating ion channels is of great significance in mTLE. In this study, we predicted the related network regulatory relationships by clustering the alterations of ion channel genes in the important pathological process of epilepsy pathogenesis, which is an important insight for the future exploration of other related pathological processes in epilepsy regarding the network regulation of miRNAs in their related expression genes, such as ion channel alterations, neuroinflammation and neuronal loss et al.

The miRNAs and their regulatory network study will have profound implications at the step of the drug development process for anti-seizures. Meanwhile, our study provides new insights into the understanding of miRNA-mediated alterations that may be critical for the onset and progression of epilepsy.

CONCLUSION

The hub mTLE ion channel-related genes and miRNAs that may regulate multiple important ion channels had been identified, while the network of miR-27a-3p regulating potassium ion channel genes was established in mTLE. Based on the miRNA-mRNA regulatory network, it is suggested that the above-mentioned ion channel genes have an important role in the pathogenesis of mTLE and the miRNA has a potential targeting role in its regulation.

Limitations

Although our study explores ion channel genes and their regulatory networks at the cellular and animal levels, it lacks phenotypic studies in epilepsy patients. In addition, how the above miRNAs are involved in the occurrence of ion channel gene expression downregulation in mTLE and the mechanisms of their involvement in regulation have not been elucidated, so it is worthwhile to investigate and explore in-depth the regulation of ion channel gene expression by miRNAs in mTLE.

DATA AVAILABILITY STATEMENT

The datasets presented in this study can be found in online repositories. The names of the repository/repositories and accession number(s) can be found in the article/**Supplementary Material**.

ETHICS STATEMENT

The animal study was reviewed and approved by the Seventh Affiliated Hospital, Sun Yat-sen University.

AUTHOR CONTRIBUTIONS

LZ conceived the idea to this paper; ZS and YL collected and analyzed the data and drafted the paper. SC, XL and KZ participated in the information registration and performed the statistical analysis. All authors read and approved the final manuscript.

FUNDING

This work was funded by grants from the National Natural Science Foundation of China (82071447, 81571266, 81771405) and the Sanming Project of Medicine in Shenzhen (No. SZSM201911003).

ACKNOWLEDGMENTS

The authors are grateful to Dr. Sebastian Guelfi team for providing high-throughput sequencing data results.

SUPPLEMENTARY MATERIAL

The Supplementary Material for this article can be found online at: https://www.frontiersin.org/articles/10.3389/fgene.2022.853529/full#supplementary-material

REFERENCES

Almeida Silva, L. F., Reschke, C. R., Nguyen, N. T., Langa, E., Sanz-Rodriguez, A., Gerbatin, R. R., et al. (2020). Genetic Deletion of microRNA-22 Blunts the Inflammatory Transcriptional Response to Status Epilepticus and Exacerbates Epilepsy in Mice. *Mol. Brain* 13, 114. doi:10.1186/s13041-020-00653-x

Boets, S., Johannesen, K. M., Destree, A., Manti, F., Ramantani, G., Lesca, G., et al. (2021). Adult Phenotype of KCNQ2 Encephalopathy. *J. Med. Genet.* doi:10.1136/jmedgenet-2020-107449

Brennan, G. P., and Henshall, D. C. (2018). microRNAs in the Pathophysiology of Epilepsy. *Neurosci. Lett.* 667, 47–52. doi:10.1016/j.neulet.2017.01.017

Bruxel, E. M., Bruno, D. C. F., do Canto, A. M., Geraldis, J. C., Godoi, A. B., Martin, M., et al. (2021). Multi-omics in Mesial Temporal Lobe Epilepsy with Hippocampal Sclerosis: Clues into the Underlying Mechanisms Leading to Disease. *Seizure* 90, 34–50. doi:10.1016/j.seizure.2021.03.002

Chang, L., Zhou, G., Soufan, O., and Xia, J. (2020). miRNet 2.0: Network-Based Visual Analytics for miRNA Functional Analysis and Systems Biology. *Nucleic Acids Res.* 48, W244–W251. doi:10.1093/nar/gkaa467

Ding, J., Adiconis, X., Simmons, S. K., Kowalczyk, M. S., Hession, C. C., Marjanovic, N. D., et al. (2020). Systematic Comparison of Single-Cell and Single-Nucleus RNA-Sequencing Methods. *Nat. Biotechnol.* 38, 737–746. doi:10.1038/s41587-020-0465-8

Dogini, D. B., Avansini, S. H., Vieira, A. S., and Lopes-Cendes, I. (2013). MicroRNA Regulation and Dysregulation in Epilepsy. *Front. Cel. Neurosci.* 7, 172. doi:10.3389/fncel.2013.00172

Englot, D. J., Morgan, V. L., and Chang, C. (2020). Impaired Vigilance Networks in Temporal Lobe Epilepsy: Mechanisms and Clinical Implications. *Epilepsia* 61, 189–202. doi:10.1111/epi.16423

Gbd 2016 Epilepsy Collaborators (2019). Global, Regional, and National burden of Epilepsy, 1990-2016: a Systematic Analysis for the Global Burden of Disease Study 2016. *Lancet Neurol.* 18, 357–375. doi:10.1016/S1474-4422(18)30454-X

Gross, C., and Tiwari, D. (2018). Regulation of Ion Channels by MicroRNAs and the Implication for Epilepsy. *Curr. Neurol. Neurosci. Rep.* 18, 60. doi:10.1007/s11910-018-0870-2

Guelfi, S., Botia, J. A., Thom, M., Ramasamy, A., Perona, M., Stanyer, L., et al. (2019). Transcriptomic and Genetic Analyses Reveal Potential Causal Drivers for Intractable Partial Epilepsy. *Brain* 142, 1616–1630. doi:10.1093/brain/awz074

Habib, N., Li, Y., Heidenreich, M., Swiech, L., Avraham-Davidi, I., Trombetta, J. J., et al. (2016). Div-Seq: Single-Nucleus RNA-Seq Reveals Dynamics of Rare Adult Newborn Neurons. *Science* 353, 925–928. doi:10.1126/science.aad7038

Henshall, D. C., Hamer, H. M., Pasterkamp, R. J., Goldstein, D. B., Kjems, J., Prehn, J. H. M., et al. (2016). MicroRNAs in Epilepsy: Pathophysiology and Clinical Utility. *Lancet Neurol.* 15, 1368–1376. doi:10.1016/s1474-4422(16)30246-0

Johnson, M. R., Behmoaras, J., Bottolo, L., Krishnan, M. L., Pernhorst, K., Santoscoy, P. L. M., et al. (2015). Systems Genetics Identifies Sestrin 3 as a Regulator of a Proconvulsant Gene Network in Human Epileptic hippocampus. *Nat. Commun.* 6, 6031. doi:10.1038/ncomms7031

Li, X., Zhang, Q., Guo, P., Fu, J., Mei, L., Lv, D., et al. (2021). Molecular Basis for Ligand Activation of the Human KCNQ2 Channel. *Cell Res* 31, 52–61. doi:10.1038/s41422-020-00410-8

Lu, J., Zhou, N., Yang, P., Deng, L., and Liu, G. (2019). MicroRNA-27a-3p Downregulation Inhibits Inflammatory Response and Hippocampal Neuronal Cell Apoptosis by Upregulating Mitogen-Activated Protein Kinase 4 (MAP2K4) Expression in Epilepsy: *In Vivo* and *In Vitro* Studies. *Med. Sci. Monit.* 25, 8499–8508. doi:10.12659/msm.916458

Lu, T. X., and Rothenberg, M. E. (2018). MicroRNA. *J. Allergy Clin. Immunol.* 141, 1202–1207. doi:10.1016/j.jaci.2017.08.034

Mooney, C., Becker, B. A., Raoof, R., and Henshall, D. C. (2016). EpimiRBase: a Comprehensive Database of microRNA-Epilepsy Associations. *Bioinformatics* 32, 1436–1438. doi:10.1093/bioinformatics/btw008

Oyrer, J., Maljevic, S., Scheffer, I. E., Berkovic, S. F., Petrou, S., and Reid, C. A. (2018). Ion Channels in Genetic Epilepsy: From Genes and Mechanisms to Disease-Targeted Therapies. *Pharmacol. Rev.* 70, 142–173. doi:10.1124/pr.117.014456

Palleria, C., Coppola, A., Citraro, R., Del Gaudio, L., Striano, S., De Sarro, G., et al. (2015). Perspectives on Treatment Options for Mesial Temporal Lobe Epilepsy with Hippocampal Sclerosis. *Expert Opin. Pharmacother.* 16, 2355–2371. doi:10.1517/14656566.2015.1084504

Raoof, R., Bauer, S., El Naggar, H., Connolly, N. M. C., Brennan, G. P., Brindley, E., et al. (2018). Dual-center, Dual-Platform microRNA Profiling Identifies Potential Plasma Biomarkers of Adult Temporal Lobe Epilepsy. *EBioMedicine* 38, 127–141. doi:10.1016/j.ebiom.2018.10.068

Singh, N. A., Charlier, C., Stauffer, D., DuPont, B. R., Leach, R. J., Melis, R., et al. (1998). A Novel Potassium Channel Gene, KCNQ2, Is Mutated in an Inherited Epilepsy of Newborns. *Nat. Genet.* 18, 25–29. doi:10.1038/ng0198-25

Smith, R. S., and Walsh, C. A. (2020). Ion Channel Functions in Early Brain Development. *Trends Neurosciences* 43, 103–114. doi:10.1016/j.tins.2019.12.004

Sosanya, N. M., Huang, P. P. C., Cacheaux, L. P., Chen, C. J., Nguyen, K., Perrone-Bizzozero, N. I., et al. (2013). Degradation of High Affinity HuD Targets Releases Kv1.1 mRNA from miR-129 Repression by mTORC1. *J. Cel Biol* 202, 53–69. doi:10.1083/jcb.201212089

Speca, D. J., Ogata, G., Mandikian, D., Bishop, H. I., Wiler, S. W., Eum, K., et al. (2014). Deletion of the Kv2.1 Delayed Rectifier Potassium Channel Leads to Neuronal and Behavioral Hyperexcitability. *Genes Brain Behav.* 13, 394–408. doi:10.1111/gbb.12120

Srivastava, P. K., Bagnati, M., Delahaye-Duriez, A., Ko, J.-H., Rotival, M., Langley, S. R., et al. (2017). Genome-wide Analysis of Differential RNA Editing in Epilepsy. *Genome Res.* 27, 440–450. doi:10.1101/gr.210740.116

Thom, M. (2014). Review: Hippocampal Sclerosis in Epilepsy: a Neuropathology Review. *Neuropathol. Appl. Neurobiol.* 40, 520–543. doi:10.1111/nan.12150

Tiwari, D., Brager, D. H., Rymer, J. K., Bunk, A. T., White, A. R., Elsayed, N. A., et al. (2019). MicroRNA Inhibition Upregulates Hippocampal A-type Potassium Current and Reduces Seizure Frequency in a Mouse Model of Epilepsy. *Neurobiol. Dis.* 130, 104508. doi:10.1016/j.nbd.2019.104508

Torkamani, A., Bersell, K., Jorge, B. S., Bjork, R. L., Jr., Friedman, J. R., Bloss, C. S., et al. (2014). De novoKCNB1mutations in Epileptic Encephalopathy. *Ann. Neurol.* 76, 529–540. doi:10.1002/ana.24263

Wang, J., Lin, Z.-J., Liu, L., Xu, H.-Q., Shi, Y.-W., Yi, Y.-H., et al. (2017). Epilepsy-associated Genes. *Seizure* 44, 11–20. doi:10.1016/j.seizure.2016.11.030

Ximerakis, M., Lipnick, S. L., Innes, B. T., Simmons, S. K., Adiconis, X., Dionne, D., et al. (2019). Single-cell Transcriptomic Profiling of the Aging Mouse Brain. *Nat. Neurosci.* 22, 1696–1708. doi:10.1038/s41593-019-0491-3

Zhang, Z., Wang, Z., Zhang, B., and Liu, Y. (2018). Downregulation of microRNA-155 by P-reoperative A-dministration of V-alproic A-cid P-revents P-ostoperative S-eizures by U-pregulating SCN1A. *Mol. Med. Rep.* 17, 1375–1381. doi:10.3892/mmr.2017.8004

Conflict of Interest: The authors declare that the research was conducted in the absence of any commercial or financial relationships that could be construed as a potential conflict of interest.

frontiers | Frontiers in Genetics

REVIEW
published: 26 May 2022
doi: 10.3389/fgene.2022.899831

Application of Induced Pluripotent Stem Cell-Derived Models for Investigating microRNA Regulation in Developmental Processes

Hongyu Chen[1,2†], *Mimi Zhang*[1,2†], *Jingzhi Zhang*[1,2], *Yapei Chen*[1,2], *Yabo Zuo*[3], *Zhishen Xie*[3], *Guanqing Zhou*[1,2], *Shehong Chen*[1,2] *and Yaoyong Chen*[1,2*]

[1]*Department of Obstetrics and Gynecology, Key Laboratory for Major Obstetric Diseases of Guangdong Province, The Third Affiliated Hospital of Guangzhou Medical University, Guangzhou, China,* [2]*Key Laboratory of Reproduction and Genetics of Guangdong Higher Education Institutes, The Third Affiliated Hospital of Guangzhou Medical University, Guangzhou, China,* [3]*Guangzhou Key Laboratory for Clinical Rapid Diagnosis and Early Warning of Infectious Diseases, KingMed School of Laboratory Medicine, Guangzhou Medical University, Guangzhou, China*

Advances in induced pluripotent stem cell (iPSC) techniques have opened up new perspectives in research on developmental biology. Compared with other sources of human cellular models, iPSCs present a great advantage in hosting the unique genotype background of donors without ethical concerns. A wide spectrum of cellular and organoid models can be generated from iPSCs under appropriate *in vitro* conditions. The pluripotency of iPSCs is orchestrated by external signalling and regulated at the epigenetic, transcriptional and posttranscriptional levels. Recent decades have witnessed the progress of studying tissue-specific expressions and functions of microRNAs (miRNAs) using iPSC-derived models. MiRNAs are a class of short non-coding RNAs with regulatory functions in various biological processes during development, including cell migration, proliferation and apoptosis. MiRNAs are key modulators of gene expression and promising candidates for biomarker in development; hence, research on the regulation of human development by miRNAs is expanding. In this review, we summarize the current progress in the application of iPSC-derived models to studies of the regulatory roles of miRNAs in developmental processes.

Keywords: microRNA, induced pluripotent stem cell, cellular model, develoment, gene regulaiton

OPEN ACCESS

Edited by:
Jian-Hong Fang,
Sun Yat-sen University, China

Reviewed by:
Qihua Fu,
Shanghai Children's Medical Center, China
Wenmin Sun,
Sun Yat-sen University, China

***Correspondence:**
Yaoyong Chen
ychen@gzhmu.edu.cn

[†]*These authors have contributed equally to this work*

Specialty section:
This article was submitted to RNA, a section of the journal Frontiers in Genetics

Received: *19 March 2022*
Accepted: *06 May 2022*
Published: *26 May 2022*

Citation:
Chen H, Zhang M, Zhang J, Chen Y, Zuo Y, Xie Z, Zhou G, Chen S and Chen Y (2022) Application of Induced Pluripotent Stem Cell-Derived Models for Investigating microRNA Regulation in Developmental Processes. Front. Genet. 13:899831. doi: 10.3389/fgene.2022.899831

INTRODUCTION

MiRNAs are short RNA molecules with 20–24 nucleotides that regulate the posttranscriptional silencing of target genes (Krol et al., 2010; Fabian and Sonenberg, 2012; Luo and Zhu, 2014; Lu and Rothenberg, 2018). MiRNAs exhibit a complex regulatory network resulting from a particular miRNA targeting multiple mRNAs and multiple miRNAs targeting the same mRNA, and affecting the expression levels of many protein-coding genes involved in functional pathways (Liu et al., 2014; Barwari et al., 2016; Luo et al., 2016; Rupaimoole and Slack, 2017). Over the past few decades, the role of miRNAs has been evaluated in a variety of biological processes (Ambros, 2004; Luo et al., 2015b; Lopez et al., 2017; Song et al., 2019). To date, numerous studies have delineated the regulatory role of miRNAs in development. For instance, miRNAs are regulating cell differentiation, proliferation, apoptosis and migration during B cell

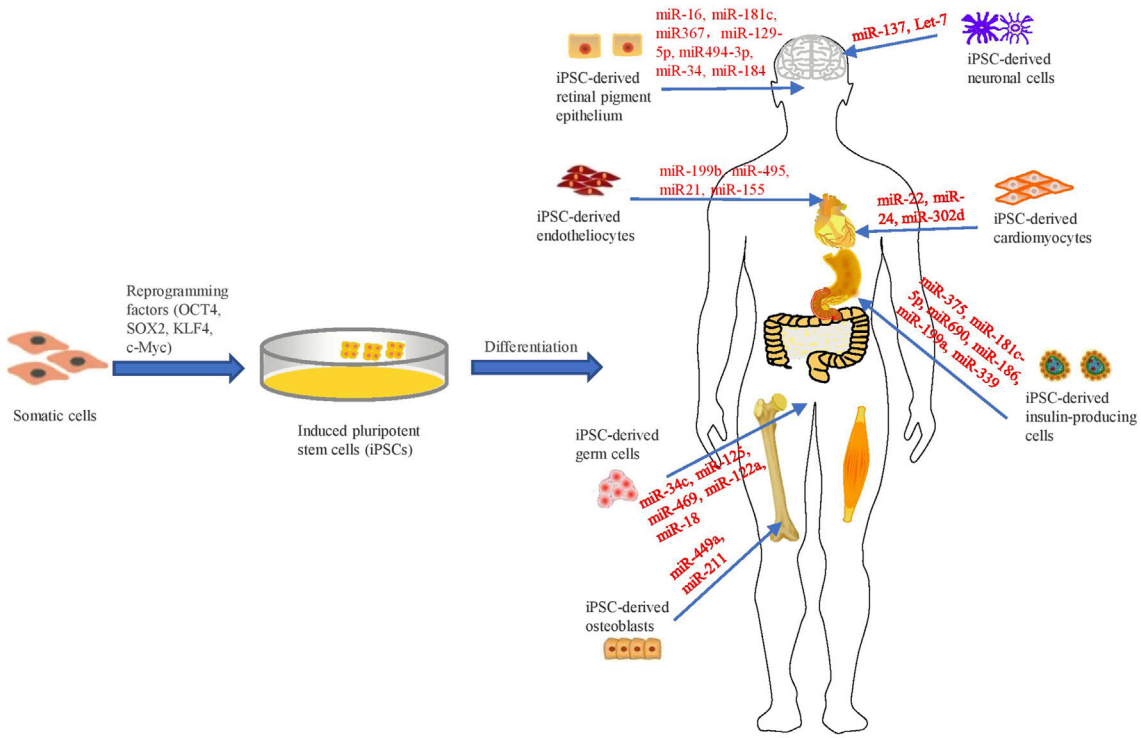

FIGURE 1 | Schematic representation of investigating the regulatory roles of miRNAs in iPSC-derived cellular models.

development by regulating a spectrum of signalling pathways, including BCR, MAPK/ERK, PI3K/AKT and NFκB pathways (Katsaraki et al., 2021). Thus, miRNAs have been characterized as valuable modulators of human development.

The investigation of miRNAs in development requires *in vitro* models derived from human pluripotent stem cells to simulate the tissue developmental procedures. Nevertheless, there are a number of shortages of human embryonic stem cell (hESC) techniques, such as ethical issues and complicated manipulation, thus preventing its wide application in clinical and basic research (Barker and de Beaufort, 2013; Luo et al., 2014). In 2006, studies were conducted to reprogram somatic cells into pluripotent stem cells with a cocktail of transcriptional factors, such as the combination of OCT4, KLF4, SOX2 and c-Myc (Takahashi and Yamanaka, 2006). This method avoids moral controversies and has led to the application of cellular programming techniques in human developmental research (Lo Sardo et al., 2017). Thus, the emergence of human induced pluripotent stem cells (hiPSC) has solved these problems (Luo et al., 2015a).

Remarkable progress has been created within the area of hiPSC over the past decade (Luo et al., 2018; Luo et al., 2021a). At present, hiPSCs can specifically differentiate into cardiomyocytes, endothelial cells, insulin-producing cells, germ cells, neuronal cells, osteoblasts, retinal pigment epithelium and so on (**Figure 1**). These cells could be ultilized for research of human development and diseases (Luo et al., 2021c). Hence, this review aims to systematically summarize the regulatory roles of miRNAs in development identified by iPSC-derived models.

CARDIOMYOCYTES

Cardiovascular diseases (CVDs), such as myocardial infarction (MI) and cardiomyopathy, are recognized as the leading lethal causes around the world and are often associated with degeneration of cardiomyocytes (CMs). CMs are fully differentiated cells with minimal proliferative potential. Given the restricted effectiveness of drug therapy in treating myocardial injuries, the development of novel therapeutic approaches for curing these disorders is of urgency. HiPSC-derived CMs (iPS-CMs) introduce a new prospect for CVD treatment. However, the molecular mechanisms regulating the development of these cells is a pivotal problem that should be solved prior to clinical usage.

For instance, a study has compared the mRNA and miRNA expression profiles of iPS-CMs and biopsies from fetal, adult and hypertensive hearts to find out the core miRNA network, which revealed miRNAs associated with human heart development (Babiarz et al., 2012). Further studies profiled the miRNAs in human iPS-CMs and revealed 96 miRNAs that could promote CM proliferation (Diez-Cuñado et al., 2018). The CM proliferation-associated miRNAs in human were quite different from those of rodent (Eulalio et al., 2012). Most human CM proliferation-associated miRNAs function by targeting the Hippo pathway, an evolutionarily conserved pathway regulating organ size (Yu and Guan, 2013). Another study also confirmed that the mRNAs encoding most components of the Hippo pathway were recruited into the RNA-induced silencing complex (RISC) in iPS-CMs (Diez-

Cuñado et al., 2018). In addition, some studies have demonstrated that miR-302d promoted CM proliferation by inhibiting LATS2 of the Hippo pathway (Xu F. et al., 2019).

Recently, miR-24 has been demonstrated as an important regulator for human heart development by using iPS-CM models (Guo et al., 2015). This is an execllent example of the complex regulatory roles of miRNAs in human development. On one hand, miR-24 has been demonstrated to suppress CM apoptosis. It is shown that delivery of miR-24 into CMs significantly alleviates cardiomyopathies, suggesting that modulating miRNA levels might be a novel therapeutic means for cardiac diseases (Qian et al., 2011; Guo et al., 2015). One study showed that miR-24 promoted functional implantation of cardiovascular progenitor cells (CPCs), in which miR-24 was utilized as a component of the antiapoptotic cocktail to enhance the survival of CPCs implantated into the MI heart tissues (Hu et al., 2011). Other studies have also identified other prosurvival roles of miR-24 in cardiac fibrosis and found that overexpression of miR-24 through lentivirus-mediated transduction reduces fibrosis and improves cardiac function in MI hearts, confirming the beneficial role of miR-24 (Guo et al., 2015). On the other hand, miR-24 has been demonstarted to exert proapoptotic effects. MiR-24 is characterized as a proapoptotic miRNA in cardiac endothelial cells, and blocking its function by injection of miR-24 antagonists can prevent apoptosis, enhance vascular distribution, and improve cardiac function after MI (Fiedler et al., 2011). However, these experiments in earlier studies were performed by viral transduction or polymeric transfection of miR-24 mimics or inhibitors, in which the protective effect observed might be partly caused by their off-target effects in non-CM cells (Guo et al., 2015).

In addition, some studies have also found that pri-miR-22/miR-22-3p is the top-ranked expressed primary miRNA transcript in heart tissues and iPS-CMs, and contributes to myocardial ischemia/reperfusion injury (Du et al., 2016; Sun et al., 2019). Some studies have confirmed the pro-apoptotic effect of miR-22 in iPS-CM (Pan and Zhu, 2018; Sun et al., 2019). Hypoxia-mediated apoptosis was augmented by miR-22 overexpression but resuced by miR-22 knockdown in iPS-CMs (Gidlöf et al., 2020). Meanwhile, this study also demonstrated that the long non-coding RNA Neat1 in the paraspeckles is the essential factor for pri-miR-22 processing in CMs. Knockdown of Neat1 could lead to significant accumulation of pri-miR-22 and consumption of mature ones in iPS-CMs (Gidlöf et al., 2020).

VASCULAR ENDOTHELIAL CELLS

MiR-199b is a highly conserved miRNA across species and capable of guiding the hiPSCs to differentiate into vascular endothelial cells (ECs) by regulating key molecular pathways, such as Notch signaling, in response to angiogenic signals. In particular, miR-199b regulates EC fate by targeting the Notch ligand JAG1, which leads to expression and secretion of VEGF via STAT3-mediated trascription (Chen et al., 2015). Nevertheless, the molecular mechanism underlying the upstream regulation remains unclear. Moreover, VEGF-induced miR-155 promotes angiogenesis by directly silencing E2F2, a E2F family transcriptional factor involved in cell proliferation, apoptosis and death (Dimova and Dyson, 2005), during EC differentiation from hiPSCs (Yang et al., 2016).

MiR-495 is a member of the DLK1-Dio3 miRNA cluster and exerts antiangiogenic effects. It is abundant in the non-EC portion while downregulated in the EC portion. It induces endothelial or angiogenic gene expression by downregulating VEZF1, a major transcriptional factor regulating EC genes, such as IGF1 and CD31, during EC differentiation and angiogenesis (Zou et al., 2010). In contrast, increasing VEZF1 expression via miR-495 blockage promotes angiogenesis post implantation of hiPSCs via enhancement of EC production. Studies have shown that the derived ECs significantly augmented the formation of new blood vessels in infarcted hearts, prevented functional deterioration and restricted the expansion of infarcted areas post transplantation in MI mice (Liang et al., 2017).

Additionally, miR-21 overexpression could enhance the Akt/TGF-β2 signal by downregulating PTEN on chromosome 10, thereby increasing the amount of ECs derived from hiPSCs (Zeng et al., 2018). Overexpression of miR-21 increased the mRNA and protein levels of TGF-β2, which is an essential cytokine for cell survival proliferation, migration and differentiation (Vargel et al., 2016). Neutralizing TGF-β2 by antibodies prohibits the expression of miR-21-induced EC markers, such as VE-CAD and CD31 (Di Bernardini et al., 2014).

INSULIN-PRODUCING CELLS

The generation of insulin-producing cells (IPCs) from hiPSCs is a promising approach to investigate the molecular mechanisms of pancreatic development and a potential source of treatment for type I diabetes (Zeng et al., 2018). MiRNAs are major posttranscriptional regulators of gene expression and thus might involve in the control of β cell development in the pancreas.

For examples, miR-375 is essential for pancreatic endocrine function as its blockage results in glucose imbalance, α cell increment and β cell reduction (Poy et al., 2009). MiR-375 and miR-186 overexpression in hiPSCs leads to differentiation into insulin-secreting β-like cells that expressing pancreatic endocrine markers, such as PDX1, GLUT2, NGN3, PAX4 and PAX6. Despite secreting less insulin than natural β cells, these hiPSC-derived β-like cells could rescue blood glucose levels after transplantation into diabetic mice (Shaer et al., 2014). In addition, miR-375 affects insulin secretion by regulating the expression of muscular dystrophy protein in MIN6 cells (Poy et al., 2004; Krek et al., 2005).

The development of organisms is a result of the reprogramming of gene regulatory networks (Hornstein and Shomron, 2006). Some studies have described miR-375 as a key regulator of pancreatic development in humans (Poy et al., 2004; Lynn et al., 2007; Bravo-Egana et al., 2008; Avnit-Sagi et al., 2012). Mice lacking miR-375 showed α/β cell imbalance and reduced β cell propagation in spite of insulin insufficiency (Avnit-Sagi et al., 2012). Studies have shown that miR-7, miR-9, miR-375 and miR-376 are dramatically upregulated throughout the islet

development (Wei et al., 2013). Some studies have found that miR-186, miR-199a and miR-339 are also upregulated during the formation of IPCs *in vitro*. The target genes of these three microRNAs include LIN28, PRDM1, CALB1, GCNB2, RBM47, PLEKHH1, RBPMS2 and PAK6 mRNA. (Joglekar et al., 2009; Chen et al., 2011; Kredo-Russo et al., 2012).

Studies have shown that miR-181c-5p accumulates gradually during the derivation of IPCs from hiPSCs. Increased phosphorylation of Smad2/3 is observed in iPSC-derived cells, and treatment with a Smad2/3 inhibitor after overexpression of miR-181c-5p had the opposite effect on IPC formation (Li et al., 2020). Similarily, other studies have also shown that miR-181c-5p is abundant in the late differentiation steps of hESC-derived IPCs, fetal pancreas, and adult islets (Liao et al., 2013; Fogel et al., 2015). Furthermore, miR-181c-5p was differentially expressed between the pancreas and the liver despite the common developmental origin of both tissues, with upregulation in the former and downregulation in latter (Porciuncula et al., 2013). Therefore, it is speculated that miR-181c-5p might play a pancreatic-specific role.

On the other hand, miR-690 overexpression dramatically delayed iPSC-derived IPC maturation and reduced insulin secretion *in vitro* and *in vivo*. Bioinformatic analysis suggested that its putative targets, such as CTNNB1, STAT3 and SOX9, were essential factors for of pancreatic endocrine development. Elevated miR-690 expression levels disrupt IPC differentiation by directly binding to Sox9. Subsequent experimental studies suggest that miR-690 could negatively modulate the Wnt signalling pathway during the pancreatic developmental process (Xu Y. et al., 2019).

In conclusion, these findings may help us better understand the process of pancreatic differentiation of hiPSCs *in vitro* and the underlying mechanisms involving miRNAs. As miRNAs could modulate certain transcriptional factors throughout the pancreatic developmental process, they could serve as novel therapeutic targets for diabetes treatment.

NEURONAL CELLS

HiPSC-derived neurons and neural progenitor cells (NPCs) are important models for investigating neurogenesis and synaptogenesis as well as their disruption in disorder statuses. Moreover, they are promising therapeutic vectors for brain disorders in the future (Zhu et al., 2013; Zhu et al., 2014). HiPSC-derived cellular and organoid models serve as an important bridge between model organism research and human postmortem brain research by providing living human cells, consisting of hiPSCs and their derived NPCs and neurons, with the composite genetic background present in patients. Hence, there is a quickly growing body of research projects using patient-specific iPSC-derived neurons to investigate neurogenesis.

For instance, iPSCs with mutations in the LRRK2 and α synuclein gene families were used to generate dopamine (DA) neurons, which exhibited higher sensitivity to oxidative stress and susceptibility to apoptosis (Byers et al., 2011; Reinhardt et al., 2013). Such phenotypes were also observed in iPSC-derived DA neurons from idiopathic Parkinson's disease (PD) patients (Sánchez-Danés et al., 2012); meanwhile, apoptotic markers were also detected in the postmortem brain of PD patients (Hartmann et al., 2000; Mogi et al., 2000). Apoptosis-related miRNAs are also associated with neuronal differentiation (Aranha et al., 2011). For examples, miR-14, let-7a and miR-34a are elevated during neural stem cell differentiation (Heman-Ackah et al., 2013).

A large number of investigations have demonstrated that miRNAs play important roles in neural development (Hsu et al., 2012; Jimenez-Mateos et al., 2012; Liu et al., 2012). In addition, abundant molecular evidences support the essential roles of miRNAs in development of schizophrenia and other neural diseases (Green et al., 2013). For instance, miRNA-seq analysis was performed to distinguish differentially expressed miRNAs in iPSC-derived neurons from schizophrenia patients with 22q11.2 deletions compared to those from healthy donors (Yang et al., 2010). They discovered that miRNA expression levels in the deleted region decreased to approximately half the normal levels, and the levels were also altered in several other miRNAs out of the deleted region. The functional annotations of the putative targets of these dysregulated miRNAs were enrich in neurological diseases, neuronal development, axon formation and other important pathways relevant with the nervous system (Zhao et al., 2015).

Finally, posttranscriptional modifications could be identified by transcriptome analysis. RNA editing is a posttranscriptional event. Adenosine to inosine (A-to-I) transition is the dominate RNA editing process and happens most frequently in RNA molecules relevant with neurotransmission (Sanjana et al., 2012), especially in a lot of brain-specific miRNAs (Nishikura, 2010). Intriguingly, comparing postmortem cerebellum of autism patients with the control ons discovered that RNA editing was more abundant in the autism samples (Eran et al., 2013). Total transcriptome analysis can also detect fusion genes (Zhang Y. et al., 2014), which is valuable for building coexpression networks that can help researchers discover gene networks and pathways that are disrupted in neuropsychiatric disorders.

MiRNAs are believed to exert key regulatory effects in a wide spectrum of neural developmental processes, such as neurogenesis, neuronal maturation, axon regeneration, synaptic development and brain plasticity (Giraldez et al., 2005; Weston et al., 2006). Let-7 family miRNAs are the highest expressed miRNAs in the mammalian brains (Lagos-Quintana et al., 2002). They were firstly identified in *Caenorhabditis elegans* (Roush and Slack, 2008) and highly conserved across species. They are the key regulators for organism development, such as cell proliferation, cell specification and terminal differentiation (Nishikura, 2010). In the developing brain, Let-7 miRNAs participate in control of various developmental processes, such as neuronal differentiation (Schwamborn et al., 2009), neuronal subtype specification (Weick et al., 2013), neuronal regeneration (Li et al., 2015) and synaptic formation (Edbauer et al., 2010). Albeit in silico models suggest that the Let-7 miRNAs are involved in modulating postsynaptic gene expression (Paschou et al., 2012), their direct functions in mature human neurons remain unclear.

One of the Let-7 members, Let-7c is located on chromosome 21; thus, it exists in an extra copy of trisomy 21 (T21) and is associated with the symptoms of mild to moderate mental retardatoin featured in this neurodevelopmental syndrome (Antonarakis, 2017). It has been reported that miRNAs encoded by chromosome 21 may be important for a comprehensive understanding of the pathophysiology of T21-related neural diseases (Izzo et al., 2017). Taken together, these investigations indicate that the Let-7 family plays an important role in modulating human neurodevelopment and provide clues to illustrating the complicated molecular aetiology of neurodevelopmental syndromes (McGowan et al., 2018).

GERM CELLS

In humans, genetic information is passed on to their offspring via germ cells (Luo et al., 2021b; Zhou et al., 2022). At present, ESCs, iPSCs and spermatogonial stem cells are the major cell sources used for generation of male germ cells expressing functional genes (Saito et al., 2015). However, their clinical utility is still challenged by several safety issues (Zhang D. et al., 2014). MiRNAs have recently emerged as important factors in translation regulation and the epigenetic control of stem cell self-renewal and pluripotent capacities (Gangaraju and Lin, 2009). Key roles of miRNA pathways in germline stem cell maintenance have been reported in vertebrate iPSCs (Gangaraju and Lin, 2009). In addition, miRNAs are very important in spermatogenesis and might play key roles in sperm mitosis, meiosis and postmeiotic stages (Wang and Xu, 2015).

The role of miRNAs in germ cell development has been functionally proven (Fernández-Pérez et al., 2018). For examples, RNA binding protein Lin28 blocks Let-7 and desuppresses Blimp1 translation in the initial stage of germ cell development (West et al., 2009). In addition, miR-125 posttranscriptionally suppress Oct4 during sperm meiosis in males (Medrano et al., 2013).

Further experimental evidence should be pursued to identify specific microRNAs that are regulating the three stages of human spermatogenesis, pachytene spermatocytes, spermatogonial cells and round spermatozoa cells (Liu Y. et al., 2015). For examples, miR-34c increased in pachytene spermatocytes and round sperm cells and prohibited survival by targeting the transcription factor ATF1 (Romero et al., 2011). In addition, miR-469 inhibited protamine and transition protein 2 (TP2) mRNA in pachytene spermatocytes and round sperm cells (Dai et al., 2011). Moreover, during spermatogenesis, miR-122a and miR-18 downregulate TP2 and heat shock factor 2, respectively (Chen et al., 2017).

RETINAL PIGMENT EPITHELIUM

The retinal pigment epithelium (RPE) is a special layer arranged at the rear of retina. Injury or RPE dysfunction can severely affect the health of photoreceptors and visual function, which is a result of potential RPE pathological blinding disease. Examples include age-related macular degeneration (AMD), Stargardt disease and retinitis pigmentosa (Greene et al., 2014). So far, there is no efficient therapy to rescue the vision; thus, iPSC-derived RPE (iPS-RPE) cells might be a source of cells to regenerate the disrupted RPE. However, before iPS-RPE cells can be used clinically, as much information as possible about the factors that modulate RPE development is of urgency to increase the production and quality of the cells for therapeutic use (Greene et al., 2014).

A study has identified 155 potential miRNA markers in iPS-RPE cells (Wang et al., 2014). Upregulated miRNAs, such as miR-181c and miR-129-5p, might drive cell specification (Naguibneva et al., 2006; Ryan et al., 2006), while downregulated miRNAs, including miR-367, miR-18b and miR-20b, are associated with mitotic division (Budde et al., 2010; Murakami et al., 2013). Putative targets of these miRNAs are relevant with cell survival, cell cycle and development.

It is of interest to evaluate the possible role of iPS-RPE miRNAs in tumorigenesis. On one hand, some iPS-RPE-upregulated miRNAs are tumour suppressors. For instance, miR-34 is a typicall tumour suppressor that prohibits tumor growth, metastasis, invasion and epithelial-mesenchymal transformation (EMT) via downregulating TP53 (Zhang et al., 2007; Nana-Sinkam and Croce, 2013). MiR-34 is generally silenced in multiple cancer types. MiR-34 expression was amplified in iPS-RPE cells by 5-fold, indicating an extremely low proliferative capacity in these terminally differentiated cells (Hermeking, 2012). Similarly, miR-16 is a tumour suppressive miRNA targeting multiple oncogenes, including EGFR, JUN and BCL2. In contrast, many iPS-RPE-downregulated miRNAs are oncogenic miRNAs (Wang et al., 2014).

MiRNAs in extracellular vesicles (EVs) derived from RPE cells might exert effects in the malignant inflammatory cycle. A specific enrichment of miR-494-3p was identified in EVs secreted from iPS-RPE cells after interaction with MPs, which might be a potential therapeutic target for the treatment of AMD (Mukai et al., 2021). AMD is the first and the third top causes of blindness in developed countries and around the world, respectively (Kuo et al., 2012). MiR-184 on chromosome 15q25.1 is a highly conserved miRNA across species (Nomura et al., 2008). MiR-137 is gradually upregulated during the differentiation of hiPSCs into RPE cells and it will downregulate PKBβ (also known as Akt2), the major downstream effector of rapamycin (mTOR) signalling pathway (Jiang et al., 2016). Hence, dysregulation of miR-137 is an important molecular event during the progression of AMD (Jiang et al., 2016).

OSTEOBLASTS

HiPSCs could provide a rich cell source for regenerative medicine and to create patient-specific cellular and organoid models to investigate both intracellular and extracellular agents in bone repair and osteoarthritis (Diekman et al., 2012). Several histone deacetylase (HDAC) inhibitors have been shown to promote osteoblast maturation and specific gene expression by upregulating Runx2 gene expression in bone marrow stem cells (Hu et al., 2013). HDAC1 changes the expression of many genes associate

TABLE 1 | Roles of miRNAs in development of various iPSC-derived cell lineages.

iPSC-Derived Cell Lineages	miRNA	Target	Effect	References
Cardiomyocytes	miR-24	Bim	Inhibit apoptosis	Guo et al. (2015)
	miR-22	HIF1A/SIRT1	Promote apoptosis	Du et al., 2016 Sun et al., 2019 Gidlöf et al. (2020)
	miR-302d	LATS2	Promote cell proliferation	Xu et al. (2019a)
Endotheliocyte	miR-199b	JAG1	Promote transcription, activation and secretion of VEGF	Chen et al., 2015 Yang et al., 2016 Dimova and Dyson, (2005)
	miR-495	VEZF1	Inhibit EC differentiation and angiogenesis	Zou et al., 2010; Liang et al., 2017
	miR-21	PTEN/VE-cad/CD31	Promote cell proliferation and differentiation	Zeng et al., 2018 Di Bernardini et al., 2014 Vargel et al. (2016)
	miR-155	E2F2	promotes angiogenesis	Dimova and Dyson, 2005 Yang et al. (2016)
Insulin-producing cells	miR-375	HNF6/INSM1/PDX1	Its increase promotes islet formation and its decrease promotes ß -cell maturation and function	Shaer et al., 2014 Poy et al., 2004 Krek et al., 2005 Hornstein and Shomron, 2006 Lynn et al., 2007 Bravo-Egana et al., 2008 Avnit-Sagi et al., 2012 Wei et al. (2013) (Joglekar et al., 2009 Chen et al., 2011 Kredo-Russo et al. (2012)
	miR-181c-5p	Smad7/TGIF2	Maintain cell-specific function	Li et al., 2020 Liao et al., 2013 Fogel et al. (2015)
	miR-690	SRY-Sox9	Inhibit cell differentiation and insulin production	Xu et al. (2019b)
	miR-186, miR-199a, miR-339	LIN28/PRDM1/CALB1/GCNB2/RBM47/PLEKHH1/RBPMS2/PAK6	Formation of IPCs *in vitro*	Joglekar et al., 2009 Chen et al., 2011 Kredo-Russo et al. (2012)
Neuronal cells	miR-137	NRXN1	Inhibit synaptic growth and maturation in the hippocampus and cortical	Green et al. (2013)
	Let-7	LIN28B	Regulates neuronal differentiation, neuronal subtype regulation and synaptic formation, as well as cell cycle regulation and tumor suppression	Giraldez et al., 2005 Weston et al., 2006 Lagos-Quintana et al., 2002 Roush and Slack, 2008 (Schwamborn et al., 2009 Weick et al., 2013 Li et al., 2015 Edbauer et al., 2010 Paschou et al., 2012 Antonarakis, 2017 Izzo et al. (2017)
Germ cells	miR-34c	ATF1	Cause round sperm cells and trigger apoptosis	Romero et al. (2011)
	miR-125	Oct4	Inhibit sperm meiosis	Medrano et al. (2013)
	miR-469	TP2	Inhibit sperm meiosis	Dai et al. (2011)
	miR-122a, miR-18	TP2/heat shock factor 2	Involved in spermatogenesis	Chen et al. (2017)

(Continued on following page)

TABLE 1 | (*Continued*) Roles of miRNAs in development of various iPSC-derived cell lineages.

iPSC-Derived Cell Lineages	miRNA	Target	Effect	References
Retinal pigment epithelium	miR-16	BCL2/JUN/EGFR	Inhibits cell proliferation, epithelial-mesenchymal transformation (EMT), metastasis, and invasion and acts as a strong tumor suppressor	Zhang et al., 2007 Nana-Sinkam and Croce, (2013)
	miR-181c	HOX-A11	Promote cell differentiation	Naguibneva et al., 2006 Ryan et al. (2006)
	miR-129-5p	CDK6/EIF2C3/CAMTA1	Antiproliferative effect	Naguibneva et al., 2006 Ryan et al. (2006)
	miR-367	HDAC2	Downregulation is associated with cell proliferation	Budde et al., 2010 Murakami et al. (2013)
	miR494-3p	TNF-α/PEDF	Candidate molecular targets for diagnosis and treatment	Mukai et al. (2021)
	miR-34	TP53/EGFR/JUN/BCL2	Inhibit tumor growth, metastasis, invasion and EMT	Zhang et al., 2007 Nana-Sinkam and Croce, (2013)
	miR-184	mTOR	Affect AMD progress	Kuo et al., 2012 Nomura et al., 2008 Liu et al., 2014 Jiang et al. (2016)
Osteoblasts	miR-449a	HDAC1/Runx2	Promote differentiation of iPS osteoblasts and growth stagnation of tumor cells	Buurman et al., 2012 Jeon et al., 2012 Okamoto et al. (2012)
	miR-211	Atg14	Promote cell differentiation	Ozeki et al. (2017)

with cell growth, survival, subtype specification and genome integrity (Buurman et al., 2012). One miRNA, miR-449a, specifically interferes with HDAC1 expression (Jeon et al., 2012; Okamoto et al., 2012). Exogenous miR-449a silencing endogenous HDAC1 expression keeps histone acetylation, induces Runx2 expression, which is a regulator of osteoblast genes (Nishimura et al., 2012), and accelerates osteoblast derivation from iPSCs (Liu T. et al., 2015).

In addition, an independent study demonstrated that a group of six miRNAs, miR-10a/b, miR-19b, miR-9, miR-124a, and miR-181a, are key regulators of the iPSC differentiation into osteoblasts (Okamoto et al., 2012). Moreover, another study has shown that miR-211 promoted iPSC differentiation into osteoblast-like cells via upregulating the expression of autophagy-related genes like ATG14 (Ozeki et al., 2017).

DISCUSSION

MiRNAs are functioning within the RNA-protein complexes known as RNA-induced silencing complexes (RISC), which regulates gene expression posttranscriptionally in higher eukaryotes (Ameres and Zamore, 2013). Their roles in human development are rapidly being discovered (**Table 1**). MiRNAs are undoubtedly involved in many stages of normal cell development through their ability to block or promote development. They can be regulated by epigenetics, which may lead to other regulatory effects. In addition, they could serve as valuable markers for patient diagnosis and prognosis, as well as promising therapeutic targets. Although the multifaceted role of miRNAs in some diseases has been extensively studied over the past few years, important information is still missing, and no single molecule has been proven to be an effective regulator of the many pathogenic pathways of disease (Katsaraki et al., 2021).

IPSC-derived models are promising tools for deepening the understanding of early developmental processes (Dvash and Benvenisty, 2004). The major advantage of iPSC-derived models over primary cells is their capacity of repeatly generating cells with specific genetic background of the donors. With this property along with their pluripotency, hiPSCs can serve as a powerful tool for human cell replacement therapies and as an *in vitro* platform for personalized drug screening and discovery (Pouton and Haynes, 2007; Stadtfeld and Hochedlinger, 2010).

The reprogramming of somatic cells derived from patients and healthy donors into iPSCs is an important step to establish human-relevant models for illustrating the molecular and cellular mechanisms underlying the disease pathology. Notably, iPSCs can also be used to develop and test new therapies *in vitro*. Here, we discuss the regulatory role of miRNAs in iPSC-derived models for human development. In the future, miRNA-related studies need to be further improved to utilize hiPSCs as powerful tools in research of developmental biology. To address this issue, new methods, such as employing ectopic miRNAs as epigenetic modulators, should also be developed to optimize existing cell reprogramming and differentiation protocols (Ferreira et al., 2018).

There is a need to more thoroughly explore the role of miRNAs in human developoment. Given their relevance, we expect miRNAs to be exploited as diagnostic markers and as therapeutic targets for developmental diseases soon.

AUTHOR CONTRIBUTIONS

YoC conceived the study. HC and ZM prepared the figure and table. HC, MZ, JZ, YpC, YZ, ZX, GZ, SC and YoC wrote and edited the manuscript. All authors read and approved the final manuscript.

FUNDING

This work was supported by grants from the Guangzhou City Science, Technology and Innovation Commission (202002030077).

REFERENCES

Ambros, V. (2004). The Functions of Animal microRNAs. *Nature* 431 (7006), 350–355. doi:10.1038/nature02871

Ameres, S. L., and Zamore, P. D. (2013). Diversifying microRNA Sequence and Function. *Nat. Rev. Mol. Cell Biol.* 14 (8), 475–488. doi:10.1038/nrm3611

Antonarakis, S. E. (2017). Down Syndrome and the Complexity of Genome Dosage Imbalance. *Nat. Rev. Genet.* 18 (3), 147–163. doi:10.1038/nrg.2016.154

Aranha, M. M., Santos, D. M., Solá, S., Steer, C. J., and Rodrigues, C. M. P. (2011). miR-34a Regulates Mouse Neural Stem Cell Differentiation. *PLoS One* 6 (8), e21396. doi:10.1371/journal.pone.0021396

Avnit-Sagi, T., Vana, T., and Walker, M. D. (2012). Transcriptional Mechanisms Controlling miR-375 Gene Expression in the Pancreas. *Exp. Diabetes Res.* 2012, 1–5. doi:10.1155/2012/891216

Babiarz, J. E., Ravon, M., Sridhar, S., Ravindran, P., Swanson, B., Bitter, H., et al. (2012). Determination of the Human Cardiomyocyte mRNA and miRNA Differentiation Network by Fine-Scale Profiling. *Stem Cells Dev.* 21 (11), 1956–1965. doi:10.1089/scd.2011.0357

Barker, R. A., and de Beaufort, I. (2013). Scientific and Ethical Issues Related to Stem Cell Research and Interventions in Neurodegenerative Disorders of the Brain. *Prog. Neurobiol.* 110, 63–73. doi:10.1016/j.pneurobio.2013.04.003

Barwari, T., Joshi, A., and Mayr, M. (2016). MicroRNAs in Cardiovascular Disease. *J. Am. Coll. Cardiol.* 68 (23), 2577–2584. doi:10.1016/j.jacc.2016.09.945

Bravo-Egana, V., Rosero, S., Molano, R. D., Pileggi, A., Ricordi, C., Domínguez-Bendala, J., et al. (2008). Quantitative Differential Expression Analysis Reveals miR-7 as Major Islet microRNA. *Biochem. Biophysical Res. Commun.* 366 (4), 922–926. doi:10.1016/j.bbrc.2007.12.052

Budde, H., Schmitt, S., Fitzner, D., Opitz, L., Salinas-Riester, G., and Simons, M. (2010). Control of Oligodendroglial Cell Number by the miR-17-92 Cluster. *Development* 137 (13), 2127–2132. doi:10.1242/dev.050633

Buurman, R., Gürlevik, E., Schäffer, V., Eilers, M., Sandbothe, M., Kreipe, H., et al. (2012). Histone Deacetylases Activate Hepatocyte Growth Factor Signaling by Repressing microRNA-449 in Hepatocellular Carcinoma Cells. *Gastroenterology* 143 (3), 811–820. e815. doi:10.1053/j.gastro.2012.05.033

Byers, B., Cord, B., Nguyen, H. N., Schüle, B., Fenno, L., Lee, P. C., et al. (2011). SNCA Triplication Parkinson's Patient's iPSC-Derived DA Neurons Accumulate α-Synuclein and Are Susceptible to Oxidative Stress. *PLoS One* 6 (11), e26159. doi:10.1371/journal.pone.0026159

Chen, B. Z., Yu, S. L., Singh, S., Kao, L. P., Tsai, Z. Y., Yang, P. C., et al. (2011). Identification of microRNAs Expressed Highly in Pancreatic Islet-like Cell Clusters Differentiated from Human Embryonic Stem Cells. *Cell. Biol. Int.* 35 (1), 29–37. doi:10.1042/CBI20090081

Chen, T., Margariti, A., Kelaini, S., Cochrane, A., Guha, S. T., Hu, Y., et al. (2015). MicroRNA-199b Modulates Vascular Cell Fate during iPS Cell Differentiation by Targeting the Notch Ligand Jagged1 and Enhancing VEGF Signaling. *Stem Cells* 33 (5), 1405–1418. doi:10.1002/stem.1930

Chen, X., Li, X., Guo, J., Zhang, P., and Zeng, W. (2017). The Roles of microRNAs in Regulation of Mammalian Spermatogenesis. *J. Anim. Sci. Biotechnol.* 8, 35. doi:10.1186/s40104-017-0166-4

Dai, L., Tsai-Morris, C.-H., Sato, H., Villar, J., Kang, J.-H., Zhang, J., et al. (2011). Testis-specific miRNA-469 Up-Regulated in Gonadotropin-Regulated Testicular RNA Helicase (GRTH/DDX25)-null Mice Silences Transition Protein 2 and Protamine 2 Messages at Sites within Coding Region. *J. Biol. Chem.* 286 (52), 44306–44318. doi:10.1074/jbc.M111.282756

Di Bernardini, E., Campagnolo, P., Margariti, A., Zampetaki, A., Karamariti, E., Hu, Y., et al. (2014). Endothelial Lineage Differentiation from Induced Pluripotent Stem Cells Is Regulated by MicroRNA-21 and Transforming Growth Factor β2 (TGF-B2) Pathways. *J. Biol. Chem.* 289 (6), 3383–3393. doi:10.1074/jbc.M113.495531

Diekman, B. O., Christoforou, N., Willard, V. P., Sun, H., Sanchez-Adams, J., Leong, K. W., et al. (2012). Cartilage Tissue Engineering Using Differentiated and Purified Induced Pluripotent Stem Cells. *Proc. Natl. Acad. Sci. U.S.A.* 109 (47), 19172–19177. doi:10.1073/pnas.1210422109

Diez-Cuñado, M., Wei, K., Bushway, P. J., Maurya, M. R., Perera, R., Subramaniam, S., et al. (2018). miRNAs that Induce Human Cardiomyocyte Proliferation Converge on the Hippo Pathway. *Cell Rep.* 23 (7), 2168–2174. doi:10.1016/j.celrep.2018.04.049

Dimova, D. K., and Dyson, N. J. (2005). The E2F Transcriptional Network: Old Acquaintances with New Faces. *Oncogene* 24 (17), 2810–2826. doi:10.1038/sj.onc.1208612

Du, J.-K., Cong, B.-H., Yu, Q., Wang, H., Wang, L., Wang, C.-N., et al. (2016). Upregulation of microRNA-22 Contributes to Myocardial Ischemia-Reperfusion Injury by Interfering with the Mitochondrial Function. *Free Radic. Biol. Med.* 96, 406–417. doi:10.1016/j.freeradbiomed.2016.05.006

Dvash, T., and Benvenisty, N. (2004). Human Embryonic Stem Cells as a Model for Early Human Development. *Best Pract. Res. Clin. Obstetrics Gynaecol.* 18 (6), 929–940. doi:10.1016/j.bpobgyn.2004.06.005

Edbauer, D., Neilson, J. R., Foster, K. A., Wang, C.-F., Seeburg, D. P., Batterton, M. N., et al. (2010). Regulation of Synaptic Structure and Function by FMRP-Associated microRNAs miR-125b and miR-132. *Neuron* 65 (3), 373–384. doi:10.1016/j.neuron.2010.01.005

Eran, A., Li, J. B., Vatalaro, K., McCarthy, J., Rahimov, F., Collins, C., et al. (2013). Comparative RNA Editing in Autistic and Neurotypical Cerebella. *Mol. Psychiatry* 18 (9), 1041–1048. doi:10.1038/mp.2012.118

Eulalio, A., Mano, M., Ferro, M. D., Zentilin, L., Sinagra, G., Zacchigna, S., et al. (2012). Functional Screening Identifies miRNAs Inducing Cardiac Regeneration. *Nature* 492 (7429), 376–381. doi:10.1038/nature11739

Fabian, M. R., and Sonenberg, N. (2012). The Mechanics of miRNA-Mediated Gene Silencing: a Look under the Hood of miRISC. *Nat. Struct. Mol. Biol.* 19 (6), 586–593. doi:10.1038/nsmb.2296

Fernández-Pérez, D., Brieño-Enríquez, M. A., Isoler-Alcaraz, J., Larriba, E., and Del Mazo, J. (2018). MicroRNA Dynamics at the Onset of Primordial Germ and Somatic Cell Sex Differentiation during Mouse Embryonic Gonad Development. *Rna* 24 (3), 287–303. doi:10.1261/rna.062869.117

Ferreira, A. F., Calin, G. A., Picanço-Castro, V., Kashima, S., Covas, D. T., and de Castro, F. A. (2018). Hematopoietic Stem Cells from Induced Pluripotent Stem Cells - Considering the Role of microRNA as a Cell Differentiation Regulator. *J. Cell Sci.* 131 (4), jcs203018. doi:10.1242/jcs.203018

Fiedler, J., Jazbutyte, V., Kirchmaier, B. C., Gupta, S. K., Lorenzen, J., Hartmann, D., et al. (2011). MicroRNA-24 Regulates Vascularity after Myocardial Infarction. *Circulation* 124 (6), 720–730. doi:10.1161/circulationaha.111.039008

Fogel, G. B., Kai, Z. S., Zargar, S., Hinton, A., Jones, G. A., Wong, A. S., et al. (2015). MicroRNA Dynamics during Human Embryonic Stem Cell Differentiation to Pancreatic Endoderm. *Gene* 574 (2), 359–370. doi:10.1016/j.gene.2015.08.027

Gangaraju, V. K., and Lin, H. (2009). MicroRNAs: Key Regulators of Stem Cells. *Nat. Rev. Mol. Cell Biol.* 10 (2), 116–125. doi:10.1038/nrm2621

Gidlöf, O., Bader, K., Celik, S., Grossi, M., Nakagawa, S., Hirose, T., et al. (2020). Inhibition of the Long Non-coding RNA NEAT1 Protects Cardiomyocytes from Hypoxia *In Vitro* via Decreased Pri-miRNA Processing. *Cell Death Dis.* 11 (8), 677. doi:10.1038/s41419-020-02854-7

Giraldez, A. J., Cinalli, R. M., Glasner, M. E., Enright, A. J., Thomson, J. M., Baskerville, S., et al. (2005). MicroRNAs Regulate Brain Morphogenesis in Zebrafish. *Science* 308 (5723), 833–838. doi:10.1126/science.1109020

Green, M. J., Cairns, M. J., Wu, J., Dragovic, M., Jablensky, A., Tooney, P. A., et al. (2013). Genome-wide Supported Variant MIR137 and Severe Negative Symptoms Predict Membership of an Impaired Cognitive Subtype of Schizophrenia. *Mol. Psychiatry* 18 (7), 774–780. doi:10.1038/mp.2012.84

Greene, W. A., Muñiz, A., Plamper, M. L., Kaini, R. R., and Wang, H.-C. (2014). MicroRNA Expression Profiles of Human iPS Cells, Retinal Pigment

Epithelium Derived from iPS, and Fetal Retinal Pigment Epithelium. *JoVE* 88, e51589. doi:10.3791/51589

Guo, C., Deng, Y., Liu, J., and Qian, L. (2015). Cardiomyocyte-specific Role of miR-24 in Promoting Cell Survival. *J. Cell. Mol. Med.* 19 (1), 103–112. doi:10.1111/jcmm.12393

Hartmann, A., Hunot, S., Michel, P. P., Muriel, M.-P., Vyas, S., Faucheux, B. A., et al. (2000). Caspase-3: A Vulnerability Factor and Final Effector in Apoptotic Death of Dopaminergic Neurons in Parkinson's Disease. *Proc. Natl. Acad. Sci. U.S.A.* 97 (6), 2875–2880. doi:10.1073/pnas.040556597

Heman-Ackah, S. M., Hallegger, M., Rao, M. S., and Wood, M. J. A. (2013). RISC in PD: the Impact of microRNAs in Parkinson's Disease Cellular and Molecular Pathogenesis. *Front. Mol. Neurosci.* 6, 40. doi:10.3389/fnmol.2013.00040

Hermeking, H. (2012). MicroRNAs in the P53 Network: Micromanagement of Tumour Suppression. *Nat. Rev. Cancer* 12 (9), 613–626. doi:10.1038/nrc3318

Hornstein, E., and Shomron, N. (2006). Canalization of Development by microRNAs. *Nat. Genet.* 38 (6), S20–S24. doi:10.1038/ng1803

Hsu, R., Schofield, C. M., Dela Cruz, C. G., Jones-Davis, D. M., Blelloch, R., and Ullian, E. M. (2012). Loss of microRNAs in Pyramidal Neurons Leads to Specific Changes in Inhibitory Synaptic Transmission in the Prefrontal Cortex. *Mol. Cell. Neurosci.* 50 (3-4), 283–292. doi:10.1016/j.mcn.2012.06.002

Hu, S., Huang, M., Nguyen, P. K., Gong, Y., Li, Z., Jia, F., et al. (2011). Novel microRNA Prosurvival Cocktail for Improving Engraftment and Function of Cardiac Progenitor Cell Transplantation. *Circulation* 124 (11 Suppl. l), S27–S34. doi:10.1161/circulationaha.111.017954

Hu, X., Zhang, X., Dai, L., Zhu, J., Jia, Z., Wang, W., et al. (2013). Histone Deacetylase Inhibitor Trichostatin A Promotes the Osteogenic Differentiation of Rat Adipose-Derived Stem Cells by Altering the Epigenetic Modifications on Runx2 Promoter in a BMP Signaling-dependent Manner. *Stem Cells Dev.* 22 (2), 248–255. doi:10.1089/scd.2012.0105

Izzo, A., Manco, R., Cristofaro, T. d., Bonfiglio, F., Cicatiello, R., Mollo, N., et al. (2017). Overexpression of Chromosome 21 miRNAs May Affect Mitochondrial Function in the Hearts of Down Syndrome Fetuses. *Int. J. Genomics* 2017, 1–10. doi:10.1155/2017/8737649

Jeon, H. S., Lee, S. Y., Lee, E. J., Yun, S. C., Cha, E. J., Choi, E., et al. (2012). Combining microRNA-449a/b with a HDAC Inhibitor Has a Synergistic Effect on Growth Arrest in Lung Cancer. *Lung Cancer* 76 (2), 171–176. doi:10.1016/j.lungcan.2011.10.012

Jiang, C., Qin, B., Liu, G., Sun, X., Shi, H., Ding, S., et al. (2016). MicroRNA-184 Promotes Differentiation of the Retinal Pigment Epithelium by Targeting the AKT2/mTOR Signaling Pathway. *Oncotarget* 7 (32), 52340–52353. doi:10.18632/oncotarget.10566

Jimenez-Mateos, E. M., Engel, T., Merino-Serrais, P., McKiernan, R. C., Tanaka, K., Mouri, G., et al. (2012). Silencing microRNA-134 Produces Neuroprotective and Prolonged Seizure-Suppressive Effects. *Nat. Med.* 18 (7), 1087–1094. doi:10.1038/nm.2834

Joglekar, M. V., Joglekar, V. M., and Hardikar, A. A. (2009). Expression of Islet-specific microRNAs during Human Pancreatic Development. *Gene Expr. Patterns* 9 (2), 109–113. doi:10.1016/j.gep.2008.10.001

Katsaraki, K., Karousi, P., Artemaki, P. I., Scorilas, A., Pappa, V., Kontos, C. K., et al. (2021). MicroRNAs: Tiny Regulators of Gene Expression with Pivotal Roles in Normal B-Cell Development and B-Cell Chronic Lymphocytic Leukemia. *Cancers* 13 (4), 593. doi:10.3390/cancers13040593

Kredo-Russo, S., Mandelbaum, A. D., Ness, A., Alon, I., Lennox, K. A., Behlke, M. A., et al. (2012). Pancreas-enriched miRNA Refines Endocrine Cell Differentiation. *Development* 139 (16), 3021–3031. doi:10.1242/dev.080127

Krek, A., Grün, D., Poy, M. N., Wolf, R., Rosenberg, L., Epstein, E. J., et al. (2005). Combinatorial microRNA Target Predictions. *Nat. Genet.* 37 (5), 495–500. doi:10.1038/ng1536

Krol, J., Loedige, I., and Filipowicz, W. (2010). The Widespread Regulation of microRNA Biogenesis, Function and Decay. *Nat. Rev. Genet.* 11 (9), 597–610. doi:10.1038/nrg2843

Kuo, C.-H., Deng, J. H., Deng, Q., and Ying, S.-Y. (2012). A Novel Role of miR-302/367 in Reprogramming. *Biochem. Biophysical Res. Commun.* 417 (1), 11–16. doi:10.1016/j.bbrc.2011.11.058

Lagos-Quintana, M., Rauhut, R., Yalcin, A., Meyer, J., Lendeckel, W., and Tuschl, T. (2002). Identification of Tissue-specific microRNAs from Mouse. *Curr. Biol.* 12 (9), 735–739. doi:10.1016/s0960-9822(02)00809-6

Li, N., Jiang, D., He, Q., He, F., Li, Y., Deng, C., et al. (2020). microRNA-181c-5p Promotes the Formation of Insulin-Producing Cells from Human Induced Pluripotent Stem Cells by Targeting Smad7 and TGIF2. *Cell Death Dis.* 11 (6), 462. doi:10.1038/s41419-020-2668-9

Li, S., Wang, X., Gu, Y., Chen, C., Wang, Y., Liu, J., et al. (2015). Let-7 microRNAs Regenerate Peripheral Nerve Regeneration by Targeting Nerve Growth Factor. *Mol. Ther.* 23 (3), 423–433. doi:10.1038/mt.2014.220

Liang, J., Huang, W., Cai, W., Wang, L., Guo, L., Paul, C., et al. (2017). Inhibition of microRNA-495 Enhances Therapeutic Angiogenesis of Human Induced Pluripotent Stem Cells. *Stem Cells* 35 (2), 337–350. doi:10.1002/stem.2477

Liao, X., Xue, H., Wang, Y.-C., Nazor, K. L., Guo, S., Trivedi, N., et al. (2013). Matched miRNA and mRNA Signatures from a hESC-Based *In Vitro* Model of Pancreatic Differentiation Reveal Novel Regulatory Interactions. *J. Cell Sci.* 126 (Pt 17), 3848–3861. doi:10.1242/jcs.123570

Liu, B., Li, J., and Cairns, M. J. (2014). Identifying miRNAs, Targets and Functions. *Briefings Bioinforma.* 15 (1), 1–19. doi:10.1093/bib/bbs075

Liu, J., Githinji, J., McLaughlin, B., Wilczek, K., and Nolta, J. (2012). Role of miRNAs in Neuronal Differentiation from Human Embryonic Stem Cell-Derived Neural Stem Cells. *Stem Cell Rev Rep* 8 (4), 1129–1137. doi:10.1007/s12015-012-9411-6

Liu, T., Hou, L., Zhao, Y., and Huang, Y. (2015a). Epigenetic Silencing of HDAC1 by miR-449a Upregulates Runx2 and Promotes Osteoblast Differentiation. *Int. J. Mol. Med.* 35 (1), 238–246. doi:10.3892/ijmm.2014.2004

Liu, Y., Niu, M., Yao, C., Hai, Y., Yuan, Q., Liu, Y., et al. (2015b). Fractionation of Human Spermatogenic Cells Using STA-PUT Gravity Sedimentation and Their miRNA Profiling. *Sci. Rep.* 5, 8084. doi:10.1038/srep08084

Lo Sardo, V., Ferguson, W., Erikson, G. A., Topol, E. J., Baldwin, K. K., and Torkamani, A. (2017). Influence of Donor Age on Induced Pluripotent Stem Cells. *Nat. Biotechnol.* 35 (1), 69–74. doi:10.1038/nbt.3749

Lopez, J. P., Fiori, L. M., Cruceanu, C., Lin, R., Labonte, B., Cates, H. M., et al. (2017). MicroRNAs 146a/b-5 and 425-3p and 24-3p Are Markers of Antidepressant Response and Regulate MAPK/Wnt-system Genes. *Nat. Commun.* 8, 15497. doi:10.1038/ncomms15497

Lu, T. X., and Rothenberg, M. E. (2018). MicroRNA. *J. Allergy Clin. Immunol.* 141 (4), 1202–1207. doi:10.1016/j.jaci.2017.08.034

Luo, Y., Chen, Y., Zhang, M., Ma, X., Zhu, D., and Chen, Y. (2021a). Generation of an Induced Pluripotent Stem Cell Line GZHMCi008-A Derived from a Patient with SRY-Positive 46,XX Testicular Disorder of Sex Development. *Stem Cell Res.* 57, 102583. doi:10.1016/j.scr.2021.102583

Luo, Y., Li, J., Zhu, D., Fan, Y., Li, S., and Sun, X. (2014). High-resolution Chromosomal Microarray Analysis of Early-Stage Human Embryonic Stem Cells Reveals an Association between X Chromosome Instability and Skewed X Inactivation. *Cell Biosci.* 4 (1), 74. doi:10.1186/2045-3701-4-74

Luo, Y., Wu, S., Yuan, J., Zhou, H., Zhong, Y., Zhang, M., et al. (2021b). Evaluation of Prognostic Factors for Clinical Pregnancy Rate Following Artificial Insemination by Husband in the Chinese Population. *Front. Med.* 8, 638560. doi:10.3389/fmed.2021.638560

Luo, Y., Xu, X., An, X., Sun, X., Wang, S., and Zhu, D. (2016). Targeted Inhibition of the miR-199a/214 Cluster by CRISPR Interference Augments the Tumor Tropism of Human Induced Pluripotent Stem Cell-Derived Neural Stem Cells under Hypoxic Condition. *Stem Cells Int.* 2016, 1–8. doi:10.1155/2016/3598542

Luo, Y., Zhang, M., Chen, Y., Chen, Y., and Zhu, D. (2021c). Application of Human Induced Pluripotent Stem Cell-Derived Cellular and Organoid Models for COVID-19 Research. *Front. Cell Dev. Biol.* 9, 720099. doi:10.3389/fcell.2021.720099

Luo, Y., and Zhu, D. (2014). Combinatorial Control of Transgene Expression by Hypoxia-Responsive Promoter and Microrna Regulation for Neural Stem Cell-Based Cancer Therapy. *BioMed Res. Int.* 2014, 1–9. doi:10.1155/2014/751397

Luo, Y., Zhu, D., Du, R., Gong, Y., Xie, C., Xu, X., et al. (2015a). Uniparental Disomy of the Entire X Chromosome in Turner Syndrome Patient-specific Induced Pluripotent Stem Cells. *Cell Discov.* 1, 15022. doi:10.1038/celldisc.2015.22

Luo, Y., Zhu, D., Lam, D. H., Huang, J., Tang, Y., Luo, X., et al. (2015b). A Double-Switch Cell Fusion-Inducible Transgene Expression System for Neural Stem Cell-Based Antiglioma Gene Therapy. *Stem Cells Int.* 2015, 1–8. doi:10.1155/2015/649080

Luo, Y., Zhu, D., Xu, X., Ge, L., Sun, X., Chen, G., et al. (2018). Generation of an Induced Pluripotent Stem Cell Line from an Adult Male with 45,X/46,XY Mosaicism. *Stem Cell Res.* 27, 42–45. doi:10.1016/j.scr.2018.01.003

Lynn, F. C., Skewes-Cox, P., Kosaka, Y., McManus, M. T., Harfe, B. D., and German, M. S. (2007). MicroRNA Expression Is Required for Pancreatic Islet Cell Genesis in the Mouse. *Diabetes* 56 (12), 2938–2945. doi:10.2337/db07-0175

McGowan, H., Mirabella, V. R., Hamod, A., Karakhanyan, A., Mlynaryk, N., Moore, J. C., et al. (2018). hsa-let-7c miRNA Regulates Synaptic and Neuronal Function in Human Neurons. *Front. Synaptic Neurosci.* 10, 19. doi:10.3389/fnsyn.2018.00019

Mogi, M., Togari, A., Kondo, T., Mizuno, Y., Komure, O., Kuno, S., et al. (2000). Caspase Activities and Tumor Necrosis Factor Receptor R1 (P55) Level Are Elevated in the Substantia Nigra from Parkinsonian Brain. *J. Neural Transm.* 107 (3), 335–341. doi:10.1007/s007020050028

Mukai, A., Otsuki, Y., Ito, E., Fujita, T., Ueno, M., Maeda, T., et al. (2021). Mitochondrial miRNA494-3p in Extracellular Vesicles Participates in Cellular Interplay of iPS-Derived Human Retinal Pigment Epithelium with Macrophages. *Exp. Eye Res.* 208, 108621. doi:10.1016/j.exer.2021.108621

Murakami, Y., Tamori, A., Itami, S., Tanahashi, T., Toyoda, H., Tanaka, M., et al. (2013). The Expression Level of miR-18b in Hepatocellular Carcinoma Is Associated with the Grade of Malignancy and Prognosis. *BMC Cancer* 13, 99. doi:10.1186/1471-2407-13-99

Naguibneva, I., Ameyar-Zazoua, M., Polesskaya, A., Ait-Si-Ali, S., Groisman, R., Souidi, M., et al. (2006). The microRNA miR-181 Targets the Homeobox Protein Hox-A11 during Mammalian Myoblast Differentiation. *Nat. Cell Biol.* 8 (3), 278–284. doi:10.1038/ncb1373

Nana-Sinkam, S. P., and Croce, C. M. (2013). Clinical Applications for microRNAs in Cancer. *Clin. Pharmacol. Ther.* 93 (1), 98–104. doi:10.1038/clpt.2012.192

Nishikura, K. (2010). Functions and Regulation of RNA Editing by ADAR Deaminases. *Annu. Rev. Biochem.* 79, 321–349. doi:10.1146/annurev-biochem-060208-105251

Nishimura, R., Wakabayashi, M., Hata, K., Matsubara, T., Honma, S., Wakisaka, S., et al. (2012). Osterix Regulates Calcification and Degradation of Chondrogenic Matrices through Matrix Metalloproteinase 13 (MMP13) Expression in Association with Transcription Factor Runx2 during Endochondral Ossification. *J. Biol. Chem.* 287 (40), 33179–33190. doi:10.1074/jbc.M111.337063

Nomura, T., Kimura, M., Horii, T., Morita, S., Soejima, H., Kudo, S., et al. (2008). MeCP2-dependent Repression of an Imprinted miR-184 Released by Depolarization. *Hum. Mol. Genet.* 17 (8), 1192–1199. doi:10.1093/hmg/ddn011

Okamoto, H., Matsumi, Y., Hoshikawa, Y., Takubo, K., Ryoke, K., and Shiota, G. (2012). Involvement of microRNAs in Regulation of Osteoblastic Differentiation in Mouse Induced Pluripotent Stem Cells. *PLoS One* 7 (8), e43800. doi:10.1371/journal.pone.0043800

Ozeki, N., Hase, N., Hiyama, T., Yamaguchi, H., Kawai-Asano, R., Nakata, K., et al. (2017). RETRACTED: MicroRNA-211 and Autophagy-Related Gene 14 Signaling Regulate Osteoblast-like Cell Differentiation of Human Induced Pluripotent Stem Cells. *Exp. Cell Res.* 352 (1), 63–74. doi:10.1016/j.yexcr.2017.01.018

Pan, H., and Zhu, L. (2018). RETRACTED: Angelica Sinensis Polysaccharide Protects Rat Cardiomyocytes H9c2 from Hypoxia-Induced Injury by Down-Regulation of microRNA-22. *Biomed. Pharmacother.* 106, 225–231. doi:10.1016/j.biopha.2018.06.120

Paschou, M., Paraskevopoulou, M. D., Vlachos, I. S., Koukouraki, P., Hatzigeorgiou, A. G., and Doxakis, E. (2012). miRNA Regulons Associated with Synaptic Function. *PLoS One* 7 (10), e46189. doi:10.1371/journal.pone.0046189

Pera, R., Simón, C., and Medrano, J. (2013). Germ Cell Differentiation from Pluripotent Cells. *Semin. Reprod. Med.* 31 (1), 014–023. doi:10.1055/s-0032-1331793

Porciuncula, A., Zapata, N., Guruceaga, E., Agirre, X., Barajas, M., and Prosper, F. (2013). MicroRNA Signatures of iPSCs and Endoderm-Derived Tissues. *Gene Expr. Patterns* 13 (1-2), 12–20. doi:10.1016/j.gep.2012.08.002

Pouton, C. W., and Haynes, J. M. (2007). Embryonic Stem Cells as a Source of Models for Drug Discovery. *Nat. Rev. Drug Discov.* 6 (8), 605–616. doi:10.1038/nrd2194

Poy, M. N., Eliasson, L., Krutzfeldt, J., Kuwajima, S., Ma, X., MacDonald, P. E., et al. (2004). A Pancreatic Islet-specific microRNA Regulates Insulin Secretion. *Nature* 432 (7014), 226–230. doi:10.1038/nature03076

Poy, M. N., Hausser, J., Trajkovski, M., Braun, M., Collins, S., Rorsman, P., et al. (2009). miR-375 Maintains Normal Pancreatic α- and β-cell Mass. *Proc. Natl. Acad. Sci. U.S.A.* 106 (14), 5813–5818. doi:10.1073/pnas.0810550106

Qian, L., Van Laake, L. W., Huang, Y., Liu, S., Wendland, M. F., and Srivastava, D. (2011). miR-24 Inhibits Apoptosis and Represses Bim in Mouse Cardiomyocytes. *J. Exp. Med.* 208 (3), 549–560. doi:10.1084/jem.20101547

Reinhardt, P., Schmid, B., Burbulla, L. F., Schöndorf, D. C., Wagner, L., Glatza, M., et al. (2013). Genetic Correction of a LRRK2 Mutation in Human iPSCs Links Parkinsonian Neurodegeneration to ERK-dependent Changes in Gene Expression. *Cell Stem Cell* 12 (3), 354–367. doi:10.1016/j.stem.2013.01.008

Romero, Y., Meikar, O., Papaioannou, M. D., Conne, B., Grey, C., Weier, M., et al. (2011). Dicer1 Depletion in Male Germ Cells Leads to Infertility Due to Cumulative Meiotic and Spermiogenic Defects. *PLoS One* 6 (10), e25241. doi:10.1371/journal.pone.0025241

Roush, S., and Slack, F. J. (2008). The Let-7 Family of microRNAs. *Trends Cell Biol.* 18 (10), 505–516. doi:10.1016/j.tcb.2008.07.007

Rupaimoole, R., and Slack, F. J. (2017). MicroRNA Therapeutics: towards a New Era for the Management of Cancer and Other Diseases. *Nat. Rev. Drug Discov.* 16 (3), 203–222. doi:10.1038/nrd.2016.246

Ryan, D. G., Oliveira-Fernandes, M., and Lavker, R. M. (2006). MicroRNAs of the Mammalian Eye Display Distinct and Overlapping Tissue Specificity. *Mol. Vis.* 12, 1175–1184.

Saito, S., Lin, Y.-C., Murayama, Y., Nakamura, Y., Eckner, R., Niemann, H., et al. (2015). Retracted Article: *In Vitro* Derivation of Mammalian Germ Cells from Stem Cells and Their Potential Therapeutic Application. *Cell. Mol. Life Sci.* 72 (23), 4545–4560. doi:10.1007/s00018-015-2020-1

Sánchez-Danés, A., Richaud-Patin, Y., Carballo-Carbajal, I., Jiménez-Delgado, S., Caig, C., Mora, S., et al. (2012). Disease-specific Phenotypes in Dopamine Neurons from Human iPS-based Models of Genetic and Sporadic Parkinson's Disease. *EMBO Mol. Med.* 4 (5), 380–395. doi:10.1002/emmm.201200215

Sanjana, N. E., Levanon, E. Y., Hueske, E. A., Ambrose, J. M., and Li, J. B. (2012). Activity-dependent A-To-I RNA Editing in Rat Cortical Neurons. *Genetics* 192 (1), 281–287. doi:10.1534/genetics.112.141200

Schwamborn, J. C., Berezikov, E., and Knoblich, J. A. (2009). The TRIM-NHL Protein TRIM32 Activates microRNAs and Prevents Self-Renewal in Mouse Neural Progenitors. *Cell* 136 (5), 913–925. doi:10.1016/j.cell.2008.12.024

Shaer, A., Azarpira, N., and Karimi, M. H. (2014). Differentiation of Human Induced Pluripotent Stem Cells into Insulin-like Cell Clusters with miR-186 and miR-375 by Using Chemical Transfection. *Appl. Biochem. Biotechnol.* 174 (1), 242–258. doi:10.1007/s12010-014-1045-5

Song, Y., Zhang, C., Zhang, J., Jiao, Z., Dong, N., Wang, G., et al. (2019). Localized Injection of miRNA-21-Enriched Extracellular Vesicles Effectively Restores Cardiac Function after Myocardial Infarction. *Theranostics* 9 (8), 2346–2360. doi:10.7150/thno.29945

Stadtfeld, M., and Hochedlinger, K. (2010). Induced Pluripotency: History, Mechanisms, and Applications. *Genes Dev.* 24 (20), 2239–2263. doi:10.1101/gad.1963910

Sun, H., Shi, K., Xie, D., Zhang, H., and Yu, B. (2019). Long Noncoding RNA C2dat1 Protects H9c2 Cells against Hypoxia Injury by Downregulating miR-22. *J. Cell. Physiology* 234 (11), 20623–20633. doi:10.1002/jcp.28667

Takahashi, K., and Yamanaka, S. (2006). Induction of Pluripotent Stem Cells from Mouse Embryonic and Adult Fibroblast Cultures by Defined Factors. *Cell* 126 (4), 663–676. doi:10.1016/j.cell.2006.07.024

Vargel, Ö., Zhang, Y., Kosim, K., Ganter, K., Foehr, S., Mardenborough, Y., et al. (2016). Activation of the TGFβ Pathway Impairs Endothelial to Haematopoietic Transition. *Sci. Rep.* 6, 21518. doi:10.1038/srep21518

Wang, H.-C., Greene, W. A., Kaini, R. R., Shen-Gunther, J., Chen, H.-I. H., Car, H., et al. (2014). Profiling the microRNA Expression in Human iPS and iPS-Derived Retinal Pigment Epithelium. *Cancer Inf.* 13s5 (Suppl. 5), CIN.S14074–35. doi:10.4137/cin.S14074

Wang, L., and Xu, C. (2015). Role of microRNAs in Mammalian Spermatogenesis and Testicular Germ Cell Tumors. *Reproduction* 149 (3), R127–R137. doi:10.1530/rep-14-0239

Wei, R., Yang, J., Liu, G.-q., Gao, M.-j., Hou, W.-f., Zhang, L., et al. (2013). Dynamic Expression of microRNAs during the Differentiation of Human

Embryonic Stem Cells into Insulin-Producing Cells. *Gene* 518 (2), 246–255. doi:10.1016/j.gene.2013.01.038

Weick, J. P., Held, D. L., Bonadurer, G. F., 3rd, Doers, M. E., Liu, Y., Maguire, C., et al. (2013). Deficits in Human Trisomy 21 iPSCs and Neurons. *Proc. Natl. Acad. Sci. U.S.A.* 110 (24), 9962–9967. doi:10.1073/pnas.1216575110

West, J. A., Viswanathan, S. R., Yabuuchi, A., Cunniff, K., Takeuchi, A., Park, I.-H., et al. (2009). A Role for Lin28 in Primordial Germ-Cell Development and Germ-Cell Malignancy. *Nature* 460 (7257), 909–913. doi:10.1038/nature08210

Weston, M. D., Pierce, M. L., Rocha-Sanchez, S., Beisel, K. W., and Soukup, G. A. (2006). MicroRNA Gene Expression in the Mouse Inner Ear. *Brain Res.* 1111 (1), 95–104. doi:10.1016/j.brainres.2006.07.006

Xu, F., Yang, J., Shang, J., Lan, F., Li, M., Shi, L., et al. (2019a). MicroRNA-302d Promotes the Proliferation of Human Pluripotent Stem Cell-Derived Cardiomyocytes by Inhibiting LATS2 in the Hippo Pathway. *Clin. Sci. (Lond)* 133 (13), 1387–1399. doi:10.1042/cs20190099

Xu, Y., Huang, Y., Guo, Y., Xiong, Y., Zhu, S., Xu, L., et al. (2019b). microRNA-690 Regulates Induced Pluripotent Stem Cells (iPSCs) Differentiation into Insulin-Producing Cells by Targeting Sox9. *Stem Cell Res. Ther.* 10 (1), 59. doi:10.1186/s13287-019-1154-8

Yang, D., Wang, J., Xiao, M., Zhou, T., and Shi, X. (2016). Role of Mir-155 in Controlling HIF-1α Level and Promoting Endothelial Cell Maturation. *Sci. Rep.* 6, 35316. doi:10.1038/srep35316

Yang, J., Cai, J., Zhang, Y., Wang, X., Li, W., Xu, J., et al. (2010). Induced Pluripotent Stem Cells Can Be Used to Model the Genomic Imprinting Disorder Prader-Willi Syndrome. *J. Biol. Chem.* 285 (51), 40303–40311. doi:10.1074/jbc.M110.183392

Yu, F.-X., and Guan, K.-L. (2013). The Hippo Pathway: Regulators and Regulations. *Genes Dev.* 27 (4), 355–371. doi:10.1101/gad.210773.112

Zeng, Z.-L., Lin, X.-l., Tan, L.-L., Liu, Y.-M., Qu, K., and Wang, Z. (2018). MicroRNAs: Important Regulators of Induced Pluripotent Stem Cell Generation and Differentiation. *Stem Cell Rev Rep* 14 (1), 71–81. doi:10.1007/s12015-017-9785-6

Zhang, B., Pan, X., Cobb, G. P., and Anderson, T. A. (2007). microRNAs as Oncogenes and Tumor Suppressors. *Dev. Biol.* 302 (1), 1–12. doi:10.1016/j.ydbio.2006.08.028

Zhang, D., Liu, X., Peng, J., He, D., Lin, T., Zhu, J., et al. (2014a). Potential Spermatogenesis Recovery with Bone Marrow Mesenchymal Stem Cells in an Azoospermic Rat Model. *Ijms* 15 (8), 13151–13165. doi:10.3390/ijms150813151

Zhang, Y., Chen, K., Sloan, S. A., Bennett, M. L., Scholze, A. R., O'Keeffe, S., et al. (2014b). An RNA-Sequencing Transcriptome and Splicing Database of Glia, Neurons, and Vascular Cells of the Cerebral Cortex. *J. Neurosci.* 34 (36), 11929–11947. doi:10.1523/jneurosci.1860-14.2014

Zhao, D., Lin, M., Chen, J., Pedrosa, E., Hrabovsky, A., Fourcade, H. M., et al. (2015). MicroRNA Profiling of Neurons Generated Using Induced Pluripotent Stem Cells Derived from Patients with Schizophrenia and Schizoaffective Disorder, and 22q11.2 Del. *PLoS One* 10 (7), e0132387. doi:10.1371/journal.pone.0132387

Zhu, D., Chen, C., Purwanti, Y. I., Du, S., Lam, D. H., Wu, C., et al. (2014). Induced Pluripotent Stem Cell-Derived Neural Stem Cells Transduced with Baculovirus Encoding CD40 Ligand for Immunogene Therapy in Mouse Models of Breast Cancer. *Hum. Gene Ther.* 25 (8), 747–758. doi:10.1089/hum.2013.160

Zhu, D., Lam, D. H., Purwanti, Y. I., Goh, S. L., Wu, C., Zeng, J., et al. (2013). Systemic Delivery of Fusogenic Membrane Glycoprotein-Expressing Neural Stem Cells to Selectively Kill Tumor Cells. *Mol. Ther.* 21 (8), 1621–1630. doi:10.1038/mt.2013.123

Zhu, D., Luo, Y., Zhou, H., Wu, S., Tang, X., Zhou, G., et al. (2022). *Chlamydia trachomatis* Infection in the Genital Tract Is Associated with Inflammation and Hypospermia in the Infertile Male of China. *Asian J. Androl.* 24 (1), 56–61. doi:10.4103/aja.aja_54_21

Zou, Z., Ocaya, P. A., Sun, H., Kuhnert, F., and Stuhlmann, H. (2010). Targeted Vezf1 -Null Mutation Impairs Vascular Structure Formation during Embryonic Stem Cell Differentiation. *Atvb* 30 (7), 1378–1388. doi:10.1161/atvbaha.109.200428

Conflict of Interest: The authors declare that the research was conducted in the absence of any commercial or financial relationships that could be construed as a potential conflict of interest.

Publisher's Note: All claims expressed in this article are solely those of the authors and do not necessarily represent those of their affiliated organizations, or those of the publisher, the editors and the reviewers. Any product that may be evaluated in this article, or claim that may be made by its manufacturer, is not guaranteed or endorsed by the publisher.

frontiers | Frontiers in Genetics

REVIEW
published: 01 June 2022
doi: 10.3389/fgene.2022.892009

Long Noncoding RNA LINC00467: Role in Various Human Cancers

Di Wu†, *Rongfei Li*†, *Jingyu Liu*, *Changcheng Zhou* and *Ruipeng Jia**

Department of Urology, Nanjing First Hospital, Nanjing Medical University, Nanjing, China

Intricate genetic mutations promote the progression of different cancer types. Long noncoding RNAs (lncRNAs) have been widely demonstrated to participate in the genomic activities of various human cancers. Long intergenic non-coding RNA 467 (LINC00467) is an upregulated lncRNA in diverse diseases, especially in several types of cancers. Functional experiments of LINC00467 revealed that LINC00467 overexpression enhanced cell chemoresistance, proliferation, migration, and invasion in several types of cancers. Moreover, overexpressed LINC00467 was associated with a poor clinical prognosis. The present evidence suggests that LINC00467 may serve as a promising prognostic indicator and become a novel cancer therapeutic target. In this review, we introduce the biologic functions of lncRNAs and describe the molecular mechanism and clinical significance of LINC00467 in detail.

Keywords: LINC00467, microrna sponge, long noncoding RNAs, cancers, biomarker, review

OPEN ACCESS

Edited by:
Detu Zhu,
Weill Cornell Medicine, United States

Reviewed by:
Wang Ma,
First Affiliated Hospital of Zhengzhou University, China
Yumin Wang,
Central South University, China

****Correspondence:***
Ruipeng Jia
ruipengj@163.com

†These authors have contributed equally to this work and share the first authorship

Specialty section:
This article was submitted to RNA, a section of the journal Frontiers in Genetics

Received: *08 March 2022*
Accepted: *16 May 2022*
Published: *01 June 2022*

Citation:
Wu D, Li R, Liu J, Zhou C and Jia R (2022) Long Noncoding RNA LINC00467: Role in Various Human Cancers. Front. Genet. 13:892009. doi: 10.3389/fgene.2022.892009

1 INTRODUCTION

Cancer, with high morbidity and mortality, has long been known as a primary life-threatening disease worldwide and imposes a huge economic and social burden on every country. (Sung et al., 2021) In recent years, the life expectancy of patients with cancer has greatly increased owing to the earlier detection and appropriate therapies. However, several cancer complications such as tumor metastasis, drug resistance, and cancer recurrence hinder the management of this disease and contribute to the high mortality associated with it. (Barik et al., 2021) Although traditionally most research about these processes has focused on the role of protein-coding RNAs (Slack and Chinnaiyan, 2019), recent efforts have focused on non-coding RNAs, which are now known to be regulatory molecules that mediate cellular processes and play an important role in tumorigenesis and cancer development. (Anastasiadou et al., 2018)

Long non-coding RNAs (lncRNAs) are RNA molecules longer than 200 nucleotides and comprise the main category of non-coding RNAs (Palazzo and Koonin, 2020) According to the latest release of the database NONCODE, the number of human lncRNAs is approximately 170,000, which is much larger than that of protein-coding RNAs. (Derrien et al., 2012; Zhao et al., 2021) Most lncRNAs are transcribed by RNA polymerase II, and then are capped at the 5′ end, ploy A tail added at the 3′ end, and edited to form biologically functional lncRNAs. (Statello et al., 2021) According to classification based on function, lncRNAs can be divided into activating ncRNAs, competing endogenous RNA (ceRNAs), and precursors for shorter functional RNA. (St Laurent et al., 2015) Most lncRNAs act as ceRNAs. The "competitive endogenous RNA hypothesis," which was put forward by Salmena et al., in 2011, proposes that lncRNAs regulate mRNA expression by targeting miRNAs through homologous miRNA response elements (MREs). By binding to MREs present in miRNAs, lncRNAs inactive them, a process known as the "molecular sponge effect", suppressing the inhibitory effect of the targeted miRNA on mRNA expression. (Salmena et al., 2011) Numerous

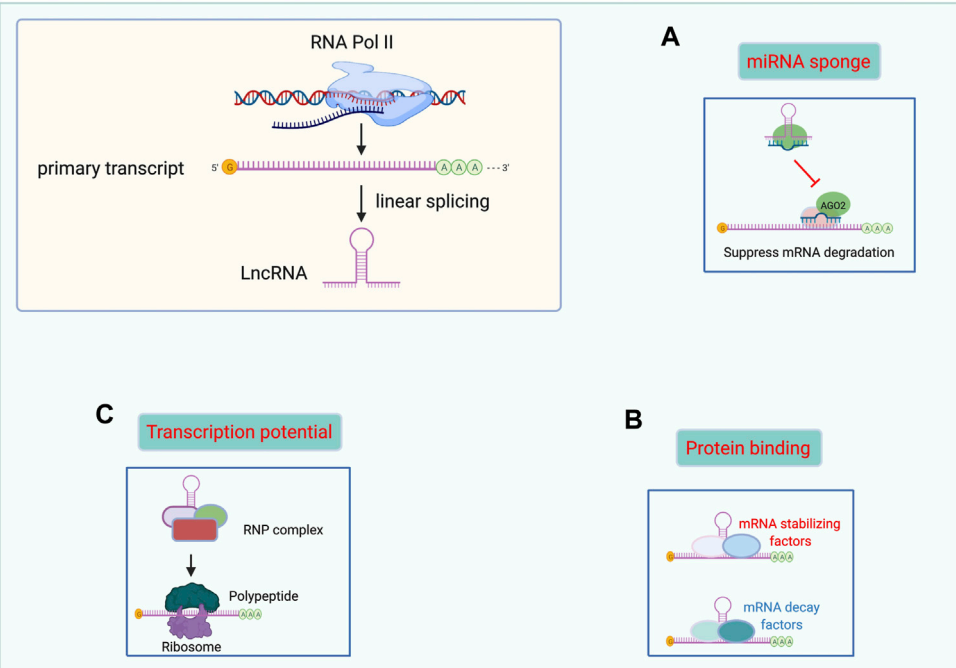

FIGURE 1 | Functional mechanisms of lncRNAs. lncRNAs can act as miRNAs sponges **(A)**, binding with proteins **(B)**, and templates for polypeptide translation **(C)**. Abbreviations: lncRNA, Long non-coding RNA. miRNAs, microRNAs. RNP complex, ribonucleoprotein complex.

posterior studies have confirmed the lncRNA-miRNA-mRNA axis established by this hypothesis, as well as the role of this axis in tumor development.

Long intergenic non-coding RNA (lincRNA) is defined as 'lncRNA not overlapping a protein-coding transcript'. (Ransohoff et al., 2018) LINC00467, a newly defined lincRNA, is located at Chromosome 1: 211,382,736-211,444,093 (GRCh38/hg38) with the length of 61,358 bases (www.genecards.org). Moreover, it encodes 28 different transcripts (www.ensembl.org). In addition to being upregulated in normal human testis and kidney tissues (Fagerberg et al., 2014), recent studies have confirmed that LINC00467 is overexpressed in various types of human tumor tissues and plays an important role in regulating gene transcription, tumor initiation, and progression.

In this review, we comprehensively summarize the different functional roles of the newly found LINC00467 in the progression of various cancers. LINC00467 mainly functions as a ceRNA and leads to the overexpression of relevant genes by sponging the corresponding miRNAs. Additionally, we present the clinical significance of LINC00467 in several human cancers and discuss its potential clinical application as an early diagnostic and prognostic biomarker and novel therapeutic target.

2 FUNCTION OF LNCRNAS

Proteins are universally acknowledged to be the basis of life. However, "non-protein-coding" is not the same as being useless. Mounting studies have demonstrated the indispensable and promising role of lncRNAs in many diseases. Herein, we summarized the main functional mechanisms of lncRNAs in the following paragraphs. Moreover, we made a figure to illustrate the function of lncRNAs more graphically. (**Figure 1**).

2.1 Acting as miRNA Sponges

The sponging of miRNAs is one of the most studied mechanisms of action of lncRNAs. As we know, some miRNAs could effectively bind to certain mRNAs in the presence of MRE, a "seed sequence" containing two to eight nucleotides. Interestingly, many lncRNAs, including lincRNAs, pseudogene transcripts, and circular RNAs share the same MRE with certain miRNAs. Then, a series of miRNAs were bound with these ceRNAs rather than mRNAs. As a result, the inhibitory effect of targeted binding of miRNA to mRNA was attenuated by lncRNAs. Through this regulatory mechanism, lncRNAs play an important role in the biological progression of many cancers. (Kazimierczyk et al., 2020) In prostate cancer, LINC01679 has been shown to inhibit cell proliferation, invasion, and tumor growth, and promote cell apoptosis *in vivo* and *in vitro* by competitively binding to miR-3150a-3p as well as by regulating the downstream gene *SLC17A9*. (Mi et al., 2021) What's more, recent evidence indicates that one lncRNAs may have several MREs to sponge different miRNAs. In acute myeloid leukemia (AML), the lncRNA MIR17HG sponges miR-21 to further promote homoharringtonine-induced AML cell apoptosis. (Yan et al., 2022) Besides MIR17HG also inhibits non-small cell lung cancer *via* functioning as a ceRNA of miR-142-3p. (Wei et al., 2020) Through this regulatory mode, lncRNAs are widely involved in the course of various diseases, including thyroid cancer (Guo et al.,

2021), renal fibrosis (Tang et al., 2021), atherosclerotic plaques (Ann et al., 2021), among others.

2.2 Interaction With Proteins

Due to their large size of hundreds, even thousands of nucleotides, lncRNAs have been shown to function as guides, signals, decoys, and scaffolds for many different proteins. (Kazimierczyk et al., 2020) Mounting evidence notes that many lncRNAs can directly bind or form complexes with some key proteins to play diverse regulatory roles including transcription and splicing, as well as gene expression. (Wu et al., 2018) A study on gallbladder cancer revealed that the lncRNA RP11-147L13.8 serves as a tumor-suppressing gene by interacting with c-Jun protein via binding to its bZIP domain (a DNA-binding and dimerization domain) and suppressing c-Jun-ser73 phosphorylation. (Zheng et al., 2021) Interestingly, another study on gallbladder cancer found that HuR protein specifically binds with lncRNAs-HGBC within the 1759–1906 nt-long region and enhances the stabilization of lncRNAs-HGBC (Hu et al., 2019) Moreover, the lncRNA AK137033 was found to interact with mRNA Sfrp2 and HuR, forming the AK137033-Sfrp2-HuR complex, which contributes to the inhibition of cardiac fibrosis. (Hao et al., 2019)

2.3 Encoding Polypeptides

LncRNA was named as 'non-coding RNA' for lack of an open reading frame. However, recent research has shown that some lncRNAs can encode polypeptides that are usually shorter than 100 amino acids and widely involved in tumorigenesis, metabolism, inflammation, and signal transduction pathways. (Ye et al., 2020) Pang et al (Pang et al., 2020) reported that the lncRNA Linc00998 encodes the micro peptide SMIM30, which facilitated HCC cell proliferation and migration and was associated with a poorer survival rate in HCC patients. Similarly, Linc00617 encodes BNLN, which maintains the stabilization of islet β cells and raises insulin secretion in islets from humans. (Li M. et al., 2021) In addition, Niu et al (Niu et al., 2020) demonstrated that the lncRNA MIR155HG encodes another micro peptide, named miPEP155, which functions as an important regulator of antigen presentation as well as a suppressor of inflammatory diseases. This new functional mechanism of lncRNAs may become a new hotspot for future research on cancer biomarkers and drug development.

3 CLINICAL SIGNIFICANCE OF LINC00467 IN VARIOUS HUMAN CANCERS

Various studies have investigated the expression of LINC00467 in different tumor tissues and corresponding controls (mostly adjacent non-malignant tissues). All studies (except that by Cai et al. (2019)) indicated that the expression of LINC00467 was upregulated in a variety of cancer tissues compared to the control group. In addition, numerous studies of different tumor types have assessed the prognosis of patients with high or low LINC00467 expression level and its association with prognostic features such as TNM (Tumor, Node, Metastasis) staging, cell differentiation, disease-free survival, and overall survival. Patients with high expression of LINC00467 tend to have advanced TNM stage, poorer cell differentiation, and shorter disease-free survival and overall survival. The details of relevant studies have been summarized in **Table 1**.

4 MOLECULAR MECHANISM OF LINC00467 IN DIVERSE HUMAN CANCERS

To date, dozens of studies have reported the effects of LINC00467 in various human cancer cell lines, including its impact on tumor cell proliferation, invasion, migration, and apoptosis (**Table 2**). In the following sections, we elaborate on the functional roles and molecular mechanism of LINC00467 in various cancers. Additionally, another figure was made to illustrate these molecular mechanisms of LINC00467. (**Figure 2**)

4.1 Function as a ceRNA

Based on the currently published research, the most reported mechanism is that LINC00467 functions as a ceRNA of a series of miRNAs. LINC00467 forms the regulatory axis of LINC00467-miRNA-mRNA by regulating downstream targeted coding genes through competitive inhibition with some certain miRNA. Through this regulatory pattern, LINC00467 could participate in the initiation and development of cancers.

4.1.1 Acute Myeloid Leukemia

In the United States, AML accounts for approximately one-third of all leukemias diagnosed and 1.2% of all annual new cancer diagnoses (Pelcovits and Niroula, 2020) The role of LINC00467 in AML pathogenesis was recently researched by Lu et al. (2021) The results of this study showed that LINC00467 expression was associated with the malignant phenotypes of AML cells and that it acted as a ceRNA of miR-339. SKI is a gene regulated by miR-339 that has been reported to promote AML development. Further investigation of the underlying mechanism verified that treatment with a miR-339 inhibitor largely diminished the influence of LINC00467 knockdown on AML cells. These results suggest that targeting the LINC00467/miR-339/SKI axis could be a suitable approach for the treatment of AML.

4.1.2 Non-Small Cell Lung Cancer

NSCLC accounts for nearly 85% of lung cancers (Herbst et al., 2008; Yin et al., 2018) and is known to be the most common cause of cancer-related death worldwide. (Siegel et al., 2018) Most of the patients diagnosed with NSCLC are already in advanced stages for which effective treatment options are still lacking (Hayden and Ghosh, 2008; Saha et al., 2020) LINC00467 regulates ERK1/2 signaling in NSCLC. Inhibiting SIRT6 and blocking the ERK1/2 signaling pathway lead to the upregulation of miR-125a-3p and the downregulation of LINC00467 in NSCLC cells. Additionally, LINC00467 upregulation or miR-125a-3p downregulation exacerbated the malignant phenotypes and DDP resistance in NSCLC cells. (Xue et al., 2021).

4.1.3 Lung Adenocarcinoma

LUAD is the commonest histological subtype of NSCLC. Early diagnosis of LUAD is particularly difficult and it is prone to

TABLE 1 | Clinical significance of LINC00467 in various human tumors. (ANCTs: adjacent non-cancerous tissues).

Cancer Type	Sample Size	Expression (tumor Vs. normal)	Clinicopathological Features	Reference
Non-small cell lung cancer (NSCLC)	91 pairs of NSCLC tissues and ANCTs	Upregulation	Advanced clinical stages, shorter overall survival and disease-free survival	Xue et al. (2021)
	GEPIA database	Not studied	Advanced clinical stages	Zhu et al. (2020)
Lung adenocarcinoma (LUAD)	60 pairs of LUAD tissues and ANCTs	Upregulation	Shorter overall survival	Wang et al. (2019)
	33 pairs of LAD tissues and ANCTs	Upregulation	Not studied	Ding et al. (2019)
Hepatocellular carcinoma (HCC)	65 HCC tissues and 31 ANCTs	Downregulation	Advanced clinical stages	Cai et al. (2019)
	56 pairs of HCC tissues and ANCTs	Upregulation	Shorter overall survival	Wang et al. (2020)
	20 pairs of HCC tissues and ANCTs	Upregulation	Not studied	Zheng et al. (2020)
	GEPIA database	Upregulation	Advanced clinical stages, poorer cell differentiation, shorter overall survival and disease-free survival	Jiang et al. (2020)
	GEPIA database	Upregulation	Contributed to Axitinib resistance	Li et al. (2021b)
Cervical Cancer Cells	54 pairs of Cervical Cancer tissues and ANCTs	Upregulation	Advanced clinical stages, shorter overall survival	Li et al. (2019)
Osteosarcoma (OS)	44 pairs of OS tissues and ANCTs	Upregulation	Advanced clinical stages, shorter overall survival	Ma et al. (2020)
	36 pairs of OS tissues and ANCTs	Upregulation	Advanced clinical stages, shorter overall survival	Yan et al. (2021)
Glioma	30 matched glioma tissues and normal tissues	Upregulation	Shorter overall survival	Jiang and Liu, (2020)
	TCGA STAD database	Upregulation	Not studied	Zhang et al. (2020)
Glioblastoma	30 matched Glioblastoma tissues and normal tissues	Upregulation	Advanced clinical stages	Liang and Tang, (2020)
Colorectal cancer (CRC)	31 pairs of CRC tissues and ANCTs	Upregulation	Shorter overall survival and disease-free survival	Bai et al. (2020)
	45 matched CRC tissues and normal tissues	Upregulation	Not studied	He et al. (2019)
	GEO dataset	Upregulation	Shorter overall survival and disease-free survival	Ge et al. (2021)
	50 CRC tissues and 10 normal tissues	Upregulation	Shorter overall survival	Li et al. (2020)
Testicular germ cell tumors (TGCT)	14 TGCT tissues and 9 ANCTs	Upregulation	Not studied	Bo et al. (2021)
Prostate cancer (PC)	60 pairs of PC tissues and ANCTs	Upregulation	Shorter overall survival	Jiang et al. (2021)
Breast Cancer	70 pairs of Breast Cancer tissues and ANCTs	Upregulation	Not studied	Zhang et al. (2021)
Esophageal squamous cell carcinoma (ESCC)	44 pairs of ESCC tissues and ANCTs	Upregulation	Not studied	Liu et al. (2021)
Head and neck squamous cell carcinoma (HNSCC)	45 HNSCC tissues and 20 ANCTs	Upregulation	Advanced clinical stages, poorer cell differentiation	Liang et al. (2021)
Gastric cancer (GC)	31 pairs of GC tissues and ANCTs	Upregulation	Not studied	Xu et al. (2021)
	TCGA STAD database	Upregulation	Shorter overall survival	Deng et al. (2021)
Bladder Cancer (BCa)	6 pairs BCa tissues and ANCTs	Upregulation	Not studied	Xiao et al. (2021)
Acute myeloid leukemia (AML)	134 BM specimens from AML patients and 40 healthy controls	Upregulation	Not studied	Lu et al. (2021)

metastasize, as a result of which it is associated with a poor prognosis. (Yang et al., 2019) LINC00467 was found to be upregulated in human LUAD tumor tissues and its expression level was found to correlate with the clinical severity of LUAD. Functional *in vitro* experiments indicated that LINC00467 promoted LUAD cell proliferation, migration, and invasion and suppressed apoptosis. Furthermore, some miRNAs sponged by LINC00467 and their downstream targets, which play a role in LUAD development, have been reported. For instance, a study found that LINC00467 can suppress apoptosis and promote proliferation and stemness of LUAD cells by sponging cytoplasmic miR-4779 or miR-7978. (Chang and Yang, 2019) Additionally, Ding et al. (2019) reported that LINC00467 promotes proliferation in LUAD cells by upregulating the expression level of CCND1, a primary regulator of the cell cycle, via sponging miR-20b-5p.

Finally, Wang et al. reported that LINC00467 DNA copy number amplification contributed to its overexpression and was positively associated with distant metastasis, immune infiltration, and poor overall survival in LUAD. In addition, LINC00467 overexpression partly originated from its DNA demethylation. Based on microarray analysis and bioinformatics, this study revealed a comprehensive miRNAs-mRNAs network that included two microRNAs (hsa-miR-1225-

TABLE 2 | Functional molecular mechanisms of LINC00467 in various cancers.

Tumor Types	Expression	Function Role	Molecular Mechanism	References
Neuroblastoma	Not Studied	neuroblastoma cell survival	Inducing DKK1 expression	Atmadibrata et al. (2014)
Acute myeloid leukemia (AML)	Upregulation	progression	LINC00467/miR-339/SKI axis	Lu et al. (2021)
Bladder Cancer (BCa)	Upregulation	Proliferation, invasion, and progression	Interacting with NF-kB-p65	Xiao et al. (2021)
Prostate cancer (PC)	Upregulation	proliferation, migration, and invasion	LINC00467/miR-494-3p/STAT3 axis	Jiang et al. (2021)
Non-small cell lung cancer (NSCLC)	Upregulation	proliferation, migration, invasion, EMT, inhibit apoptosis	LINC00467/miR-125a-3p/SIRT6 axis	Xue et al. (2021)
		progression, proliferation, and metastasis	Enhancing the Akt signaling pathway	Zhu et al. (2020)
Lung adenocarcinoma (LUAD)	Upregulation	proliferation, migration	Silencing DKK1 to activate the Wnt/b-catenin signaling pathway	Yang et al. (2019)
		proliferation, stemness, inhibit apoptosis	Sponging miR-4779 and miR-7978	Chang and Yang, (2019)
		proliferation, migration, and invasion, inhibit apoptosis	Repressing HTRA3	Wang et al. (2019)
		proliferation and cell cycle progression	LINC00467/miR-20b-5p/CCND1 axis	Ding et al. (2019)
		Not studied	LINC00467/hsa-miR-1225-5p, hsa-miR-575/ BARX2, BCL9, KCNK1, KIAA1324, TMEM182	Wang et al. (2021)
Cervical cancer	Upregulation	proliferation, migration, invasion, and EMT	LINC00467/miR-107/KIF23 axis	Li et al. (2019)
Hepatocellular carcinoma (HCC)	Upregulation	proliferation, invasion, repressed apoptosis	LINC00467/miR-509-3p/PDGFRA axis	Li et al. (2021b)
		proliferation metastasis, inhibit apoptosis	Binding with IGF2BP3	Jiang et al. (2020)
		proliferation, progression, migration, inhibit apoptosis	Inhibiting NR4A3	Wang et al. (2020)
		proliferation, invasion, inhibit apoptosis	LINC00467/miR-18a-5p/NEDD9 axis	Zheng et al. (2020)
	Upregulation	impeding cell viability, proliferation, migration, and invasion	LINC00467/miR-9-5p/PPARA axis	Cai et al. (2019)
Osteosarcoma (OS)	Upregulation	proliferation, migration, invasion, inhibit apoptosis	LINC00467/miR-217/HMGA1 axis	Ma et al. (2020)
	Upregulation	proliferation, migration, invasion, and EMT	LINC00467/miR-217/KPNA4 axis	Yan et al. (2021)
Colorectal cancer (CRC)	Upregulation	proliferation, invasion	Not studied	He et al. (2019)
	Upregulation	proliferation, metastasis, inhibit apoptosis	Sponging miR-451a	Bai et al. (2020)
	Upregulation	Chemoresistance to 5-FU, metastasis	LINC00467/miR-133b/FTL axis	Li et al. (2020)
	Upregulation	proliferation	Encoding ASAP	Ge et al. (2021)
Testicular germ cell tumors (TGCT)	Upregulation	migration, invasion, inhibit immune cells activation and infiltration	Activating AKT3	Bo et al. (2021)
Breast Cancer	Upregulation	proliferation, migration, invasion, and EMT	LINC00467/miR-138-5p/LIN28B axis	Zhang et al. (2021)
Esophageal squamous cell carcinoma (ESCC)	Upregulation	proliferation, invasion, inhibit apoptosis	LINC00467/miR-485-5p/DPAGT1 axis	Liu et al. (2021)
Head and neck squamous cell carcinoma (HNSCC)	Upregulation	proliferation, migration, EMT, invasion	LINC00467/miR-299-5p/USP48 axis	Chen and Ding, (2020)
	Upregulation	invasion and inhibit apoptosis	LINC00467/miR-1285-3p/TFAP2A axis	Liang et al. (2021)
Gastric cancer (GC)	Upregulation	invasion, proliferation, inhibit apoptosis	Enhancing ITGB3 level	Xu et al. (2021)
	Upregulation	proliferation, migration, and invasion	LINC00467/miR-7-5p/EGFR axis	Deng et al. (2021)
Glioma	Upregulation	viability, migration, and invasion	LINC00467/miR-200a/E2F3 axis	Gao et al. (2020)
	Upregulation	proliferation, invasion, cell cycle, inhibit apoptosis	LINC00467/DNMT1/lp53 axis	Zhang et al. (2020)
	Upregulation	proliferation, inhibit apoptosis	LINC00467/miR-339-3p/IP6K2 axis	Liang and Tang, (2020)
	Upregulation	proliferation, invasion, inhibit apoptosis	Sponging miR-485-5p	Jiang and Liu, (2020)

5p, hsa-miR-575) and five mRNAs (BARX2, BCL9, KCNK1, KIAA1324, TMEM182) specific to LINC00467 in LUAD. Through bioinformatic analysis, two potential prognostic biomarkers (BARX2 and BCL9) for LUAD were revealed. (Wang et al., 2021) Based on the results of these reports, LINC00467 stands as a potential diagnostic and prognostic biomarker, as well as a suitable therapeutic target for LUAD.

4.1.4 Cervical Cancer

In the developing world, cervical cancer remains the second most common cancer among women, thereby placing a heavy economic burden on society.(Hillmann et al., 2013; Siva et al., 2015) It has been reported that cytoplasmic LINC00467 plays an important role in the progression of cervical cancer by competitively sponging miR-107 to downregulate the

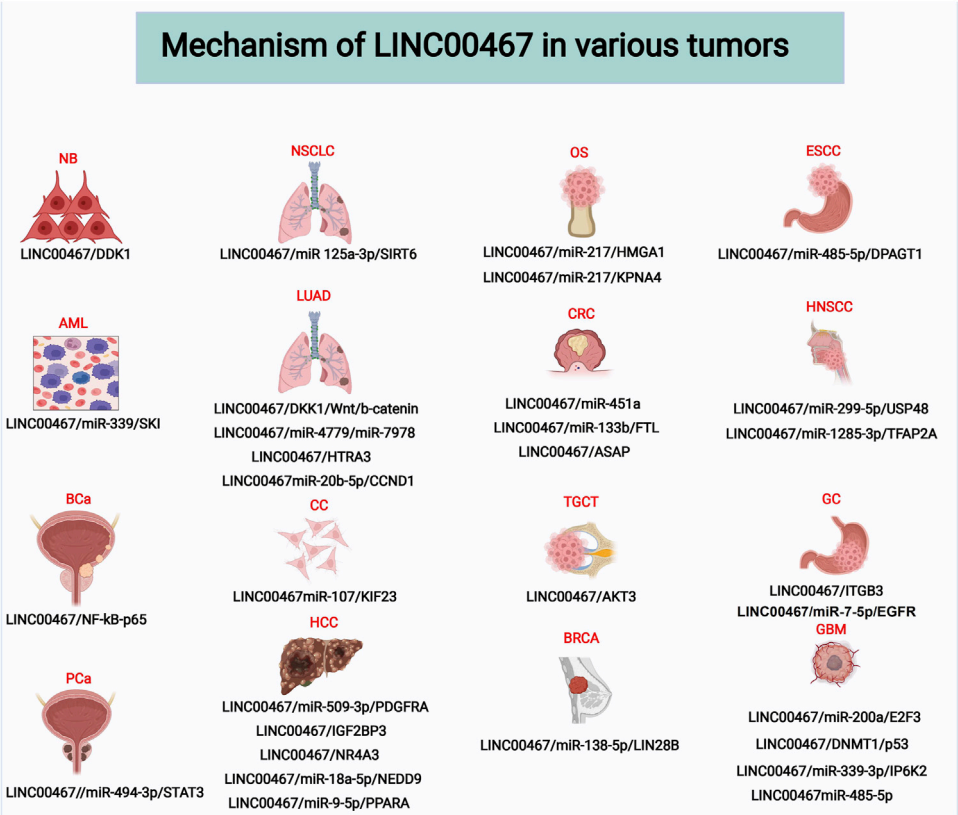

FIGURE 2 | Molecular mechanisms of LINC00467 in various tumors. Abbreviations: NB, Neuroblastoma; NSCLC, Non-small cell lung cancer; OS, Osteosarcoma; ESCC, Esophageal squamous cell carcinoma; AML, Acute Myeloid Leukemia; LUAD, Lung adenocarcinoma; CRC, Colorectal cancer; HNSCC, Head and neck squamous cell carcinoma; BCa, Bladder Cancer; CC, Cervical cancer; TGCT, Testicular germ cell tumor; GC, Gastric cancer; PCa, Prostate cancer; HCC, Hepatocellular carcinoma; BRCA, Breast Cancer; GBM, Glioblastoma.

expression of the downstream gene KIF23. LINC00467 silencing or miR-107 overexpression inhibited cervical cancer cell proliferation, migration, invasion, epithelial-mesenchymal transition (EMT), and tumorigenic ability *in vivo*, further suggesting that targeting LINC00467 may be a novel therapeutic strategy for patients with cervical cancer. (Li et al., 2019).

4.1.5 Hepatocellular Carcinoma

HCC is a prevalent human malignancy with high morbidity and mortality worldwide.(Maluccio and Covey, 2012; Laursen, 2014) Exploring novel therapeutic targets for HCC remains a pressing challenge nowadays (Dhar et al., 2018; Andrade et al., 2019) LINC00467 expression is upregulated in HCC cells and is related to HCC progression. Additionally, miR-509-3p and platelet-derived growth factor receptor alpha (PDGFRA), which are targets of LINC00467, promoted proliferation and invasion, repressed apoptosis, and ameliorated the resistance to axitinib, the commonly-used drug for HCC (Chan et al., 2017; Li W. et al., 2021) Moreover, Zheng et al. described that silencing LINC00467 could modulate HCC cell growth and development by targeting the miR-18a-5p/NEDD9 axis. (Zheng et al., 2020) Interestingly, one study reported that the expression of LINC00467 was significantly decreased in HCC tissues, especially in metastatic HCC tissues, which is in contrast to the results of other relevant studies on LINC00467 in HCC. Furthermore, it was reported that LINC00467 exerted a tumor suppressor role by reducing cell viability, proliferation, migration, and invasion by regulating the miR-9-5a/PPARA signaling axis in HCC. (Cai et al., 2019).

4.1.6 Osteosarcoma

OS, which mainly occurs in children and adolescents, has a poor prognosis and low survival rate due to its rapid progression and metastasis ability.(Wycislo and Fan, 2015; Marko et al., 2016) Ma et al. reported that LINC00467 expression was increased in OS cell lines, and that overexpression of LINC00467 increased cell proliferation, migration, and invasion, and decreased cell apoptosis by upregulating the expression of high mobility group A1 (HMGA1) by targeting miR-127 in OS. (Ma et al., 2020) Additionally, it was reported that LINC00467-mediated sponging of miR-127 also regulated the expression of karyopherin subunit α 4 (KPNA4), contributing to OS progression. (Yan et al., 2021).

4.1.7 Colorectal Cancer

CRC is the second leading cause of cancer-related mortality worldwide, partly due to the lack of effective

treatments.(Walsh and Terdiman, 2003; Sunkara and Hébert, 2015; Sung et al., 2021) LINC00467 expression level has been reported to be significantly increased in CRC tissues and cell lines. Silencing its expression resulted in the inhibition of CRC cell proliferation, invasion, and EMT. (He et al., 2019) Another study using data from 31 CRC patients further elucidated that LINC00467 upregulation was closely associated with metastasis and TNM stage in CRC. Moreover, the authors reported that overexpression of miR-451a reduced the level of LINC00467 in CRC cells. (Bai et al., 2020) Additionally, LINC00467 has also been suggested to play other biological roles in CRC cells, including mediating chemoresistance to 5-FU and metastasis, through the miR-133b/ferritin light chain (FTL) axis. (Li et al., 2020).

4.1.8 Prostate Carcinoma

PC, which is a heterogeneous disease, is the most common non-skin male malignancy in the Western world. (Haffner et al., 2021) LINC00467 expression is upregulated in PC tissues and cells. Meanwhile, LINC00467 knockdown reduced PC cell proliferation, migration, and invasion via regulation of the miR-494-3p/STAT3 axis. Additionally, it has also been shown that downregulation of LINC00467 inhibited M2 macrophage polarization and suppressed the migration and invasion of PC cells by activating the STAT3 pathway. These results suggest that inhibiting LINC00467 may be an effective therapeutic strategy for patients with PC. (Jiang et al., 2021).

4.1.9 Breast Cancer

Breast cancer is the most common type of malignancy among women and is associated with a high number of cancer-related deaths worldwide. (Jemal et al., 2011) Zhang et al. reported that silencing LINC00467 hindered the proliferation, migration, invasion, and EMT of breast cancer cell lines *in vitro*, whereas overexpression of LINC00467 predicted poor overall survival. Additional experiments have revealed that LINC00467 sponges miR-138-5p while directly interacting with LIN28B, a significant oncogene in breast cancer, to elevate its protein level. (Zhang et al., 2021).

4.1.10 Esophageal Squamous Cell Carcinoma

ESCC, an important subtype of esophageal carcinoma, is the most common primary gastrointestinal malignant tumor. It has a relatively low 5-years survival rate and a high incidence, with more than 400,000 newly-diagnosed cases annually worldwide (Luo et al., 2019; Sugimura et al., 2019) LINC00467 expression is upregulated in ESCC tissues and cell lines, and high LINC00467 expression is correlated with the promotion of cell proliferation and inhibition of cell apoptosis. More importantly, LINC00467 facilitated ESCC progression by sponging miR-485-5p and modulating DPAGT1 levels. (Liu et al., 2021).

4.1.11 Head and Neck Squamous Cell Carcinoma

HNSCC, which mainly affects the oral cavity, pharynx, and larynx, is among one the ten malignancies with more than 600,000 new cases worldwide annually (Siegel et al., 2017; Xu et al., 2020) The notable upregulation of LINC00467 in HNSCC promotes cell growth, cell migration, and EMT by sponging miR-299-5p, thereby upregulating the expression of the oncogene tumor ubiquitin specific protease-48 (USP48), ultimately leading to HNSCC progression. (Chen and Ding, 2020) Additionally, Liang et al. reported that LINC00467 over-expression in HNSCC patients promoted cell invasion and inhibited apoptosis by sponging miR-1285-3p and modulating the expression level of TFAP2A, a downstream target of miR-1285-3p. (Liang et al., 2021).

4.1.12 Gastric Cancer

GC is an aggressive malignant tumor with a high mortality rate that is often diagnosed at an advanced stage. (Abdi et al., 2020) A study found that LINC00467 knockdown inhibited proliferation, migration, and invasion of GC cells. Furthermore, researchers revealed that LINC00467 promotes GC progression by directly regulating miR-7-5p/EGFR (epidermal growth factor receptor) axis. (Deng et al., 2021).

4.1.13 Glioma

Gliomas are tumors derived from the neuroepithelial ectoderm that stand among the most prevalent intracranial tumors, accounting for approximately 40% of all brain tumors. (Chen et al., 2017) Gao et al. demonstrated that high LINC00467 expression is a distinctive feature of glioma cell lines compared with normal cell lines. Moreover, LINC00467 was shown to promote the viability, migration, and invasion of glioma cells, and its expression level was negatively correlated with that of miRNA-200a, but positively correlated with E2F3 expression. LINC00467 accelerated the progression of gliomas by regulating the miR-200a/E2F3 axis. (Gao et al., 2020) Zhang et al. showed that increased LINC00467 expression in glioma cell lines promoted tumor proliferation, invasion, and cell cycle progression, but inhibited cell apoptosis by binding to DNMT1 to inhibit the expression of the tumor suppressor P53. (Zhang et al., 2020) In addition, another study found that LINC00467 exerted its biological function, including accelerating the proliferation and invasion abilities of glioma cells, as well as attenuating apoptosis, by sponging miRNA-485-5p (Jiang and Liu, 2020).

Glioblastoma, which is considered an advanced stage of glioma, is associated with a lower overall survival rate than glioma. (Zhang et al., 2019; Pelcovits and Niroula, 2020) LINC00467 knockdown was demonstrated to hinder cell proliferation while promoting cell apoptosis in glioblastoma by sponging miR-339-3p and regulating its target downstream gene, IP6K2. (Liang and Tang, 2020).

4.2 Other Functional Mechanisms

Except for functioning as a ceRNA in the underlying mechanisms of various human cancers, LINC00467 can also play different biological roles by interacting with certain proteins, regulating classical signaling pathways, or encoding micro peptides.

4.2.1 Neuroblastoma

Neuroblastoma is a malignant embryonal tumor frequently diagnosed in children that usually occurs in the abdomen and

has a high metastatic burden. (Park and Cheung, 2020) The role of LINC00467 in human cancers was first reported by Atmadibrata et al., who identified that LINC00467 transcription was regulated by N-Myc, a type of Myc oncoprotein that is associated with neuroblastoma occurrence. (Atmadibrata et al., 2014) In this study, it was demonstrated that N-Myc could reduce LINC00467 and *RD3* gene promoter activity by directly binding to the Sp1-binding site-enriched region. Through this regulatory mechanism, N-Myc could downregulate the expression of LINC00467 and *RD3*. Moreover, LINC00467 could reduce the mRNA expression of its neighboring protein-coding gene *RD3*. To conclude, N-Myc-mediated suppression of *RD3* mRNA expression could be blocked by N-Myc-mediated suppression of LINC00467. Furthermore, LINC00467 knockdown reduced the survival of neuroblastoma cells by inducing the expression of *DKK1*, a classic tumor suppressor gene. However, in this study, the specific roles of LINC00467 in neuroblastoma cells were not investigated in detail.

4.2.2 Bladder Cancer

Bladder cancer, which mainly occurs in men, is the most common malignancy of the genitourinary system. (Bray et al., 2018) A recent study on the underlying molecular mechanisms of bladder cancer validated that LINC00467 is highly expressed in bladder cancer tissues and cells. LINC00467 was also demonstrated to be a promotion of bladder cancer cell proliferation and invasion. Using the catRAPID algorithm, it was predicted that LINC00467 could bind to NF-kB p65 through several binding sites. Further functional experiments showed that LINC00467 binding to NF-kB p65 increased the stability of this transcription factor and its nuclear translocation, a subcellular process in which NF-kB p65 could be transported into the cell nucleus to regulate gene expression. Moreover, rescue assays demonstrated that LINC00467 could promote the progression of bladder cancer through the NF-κB signaling pathway, which is closely correlated with the occurrence and development of tumors. (Xiao et al., 2021)

4.2.3 LUAD

In LUAD, except for sponging miRNAs, LINC00467 could also exert its function through other molecular mechanisms. A study confirmed that LINC00467 inhibited the expression of HtrA serine peptidase 3 (HTRA3), a downstream gene of LINC00467, by recruiting EZH2 to the HTRA3 promoter, thereby regulating the characteristics of LUAD cells. (Wang et al., 2019) Yang et al. (2019) discovered that STAT1 (signal transducer and activator of transcription 1)-mediated upregulation of LINC00467 promoted LUAD cell proliferation and migration by recruiting enhancer of zeste homolog 2 (EZH2) to downregulate DKK1, which resulted in the inhibition of the Wnt/β-catenin signaling pathway.

4.2.4 NSCLC

In another study, Using the GEPIA and Kaplan–Meier Plotter databases, Zhu et al. found that LINC00467 is highly overexpressed in NSCLC tissues and is associated with advanced clinical stages and poor prognosis. Furthermore, functional experiments confirmed that LINC00467 upregulation was due to TDG (Thymine DNA Glycosylase)-mediated acetylation. Additionally, LINC00467 has been proven to promote NSCLC cell proliferation and metastasis by regulating the Akt signaling pathway. (Zhu et al., 2020).

4.2.5 HCC

LINC00467 can also regulate the initiation and development of HCC through interacting with certain proteins and participating in post-transcriptionally modification. Jiang et al. reported that upregulation of LINC00467 facilitated proliferation and metastasis but hindered cell apoptosis in HCC. A series of functional experiments revealed that the underlying mechanism relied on the direct binding between LINC00467 and insulin-like growth factor-2 messenger RNA-binding protein 3 (IGF2BP3), which increased the stability of the transcript encoding the tumor necrosis factor receptor-associated factor 5 (TRAF5). (Jiang et al., 2020) In addition, LINC00467 can post-transcriptionally reduce the expression of the tumor suppressor NR4A3 by regulating Dicer-dependent RNA splicing, which ultimately contributes to HCC tumorigenesis. (Wang et al., 2020)

4.2.6 CRC

To date, there has only been one article of LINC00467 working by encoding a micro peptide. A study focusing on the role of ATP synthase-associated peptide (ASAP), a micro peptide encoded by LINC00467, reported that ASAP facilitated tumor proliferation through the regulation of mitochondrial ATP production in CRC. Moreover, ASAP expression was negatively correlated with the prognosis of patients with CRC. (Ge et al., 2021).

4.2.7 Testicular Germ Cell Tumors

TGCTs, which can be classified as seminoma or non-seminoma tumors, mainly occur in men aged 20–40 years. In China, its incidence is one every 100,000 people. Furthermore, in China as well as worldwide, the incidence of this disease is gradually increasing (Chia et al., 2010; Greene et al., 2010; Shanmugalingam et al., 2013) Bo et al. reported that LINC00467 can promote TGCT cell migration and invasion by controlling the expression level of AKT3 and affecting the total AKT phosphorylation level. Interestingly, LINC00467 could also inhibit the infiltration of immune cells as well as their activation, indicating that it may be a potential target for anti-PD-1 immunotherapy. (Bo et al., 2021)

4.2.8 GC

In GC, Xu et al. reported that the upregulation of LINC00467 in patients with GC was positively associated with tumor differentiation and the TNM stage. Functional experiments revealed that overexpression of LINC00467 increases GC cell viability and proliferation while suppressing apoptosis by enhancing ITGB3 (integrin subunit beta 3) levels. (Xu et al., 2021)

5 DISCUSSION

Recent studies have shown that LINC00467 overexpression is associated with numerous diseases, especially with the

progression of various types of tumors. However, the role of LINC00467 in HCC is controversial. In addition, several studies have confirmed that high expression of LINC00467 is associated with poor prognosis in various tumor types. Functional experiments on cancer cells showed that LINC00467 could promote the proliferation, invasion, migration, and inhibition of apoptosis of tumor cells, while silencing LINC00467 exerted the opposite effects. However, owing to the different sample sizes and procedures of each study, the results are non-concluding, and a larger study or multicentre joint studies are needed to further verify these conclusions. Additionally, studying LINC00467 expression levels in human blood or other body fluids would be beneficial for evaluating its clinical application as a promising biomarker for the early diagnosis and prognosis of various diseases. Moreover, silencing LINC00467 could be a suitable therapeutic strategy, but more studies are needed to verify this. *In vivo* studies of LINC00467 with cell-derived and patient-derived xenograft animal models are required to further assess the role of LINC00467 in tumor progression, avoid the limitations of *in vitro* studies, and test new treatment options. However, some of the studies referred to in this paper, such as those conducted for OS, CRC, TGCT, GC, glioma, esophageal cancer, and HNSCC, were performed only *in vitro* without further *in vivo* validation of their findings.

LINC00467 has been demonstrated to function through diverse regulatory mechanisms, mainly acting as a ceRNA of a series of miRNAs, including miR-339, miR-494-3p, miR-125A-3p, miR-4779, miR-7978, miR-20b-5p, miR-107, miR-509-3p, miR-18a-5p, miR-9-5p, miR-217, miR-451A, miR-138-5p, miR-485-5p, miR-299-5p, miR-1285-3p, miR-7-5p, miR-200a, miR-339-3p, and miR-485-5p. By sponging these miRNAs, LINC00467 alters the expression level of downstream genes and influences cell signalling pathways. Central signalling cascades have been found among the pathways regulated by LINC00467; for example, the Wnt/B-catenin pathway in LUAD. However, a few studies failed to fully elucidate the mechanism of action of LINC00467 in some diseases. For example, a study found that LINC00467 could competingly bind with miR-451a, but its downstream gene was not studied. (Bai et al., 2020) Additionally, Bo et al. reported that LINC00467 promotes TGCT cell invasion and migration by activating AKT3. However, the detailed regulatory mechanism between LINC00467 and AKT3 is not illustrated. (Bo et al., 2021) Herein, we expect more comprehensive and in-depth studies to advance the clinical application of LINC00467 in the future.

It is worth noting that studies on HCC have shown that LINC00467 expression is higher in HCC tissues than in controls (Jiang et al., 2020; Wang et al., 2020; Zheng et al., 2020) However, Cai et al. (2019) reported the opposite result in their clinical samples. Furthermore, they found that LINC00467 expression in HCC tissues with metastasis was lower than that in non-metastatic tissues. This contradiction needs to be assessed by further validation with more clinical samples of HCC. Meanwhile, several studies reported that LINC00467 plays a carcinogenic role in HCC by sponging miR-18a-5p or miR-509-3p (Zheng et al., 2020; Li W. et al., 2021), inhibiting NR4A3 (Wang et al., 2020), and binding to IGF2BP3. (Jiang et al., 2020) Cai et al. (2019) studied the LINC00467/miR-9-5p/PPARA axis and concluded that LINC00467 exerts a tumor-suppressive effect in HCC tissues. If the data is real, this contradiction on HCC indicates that LINC00467 plays different roles depending on the cell type.

In addition to regulating the expression level of downstream genes, LINC00467 also functions as a protein-coding RNA, as it encodes several short peptides. Before Andrews and Rothnagel (2014) and Bazzini et al. (2014) reported that ncRNAs could encode hundreds of functional micro peptides, lncRNAs had long been regarded as "transcriptional noise". Soon afterward, Anderson et al. (2015) found a novel micro peptide myoregulin (MLN), encoded by a lncRNA, plays an important role in regulating skeletal muscle physiology. Similarly, in CRC, LINC00467 can encode a short peptide ASAP, which promotes CRC cell proliferation. Although current studies on LINC00467 and other lncRNAs mainly focus on their interaction with miRNA or proteins, further investigation into the function of these micro peptides encoded by short open reading frames is needed.

Exosomes are a subtype of extracellular vesicles with a diameter of 40–150 nm, secreted by almost all types of living cells (Cocucci and Meldolesi, 2015) An increasing number of studies have confirmed that exosomes are responsible for many biological functions as they transport a large number of functional units, such as DNA, RNA, and proteins. Data from the GEO databases shows that one of the LINC00467 transcripts (NONCODE ID: NONHSAT225914.1) is expressed in exosomes of some samples, such as those from tuberculosis patient serum and HepG2s (Hepatocellular Carcinoma Cell Line Exosomes). Further studies should be conducted to determine the role of exosome-mediated transport of LINC00467 in various diseases.

In this review, the latest research progress on LINC00467 is summarized, and its biological mechanisms and clinical application value in various tumors are detailed. The described studies highlight that LINC00467 plays a remarkable role as an oncogene. Further research on LINC00467 and its mechanism of action may contribute to its use for disease diagnosis, targeted therapy, and prognostic evaluation in the future.

AUTHOR CONTRIBUTIONS

DW, RL, and JL: conception and literature search. DW, CZ, and RJ: manuscript writing and final approval. All authors contributed to the article and approved the submitted version. DW and RL contributed equally to this work and share first authorship.

FUNDING

This work was supported by National Natural Science Foundation of China Grants (92049111,81570613), Jiangsu Province "Science and Education Strong Guard" Engineering Leading Talent and Innovation Team Project (CXTDC2016003), Nanjing Medical Science and Technology Development Project (ZDX16006), Jiangsu Provincial Medical Innovation Team (2016), and Jiangsu Provincial Social Development Project (BE2017615).

REFERENCES

Abdi, E., Latifi-Navid, S., Abdi, F., and Taherian-Esfahani, Z. (2020). Emerging Circulating MiRNAs and LncRNAs in Upper Gastrointestinal Cancers. *Expert Rev. Mol. diagnostics* 20, 1121–1138. doi:10.1080/14737159.2020.1842199

Anastasiadou, E., Jacob, L. S., and Slack, F. J. (2018). Non-coding RNA Networks in Cancer. *Nat. Rev. Cancer* 18, 5–18. doi:10.1038/nrc.2017.99

Anderson, D. M., Anderson, K. M., Chang, C.-L., Makarewich, C. A., Nelson, B. R., Mcanally, J. R., et al. (2015). A Micropeptide Encoded by a Putative Long Noncoding RNA Regulates Muscle Performance. *Cell* 160, 595–606. doi:10.1016/j.cell.2015.01.009

Andrade, F. D. O., Furtado, K. S., Heidor, R., Sandri, S., Hebeda, C. B., Miranda, M. L. P., et al. (2019). Antiangiogenic Effects of the Chemopreventive Agent Tributyrin, a Butyric Acid Prodrug, during the Promotion Phase of Hepatocarcinogenesis. *Carcinogenesis* 40, 979–988. doi:10.1093/carcin/bgy190

Andrews, S. J., and Rothnagel, J. A. (2014). Emerging Evidence for Functional Peptides Encoded by Short Open Reading Frames. *Nat. Rev. Genet.* 15, 193–204. doi:10.1038/nrg3520

Ann, S.-J., Bang, H., Lee, C. J., Oh, J., Park, S., Kang, S.-M., et al. (2021). LncRNA HSPA7 in Human Atherosclerotic Plaques Sponges miR-223 and Promotes the Proinflammatory Vascular Smooth Muscle Cell Transition. *Exp. Mol. Med.* 53, 1842–1849. doi:10.1038/s12276-021-00706-8

Atmadibrata, B., Liu, P. Y., Sokolowski, N., Zhang, L., Wong, M., Tee, A. E., et al. (2014). The Novel Long Noncoding RNA Linc00467 Promotes Cell Survival but Is Down-Regulated by N-Myc. *PloS one* 9, e88112. doi:10.1371/journal.pone.0088112

Bai, Y., Wu, H., Han, B., Xu, K., Liu, Y., Liu, Y., et al. (2020). Long Intergenic Non-protein Coding RNA-467 Targets microRNA-451a in Human Colorectal Cancer. *Oncol. Lett.* 20, 124. doi:10.3892/ol.2020.11987

Barik, G. K., Sahay, O., Behera, A., Naik, D., and Kalita, B. (2021). Keep Your Eyes Peeled for Long Noncoding RNAs: Explaining Their Boundless Role in Cancer Metastasis, Drug Resistance, and Clinical Application. *Biochimica Biophysica Acta (BBA) - Rev. Cancer* 1876, 188612. doi:10.1016/j.bbcan.2021.188612

Bazzini, A. A., Johnstone, T. G., Christiano, R., Mackowiak, S. D., Obermayer, B., Fleming, E. S., et al. (2014). Identification of Small ORFs in Vertebrates Using Ribosome Footprinting and Evolutionary Conservation. *EMBO J.* 33, 981–993. doi:10.1002/embj.201488411

Bo, H., Zhu, F., Liu, Z., Deng, Q., Liu, G., Li, R., et al. (2021). Integrated Analysis of High-Throughput Sequencing Data Reveals the Key Role of LINC00467 in the Invasion and Metastasis of Testicular Germ Cell Tumors. *Cell Death Discov.* 7, 206. doi:10.1038/s41420-021-00588-9

Bray, F., Ferlay, J., Soerjomataram, I., Siegel, R. L., Torre, L. A., and Jemal, A. (2018). Global Cancer Statistics 2018: GLOBOCAN Estimates of Incidence and Mortality Worldwide for 36 Cancers in 185 Countries. *CA A cancer J. Clin.* 68, 394–424. doi:10.3322/caac.21492

Cai, K., Li, T., Guo, L., Guo, H., Zhu, W., Yan, L., et al. (2019). Long Non-coding RNA LINC00467 Regulates Hepatocellular Carcinoma Progression by Modulating miR-9-5p/PPARA Expression. *Open Biol.* 9, 190074. doi:10.1098/rsob.190074

Chan, S. L., Yeo, W., Mo, F., Chan, A. W. H., Koh, J., Li, L., et al. (2017). A Phase 2 Study of the Efficacy and Biomarker on the Combination of Transarterial Chemoembolization and Axitinib in the Treatment of Inoperable Hepatocellular Carcinoma. *Cancer* 123, 3977–3985. doi:10.1002/cncr.30825

Chang, Y., and Yang, L. (2019). LINC00467 Promotes Cell Proliferation and Stemness in Lung Adenocarcinoma by Sponging miR-4779 and miR-7978. *J. Cell Biochem.* doi:10.1002/jcb.29510

Chen, R., Smith-Cohn, M., Cohen, A. L., and Colman, H. (2017). Glioma Subclassifications and Their Clinical Significance. *Neurotherapeutics* 14, 284–297. doi:10.1007/s13311-017-0519-x

Chen, Y., and Ding, Y. (2020). LINC00467 Enhances Head and Neck Squamous Cell Carcinoma Progression and the Epithelial-Mesenchymal Transition Process via miR-299-5p/ubiquitin Specific Protease-48 axis. *J. Gene Med.* 22, e3184. doi:10.1002/jgm.3184

Chia, V. M., Quraishi, S. M., Devesa, S. S., Purdue, M. P., Cook, M. B., and Mcglynn, K. A. (2010). International Trends in the Incidence of Testicular Cancer, 1973-2002. *Cancer Epidemiol. Biomarkers Prev.* 19, 1151–1159. doi:10.1158/1055-9965.epi-10-0031

Cocucci, E., and Meldolesi, J. (2015). Ectosomes and Exosomes: Shedding the Confusion between Extracellular Vesicles. *Trends Cell Biol.* 25, 364–372. doi:10.1016/j.tcb.2015.01.004

Deng, L.-H., Zhao, H., Bai, L.-P., Xie, J., Liu, K., and Yan, F. (2021). Linc00467 Promotion of Gastric Cancer Development by Directly Regulating miR-7-5p Expression and Downstream Epidermal Growth Factor Receptor. *Bioengineered* 12, 9484–9495. doi:10.1080/21655979.2021.1996014

Derrien, T., Johnson, R., Bussotti, G., Tanzer, A., Djebali, S., Tilgner, H., et al. (2012). The GENCODE V7 Catalog of Human Long Noncoding RNAs: Analysis of Their Gene Structure, Evolution, and Expression. *Genome Res.* 22, 1775–1789. doi:10.1101/gr.132159.111

Dhar, D., Antonucci, L., Nakagawa, H., Kim, J. Y., Glitzner, E., Caruso, S., et al. (2018). Liver Cancer Initiation Requires P53 Inhibition by CD44-Enhanced Growth Factor Signaling. *Cancer Cell* 33, 1061–e6. doi:10.1016/j.ccell.2018.05.003

Ding, H., Luo, Y., Hu, K., Liu, P., and Xiong, M. (2019). Linc00467 Promotes Lung Adenocarcinoma Proliferation via Sponging miR-20b-5p to Activate CCND1 Expression. *Ott* 12, 6733–6743. doi:10.2147/ott.s207748

Fagerberg, L., Hallström, B. M., Oksvold, P., Kampf, C., Djureinovic, D., Odeberg, J., et al. (2014). Analysis of the Human Tissue-specific Expression by Genome-wide Integration of Transcriptomics and Antibody-Based Proteomics. *Mol. Cell. Proteomics* 13, 397–406. doi:10.1074/mcp.m113.035600

Gao, S., Duan, H., An, D., Yi, X., Li, J., and Liao, C. (2020). Knockdown of Long Non-coding RNA LINC00467 Inhibits Glioma Cell Progression via Modulation of E2F3 Targeted by miR-200a. *Cell Cycle* 19, 2040–2053. doi:10.1080/15384101.2020.1792127

Ge, Q., Jia, D., Cen, D., Qi, Y., Shi, C., Li, J., et al. (2021). Micropeptide ASAP Encoded by LINC00467 Promotes Colorectal Cancer Progression by Directly Modulating ATP Synthase Activity. *J. Clin. Invest.* 131. doi:10.1172/JCI152911

Greene, M. H., Kratz, C. P., Mai, P. L., Mueller, C., Peters, J. A., Bratslavsky, G., et al. (2010). Familial Testicular Germ Cell Tumors in Adults: 2010 Summary of Genetic Risk Factors and Clinical Phenotype. *Endocrine-related cancer* 17, R109–R121. doi:10.1677/erc-09-0254

Guo, K., Qian, K., Shi, Y., Sun, T., and Wang, Z. (2021). LncRNA-MIAT Promotes Thyroid Cancer Progression and Function as ceRNA to Target EZH2 by Sponging miR-150-5p. *Cell Death Dis.* 12, 1097. doi:10.1038/s41419-021-04386-0

Haffner, M. C., Zwart, W., Roudier, M. P., True, L. D., Nelson, W. G., Epstein, J. I., et al. (2021). Genomic and Phenotypic Heterogeneity in Prostate Cancer. *Nat. Rev. Urol.* 18, 79–92. doi:10.1038/s41585-020-00400-w

Hao, K., Lei, W., Wu, H., Wu, J., Yang, Z., Yan, S., et al. (2019). LncRNA-Safe Contributes to Cardiac Fibrosis through Safe-Sfrp2-HuR Complex in Mouse Myocardial Infarction. *Theranostics* 9, 7282–7297. doi:10.7150/thno.33920

Hayden, M. S., and Ghosh, S. (2008). Shared Principles in NF-Kb Signaling. *Cell* 132, 344–362. doi:10.1016/j.cell.2008.01.020

He, X., Li, S., Yu, B., Kuang, G., Wu, Y., Zhang, M., et al. (2019). Up-regulation of LINC00467 Promotes the Tumourigenesis in Colorectal Cancer. *J. Cancer* 10, 6405–6413. doi:10.7150/jca.32216

Herbst, R. S., Heymach, J. V., and Lippman, S. M. (2008). Lung Cancer. *N. Engl. J. Med.* 359, 1367–1380. doi:10.1056/nejmra0802714

Hillmann, E. D. C., Dos Reis, R., Monego, H., Appel, M., Hammes, L. S., Rivoire, W. A., et al. (2013). Cervical Digital Photography for Screening of Uterine Cervix Cancer and its Precursor Lesions in Developing Countries. *Arch. Gynecol. Obstet.* 288, 183–189. doi:10.1007/s00404-013-2745-8

Hu, Y.-P., Jin, Y.-P., Wu, X.-S., Yang, Y., Li, Y.-S., Li, H.-F., et al. (2019). LncRNA-HGBC Stabilized by HuR Promotes Gallbladder Cancer Progression by Regulating miR-502-3p/SET/AKT axis. *Mol. Cancer* 18, 167. doi:10.1186/s12943-019-1097-9

Jemal, A., Bray, F., Center, M. M., Ferlay, J., Ward, E., and Forman, D. (2011). Global Cancer Statistics. *CA a cancer J. Clin.* 61, 69–90. doi:10.3322/caac.20107

Jiang, H., Deng, W., Zhu, K., Zeng, Z., Hu, B., Zhou, Z., et al. (2021). LINC00467 Promotes Prostate Cancer Progression via M2 Macrophage Polarization and the miR-494-3p/STAT3 Axis. *Front. Oncol.* 11, 661431. doi:10.3389/fonc.2021.661431

Jiang, W., Cheng, X., Wang, T., Song, X., Zheng, Y., and Wang, L. (2020). LINC00467 Promotes Cell Proliferation and Metastasis by Binding with IGF2BP3 to Enhance the mRNA Stability of TRAF5 in Hepatocellular Carcinoma. *J. Gene Med.* 22, e3134. doi:10.1002/jgm.3134

Jiang, X. H., and Liu, Y. Y. (2020). LINC00467 Promotes Proliferation and Invasion in Glioma via Interacting with miRNA-485-5p. *Eur. Rev. Med. Pharmacol. Sci.* 24, 766–772. doi:10.26355/eurrev_202001_20057

Kazimierczyk, M., Kasprowicz, M. K., Kasprzyk, M. E., and Wrzesinski, J. (2020). Human Long Noncoding RNA Interactome: Detection, Characterization and Function. *Int. J. Mol. Sci.* 21. doi:10.3390/ijms21031027

Laursen, L. (2014). A Preventable Cancer. *Nature* 516, S2–S3. doi:10.1038/516s2a

Li, G.-C., Xin, L., Wang, Y.-S., and Chen, Y. (2019). Long Intervening Noncoding 00467 RNA Contributes to Tumorigenesis by Acting as a Competing Endogenous RNA against miR-107 in Cervical Cancer Cells. *Am. J. Pathology* 189, 2293–2310. doi:10.1016/j.ajpath.2019.07.012

Li, M., Shao, F., Qian, Q., Yu, W., Zhang, Z., Chen, B., et al. (2021). A Putative Long Noncoding RNA-Encoded Micropeptide Maintains Cellular Homeostasis in Pancreatic β Cells. *Mol. Ther. - Nucleic Acids* 26, 307–320. doi:10.1016/j.omtn.2021.06.027

Li, W., He, Y., Chen, W., Man, W., Fu, Q., Tan, H., et al. (2021). Knockdown of LINC00467 Contributed to Axitinib Sensitivity in Hepatocellular Carcinoma through miR-509-3p/PDGFRA axis. *Gene Ther.* 28, 634–645. doi:10.1038/s41434-020-0137-9

Li, Z., Liu, J., Chen, H., Zhang, Y., Shi, H., Huang, L., et al. (2020). Ferritin Light Chain (FTL) Competes with Long Noncoding RNA Linc00467 for miR-133b Binding Site to Regulate Chemoresistance and Metastasis of Colorectal Cancer. *Carcinogenesis* 41, 467–477. doi:10.1093/carcin/bgz181

Liang, R., and Tang, Y. (2020). LINC00467 Knockdown Repressed Cell Proliferation but Stimulated Cell Apoptosis in Glioblastoma via miR-339-3p/IP6K2 axis. *Cbm* 28, 169–180. doi:10.3233/cbm-190939

Liang, Y., Cheng, G., Huang, D., and Yuan, F. (2021). Linc00467 Promotes Invasion and Inhibits Apoptosis of Head and Neck Squamous Cell Carcinoma by Regulating miR-1285-3p/TFAP2A. *Am. J. Transl. Res.* 13, 6248–6259.

Liu, Z., Yang, S., Chen, X., Dong, S., Zhou, S., and Xu, S. (2021). LncRNA LINC00467 Acted as an Oncogene in Esophageal Squamous Cell Carcinoma by Accelerating Cell Proliferation and Preventing Cell Apoptosis via the miR-485-5p/DPAGT1 axis. *J. Gastroenterology hepatology* 36, 721–730. doi:10.1111/jgh.15201

Lu, J., Wu, X., Wang, L., Li, T., and Sun, L. (2021). Long Noncoding RNA LINC00467 Facilitates the Progression of Acute Myeloid Leukemia by Targeting the miR-339/SKI Pathway. *Leukemia Lymphoma* 62, 428–437. doi:10.1080/10428194.2020.1832667

Luo, H., Song, H., Mao, R., Gao, Q., Feng, Z., Wang, N., et al. (2019). Targeting Valosin-containing Protein Enhances the Efficacy of Radiation Therapy in Esophageal Squamous Cell Carcinoma. *Cancer Sci.* 110, 3464–3475. doi:10.1111/cas.14184

Ma, H. Z., Wang, J., Shi, J., Zhang, W., and Zhou, D. S. (2020). LncRNA LINC00467 Contributes to Osteosarcoma Growth and Metastasis through Regulating HMGA1 by Directly Targeting miR-217. *Eur. Rev. Med. Pharmacol. Sci.* 24, 5933–5945. doi:10.26355/eurrev_202006_21486

Maluccio, M., and Covey, A. (2012). Recent Progress in Understanding, Diagnosing, and Treating Hepatocellular Carcinoma. *CA a cancer J. Clin.* 62, 394–399. doi:10.3322/caac.21161

Marko, T. A., Diessner, B. J., and Spector, L. G. (2016). Prevalence of Metastasis at Diagnosis of Osteosarcoma: An International Comparison. *Pediatr. Blood Cancer* 63, 1006–1011. doi:10.1002/pbc.25963

Mi, Y.-Y., Sun, C.-Y., Zhang, L.-F., Wang, J., Shao, H.-B., Qin, F., et al. (2021). Long Non-coding RNAs LINC01679 as a Competitive Endogenous RNAs Inhibits the Development and Progression of Prostate Cancer via Regulating the miR-3150a-3p/SLC17A9 Axis. *Front. Cell Dev. Biol.* 9, 737812. doi:10.3389/fcell.2021.737812

Niu, L., Lou, F., Sun, Y., Sun, L., Cai, X., Liu, Z., et al. (2020). A Micropeptide Encoded by lncRNA MIR155HG Suppresses Autoimmune Inflammation via Modulating Antigen Presentation. *Sci. Adv.* 6, eaaz2059. doi:10.1126/sciadv.aaz2059

Palazzo, A. F., and Koonin, E. V. (2020). Functional Long Non-coding RNAs Evolve from Junk Transcripts. *Cell* 183, 1151–1161. doi:10.1016/j.cell.2020.09.047

Pang, Y., Liu, Z., Han, H., Wang, B., Li, W., Mao, C., et al. (2020). Peptide SMIM30 Promotes HCC Development by Inducing SRC/YES1 Membrane Anchoring and MAPK Pathway Activation. *J. hepatology* 73, 1155–1169. doi:10.1016/j.jhep.2020.05.028

Park, J. A., and Cheung, N.-K. V. (2020). Targets and Antibody Formats for Immunotherapy of Neuroblastoma. *Jco* 38, 1836–1848. doi:10.1200/jco.19.01410

Pelcovits, A., and Niroula, R. (2020). Acute Myeloid Leukemia: A Review. *R. I. Med. J. (2013)* 103, 38–40.

Ransohoff, J. D., Wei, Y., and Khavari, P. A. (2018). The Functions and Unique Features of Long Intergenic Non-coding RNA. *Nat. Rev. Mol. Cell Biol.* 19, 143–157. doi:10.1038/nrm.2017.104

Saha, S., Kiran, M., Kuscu, C., Chatrath, A., Wotton, D., Mayo, M. W., et al. (2020). Long Noncoding RNA DRAIC Inhibits Prostate Cancer Progression by Interacting with IKK to Inhibit NF-Kb Activation. *Cancer Res.* 80, 950–963. doi:10.1158/0008-5472.can-19-3460

Salmena, L., Poliseno, L., Tay, Y., Kats, L., and Pandolfi, P. P. (2011). A ceRNA Hypothesis: the Rosetta Stone of a Hidden RNA Language? *Cell* 146, 353–358. doi:10.1016/j.cell.2011.07.014

Shanmugalingam, T., Soultati, A., Chowdhury, S., Rudman, S., and Van Hemelrijck, M. (2013). Global Incidence and Outcome of Testicular Cancer. *Clin. Epidemiol.* 5, 417–427. doi:10.2147/CLEP.S34430

Siegel, R. L., Miller, K. D., and Jemal, A. (2017). Cancer Statistics, 2017. *CA Cancer J. Clin.* 67, 7–30. doi:10.3322/caac.21387

Siegel, R. L., Miller, K. D., and Jemal, A. (2018). Cancer Statistics, 2018. *CA Cancer J. Clin.* 68, 7–30. doi:10.3322/caac.21442

Siva, S., Deb, S., Young, R. J., Hicks, R. J., Callahan, J., Bressel, M., et al. (2015). 18F-FDG PET/CT Following Chemoradiation of Uterine Cervix Cancer Provides Powerful Prognostic Stratification Independent of HPV Status: a Prospective Cohort of 105 Women with Mature Survival Data. *Eur. J. Nucl. Med. Mol. Imaging* 42, 1825–1832. doi:10.1007/s00259-015-3112-8

Slack, F. J., and Chinnaiyan, A. M. (2019). The Role of Non-coding RNAs in Oncology. *Cell* 179, 1033–1055. doi:10.1016/j.cell.2019.10.017

Statello, L., Guo, C.-J., Chen, L.-L., and Huarte, M. (2021). Gene Regulation by Long Non-coding RNAs and its Biological Functions. *Nat. Rev. Mol. Cell Biol.* 22. doi:10.1038/s41580-020-00315-9

St. Laurent, G., Wahlestedt, C., and Kapranov, P. (2015). The Landscape of Long Noncoding RNA Classification. *Trends Genet.* 31, 239–251. doi:10.1016/j.tig.2015.03.007

Sugimura, K., Miyata, H., Shinno, N., Ushigome, H., Asukai, K., Yanagimoto, Y., et al. (2019). Prognostic Factors for Esophageal Squamous Cell Carcinoma Treated with Neoadjuvant Docetaxel/Cisplatin/5-Fluorouracil Followed by Surgery. *Oncology* 97, 348–355. doi:10.1159/000502342

Sung, H., Ferlay, J., Siegel, R. L., Laversanne, M., Soerjomataram, I., Jemal, A., et al. (2021). Global Cancer Statistics 2020: GLOBOCAN Estimates of Incidence and Mortality Worldwide for 36 Cancers in 185 Countries. *CA A Cancer J. Clin.* 71, 209–249. doi:10.3322/caac.21660

Sunkara, V., and Hébert, J. R. (2015). The Colorectal Cancer Mortality-To-Incidence Ratio as an Indicator of Global Cancer Screening and Care. *Cancer* 121, 1563–1569. doi:10.1002/cncr.29228

Tang, S., Xiao, G., Yuan, Q., Lin, W., Yuan, X., Fang, X., et al. (2021). Long Non-coding RNA ENST00000453774.1 Confers an Inhibitory Effect on Renal Fibrosis by Inhibiting miR-324-3p to Promote NRG1 Expression. *Front. Cell Dev. Biol.* 9, 580754. doi:10.3389/fcell.2021.580754

Walsh, J. M. E., and Terdiman, J. P. (2003). Colorectal Cancer Screening. *JAMA* 289, 1288–1296. doi:10.1001/jama.289.10.1288

Wang, H., Guo, Q., Nampoukime, K. P. B., Yang, P., and Ma, K. (2020). Long Non-coding RNA LINC00467 Drives Hepatocellular Carcinoma Progression via Inhibiting NR4A3. *J. Cell Mol. Med.* 24, 3822–3836. doi:10.1111/jcmm.14942

Wang, W., Bo, H., Liang, Y., and Li, G. (2021). LINC00467 Is Upregulated by DNA Copy Number Amplification and Hypomethylation and Shows ceRNA Potential in Lung Adenocarcinoma. *Front. Endocrinol. (Lausanne)* 12, 802463. doi:10.3389/fendo.2021.802463

Wang, X., Liu, H., Shen, K., Pan, X., Wei, Y., Lv, T., et al. (2019). Long Intergenic Non-coding RNA 00467 P-romotes L-ung A-denocarcinoma P-roliferation, M-igration and I-nvasion by B-inding with EZH2 and R-epressing HTRA3 E-xpression. *Mol. Med. Rep.* 20, 640–654. doi:10.3892/mmr.2019.10292

Wei, S., Liu, J., Li, X., and Liu, X. (2020). LncRNA MIR17HG Inhibits Non-small Cell Lung Cancer by Upregulating miR-142-3p to Downregulate Bach-1. *BMC Pulm. Med.* 20, 78. doi:10.1186/s12890-020-1112-3

Wu, Z. R., Yan, L., Liu, Y. T., Cao, L., Guo, Y. H., Zhang, Y., et al. (2018). Inhibition of mTORC1 by lncRNA H19 via Disrupting 4E-BP1/Raptor Interaction in Pituitary Tumours. *Nat. Commun.* 9, 4624. doi:10.1038/s41467-018-06853-3

Wycislo, K. L., and Fan, T. M. (2015). The Immunotherapy of Canine Osteosarcoma: a Historical and Systematic Review. *J. Vet. Intern Med.* 29, 759–769. doi:10.1111/jvim.12603

Xiao, J., Gong, L., Xiao, M., He, D., Xiang, L., Wang, Z., et al. (2021). LINC00467 Promotes Tumor Progression via Regulation of the NF-Kb Signal Axis in Bladder Cancer. *Front. Oncol.* 11, 652206. doi:10.3389/fonc.2021.652206

Xu, L., Liu, C., Ye, Z., Wu, C., Ding, Y., and Huang, J. (2021). Overexpressed LINC00467 Promotes the Viability and Proliferation yet Inhibits Apoptosis of Gastric Cancer Cells via Raising ITGB3 Level. *Tissue Cell* 73, 101644. doi:10.1016/j.tice.2021.101644

Xu, Q., Ma, H., Chang, H., Feng, Z., Zhang, C., and Yang, X. (2020). The Interaction of Interleukin-8 and PTEN Inactivation Promotes the Malignant Progression of Head and Neck Squamous Cell Carcinoma via the STAT3 Pathway. *Cell Death Dis.* 11, 405. doi:10.1038/s41419-020-2627-5

Xue, F., Yang, C., Yun, K., Jiang, C., Cai, R., Liang, M., et al. (2021). Reduced LINC00467 Elevates microRNA-125a-3p to Suppress Cisplatin Resistance in Non-small Cell Lung Cancer through Inhibiting Sirtuin 6 and Inactivating the ERK1/2 Signaling Pathway. *Cell Biol. Toxicol.* doi:10.1007/s10565-021-09637-6

Yan, J., Fang, T., Zhang, M., and Zhou, Q. (2021). LINC00467 Facilitates Osteosarcoma Progression by Sponging miR-217 to R-egulate KPNA4 E-xpression. *Int. J. Mol. Med.* 47. doi:10.3892/ijmm.2021.4859

Yan, J., Yao, L., Li, P., Wu, G., and Lv, X. (2022). Long Non-coding RNA MIR17HG Sponges microRNA-21 to Upregulate PTEN and Regulate Homoharringtonine-Based Chemoresistance of Acute Myeloid Leukemia Cells. *Oncol. Lett.* 23, 24. doi:10.3892/ol.2021.13142

Yang, J., Liu, Y., Mai, X., Lu, S., Jin, L., and Tai, X. (2019). STAT1-induced Upregulation of LINC00467 Promotes the Proliferation Migration of Lung Adenocarcinoma Cells by Epigenetically Silencing DKK1 to Activate Wnt/β-Catenin Signaling Pathway. *Biochem. Biophysical Res. Commun.* 514, 118–126. doi:10.1016/j.bbrc.2019.04.107

Ye, M., Zhang, J., Wei, M., Liu, B., and Dong, K. (2020). Emerging Role of Long Noncoding RNA-Encoded Micropeptides in Cancer. *Cancer Cell Int.* 20, 506. doi:10.1186/s12935-020-01589-x

Yin, D., Lu, X., Su, J., He, X., De, W., Yang, J., et al. (2018). Long Noncoding RNA AFAP1-AS1 Predicts a Poor Prognosis and Regulates Non-small Cell Lung Cancer Cell Proliferation by Epigenetically Repressing P21 Expression. *Mol. Cancer* 17, 92. doi:10.1186/s12943-018-0836-7

Zhang, J., Jiang, J., Zhao, L., Zhang, J., Shen, N., Li, S., et al. (2019). Survival Prediction of High-Grade Glioma Patients with Diffusion Kurtosis Imaging. *Am. J. Transl. Res.* 11, 3680–3688.

Zhang, Y., Jiang, X., Wu, Z., Hu, D., Jia, J., Guo, J., et al. (2020). Long Noncoding RNA LINC00467 Promotes Glioma Progression through Inhibiting P53 Expression via Binding to DNMT1. *J. Cancer* 11, 2935–2944. doi:10.7150/jca.41942

Zhang, Y., Sun, Y., Ding, L., Shi, W., Ding, K., and Zhu, Y. (2021). Long Non-coding RNA LINC00467 Correlates to Poor Prognosis and Aggressiveness of Breast Cancer. *Front. Oncol.* 11, 643394. doi:10.3389/fonc.2021.643394

Zhao, L., Wang, J., Li, Y., Song, T., Wu, Y., Fang, S., et al. (2021). NONCODEV6: an Updated Database Dedicated to Long Non-coding RNA Annotation in Both Animals and Plants. *Nucleic acids Res.* 49, D165–D171. doi:10.1093/nar/gkaa1046

Zheng, B., Wang, J., Fan, K., Sun, W., Wan, W., Gao, Z., et al. (2021). lncRNA RP11-147L13.8 Suppresses Metastasis and Chemo-Resistance by Modulating the Phosphorylation of C-Jun Protein in GBC. *Mol. Ther. - Oncolytics* 23, 124–137. doi:10.1016/j.omto.2021.08.016

Zheng, Y., Nie, P., and Xu, S. (2020). Long Noncoding RNA Linc00467 Plays an Oncogenic Role in Hepatocellular Carcinoma by Regulating the miR-18a-5p/NEDD9 axis. *J. Cell Biochem.* 121, 3135–3144. doi:10.1002/jcb.29581

Zhu, Y., Li, J., Bo, H., He, D., Xiao, M., Xiang, L., et al. (2020). LINC00467 Is Up-Regulated by TDG-Mediated Acetylation in Non-small Cell Lung Cancer and Promotes Tumor Progression. *Oncogene* 39, 6071–6084. doi:10.1038/s41388-020-01421-w

Conflict of Interest: The authors declare that the research was conducted in the absence of any commercial or financial relationships that could be construed as a potential conflict of interest.

Publisher's Note: All claims expressed in this article are solely those of the authors and do not necessarily represent those of their affiliated organizations, or those of the publisher, the editors and the reviewers. Any product that may be evaluated in this article, or claim that may be made by its manufacturer, is not guaranteed or endorsed by the publisher.

frontiers | Frontiers in Genetics

ORIGINAL RESEARCH
published: 08 June 2022
doi: 10.3389/fgene.2022.882324

Construction of Immune-Related ceRNA Network in Dilated Cardiomyopathy: Based on Sex Differences

Chang Liu[1,2†], *Jian Liu*[1,2†], *Daihong Wu*[1,2], *Shaoling Luo*[1,2], *Weijie Li*[1,2], *Lushan Chen*[1,2], *Zhen Liu*[1,2*] and *Bingbo Yu*[1,2*]

[1]Department of Cardiology, Guangzhou First People's Hospital, School of Medicine, South China University of Technology, Guangzhou, China, [2]Department of Cardiology, Guangzhou First People's Hospital, Guangzhou Medical University, Guangzhou, China

OPEN ACCESS

Edited by:
Jian-Hong Fang,
Sun Yat-sen University, China

Reviewed by:
Mingguo Xu,
Shenzhen Children's Hospital, China
Xiaoxian Qian,
Third Affiliated Hospital of Sun Yat-sen University, China
Ruijie Zhang,
Harbin Medical University, China

***Correspondence:**
Zhen Liu
lz71826@163.com
Bingbo Yu
yby5689@163.com

†These authors have contributed equally to this work

Specialty section:
This article was submitted to RNA, a section of the journal Frontiers in Genetics

Received: 23 February 2022
Accepted: 26 April 2022
Published: 08 June 2022

Citation:
Liu C, Liu J, Wu D, Luo S, Li W, Chen L, Liu Z and Yu B (2022) Construction of Immune-Related ceRNA Network in Dilated Cardiomyopathy: Based on Sex Differences. Front. Genet. 13:882324. doi: 10.3389/fgene.2022.882324

Background: Immune targeted therapy has become an attractive therapeutic approach for patients with dilated cardiomyopathy (DCM) recently. Genetic predisposition and gender play a critical role in immune-related responses of DCM. This study aimed to perform a bioinformatics analysis of molecular differences between male and female samples and identify immune-related ceRNA network in DCM.

Methods: The gene expression microarray and clinical features dataset of GSE19303 was downloaded from the GEO. The raw data were preprocessed, followed by identification of differentially expressed genes (DEGs) between male and female DCM samples. Crucial functions and pathway enrichment analysis of DEGs were investigated through GO analysis and KEGG pathway analysis, respectively. A lncRNA–miRNA–mRNA network was constructed and a central module was extracted from the ceRNA network.

Results: Compared with the female group, the male group benefits more from IA/IgG immunotherapy. Male patients of DCM had a significant positive correlation with the abundance of inflammatory cells (B cells, memory B cells, $CD8^+$ Tem cells, and NK cells). Sex difference DEGs had a widespread impact on the signaling transduction, transcriptional regulation, and metabolism in DCM. Subsequently, we constructed an immune-related ceRNA network based on sex differences in DCM, including five lncRNAs, six miRNAs, and 29 mRNAs. Furthermore, we extracted a central module from the ceRNA network, including two lncRNAs (XIST and LINC00632), three miRNAs (miR-1-3p, miR-17-5p, and miR-22-3p), and six mRNAs (CBL, CXCL12, ESR1, IGF1R, IL6ST, and STC1). Among these DEGs, CBL, CXCL12, and IL6ST expression was considered to be associated with inflammatory cell infiltration in DCM.

Conclusions: The identified ceRNA network and their enriched pathways may provide genetic insights into the phenotypic diversity of female and male patients with DCM and may provide a basis for development of sex-related individualization of immunotherapy.

Keywords: dilated cardiomyopathy, immunotherapy, sex differences, ceRNA network, gene regulation, bioinformatics

INTRODUCTION

Globally, dilated cardiomyopathy (DCM) is one of the most common forms of cardiomyopathy, and it represents a leading cause of cardiac transplantation in children and adults (Martinez et al., 2021). Contemporary estimates of the DCM prevalence range from one in 2,500 to one in 250 people (Merlo et al., 2018). Theoretically, DCM is a heart muscle disease characterized by left or biventricular dilatation and systolic dysfunction in the absence of coronary artery disease, hypertension, valvular disease, or congenital heart disease (WJ et al., 2017). The important feature of DCM is the structural or functional abnormalities of the heart muscle, which leads to complications such as heart failure and arrhythmia and results in substantial morbidity and mortality (P et al., 1996). It is increasingly appreciated that DCM is more than a single-disease entity of "nonischemic" heart failure but rather represents a unique family of heart muscle diseases with complex interactions between genetic predisposition, infection, inflammation, autoimmune diseases, endocrine, and environmental precipitants (Asher et al., 2021).

Male sex is a key risk factor for progression to heart failure following a large number of cardiovascular conditions, including DCM (Cannata et al., 2020). Studies reported gender data for nongenetic DCM with an average overall sex ratio of 2.5:1, male to female (Jain et al., 2021). However, few clinical studies have specifically investigated gender-related differences in the incidence or pathogenic mechanisms of DCM. It was found that men with acute DCM had higher expression of apoptosis-related proteins than that of women and higher expression levels associated with lower left ventricular ejection fraction (LVEF; the fraction of the volume of fluid ejected from the left ventricle with each contraction) (Sheppard et al., 2005a).

The most common causes of DCM are infections and autoimmunity. Enteroviruses, adenoviruses, and herpesviruses are commonly found in patients with DCM (Maekawa et al., 2007). Virus infection triggers the recruitment of inflammatory cells including mast cells, macrophages, helper T cells, and B cells (Schultheiss et al., 2019). These immune cells release cytokines, such as transforming growth factor-β1 (TGFβ1), interleukin (IL), and tumor necrosis factor (TNF), and other mediators that promote remodeling, collagen deposition, and fibrosis (Epelman et al., 2015). In addition, a number of factors, including the components of innate immunity and profibrotic cytokines, have been identified in animal models as important pathogenic mechanisms that increase inflammation and susceptibility to chronic DCM (Elamm et al., 2012). Correspondingly, immunoadsorption with subsequent immunoglobulin substitution (IA/IgG) therapy could improve LVEF, LVIDD, and NYHA classes of DCM (Ameling et al., 2016).

With the rapid development of sequencing technologies, an increasing number of competing endogenous RNAs (ceRNAs), such as microRNA (miRNA), long noncoding RNA (lncRNA), and circular RNA (circRNA), have been found to be involved in DCM progression (Lin et al., 2021). The genes most commonly known to cause DCM, including TTN, LMNA, MYH7, BAG3, TNNT2, and others, were identified initially in large DCM pedigrees (Schultheiss et al., 2019). Interestingly, a number of circRNAs are generated from genes which are associated with cardiovascular diseases, such as TTN and RYR2 (Tan et al., 2017). In addition, emerging evidence reveals critical roles for lncRNAs in the development and progression of DCM (Chen et al., 2021). Moreover, downregulation of the miRNA-221/222 family associated with heart failure enables profibrotic TGF-β signaling in pressure-overloaded hearts (Verjans et al., 2018).

Historically, pharmacological therapy (ACE inhibitors and β-blockers) and cardiac resynchronization therapy (CRT) are standard treatments for heart failure in DCM, but they all have limitations. Recently, immunotherapies have become an attractive therapeutic strategy in DCM. Moreover, sex differences and gene expression influence the efficacy of immunotherapies (Jain et al., 2021). Therefore, to provide personalized immunotherapy for DCM patients, it is crucial to identify key genes and pathways that may be related to the phenotypic diversity of male and female patients. In our study, we used a GSE19303 gene expression microarray of the myocardial biopsy samples from DCM patients. First, we found that immunotherapy significantly improved the clinical outcome of male DCM patients. Furthermore, we identified the sex-related DEGs in DCM and constructed pathways and functional enrichment analysis. We identified sex difference immune–related ceRNA network with high reliability, and our results showed that the lncRNA–miRNA–mRNA network may provide a new understanding of the mechanisms and potential therapeutic targets for DCM.

MATERIALS AND METHODS

Data Source

The GSE19303 gene expression microarray and clinical features dataset was obtained from Gene Expression Omnibus (http://ncbi.nlm.nih.gov/geo/). The dataset contained a total of 81 endomyocardial biopsy samples, 40 baseline biopsies from patients with DCM, 33 of 40 patients had received immunotherapy (immunoadsorption with subsequent immunoglobulin substitution (IA/IgG) treatment), 33 follow-up biopsies of DCM patients collected 6 months after the treatment, and eight biopsies from individuals without DCM (Ameling et al., 2016). Among them, 40 baseline and 33 follow-up endomyocardial biopsy samples from DCM patients were utilized in our study and were divided into groups of different sexes. The male patient group contained 28 samples, and the female patient group included 12 samples. The platform for the gene expression profiles was GPL570 [HG-U133_Plus_2] Affymetrix Human Genome U133 Plus 2.0 Array (Affymetrix; Thermo Fisher Scientific, Inc., Waltham, MA, United States).

Research Design and Data Preprocessing

We retrieved the expression matrix from the GEO database and preprocessed it by using the robust multiarray analysis (RMA) method (http://www.bioconductor.org/). After log2 transformation and quantile normalization of the expression data, we annotated the converted probe ID for each gene to a gene symbol utilizing hgu133plus2. db, org. Hs.eg.db, and the

annotate package in Bioconductor (http://www.bioconductor.org/). If a gene's symbol corresponded with the multiple probe IDs, the expression level of that gene was represented by the mean of the probes.

Clinical Features Analysis

T-tests or paired t-tests were used to test for differences, and outlier samples were assessed using 1.5 times the interquartile range of the differences, and Shapiro–Wilk normality test was used for normality tests. A p-value less than 0.05 is considered statistically significant.

Immune Cell Infiltration Abundance Analysis

IOBR (Immuno-Oncology Biological Research) is a computational tool for immuno-tumor biology research (Zeng et al., 2021). Here, based on our expression profiles, we use the IOBR package in R to analyze the immune cell infiltration abundance of GSE19303 datasets. The xCell method was selected to calculate infiltration abundance of 64 kinds of immune cells, stem cells, and stromal cells in each sample (Aran et al., 2017). The DEGs of the ceRNA network were divided into the high-expression and low-expression groups by the median. The relationship between DEG expression and the fractions of immune cells was investigated by Wilcoxon test. The results were visualized using the ggplot packages in R software.

Identification of Sex Difference Differentially Expressed Genes

The Linear Models for Microarray Analysis (Limma) package in R software was applied to identify the differentially expressed genes (DEGs) in the male DCM samples compared with the female DCM ones, based on Student's t-test. Adjusted p-values were calculated using the Benjamini–Hochberg method. The significant DEGs were selected with a threshold of p-value < 0.05 and fold change>1.5. We obtained the volcano plot utilizing the pheatmap package in R.

Moreover, we excluded the genes in the Y chromosomes and then compared the male and female DCM samples again using the Limma package. p-value < 0.05 and fold change>1.5 were selected to be the cutoff criteria of the significant DEGs. We obtained another volcano and heatmap plot. In order to plot the differentially expressed lncRNAs (DE-lncRNAs), we used the pheatmap package in R to construct a heatmap.

Functional Enrichment Analysis

In order to explore the potential functions and pathways that may be altered by the DEGs, we applied the clusterProfiler package in R to perform the functional and pathway enrichment analyses of the identified DEGs. The Gene Ontology (GO; http://www.geneontology.org/) database was used to determine the biological processes (BPs) that the DEGs may be involved in. In addition, according to the modified Fisher's exact test, the Kyoto Encyclopedia of Genes and Genomes (KEGG; http://www.genome.jp/kegg/pathway.html) database was used for pathway enrichment analysis of the identified DEGs. The selection criteria for the significant GO terms and pathways were $p < 0.05$, and the number of enriched genes were (also called count) > 2. The plots were performed by the ggplot2 package in R.

Gene Set Enrichment Analysis

GSEA software (version 3.0) and c2. all.v7.4. symbols.gmt subcollection were obtained from the GSEA website (http://software.broadinstitute.org/gsea/index.jsp) (Subramanian et al., 2005). We divided the samples into two groups by sex. The minimum gene set was 5 and the maximum gene set was 5,000, with 1,000 resampling. p-value < 0.05 (as needed) or FDR <0.25 (as needed) were considered statistically significant.

Screening of Sex Difference Immune-Related Genes

Potential interactions between DE-lncRNAs and DE-miRNAs and between DE-miRNAs and DEGs were predicted using DIANA (https://diana.e-ce.uth.gr/lncbasev3) (Karagkouni et al., 2020) and ENCORI databases (https://starbase.sysu.edu.cn/index.php) (Li et al., 2014), respectively. Only the lncRNA–miRNA and miRNA-DEG interactors, that had an opposite expression trend, were used to construct the ceRNA network. The immune gene list was obtained from the Immunology Database and Analysis Portal (IMMPORT) database (http://www.immport.org/) (Bhattacharya et al., 2014). The Venny online tool was used to analyze the overlapping genes (http://jvenn.toulouse.inra.fr/app/example.html) (Bardou et al., 2014).

ceRNA Network Enrichment Analysis

Coexpression patterns in 29 immune-related DEGs were analyzed using Pearson's correlation coefficient, and the results were visualized using the heatmap packages in R software. Cytoscape software (version 3.8.2, https://cytoscape.org) was used to develop the ceRNA network. For gene set functional enrichment analysis, we used the GO and KEGG annotations of genes in the R package org. Hs.eg.db (version 3.1.0) as the background to map the genes to the background set using the R package clusterProfiler (version 3.14.3) to perform enrichment analysis to obtain gene set enrichment results. p-value < 0.05 was considered statistically significant.

Predicted Protein–Protein Interaction Network Analysis

A protein–protein interaction (PPI) network, comprising 50 ceRNA network coexpression proteins, was constructed by GeneMANIA (http://genemania.org/) (Warde-Farley et al., 2010). These nodes represent genes that are closely related to the ceRNA network in terms of physical interactions, shared protein domains, predictions, colocalization, pathway,

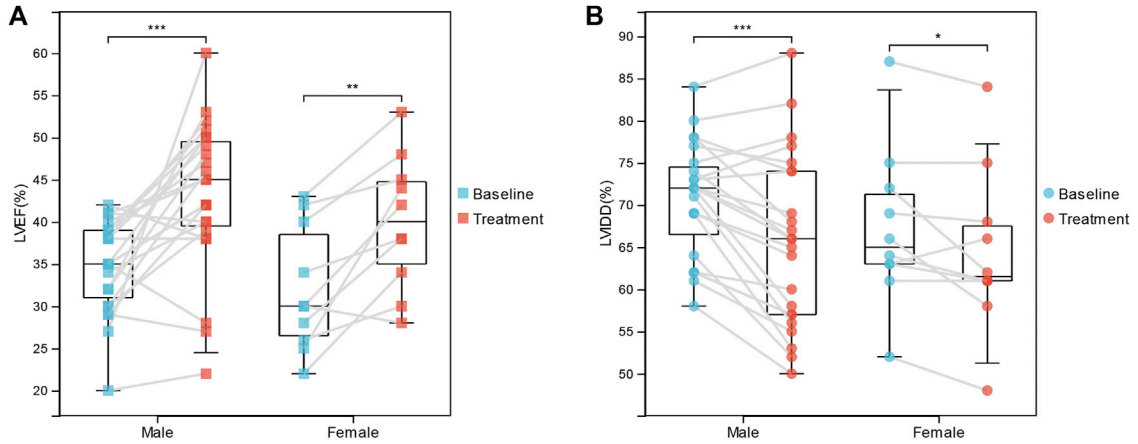

FIGURE 1 | Correlations Between IgG immunotherapy and Clinical Outcome Features. **(A)** LVEF in paired baseline and IgG treatment DCM patients. **(B)** LVIDD in paired baseline and IgG treatment DCM patients. *, $p < 0.05$; **, $p < 0.01$; and ***, $p < 0.001$.

coexpression, and genetic interactions. We use NetworkAnalyst (version 3.0, https://www.networkanalyst.ca/) to carry out the heart (left ventricle)-specific PPI, TF-miRNA interactions, and protein–chemical interaction analysis on the ceRNA network coexpression module (Zhou et al., 2019). In these networks, the nodes represent individual genes/proteins/chemicals, while the edges which connect the nodes correspond to a known, curated interaction between a given pair of nodes.

Tool Usage

All the statistical analyses were performed using R (version 3.6.4) or SPSS (version 19.0), and a *p*-value less than 0.05 is considered statistically significant. The plots were performed by R, Cytoscape software (version 3.8.2, https://cytoscape.org), or SangerBox tools (version 3.0, http://www.sangerbox.com/tool).

RESULTS

Baseline Clinical Characteristics of Dilated Cardiomyopathy Patients

The RNA array data for a total of 40 DCM patients were acquired from the GES19303 dataset. The detailed baseline clinical features are listed in **Supplementary Table S1**. Among the 40 participants, 28 were male and 12 were female. DCM patient gender (male vs. female) was significantly correlated with age (52.2 ± 9.21 years vs. 45.42 ± 8.08 years, $p = 0.032$) and Epstein–Barr virus (EBV) infection (0/28 vs. 2/12, $p = 0.027$). However, gender was not significantly correlated with other clinical features such as LVEF, LVIDD, BMI, inflammation index, total virus infection, PVB19 infection, HHV6 infection, HSV1 infection, and IgG treatment.

Immunotherapy Significantly Improves the Clinical Outcome of Dilated Cardiomyopathy Patients

Moreover, we investigated the association between IA/IgG treatment and clinical outcome features in DCM patients. In female patients, immunotherapy was significantly correlated with LVEF (32.00 ± 7.44% vs. 40.00 ± 7.93%, $p = 0.002$) and LVIDD (67.20 ± 9.40% vs. 64.40 ± 9.79%, $p = 0.047$). For male patients, immunotherapy was more significantly correlated with LVEF (34.70 ± 5.43% vs. 43.22 ± 8.88%, $p = 3.74E\text{-}04$) and LVIDD (70.74 ± 6.72% vs. 65.70 ± 10.30%, $p = 1.417E\text{-}04$) (**Figures 1A,B**). However, IgG treatment was not significantly correlated with the inflammation index (**Table 1**). These results suggest that IA/IgG immunotherapy could significantly improve the outcome of DCM especially in male patients.

Sex is Correlated With Immune Infiltration Levels in Dilated Cardiomyopathy

To gain insight into potential target immune cells of DCM IA/IgG immunotherapy, we estimated the composition of the microenvironment in baseline DCM patients by using the xCell algorithm. Our result showed that the composition of the microenvironment of DCM was complex (**Figure 2A**). The top five abundant cell types were multipotent progenitors (MPPs), mesenchymal stem cells (MSCs), natural killer T cells (NKTs), immature dendritic cells (iDCs), and microvascular endothelial cells (mv endothelial cells) (**Figure 2B**). Moreover, when compared with the female DCM patients, male DCM patients had a significant positive correlation with abundance of B cells, memory B cells, effect memory $CD8^+$ cells, and NK cells (**Figure 2C**). These results suggest that sex-differentiated microenvironments may contribute to differences in immunotherapy efficacy.

TABLE 1 | Correlations between IA/IgG immunotherapy and clinical features of DCM in male and female patients.

Clinical Characteristics	Baseline	Follow up	*p* value
Male patients	—	—	—
LVEF (%)	34.70 ± 5.43	43.22 ± 8.88	**3.74E-04**
LVIDD (%)	70.74 ± 6.72	65.70 ± 10.30	**1.417E-04**
Inflammation index ($CD68^+$ + $CD3^+$) %	21.26 ± 12.17	17.87 ± 8.88	0.271
Female patients	—	—	—
LVEF (%)	32.00 ± 7.44	40.00 ± 7.93	**0.002**
LVIDD (%)	67.20 ± 9.40	64.40 ± 9.79	**0.047**
Inflammation index ($cd68^+$ + $cd3^+$) %	16.80 ± 5.55	13.70 ± 7.66	0.132

Bold values indicate $p < 0.05$.

Identification of Sex Difference Differentially Expressed Genes in Dilated Cardiomyopathy

A total of 1,138 DEGs were finally screened from the comparison of male DCM samples with female DCM samples, including 579 upregulated and 556 downregulated DEGs (**Figure 3A**). Considering that genes in the Y chromosome is few in number and misleading, we removed the genes in the Y chromosome in the subsequent analyses. After excluding the genes in the Y chromosomes, we obtained 1,071 DEGs, of which 542 were upregulated and 529 were downregulated in the male group (**Figure 3B**). The top 50 significant positive and negative sex-related DEGs correlated with DCM are shown in the heatmap (**Figure 3C**). Interestingly, there were 68 differentially expressed lncRNAs (DE-lncRNAs) and five differentially expressed miRNAs (DE-miRNAs) in DEGs, and the top 50 significant DE-lncRNAs are shown in the heatmap (**Figure 3D**).

Sex Difference Signaling Pathways and Functional Enrichment Analysis in Dilated Cardiomyopathy

The upregulated and downregulated DEGs were processed separately for the GO and KEGG pathway analyses. The significantly enriched biological processes (BPs) were negative regulation of cellular process, negative regulation of programmed cell death, cardiovascular system development, ncRNA metabolic process, and RNA modification (**Figure 4A**). The significantly enriched cellular components (CCs) were the cytoskeleton, endoplasmic reticulum part, extracellular matrix, complex of collagen trimers, and RNA polymerase I transcription factor complex (**Figure 4B**). The significantly enriched molecular functions (MFs) were molecular function regulator, signaling receptor binding, extracellular matrix structural constituent, core promoter binding, and antiporter activity (**Figure 4C**). The significantly enriched KEGG were focal adhesion, tight junction, amebiasis, ECM–receptor interaction, and amino-acid metabolism (**Figure 4D**). These results suggest that there is a widespread impact of sex difference on the signaling transduction, transcriptional regulation, and metabolism.

To confirm the abovementioned results, we performed GSEA on the sex-related DEGs to identify Gene Ontology and signaling pathways that were differentially activated in DCM. The top 20 significant positive and negative enrichment pathways are shown in **Figure 5A**. GSEA showed that significant positively enriched pathways in male are aminoacyl tRNA biosynthesis, TP53 targets apoptotic, protein repair, RNA polymerase I transcription initiation, and TRAIL signaling. (**Figure 5B**). Gene sets related to collagens, TGF-beta receptor signaling, epithelial-to-mesenchymal transition, degradation of the extracellular matrix, and IL6 signaling showed enrichment in the female DCM patients (**Figure 5C**).

Construction of Sex Difference Immune-Related ceRNA Network

Among the 68 DE-lncRNAs and five DE-miRNAs, five DE-lncRNAs (ARHGEF7-IT1, LINC00632, LINC02135, TEX36-AS1, and X-inactive specific transcript (XIST)) were predicted to interact with four DE-miRNAs (miR-1-3p, miR-17-5p, miR-22-3p, and miR-146a-5p) by the DIANA database. The four DE-miRNAs were predicted to interact with a total of 7,747 genes by the ENCORI database (**Figure 6A**). To further construct the sex difference immune-related ceRNA network, the Venny method was used to analyze the intersection between DEGs, miR-related genes, and immune genes (**Figure 6B**). The coexpression plot among these 29 genes is presented in **Figure 6C**. These DE-lncRNA–miRNA–immune gene interaction pairs were integrated to construct the ceRNA network (**Figure 6D**). Furthermore, we extracted a central module from the ceRNA network, including two lncRNAs (XIST and LINC00632), three miRNAs (miR-1-3p, miR-17-5p, and miR-22-3p), and six mRNAs (Casitas B-Lineage Lymphoma Proto-Oncogene (CBL), C-X-C Motif Chemokine Ligand 12 (CXCL12), Estrogen Receptor 1 (ESR1), Insulin-like Growth Factor 1 Receptor (IGF1R), Interleukin 6 Cytokine Family Signal Transducer (IL6ST), and Stanniocalcin 1 (STC1)) (**Figure 6E**).

GO and KEGG enrichment analyses were conducted to investigate the functions of the ceRNA network. GO_BP analysis showed that ceRNA network was significantly enriched in programmed cell death, immune system

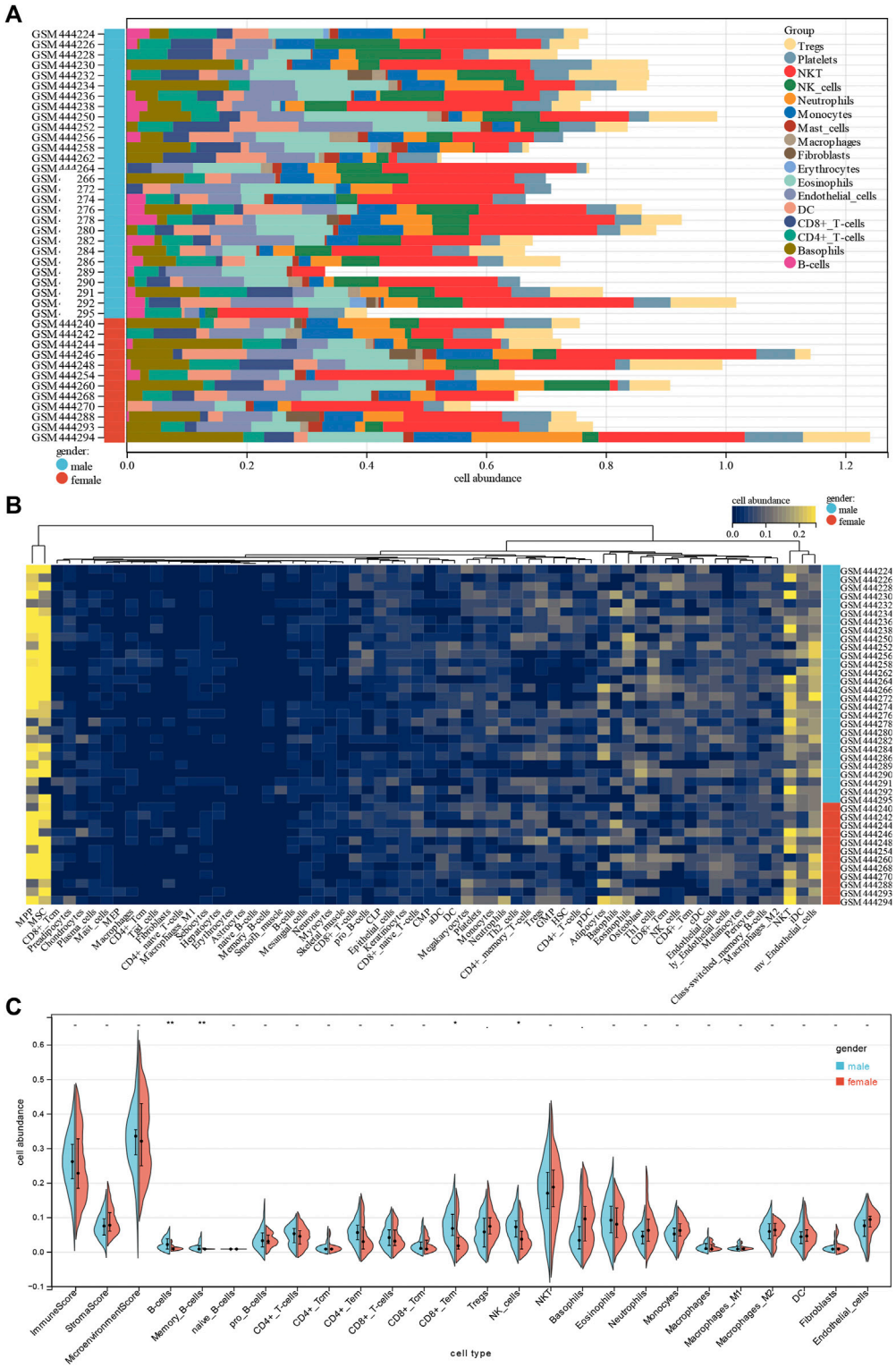

FIGURE 2 | Correlations of gender with immune infiltration level in DCM tissues. **(A)** Distribution of immune cell infiltration in each sample. **(B)** Heatmap of immune cell types. **(C)** Violin plot of infiltrating immune cells.

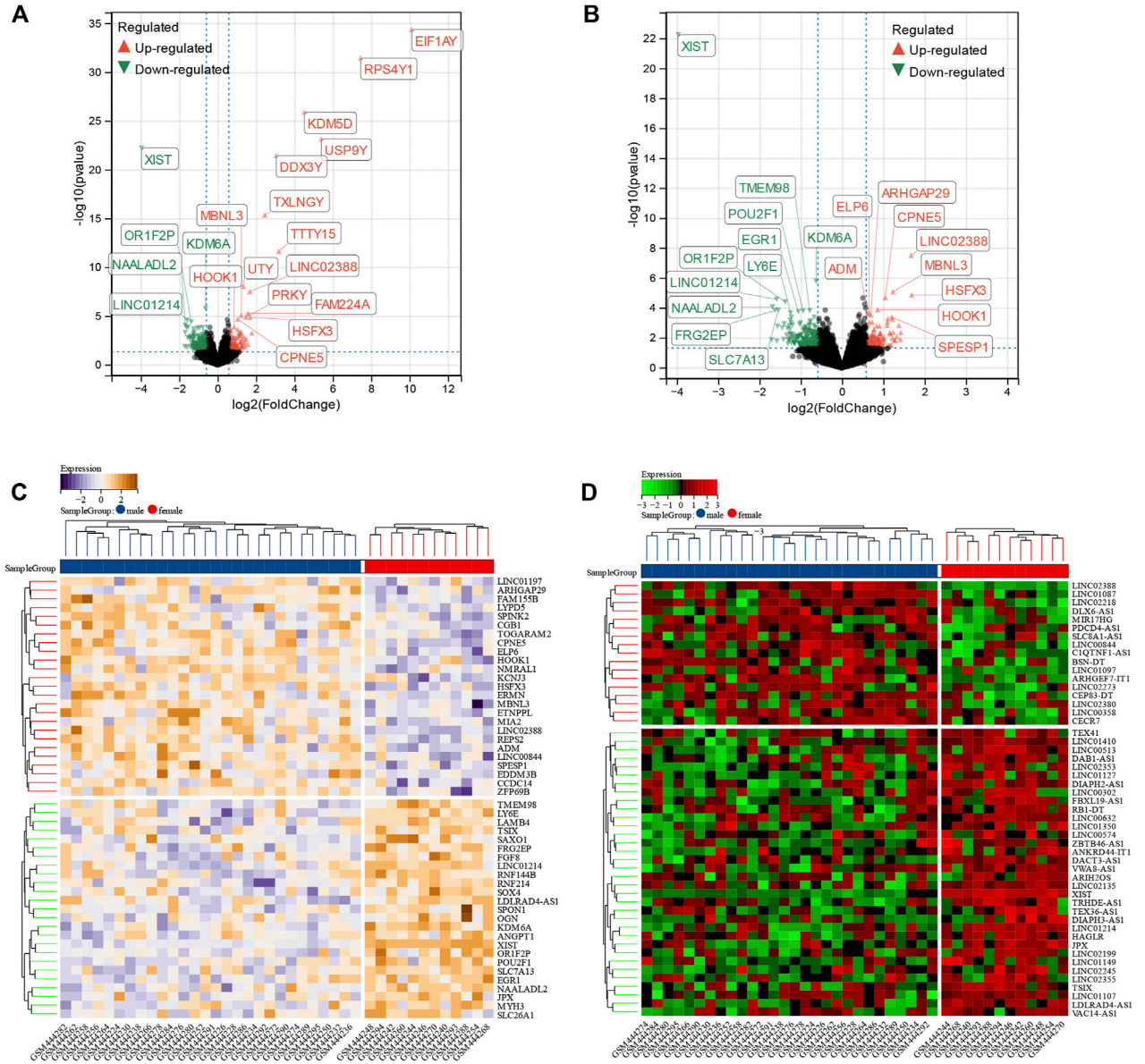

FIGURE 3 | Identification of sex difference DEGs in DCM. **(A)** The volcano plot of all DEGs of male and female DCM patient myocardial tissues. The differences are set as *p* value<0.05 and |log FC| >1.5. **(B)** The volcano plot of all DEGs of male and female DCM patients after excluding the genes on Y chromosomes. The differences are set as *p* value<0.05 and |log FC| >1.5. **(C)** Heatmap showing 50 significantly DEGs of male and female DCM patients after excluding the genes on Y chromosomes. **(D)** Heatmap showing 50 significant DE-lncRNAs of male and female DCM patients after excluding the genes on Y chromosomes.

process, and heart development (**Figure 7A**). GO_CC analysis showed that the ceRNA network was significantly enriched in the cell surface, endoplasmic reticulum, and collagen-containing extracellular matrix (**Figure 7B**). GO_MF analysis showed that the ceRNA network was significantly enriched in molecular function regulator, cytokine activity, and RNA polymerase II transcription factor binding (**Figure 7C**). The KEGG pathway enrichment analysis showed that ceRNA network was significantly enriched in cytokine–cytokine receptor interaction, Ras signaling pathway, and natural killer cell–mediated cytotoxicity (**Figure 7D**).

Regulators of Sex Difference Immune-Related ceRNA Network in Dilated Cardiomyopathy

The protein–protein interaction (PPI) network was assembled based on the ceRNA network in the DCM cohort by GeneMANIA. The analysis showed that the 50 most significantly coexpressed genes play roles in peptidyl-

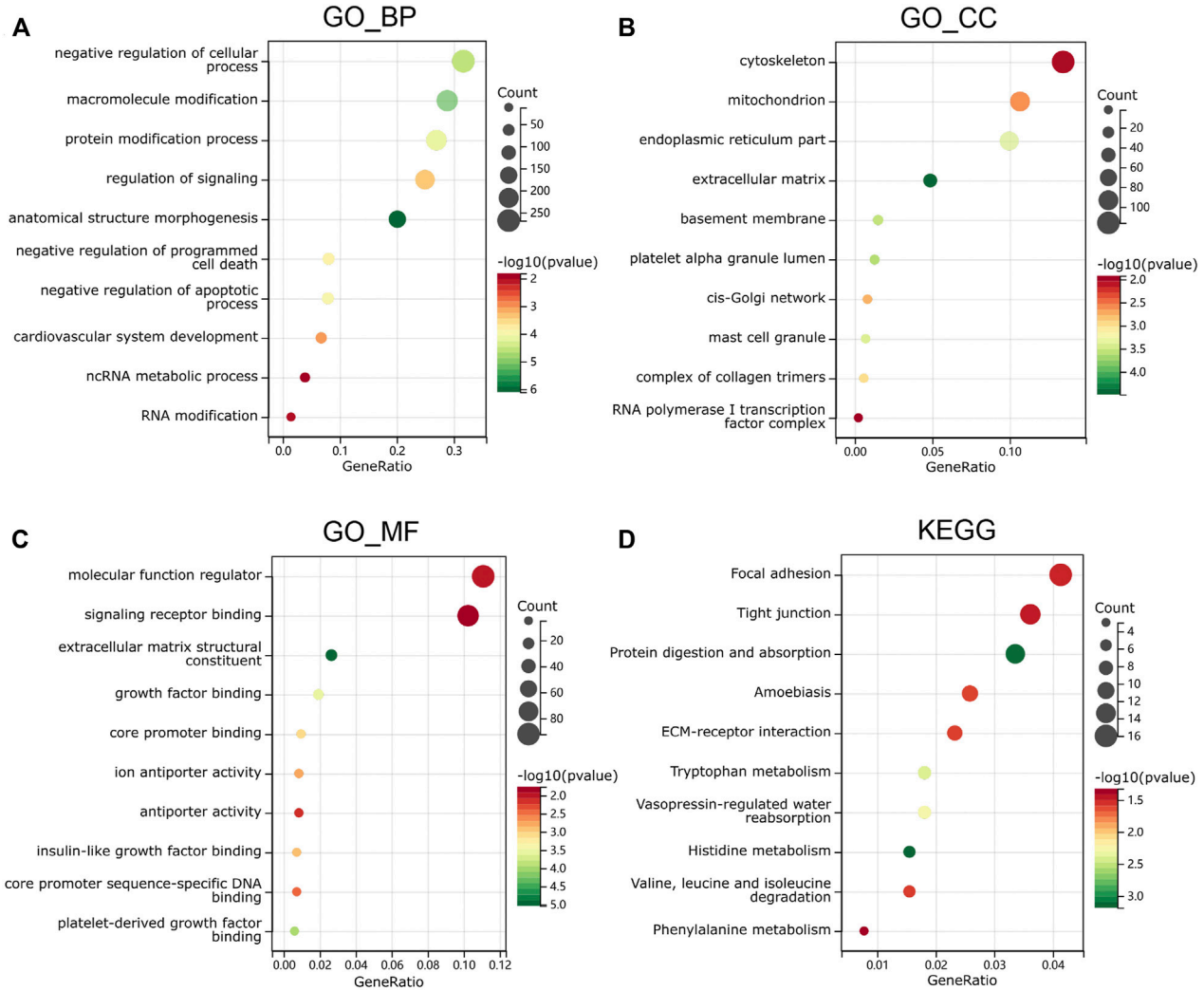

FIGURE 4 | Functional enrichment analysis in GO and KEGG. **(A)** biological process, **(B)** molecular function and **(C)** cell composition of GO enrichment analysis. **(D)** Kyoto Encyclopedia of Genes and Genomes analysis results of differentially expressed gender-related genes between male and female. The words on the left indicates enriched terms, the size of the balls indicates the number of the genes enriched and the color indicates the level of the enrichment.

tyrosine phosphorylation, leukocyte chemotaxis, and the vascular process in the circulatory system (**Figure 8A**). Next, the ceRNA network was assembled based on the heart (left ventricle)-specific data collected from the DifferentialNet database (Basha et al., 2018) by NetworkAnalyst (**Figure 8B**). The top five hub proteins were CBL, FYN Proto-Oncogene (FYN), Kinase Insert Domain Receptor (KDR), ESR1, and Histone Deacetylase 1 (HDAC1) (**Supplementary Table S2**). Furthermore, a graph of TF-miRNA coregulatory interactions of the ceRNA network was constructed based on the RegNetwork database (Liu et al., 2015) (**Figure 8C**). From this, the top five TFs identified were Myelocytomatosis Oncogene (MYC), Nuclear Factor Kappa B Subunit 1 (NFKB1), Specificity Protein 1 (SP1), MYC Associated Factor X (MAX), and Upstream Transcription Factor 1 (USF1) (**Supplementary Table S3**).

Identifies Potential Target Drugs of Sex Difference Immune-Related ceRNA Network

To gain insight into the potential target drugs based on our established ceRNA network, we examined protein–chemical interactions from the Comparative Toxicogenomics Database (CTD) (Davis et al., 2021) (**Figure 8D**). Excluding hazardous chemicals, the top five drugs were 4-fluorobenzoyl-TN-14003, polyphenon E, 3-(4-methylphenylsulfonyl)-2-propenenitrile, deoxyglucose, and arachidonic acid (**Supplementary Table S4**). 4-fluoro benzoyl-TN-14003(BKT140, motixafortide) is a high-affinity CXCR4 antagonist, which can inhibit the migration of prostate cancer cells (Peng and Kopecek, 2014). BKT140 has been tested in stimulating megakaryopoiesis and platelet production (Abraham et al., 2013). Polyphenon E is a green tea polyphenol preparation which possesses potent antioxidative and

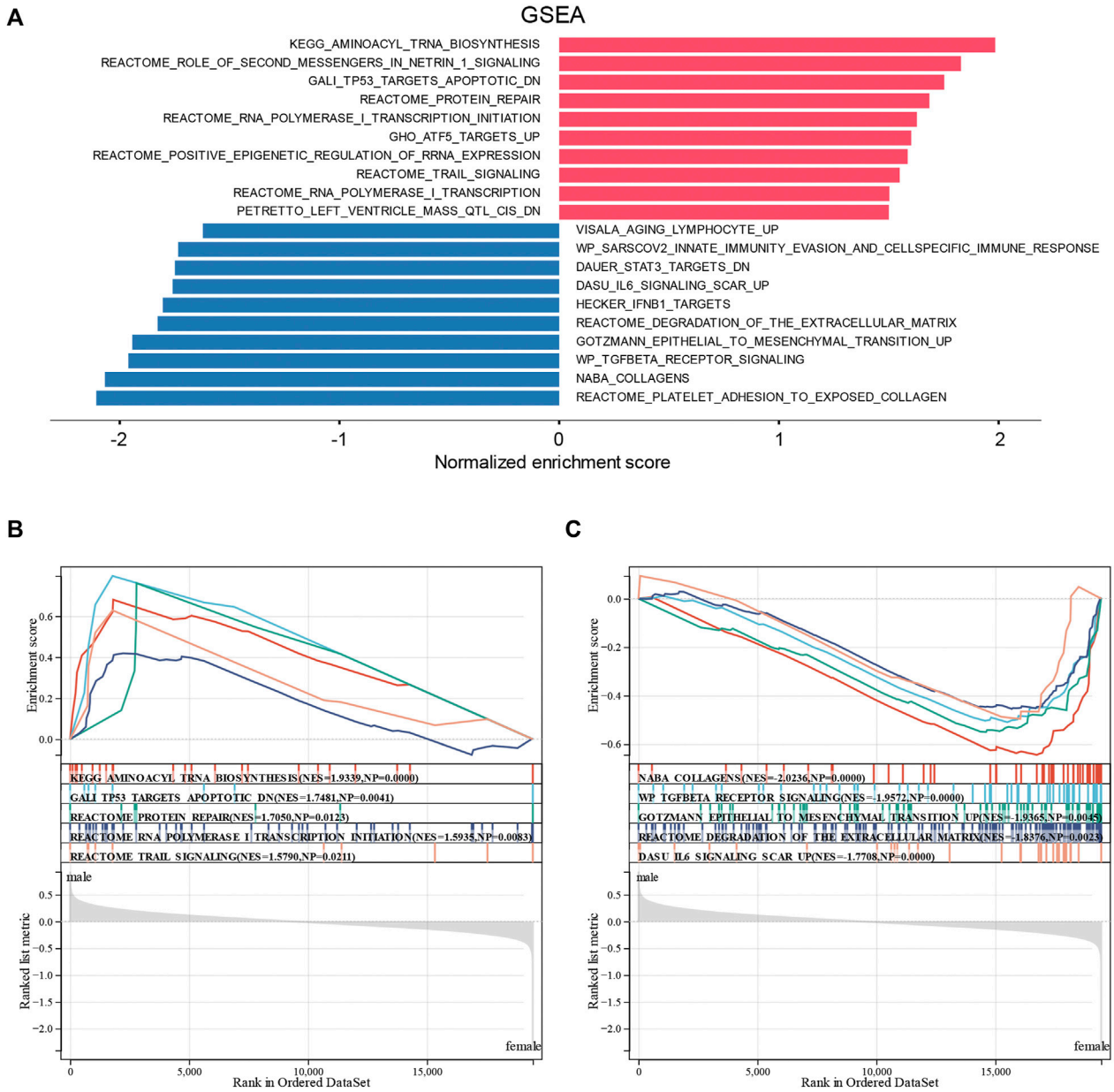

FIGURE 5 | Enrichment plots from GSEA. **(A)** Significantly enriched pathway annotations of DCM. **(B)** Significantly positive enriched pathways in male DCM patients. **(C)** Significantly positive enriched pathways in female DCM patients.

anti-inflammatory properties (Bornhoeft et al., 2012). 3-(4-methylphenylsulfonyl)-2-propenenitrile (BAY11-7,082) is an NF-kappaB inhibitor, which can protect the myocardial infarction heart from cardiac dysfunction in the mouse model (Martinez-Martinez et al., 2017). Moreover, BAY11-7,082 significantly reduced the TNF and IL-6 protein expression in atherogenesis (Vallejo et al., 2018). Deoxyglucose (2-DG) is a glucose molecule which cannot undergo further glycolysis. 2-DG can antagonize DOX-induced cardiomyocyte death, which is mediated through multiple mechanisms, including the preservation of ATP content, the activation of AMPK, and the inhibition of autophagy (Chen et al., 2011). Arachidonic acid (AA) is an essential fatty acid, which can be found in fish and certain plant oils. Higher *in vivo* circulating and tissue levels of AA were associated with lower risk of major cardiovascular events (Marklund et al., 2019). In addition, sex differences in the AA levels could be an important underlying mechanism for different effects of sex hormones and cardiovascular disease differences between males and females (Gerges and El-Kadi, 2021). Based on the previous research, these drugs show promising potential as novel therapies against DCM *via* the immune-related ceRNA network. However, further evaluation is still needed.

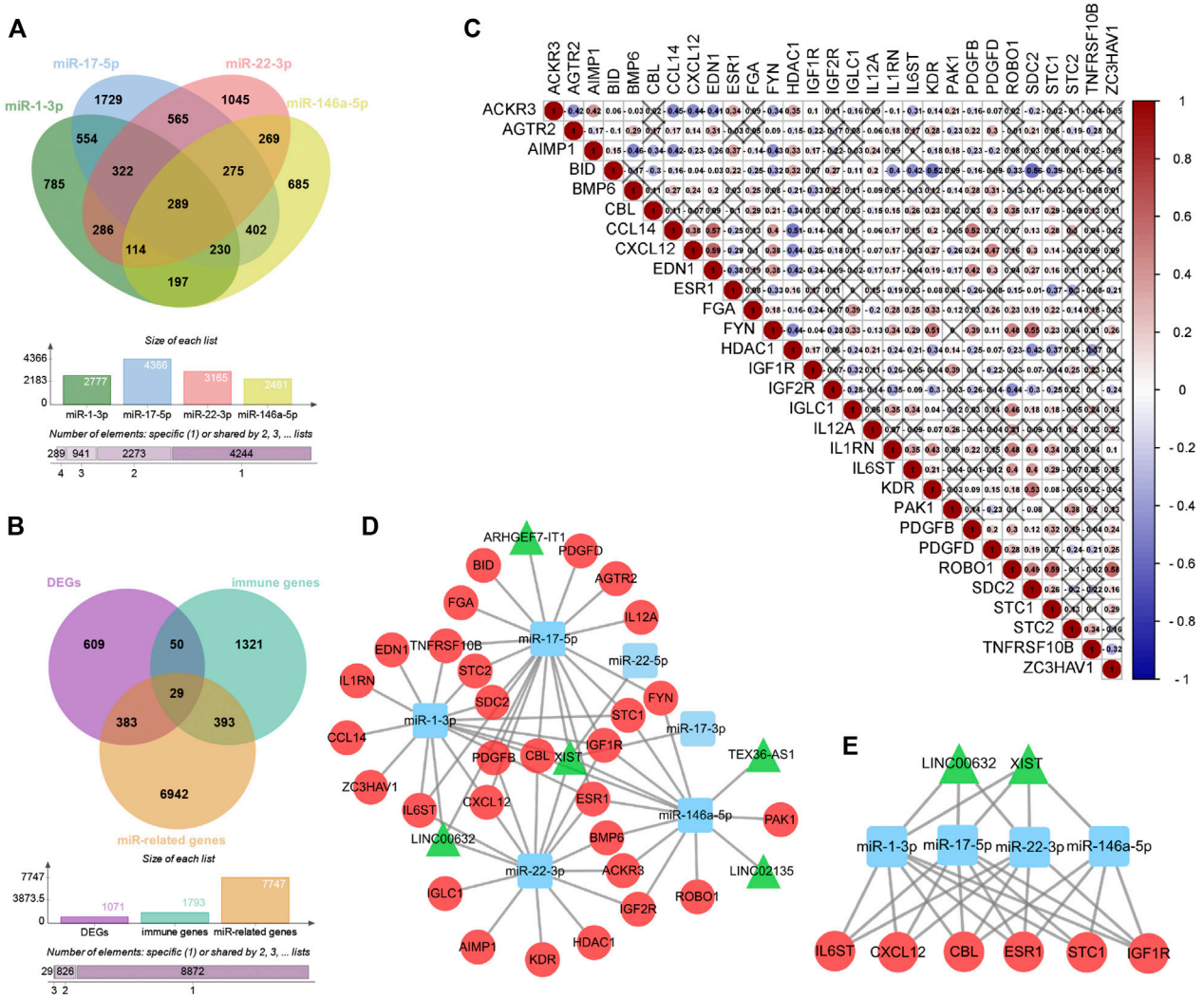

FIGURE 6 | Construction of Sex difference Immune-related ceRNA Networks. **(A)** Intersection between four kinds of microRNAs. **(B)** Intersection between DEGs, miR-related genes and immune genes. **(C)** Co-expression analysis of immune-related DE-mRNAs. **(D)** ceRNA network among lncRNAs, miRNAs, and mRNAs, Circular, mRNAs; triangle, lncRNAs; square, miRNAs. **(E)** Central module from the ceRNA network.

Correlation of Immune Cell Infiltration and ceRNA Network

For further analysis, the DEGs of the ceRNA network were divided to the high-expression and low-expression groups by median. The correlation between immune cell abundance and DEGs was analyzed by the Wilcoxon test. CBL expression had a significant positive correlation with macrophages (p = 0.03), neutrophils (p = 0.008), and fibroblasts (p = 0.02). Moreover, CBL expression had a significant negative correlation with CD8+Tem (p = 0.0096) and conventional DC (cDC, p = 0.0056) (**Figure 9A**). CXCL12 expression had a significant positive correlation with M1 macrophages (p = 0.03), activated DCs (aDC, p = 0.0035), MSCs (p = 0.02), lymphatic endothelial cells (ly endothelial cells, p = 0.04), and mv endothelial cells (p = 0.0032). Furthermore, CXCL12 expression had a significant negative correlation with B-cells (p = 0.01), Treg (p = 0.03), M2 macrophages (p = 0.04), hematopoietic stem cells (HSC, p = 0.04), and common lymphoid progenitor (CLP, p = 0.0067) (**Figure 9B**). IL6ST expression had a significant positive correlation with Tregs (p = 0.0014) and myocytes (p = 0.03). Moreover, IL6ST expression had a significant negative correlation with iDC (p = 0.02), ly endothelial cells (p = 0.0044), and mv endothelial cells (p = 0.01) (**Figure 9C**). However, ESR1, IGF1R, XIST, and LINC00632 expression had no significant correlation with most immune cells in DCM.

DISCUSSION

The etiology of DCM can be broadly categorized into genetic, acquired, or mixed (Martinez et al., 2021). Susceptibility in the

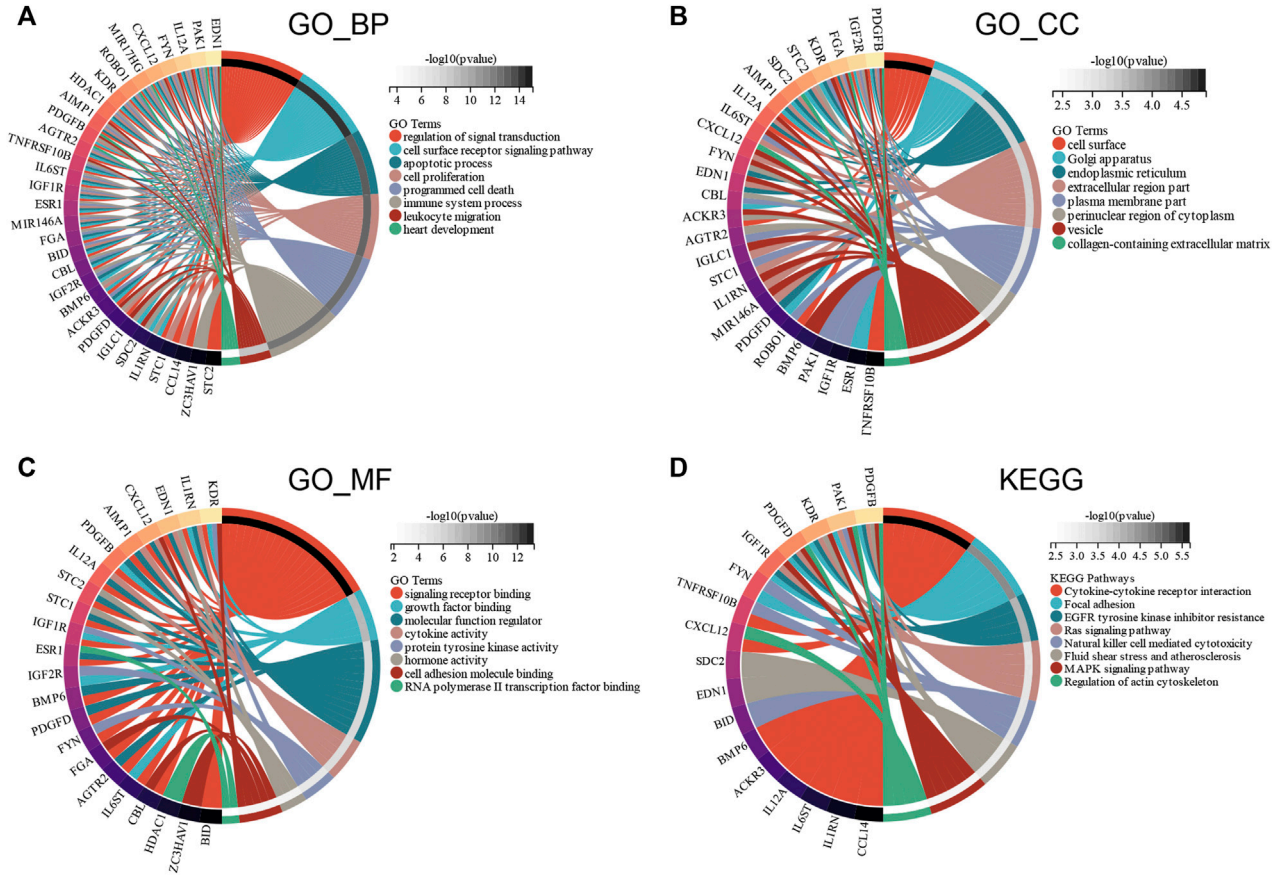

FIGURE 7 | Functional enrichment analysis of ceRNA Network. **(A)** biological process, **(B)** molecular function, **(C)** cell composition and **(D)** KEGG analysis results of differentially expressed immune-related genes between male and female.

model systems to an elevated innate immune response is dependent on at least two factors: 1) male sex (e.g., testosterone) and 2) genetic background (Elamm et al., 2012). Males significantly more often developed relevant reduction of LVEF, malignant ventricular arrhythmias, and end-stage heart failure compared with females, and the mortality was also higher in males (Meyer et al., 2014). For a reason, these so-called sex hormones bind to the nuclear-associated receptors in cardiac cells such as cardiomyocytes and fibroblasts, where they influence cell function (e.g., apoptosis and fibrosis) (Sheppard et al., 2005b). Moreover, sex hormone receptors are located on/in many cells of the immune system, including T cells, B cells, monocytes, macrophages, DCs, and mast cells in humans, which activate the sex-specific immune response (Jain et al., 2021). With the intent to gain new genetic insight to understand the phenotypic differences between female and male patients with DCM, we performed this study and identified a set of critical DEGs which may facilitate therapeutic individualization. In this study, we obtained a total of 1,071 DEGs (542 upregulated genes and 529 downregulated genes) between the male and female DCM samples. The DEGs were processed separately for GO and KEGG pathway analyses. The most significantly enriched terms included "regulation of programmed cell death," "cardiovascular system development," and "ncRNA metabolic process."

Viral infections of the heart were considered to be possible triggers or contributors for the development of the disease in a large number of the DCM patients (Kuhl et al., 2005). The most common viruses that induced inflammatory cardiomyopathy include adenoviruses and enteroviruses; vasculotropic viruses; human immunodeficiency virus (HIV), hepatitis C virus (HCV), influenza A virus and influenza B virus; and viruses from the Coronaviridae family and the Herpesviridae family (Tschope et al., 2021). Epstein–Barr virus belonging to the Herpesviridae family is ubiquitous in population and causes a latent, life-long B lymphocyte infection in more than 90% adults worldwide (Macsween and Crawford, 2003). The identification of intramyocyte EBV genome in inflammatory cardiomyopathy patients was up to 6.3% (Chimenti et al., 2004). Moreover, high numbers of EBV-encoded RNA copies were found in the CD8+T cells from endomyocardial biopsies of a female patient with life-threatening perimyocarditis and caused a severe chronic active infection (Richter et al., 2013). We found that DCM patient gender was significantly correlated with EBV infection. Both the sexes have the same seroprevalence of EBV. Nonetheless, EBV antibody titers in females are generally higher than those in males (Keane et al., 2021). Gender and sex hormone estradiol have been demonstrated to alter EBV latency III functions and regulate

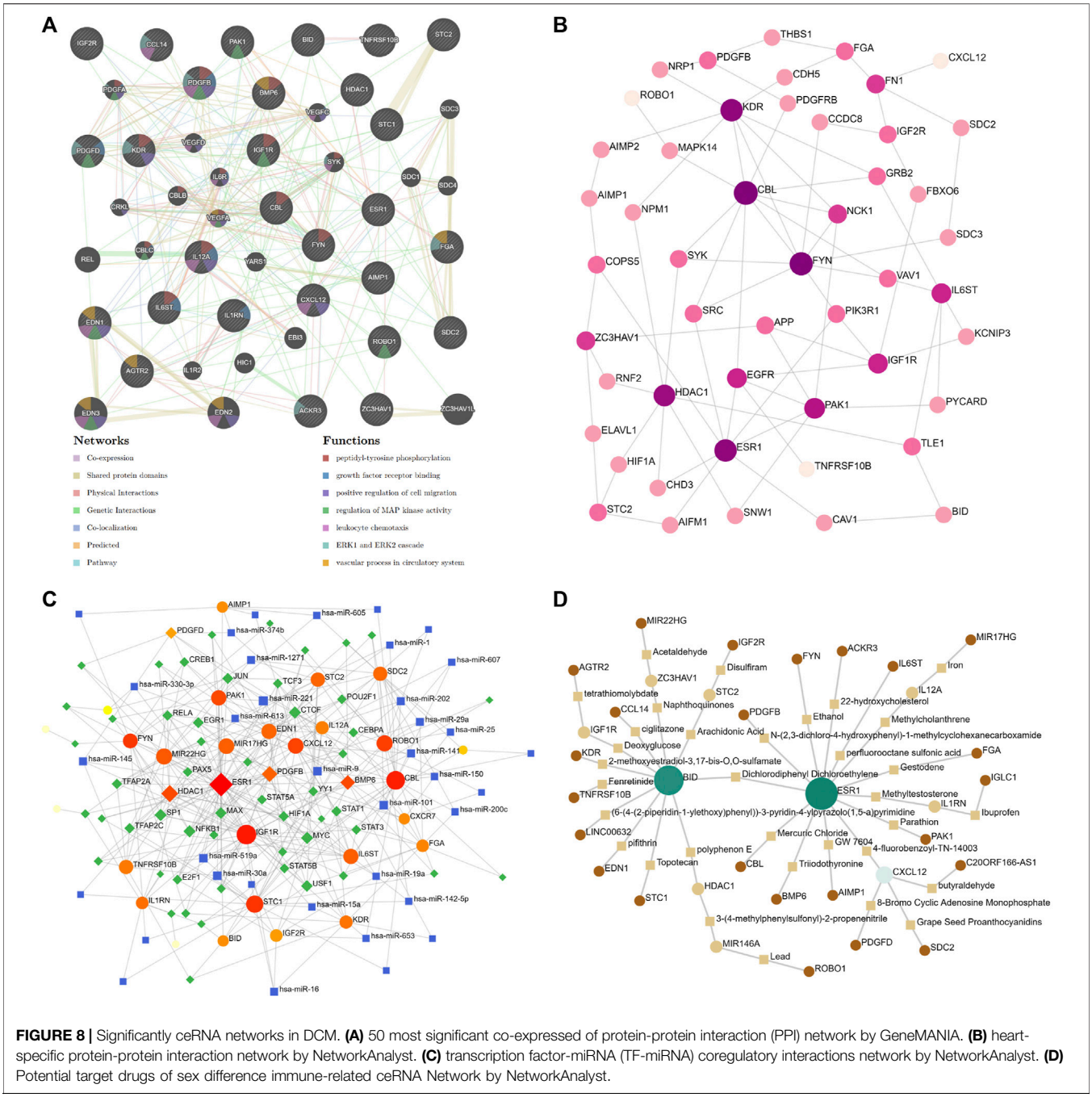

FIGURE 8 | Significantly ceRNA networks in DCM. **(A)** 50 most significant co-expressed of protein-protein interaction (PPI) network by GeneMANIA. **(B)** heart-specific protein-protein interaction network by NetworkAnalyst. **(C)** transcription factor-miRNA (TF-miRNA) coregulatory interactions network by NetworkAnalyst. **(D)** Potential target drugs of sex difference immune-related ceRNA Network by NetworkAnalyst.

multiple sclerosis (MS) risk genes differently among both sexes (Keane et al., 2021). However, whether gender and sex hormones affect EBV infection in the myocardium of DCM patients still warrants further research.

In addition to sex differences, genetic predisposition plays a crucial role in the DCM process. The ceRNA network has been proven to be involved in various heart diseases, including DCM (Tao et al., 2019). In this study, we constructed an immune-related ceRNA network based on sex difference in DCM, including five lncRNAs, six miRNAs, and 29 mRNAs. Furthermore, we extracted a central module from the ceRNA network, including two lncRNAs (XIST and LINC00632), three miRNAs (miR-1-3p, miR-17-5p, and miR-22-3p), and six mRNAs (CBL, CXCL12, ESR1, IGF1R, IL6ST, and STC1). Recent studies found that XIST protects the hypoxia-induced cardiomyocyte injury by regulating different kinds of miRNAs (Chen et al., 2018; Fan et al., 2020; Xiao et al., 2021). LINC00632 inhibits IL-13–induced inflammatory cytokine and mucus production (Yue et al., 2020). Li et al. (2018) indicated that miR-1-3p, which correlates with the left ventricular function of HCM, can serve as a potential target and differentiate HCM from DCM. Zhao et al. (2021) reported that miR-17-5p–mediated

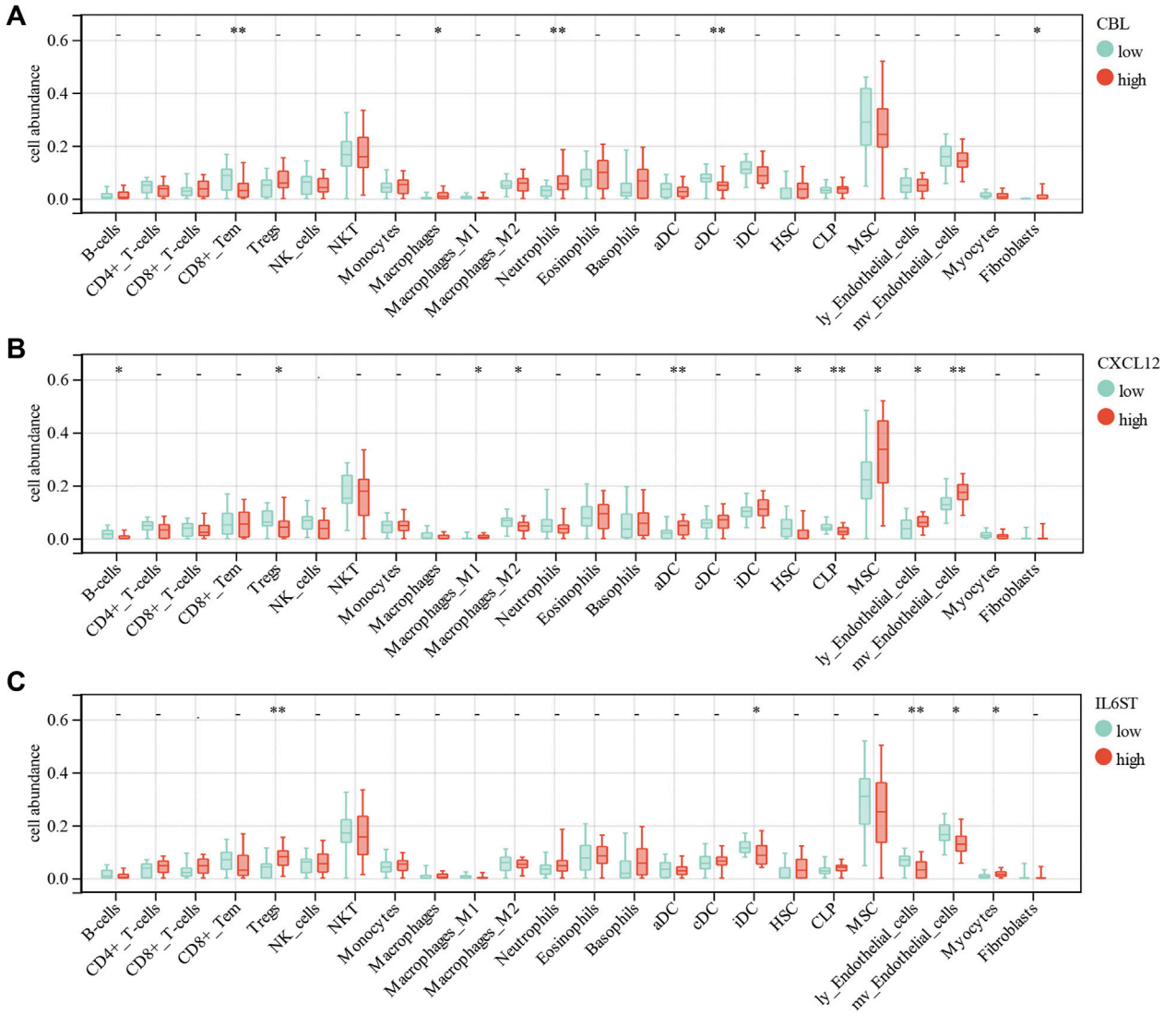

FIGURE 9 | Correlations of low/high **(A)** CBL, **(B)** CXCL12 and **(C)** IL6ST expression with immune cells infiltration in DCM.

endoplasmic reticulum stress promotes acute myocardial ischemia injury. Serially measured circulating miR-22-3p is a biomarker for adverse clinical outcome in patients with chronic heart failure (van Boven et al., 2017). CBL (c-Cbl) is an adapter protein with intrinsic E3 ubiquitin ligase activity that targets the receptor and nonreceptor tyrosine kinases, resulting in their ubiquitination and downregulation. Yang et al. (2016). demonstrated that c-Cbl mediates the ubiquitination/degradation of integrin β1, which leads to DCM. Rafiq et al. (2014) reported that c-Cbl activation promotes myocyte apoptosis, inhibits angiogenesis, and causes adverse cardiac remodeling after myocardial infarction. CXCL12, also known as stromal cell–derived factor-1 (SDF-1), plays a role in many diverse cellular functions, including embryogenesis, immune surveillance, and inflammation response. SDF-1β inhibits palmitate-induced cardiomyocyte fibrosis through the activation of the p38β MAPK signaling pathway (Tian et al., 2021). Jorbenadze et al. (2014) demonstrated that platelet-bound SDF-1 is especially increased in patients with severe impairment of left ventricular systolic function in heart failure. IL6ST, also known as gp130, is a signal transducer shared by many cytokines, including IL-6, ciliary neurotrophic factor (CNTF), leukemia inhibitory factor (LIF), and oncostatin M (OSM). Gp130 activation is sufficient to promote cardiomyocyte proliferation by activating Yap through Src during heart regeneration (Li et al., 2020). MiR-223-3p can directly combine with IL-6ST 3′ untranslatable regions (UTR) and hold back the IL-6 expression and decrease the expression of p-STAT3 and NF-κB p65 in Kawasaki-related heart disease (Wang et al., 2019).

Immune-targeted therapy has become an attractive therapeutic strategy in DCM recently. Damaged cardiac tissue and infections strongly induce the innate immune response, activating Toll-like receptors (TLRs) and the inflammasome, resulting in the release of the proinflammatory cytokines

(Yajima and Knowlton, 2009). Immune cells needed for immune defense, such as macrophages, NK cells, and CD8 T cells, are also important in the early cardiac cellular response in the viral-related DCM models (Elamm et al., 2012). In the case of autoimmune DCM, B cells produce autoantibodies that form immune complexes with self-antigens and complement components (Liu et al., 2000). In addition, the proinflammatory markers, c-fos, IL-6, iNOS, and IL-1β, were upregulated only in the hearts of male but not female rats with autoimmune myocarditis (Barcena et al., 2021). Several clinical trials indicated that immunosuppressive therapies can significantly improve LVEF in patients with inflammatory DCM (Schultheiss et al., 2019). Ameling et al. (2016) demonstrated that immunoadsorption with subsequent immunoglobulin substitution (IA/IgG) improved LVEF, LVIDD, and NYHA classes and inflammation status in DCM patients, accompanied by lower expression of connective tissue growth factor, fibronectin, and collagen type I. However, the response rates to this therapeutic intervention are characterized by considerable interindividual variability (Ameling et al., 2013). Our results, partly in line with the findings of the previous studies, showed that the male sex was significantly positively correlated with inflammatory cell (B cells, memory B cells, CD8+Tem, and NK cells) infiltration.

In summary, in this comprehensive study, we found sex differences in the outcome of immunotherapy in DCM patients. In addition, male DCM patients had a significant positive correlation with the abundance of inflammatory cells (B cells, memory B cells, $CD8^+$ Tem cells, and NK cells). Sex difference DEGs had a widespread impact on the signaling transduction, transcriptional regulation, and metabolism in DCM. Subsequently, we constructed an immune-related ceRNA network based on sex differences in DCM, including five lncRNAs, six miRNAs, and 29 mRNAs. This ceRNA network can regulate a variety of immune-related signaling pathways in DCM. Among this ceRNA network, CBL, CXCL12, and IL6ST were considered to be important DEGs associated with immune cell infiltration. Together, our findings suggest that the sex difference ceRNA network plays a crucial role in immune response regulation in DCM, yet the underlying mechanism still needed further validation.

DATA AVAILABILITY STATEMENT

The original contributions presented in the study are included in the article/**Supplementary Material**. Further inquiries can be directed to the corresponding authors.

AUTHOR CONTRIBUTIONS

Conceptualization, CL and BY; data curation, CL and JL; methodology, CL and DW; resources, CL and ZL; software, CL, SL, and WL; visualization, CL and LC; original draft, CL; review and editing, JL; supervision, ZL and BY.

SUPPLEMENTARY MATERIAL

The Supplementary Material for this article can be found online at: https://www.frontiersin.org/articles/10.3389/fgene.2022.882324/full#supplementary-material

REFERENCES

Abraham, M., Weiss, I. D., Wald, H., Wald, O., Nagler, A., Beider, K., et al. (2013). Sequential Administration of the High Affinity CXCR4 Antagonist BKT140 Promotes Megakaryopoiesis and Platelet Production. *Br. J. Haematol.* 163, 248–259. doi:10.1111/bjh.12501

Ameling, S., Bhardwaj, G., Hammer, E., Beug, D., Steil, L., Reinke, Y., et al. (2016). Changes of Myocardial Gene Expression and Protein Composition in Patients with Dilated Cardiomyopathy after Immunoadsorption with Subsequent Immunoglobulin Substitution. *Basic Res. Cardiol.* 111, 53. doi:10.1007/s00395-016-0569-y

Ameling, S., Herda, L. R., Hammer, E., Steil, L., Teumer, A., Trimpert, C., et al. (2013). Myocardial Gene Expression Profiles and Cardiodepressant Autoantibodies Predict Response of Patients with Dilated Cardiomyopathy to Immunoadsorption Therapy. *Eur. Heart J.* 34, 666–675. doi:10.1093/eurheartj/ehs330

Aran, D., Hu, Z., and Butte, A. J. (2017). xCell: Digitally Portraying the Tissue Cellular Heterogeneity Landscape. *Genome Biol.* 18, 220. doi:10.1186/s13059-017-1349-1

Asher, C., Puyol-Antón, E., Rizvi, M., Ruijsink, B., Chiribiri, A., Razavi, R., et al. (2021). The Role of AI in Characterizing the DCM Phenotype. *Front. Cardiovasc. Med.* 8, 787614. doi:10.3389/fcvm.2021.787614

Barcena, M. L., Jeuthe, S., Niehues, M. H., Pozdniakova, S., Haritonow, N., Kühl, A. A., et al. (2021). Sex-Specific Differences of the Inflammatory State in Experimental Autoimmune Myocarditis. *Front. Immunol.* 12, 686384. doi:10.3389/fimmu.2021.686384

Bardou, P., Mariette, J., Escudié, F., Djemiel, C., and Klopp, C. (2014). Jvenn: an Interactive Venn Diagram Viewer. *BMC Bioinforma.* 15, 293. doi:10.1186/1471-2105-15-293

Basha, O., Shpringer, R., Argov, C. M., and Yeger-Lotem, E. (2018). The DifferentialNet Database of Differential Protein-Protein Interactions in Human Tissues. *Nucleic Acids Res.* 46, D522–D526. doi:10.1093/nar/gkx981

Bhattacharya, S., Andorf, S., Gomes, L., Dunn, P., Schaefer, H., Pontius, J., et al. (2014). ImmPort: Disseminating Data to the Public for the Future of Immunology. *Immunol. Res.* 58, 234–239. doi:10.1007/s12026-014-8516-1

Bornhoeft, J., Castaneda, D., Nemoseck, T., Wang, P., Henning, S. M., and Hong, M. Y. (2012). The Protective Effects of Green Tea Polyphenols: Lipid Profile, Inflammation, and Antioxidant Capacity in Rats Fed an Atherogenic Diet and Dextran Sodium Sulfate. *J. Med. Food* 15, 726–732. doi:10.1089/jmf.2011.0258

Cannatà, A., Fabris, E., Merlo, M., Artico, J., Gentile, P., Pio Loco, C., et al. (2020). Sex Differences in the Long-Term Prognosis of Dilated Cardiomyopathy. *Can. J. Cardiol.* 36, 37–44. doi:10.1016/j.cjca.2019.05.031

Chen, K., Xu, X., Kobayashi, S., Timm, D., Jepperson, T., and Liang, Q. (2011). Caloric Restriction Mimetic 2-deoxyglucose Antagonizes Doxorubicin-Induced Cardiomyocyte Death by Multiple Mechanisms. *J. Biol. Chem.* 286, 21993–22006. doi:10.1074/jbc.m111.225805

Chen, Y. X., Ding, J., Zhou, W. E., Zhang, X., Sun, X. T., Wang, X. Y., et al. (2021). Identification and Functional Prediction of Long Non-coding RNAs in Dilated Cardiomyopathy by Bioinformatics Analysis. *Front. Genet*. 12, 648111. doi:10.3389/fgene.2021.648111

Chen, Y., Liu, X., Chen, L., Chen, W., Zhang, Y., Chen, J., et al. (2018). The Long Noncoding RNA XIST Protects Cardiomyocyte Hypertrophy by Targeting miR-330-3p. *Biochem. Biophysical Res. Commun.* 505, 807–815. doi:10.1016/j.bbrc.2018.09.135

Chimenti, C., Russo, A., Pieroni, M., Calabrese, F., Verardo, R., Thiene, G., et al. (2004). Intramyocyte Detection of Epstein-Barr Virus Genome by Laser Capture Microdissection in Patients with Inflammatory Cardiomyopathy. *Circulation* 110, 3534–3539.doi:10.1161/01.cir.0000148823.08092.0e

Davis, A. P., Grondin, C. J., Johnson, R. J., Sciaky, D., Wiegers, J., Wiegers, T. C., et al. (2021). Comparative Toxicogenomics Database (CTD): Update 2021. *Nucleic Acids Res.* 49, D1138–D1143. doi:10.1093/nar/gkaa891

Elamm, C., Fairweather, D., and Cooper, L. T. (2012). Pathogenesis and Diagnosis of Myocarditis. *Heart* 98, 835–840. doi:10.1136/heartjnl-2012-301686

Epelman, S., Liu, P. P., and Mann, D. L. (2015). Role of Innate and Adaptive Immune Mechanisms in Cardiac Injury and Repair. *Nat. Rev. Immunol.* 15, 117–129. doi:10.1038/nri3800

Fan, J.-L., Zhu, T.-T., Xue, Z.-Y., Ren, W.-Q., Guo, J.-Q., Zhao, H.-Y., et al. (2020). lncRNA-XIST Protects the Hypoxia-Induced Cardiomyocyte Injury through Regulating the miR-125b-Hexokianse 2 axis. *Vitro Cell.Dev.Biol.-Animal* 56, 349–357. doi:10.1007/s11626-020-00459-0

Gerges, S. H., and El-Kadi, A. O. S. (2021). Sex Differences in Eicosanoid Formation and Metabolism: A Possible Mediator of Sex Discrepancies in Cardiovascular Diseases. *Pharmacol. Ther.* doi:10.1016/j.pharmthera.2021.108046

Jain, A., Norton, N., Bruno, K. A., Cooper, L. T., JR., Atwal, P. S., and Fairweather, D. (2021). Sex Differences, Genetic and Environmental Influences on Dilated Cardiomyopathy. *J. Clin. Med.* 10. doi:10.3390/jcm10112289

Jorbenadze, R., Schleicher, E., Bigalke, B., Stellos, K., and Gawaz, M. (2014). Expression of Platelet-Bound Stromal-Cell Derived Factor-1 (SDF-1) and Number of CD34+progenitor Cells in Patients with Congestive Heart Failure. *Platelets* 25, 409–415. doi:10.3109/09537104.2013.829913

Karagkouni, D., Paraskevopoulou, M. D., Tastsoglou, S., Skoufos, G., Karavangeli, A., Pierros, V., et al. (2020). DIANA-LncBase V3: Indexing Experimentally Supported miRNA Targets on Non-coding Transcripts. *Nucleic Acids Res.* 48, D101–D110. doi:10.1093/nar/gkz1036

Keane, J. T., Afrasiabi, A., Schibeci, S. D., Fewings, N., Parnell, G. P., Swaminathan, S., et al. (2021). Gender and the Sex Hormone Estradiol Affect Multiple Sclerosis Risk Gene Expression in Epstein-Barr Virus-Infected B Cells. *Front. Immunol.* 12, 732694. doi:10.3389/fimmu.2021.732694

Kühl, U., Pauschinger, M., Noutsias, M., Seeberg, B., Bock, T., Lassner, D., et al. (2005). High Prevalence of Viral Genomes and Multiple Viral Infections in the Myocardium of Adults with "idiopathic" Left Ventricular Dysfunction. *Circulation* 111, 887–893. doi:10.1161/01.CIR.0000155616.07901.35

Li, J.-H., Liu, S., Zhou, H., Qu, L.-H., and Yang, J.-H. (2014). starBase v2.0: Decoding miRNA-ceRNA, miRNA-ncRNA and Protein-RNA Interaction Networks from Large-Scale CLIP-Seq Data. *Nucl. Acids Res.* 42, D92–D97. doi:10.1093/nar/gkt1248

Li, M., Chen, X., Chen, L., Chen, K., Zhou, J., and Song, J. (2018). MiR-1-3p that Correlates with Left Ventricular Function of HCM Can Serve as a Potential Target and Differentiate HCM from DCM. *J. Transl. Med.* 16, 161. doi:10.1186/s12967-018-1534-3

Li, Y., Feng, J., Song, S., Li, H., Yang, H., Zhou, B., et al. (2020). gp130 Controls Cardiomyocyte Proliferation and Heart Regeneration. *Circulation* 142, 967–982. doi:10.1161/circulationaha.119.044484

Lin, Z., Zhao, Y., Dai, F., Su, E., Li, F., and Yan, Y. (2021). Analysis of Changes in Circular RNA Expression and Construction of ceRNA Networks in Human Dilated Cardiomyopathy. *J. Cell. Mol. Medi* 25, 2572–2583. doi:10.1111/jcmm.16251

Liu, P., Aitken, K., Kong, Y.-Y., Opavsky, M. A., Martino, T., Dawood, F., et al. (2000). The Tyrosine Kinase P56lck Is Essential in Coxsackievirus B3-Mediated Heart Disease. *Nat. Med.* 6, 429–434. doi:10.1038/74689

Liu, Z. P., Wu, C., Miao, H., and Wu, H. (2015). *RegNetwork: An Integrated Database of Transcriptional and Post-transcriptional Regulatory Networks in Human and Mouse*. Database, Oxford.

Macsween, K. F., and Crawford, D. H. (2003). Epstein-Barr Virus-Recent Advances. *Lancet Infect. Dis.* 3, 131–140. doi:10.1016/s1473-3099(03)00543-7

Maekawa, Y., Ouzounian, M., Opavsky, M. A., and Liu, P. P. (2007). Connecting the Missing Link between Dilated Cardiomyopathy and Viral Myocarditis. *Circulation* 115, 5–8. doi:10.1161/circulationaha.106.670554

Marklund, M., Wu, J. H. Y., Imamura, F., Del Gobbo, L. C., Fretts, A., De Goede, J., et al. (2019). Biomarkers of Dietary Omega-6 Fatty Acids and Incident Cardiovascular Disease and Mortality. *Circulation* 139, 2422–2436. doi:10.1161/circulationaha.118.038908

Martinez, H. R., Beasley, G. S., Miller, N., Goldberg, J. F., and Jefferies, J. L. (2021). Clinical Insights into Heritable Cardiomyopathies. *Front. Genet.* 12, 663450. doi:10.3389/fgene.2021.663450

Martínez-Martínez, E., Buonafine, M., Boukhalfa, I., Ibarrola, J., Fernández-Celis, A., Kolkhof, P., et al. (2017). Aldosterone Target NGAL (Neutrophil Gelatinase-Associated Lipocalin) Is Involved in Cardiac Remodeling after Myocardial Infarction through NFκB Pathway. *Hypertension* 70, 1148–1156. doi:10.1161/hypertensionaha.117.09791

Merlo, M., Cannatà, A., Gobbo, M., Stolfo, D., Elliott, P. M., and Sinagra, G. (2018). Evolving Concepts in Dilated Cardiomyopathy. *Eur. J. Heart Fail* 20, 228–239. doi:10.1002/ejhf.1103

Meyer, S., Van Der Meer, P., Van Tintelen, J. P., and Van Den Berg, M. P. (2014). Sex Differences in Cardiomyopathies. *Eur. J. Heart Fail* 16, 238–247. doi:10.1002/ejhf.15

P, R., W, M., B, M., B, M., J, O. C., et al. (1996). Report of the 1995 World Health Organization/International Society and Federation of Cardiology Task Force on the Definition and Classification of Cardiomyopathies. *Circulation* 93, 841–842.

Peng, Z.-H., and Kopeček, J. (2014). HPMA Copolymer CXCR4 Antagonist Conjugates Substantially Inhibited the Migration of Prostate Cancer Cells. *ACS Macro Lett.* 3, 1240–1243. doi:10.1021/mz5006537

Rafiq, K., Kolpakov, M. A., Seqqat, R., Guo, J., Guo, X., Qi, Z., et al. (2014). c-Cbl Inhibition Improves Cardiac Function and Survival in Response to Myocardial Ischemia. *Circulation* 129, 2031–2043. doi:10.1161/circulationaha.113.007004

Richter, J., Quintanilla-Martinez, L., Bienemann, K., Zeus, T., Germing, U., Sander, O., et al. (2013). An Unusual Presentation of a Common Infection. *Infection* 41, 565–569. doi:10.1007/s15010-012-0321-y

Schultheiss, H.-P., Fairweather, D., Caforio, A. L. P., Escher, F., Hershberger, R. E., Lipshultz, S. E., et al. (2019). Dilated Cardiomyopathy. *Nat. Rev. Dis. Prim.* 5, 32. doi:10.1038/s41572-019-0084-1

Sheppard, R., Bedi, M., Kubota, T., Semigran, M. J., Dec, W., Holubkov, R., et al. (2005a). Myocardial Expression of Fas and Recovery of Left Ventricular Function in Patients with Recent-Onset Cardiomyopathy. *J. Am. Coll. Cardiol.* 46, 1036–1042. doi:10.1016/j.jacc.2005.05.067

Subramanian, A., Tamayo, P., Mootha, V. K., Mukherjee, S., Ebert, B. L., Gillette, M. A., et al. (2005). Gene Set Enrichment Analysis: a Knowledge-Based Approach for Interpreting Genome-wide Expression Profiles. *Proc. Natl. Acad. Sci. U.S.A.* 102, 15545–15550. doi:10.1073/pnas.0506580102

Tan, W. L., Lim, B. T., Anene-Nzelu, C. G., Ackers-Johnson, M., Dashi, A., See, K., et al. (2017). A Landscape of Circular RNA Expression in the Human Heart. *Cardiovasc Res.* 113, 298–309. doi:10.1093/cvr/cvw250

Tao, L., Yang, L., Huang, X., Hua, F., and Yang, X. (2019). Reconstruction and Analysis of the lncRNA-miRNA-mRNA Network Based on Competitive Endogenous RNA Reveal Functional lncRNAs in Dilated Cardiomyopathy. *Front. Genet.* 10, 1149. doi:10.3389/fgene.2019.01149

Tian, Y., Wang, Z., Zheng, X., Song, W., Cai, L., Rane, M., et al. (2021). KLF15 Negatively Regulates Cardiac Fibrosis by Which SDF-1β Attenuates Cardiac Fibrosis in Type 2 Diabetic Mice. *Toxicol. Appl. Pharmacol.* 427, 115654. doi:10.1016/j.taap.2021.115654

Tschöpe, C., Ammirati, E., Bozkurt, B., Caforio, A. L. P., Cooper, L. T., Felix, S. B., et al. (2021). Myocarditis and Inflammatory Cardiomyopathy: Current Evidence and Future Directions. *Nat. Rev. Cardiol.* 18, 169–193. doi:10.1038/s41569-020-00435-x

Vallejo, A., Chami, B., Dennis, J. M., Simone, M., Ahmad, G., Abdo, A. I., et al. (2018). NFκB Inhibition Mitigates Serum Amyloid A-Induced Pro-atherogenic Responses in Endothelial Cells and Leukocyte Adhesion and Adverse Changes to Endothelium Function in Isolated Aorta. *Int. J. Mol. Sci.* 20. doi:10.3390/ijms20010105

Van Boven, N., Akkerhuis, K. M., Anroedh, S. S., Rizopoulos, D., Pinto, Y., Battes, L. C., et al. (2017). Serially Measured Circulating miR-22-3p Is a Biomarker for Adverse Clinical Outcome in Patients with Chronic Heart Failure: The Bio-SHiFT Study. *Int. J. Cardiol.* 235, 124–132. doi:10.1016/j.ijcard.2017.02.078

Verjans, R., Peters, T., Beaumont, F. J., Van Leeuwen, R., Van Herwaarden, T., Verhesen, W., et al. (2018). MicroRNA-221/222 Family Counteracts Myocardial Fibrosis in Pressure Overload-Induced Heart Failure. *Hypertension* 71, 280–288. doi:10.1161/hypertensionaha.117.10094

Wang, X., Ding, Y. Y., Chen, Y., Xu, Q. Q., Qian, G. H., Qian, W. G., et al. (2019). MiR-223-3p Alleviates Vascular Endothelial Injury by Targeting IL6ST in Kawasaki Disease. *Front. Pediatr.* 7, 288. doi:10.3389/fped.2019.00288

Warde-Farley, D., Donaldson, S. L., Comes, O., Zuberi, K., Badrawi, R., Chao, P., et al. (2010). The GeneMANIA Prediction Server: Biological Network

Integration for Gene Prioritization and Predicting Gene Function. *Nucleic Acids Res.* 38, W214–W220. doi:10.1093/nar/gkq537

Wj, M., Bj, M., and G, T. (2017). Classification, Epidemiology, and Global Burden of Cardiomyopathies. *Circulation Res.* 121, 722–730.

Xiao, X., He, Z., Tong, S., Dai, L., Xiao, Q., Qin, Z., et al. (2021). lncRNA XIST Knockdown Suppresses Hypoxia/reoxygenation (H/R)-induced Apoptosis of H9C2 Cells by Regulating miR -545-3p/G3BP2. *IUBMB Life* 73, 1103–1114. doi:10.1002/iub.2512

Yajima, T., and Knowlton, K. U. (2009). Viral Myocarditis. *Circulation* 119, 2615–2624. doi:10.1161/circulationaha.108.766022

Yang, N., Yu, F., Shao, G., Fu, Y., and Kong, W. (2016). The E3 Ubiquitin Ligase C-Cbl Mediates Integrin β1 Ubiquitination during Dilated Cardiomyopathy. *Biochem. Biophysical Res. Commun.* 479, 728–735. doi:10.1016/j.bbrc.2016.09.144

Yue, L., Yin, X., Hao, F., Dong, J., Ren, X., Xu, O., et al. (2020). Long Noncoding RNA Linc00632 Inhibits Interleukin-13-Induced Inflammatory Cytokine and Mucus Production in Nasal Epithelial Cells. *J. Innate Immun.* 12, 116–128. doi:10.1159/000500420

Zeng, D., Ye, Z., Shen, R., Yu, G., Wu, J., Xiong, Y., et al. (2021). IOBR: Multi-Omics Immuno-Oncology Biological Research to Decode Tumor Microenvironment and Signatures. *Front. Immunol.* 12, 687975. doi:10.3389/fimmu.2021.687975

Zhao, L., Jiang, S., Wu, N., Shi, E., Yang, L., and Li, Q. (2021). MiR-17-5p-mediated Endoplasmic Reticulum Stress Promotes Acute Myocardial Ischemia Injury through Targeting Tsg101. *Cell Stress Chaperones* 26, 77–90. doi:10.1007/s12192-020-01157-2

Zhou, G., Soufan, O., Ewald, J., Hancock, R. E. W., Basu, N., and Xia, J. (2019). NetworkAnalyst 3.0: a Visual Analytics Platform for Comprehensive Gene Expression Profiling and Meta-Analysis. *Nucleic Acids Res.* 47, W234–W241. doi:10.1093/nar/gkz240

Conflict of Interest: The authors declare that the research was conducted in the absence of any commercial or financial relationships that could be construed as a potential conflict of interest.

Publisher's Note: All claims expressed in this article are solely those of the authors and do not necessarily represent those of their affiliated organizations, or those of the publisher, the editors, and the reviewers. Any product that may be evaluated in this article, or claim that may be made by its manufacturer, is not guaranteed or endorsed by the publisher.

Frontiers in Genetics

Highlights genetic and genomic inquiry relating to all domains of life

The most cited genetics and heredity journal, which advances our understanding of genes from humans to plants and other model organisms. It highlights developments in the function and variability of the genome, and the use of genomic tools.

Discover the latest Research Topics

See more →

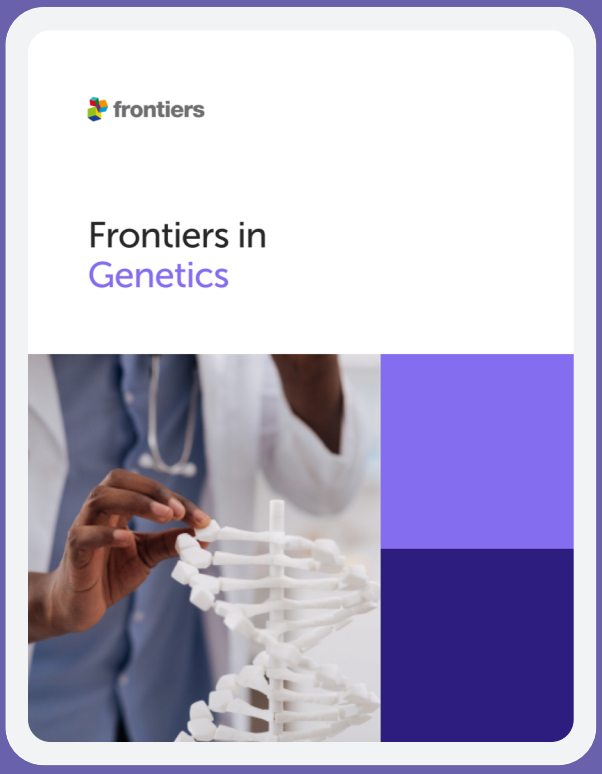

Frontiers

Avenue du Tribunal-Fédéral 34
1005 Lausanne, Switzerland
frontiersin.org

Contact us

+41 (0)21 510 17 00
frontiersin.org/about/contact